UNIVERSITY OF CALIFORNIA
RIVERSIDE

# From Discovery-Based to Targeted Proteomics

A Dissertation submitted in partial satisfaction
of the requirements for the degree of

Doctor of Philosophy

in

Environmental Toxicology

by

Lei Guo

March 2015

Dissertation Committee:

Dr. Yinsheng Wang, Chairperson
Dr. Quan Cheng
Dr. Huiwang Ai

The Dissertation of Lei Guo is approved:

---

---

---

Committee Chairperson

University of California, Riverside

# ACKNOWLEDGMENTS

I would like to express my sincere gratitude to my graduate advisor, Prof. Yinsheng Wang, who provided the opportunity, guidance and financial support in all my projects for my PhD study. During these five years, he gave me many constructive ideas both for my research and future career plan. Without his help and support, it would not be possible for me to complete my doctoral study successfully. I would also like to thank his family for their help and kindness.

I would like to thank all the members of my dissertation committee, Prof. Quan Cheng and Prof. Huiwang Ai. Their review and evaluation of this work as well as their valuable suggestions and generous help during my PhD study are deeply appreciated. I would also like to thank Prof. David Eastmond, Prof. Sarjeet Gill and Prof. Roger Atkinson for all their patient help and instructions of the curricula in graduate school.

I would like to thank Mr. Songqin Pan in the Proteomics Core for his help and advises in mass spectrometers. I would like to thank the staff members in Mass Spectrometry Facility, Dr. Richard Kondrat and Mr. Ron New for their help with Thermo TSQ vantage use.

I also appreciate all the help and friendship from current and former members of the Wang group. Especially, I would like to thank Dr. Yongsheng Xiao for his advices, instructions and help in my research. I would like to thank Dr. Lei Xiong for her help and guidance with discovery-based proteomic study when I first started my research here. I would like to express my sincere thanks to Dr. Xiaoli Dong and her husband Dr.

Xinning Jiang for their great contribution of setting up instrument and bioinfomatic tools, as well as constructive advices for my proteomic studies. I would like to thank Dr. Xiaoxia Dai and Dr. Changjun You for their help and discussion with all the biological experiments. I would also like to thank Lijuan Fu for all the valuable discussion of the triple quadrupole mass spectrometer and friendship, Weili Miao for her help in my experiments and all other former and current group members: Dr. Qiongwei Yu, Dr. Tao Bing, Dr. Jin Wang, Dr. John Prins, Dr. Qianqian Zhai, Dr. Debin Ji, Dr. Jianshuang Wang, Dr. Qian Cai, Dr. Ashley Swanson, Shuo Liu, Pengcheng Wang, Preston Williams, Eric Stephens, Zi Wang, Nicole Williams, Ji Jiang, Yang Yu, Ming Huang, Yuxiang Cui and Jiabin Wu.

I am also appreciative of my friends and fellow graduate students or postdocs in the Environmental Toxicology Graduate Program and Department of Chemistry, especially from the Ai, Zhong, Feng and Julian group. I'd like to thank Dr. Xing Zhang, Dr. Shang Zeng, Dr. Yunhua Liu, Fei Bu, Yichong Fan, Yang Liu, Wei Ren, April Ranney, Monique Williams and Daniel Wasik, for the helpful discussion, technical support and friendship.

I would also like to thank staff from the Environmental Toxicology Graduate Program and Department of Chemistry for providing prompt assistance of administrative matters. They are Ms. Dawn Loyola, Dr. Kevin Simpson, Ms. Barbara Outzen, Ms. Tina Enriquez, Mr. Jaime Matute and Mr. Prisciliano Saavedra.

I would also thank the financial support for my PhD study by the Environmental Toxicology Graduate Program and Department of Chemistry, UC Riverside.

I would like to thank my husband, Dr. Yongsheng Xiao. Without his company, support, love and encouragement, I would not be able to complete my PhD study and find a job successfully.

Finally, I would like to express my deepest gratitude to my parents Haoyuan Guo and Jinying Cao, my grandmother Xiuchun Tang, and my parents in-law Mingxing Xiao and Yong Chen for their dedication, love and support.

Best wishes to them all!

# COPYRIGHT ACKNOWLEDGEMENTS

The text and figures in Chapter 2, in part or full, are a reprint of the material as it appears in Journal of Proteome Research 2013, 12(7):3511-3518. The coauthors (listed in the publication) Lei Guo designed and performed research, analyzed data and wrote the paper, Dr. Yongsheng Xiao designed and performed research and analyzed data, Dr. Yinsheng Wang designed, directed and supervised the research, analyzed data and wrote the paper that forms the basis of this chapter.

The text and figures in Chapter 3, in part or full, are a reprint of the material as it appears in Toxicology and Applied Pharmacology 2014, 277(1):21-29. The coauthors (listed in the publication) Lei Guo designed and performed research, analyzed data and wrote the paper, Dr. Yongsheng Xiao designed and performed research and analyzed data, Dr. Yinsheng Wang designed, directed and supervised the research, analyzed data and wrote the paper that forms the basis of this chapter.

The text and figures in Chapter 4, in part or full, are a reprint of the material as it appears in Analytical Chemistry 2014, 86(21):10700-10707. The coauthors (listed in the publication) Lei Guo designed and performed research, analyzed data and wrote the paper, Dr. Yongsheng Xiao designed and performed research and analyzed data, Dr. Yinsheng Wang designed, directed and supervised the research, analyzed data and wrote the paper that forms the basis of this chapter.

The text and figures in Chapter 5, in part or full, are a reprint of the material as it appears in Journal of Proteome Research 2015, 14(1):193-201. The coauthors (listed in

the publication) Lei Guo designed and performed research, analyzed data and wrote the paper, Dr. Yongsheng Xiao designed and performed research and analyzed data, Dr. Ming Fan performed the research, Dr. Jian Jian Li designed the research and wrote paper, Dr. Yinsheng Wang designed, directed and supervised the research, analyzed data and wrote the paper that forms the basis of this chapter.

# DEDICATION

To my husband Yongsheng Xiao, my parents Haoyuan Guo and Jinying Cao, my grandmother Xiuchun Tang, and my parents in-law Mingxing Xiao and Yong Chen. I deeply appreciate all your love, patience, support and company!

ABSTRACT OF THE DISSERTATION

From Discovery-Based to Targeted Proteomics

by

Lei Guo

Doctor of Philosophy, Graduate Program in Environmental Toxicology
University of California, Riverside, March 2015
Dr. Yinsheng Wang, Chairperson

Mass spectrometry-based proteomic approaches have become the method of choice for performing discovery-based quantitative global proteomic analysis, as well as targeted proteomics for the reproducible analysis of a selected set of proteins. In this dissertation, we reported the application of these approaches in the profiling of global proteome with discovery-based proteomics approach, and profiling of global kinome with targeted proteomic analysis.

In Chapter two, we studied hexavalent chromium [Cr(VI)]-induced alteration of proteomic landscape in human skin fibroblast cells. We utilized MS-based quantitative approach for assessing the global proteome alteration in response to Cr(VI) treatment. Here with the use of in-gel digestion and mass spectrometry analysis in data-dependant mode, we were able to quantify ~4600 unique proteins, among which around 10% exhibited significant alterations in expression levels upon a 24-h treatment with 0.5 μM

$K_2Cr_2O_7$. From these results, we revealed that Cr(VI) induced its cytotoxic effect via activating the cholesterol biosynthesis pathway.

In Chapter three, we combined the filter-aided sample preparation method with LC-MS/MS analysis to reveal monomethylarsonous acid [MMA(III)]-induced alteration in the protein expression level in human skin fibroblasts. From our study, among the ~6500 quantified unique proteins, ~300 displayed significant changes in expression after exposure with 2 μM MMA(III) for 24 h. Subsequent analysis revealed the inhibition of *de novo* cholesterol biosynthesis upon MMA(III) treatment.

In Chapter four, we applied adenosine triphosphate (ATP) affinity probe and scheduled multiple-reaction monitoring analysis for profiling global kinome in human cells in response to arsenite treatment. From the quantification of ~250 kinases, we found the expression of several kinases involved in cell cycle progression was changed significantly upon arsenite treatment. The up-regulation of cyclin-dependant kinase 1 was further verified.

In Chapter five, we utilized stable isotope-labeled ATP affinity probe in conjunction with scheduled MRM analysis for profiling global kinome signatures of the radioresistant MCF-7/C6 breast cancer cells. We rigorously quantified 120 kinases, of which one third exhibited significant differences in expression levels or ATP binding affinities. Several kinases involved in cell cycle progression and DNA damage response quantified may be involved in the development of radioresistance in cancer cells.

# TABLE OF CONTENTS

# LIST OF FIGURES

# LIST OF TABLES

# Chapter 1

# General Overview

## 1.1 Introduction

In the well-known "central dogma of molecular biology",[1] protein is the final product of the entire process of genetic information flow. Regulations involving DNA replication, transcription and RNA translation can all affect differential expression and post-translational modifications of proteins, which may in turn function as key regulators for these processes.[2] Proteins are also active cellular components that participate in and regulate a variety of cellular processes.[3] Knowledge of protein expression, turnover and modifications can offer vital insights into the modes of action behind endogenous or exogenous stimuli or diseases.[4] Collectively, the studies about the identities, quantities and physiological functions of all proteins are referred as "Proteomics".[5] Different aspects of proteomics have been studied, ranging from protein identification, quantification, post-translational modification and cellular function to protein-protein, protein-DNA and protein-RNA interactions.[6]

In the field of quantitative protein profiling, different global approaches have been developed to perform protein analysis on a proteomic scale (Figure 1.1).[7] The analysis of comparative protein expression pattern is initially achieved by high-resolution two-dimensional (2D) gel electrophoresis.[8] 2D gel electrophoresis is achieved by sequential orthogonal separation of proteins based on two different properties. The two dimensions

of separations can be achieved through isoelectric point by isoelectric focusing and protein molecular weight by SDS electrophoresis.[9] The proteins can then be detected after silver or Coomassie Brilliant Blue staining by software-based image analysis.[10] However, the reliability of this approach may be compromised by overlapped spots, mismatched spots or different gel running conditions.

Alternatively, with the advancement of mass spectrometry instrumentation and its successful application in the detection of complex large molecules, along with the development of bioinformatic tools, the mass spectrometry-based quantitative proteomics study has become an indispensable tool for global proteome profiling.[11] Compared to conventional proteomic approaches, the MS-based method provides higher throughput and increased reliability.[12] The mass spectrum can reliably reveal the sequence and amount of a peptide, which minimizes the possibility of false identification and quantification caused by interferences.

In this chapter, I will first review the common strategies for quantitative proteomic study, including metabolic, chemical labeling and label-free quantification. Subsequently, the general workflow, including diverse sample preparation methods, mass spectrometry instrumentation and operating principles, as well as applications will be discussed in detail for both discovery-based and targeted proteomic studies, respectively.

**1.2 Mass spectrometry-based quantitative proteomics**

Mass spectrometry-based proteomics has been applied to the study of protein-protein interactions by affinity-based isolations, the mapping of organelles, and quantitative proteome profiling from various species.[12] The capability of mass

spectrometry to precisely quantify thousands of proteins from complex samples exerts great influence in different fields of biology and pharmacy.[13]

In general, proteomic analysis can be achieved by either detecting intact proteins or peptides digested by protease. First, intact proteins or large peptide fragments can be ionized and directly analyzed by mass spectrometers.[14] On the other hand, mass spectrometric analysis can be conducted on proteolytically digested peptides, which is known as bottom-up proteomics.[15] Given the relatively mature development of bottom-up proteomic approach, it is commonly adopted in global proteome profiling.

The entire process of MS-based quantitative proteomics is a multi-step operation. Multiple options for each step can satisfy special demands for analyzing complex samples from different aspects. Different methods are utilized for the MS-based quantification of proteins.[16] It can be achieved through measurement of the absolute value of the protein amount in comparison with known amount of synthetic, heavy isotopologues of target peptides. The absolute amount of a peptide is calculated by the pre-determined calibration curve of the standards.[17] On the other hand, this can be achieved through relative quantification. One approach is the "label-free quantification", in which spectra of the same peptide from two separate mass spectrometric analyses are compared.[18] An improved alternative is to use stable isotope-labeled analyte as control to obtain the relevant protein amount, which increases the quantification accuracy and eliminates systematic variation of sample processing and MS measurement.[19] The general principle of this method is based on the fact that chemically identical analyte pairs with different isotopes co-elute in the chromatography, and the analytes can be

differentiated on the spectrum via the mass difference introduced by stable isotope labeling.[12] Thus, through relative signal intensities, ratios of protein expression in tested samples can be determined.

As mentioned above, unlike the MS-based quantification of small molecules, which normally uses unlabeled internal standards or spiked-in synthetic stable isotope-labeled standards as control for the measurement,[20] the quantification of proteins can be achieved through direct labeling of protein components through chemical or metabolic labeling. The use of such internal standard of analyte pairs will reduce the variation arising from sample preparation and chromatographic analysis.

Comparison of the representative labeling approaches and relevant structures of the labeling reagents are illustrated in Figure 1.2 and 1.3.

### 1.2.1 ICAT

Isotope-coded affinity tag (ICAT) is one of the most commonly used chemical isotope labeling methods for understanding global proteome dynamics in a cell, tissue or organism.[21] As shown in Figure 1.3A, the ICAT probe consists of three parts, which include a thiol-reactive iodoacetyl group, a labeled linker, and a biotin moiety that enables enrichment and purification. The iodoacetyl group is a chemical crosslinking group that binds and subsequently labels only the free thiols on the cysteine residue. The light and heavy labeled peptides can then be differentiated by the mass difference due to isotope labeling with either deuterium or carbon-13 in the heavy form of the tag.

For ICAT labeling, cell lysates from two different states of cells to be investigated are labeled separately with light or heavy form of the probes. At this step, the tag is

covalently attached to the thiol groups of cysteines in all the proteins. The cell lysates are subsequently combined and mixed in equal amount. After enzymatic digestions, normally with trypsin, the resulting peptides will be fractionated to reduce sample complexity via high-performance liquid chromatography, thus facilitates quantification of proteins in low abundance. Subsequently, each fraction will be purified with affinity enrichment of avidin, followed by analysis via mass spectrometers. The identity of each peptide is verified through analyzing peptide fragment ions in the tandem MS; however, quantification of a peptide is via comparison of signal intensities for the corresponding light and heavy forms of the peptide in MS. Thus, the amount of the proteins from which the peptides are derived can be determined.

The ICAT labeling strategy has been broadly applied to the MS-based quantitative analysis of the entire proteome for cells, tissues, and organelles.[22] Unlike traditional metabolic labeling method, this chemical labeling strategy reduces the cost of labeling and is more practical for the analysis of complex clinical samples.[23] However, since the tag only attaches to the cysteine residue, which is only present in less than one third of the total human tryptic peptides, this method could give rise to incomplete proteome coverage.[24] To solve this problem, an alternative labeling method called dimethyl labeling is adopted.[25] Unlike the ICAT strategy, the dimethylation uses labeled formaldehyde and sodium cyanoborohydride with stable isotopes such as deuterium and carbon-13, which reacts with the primary amine on the N-termini of peptides or the side chain of lysine residue.[25] This method has been widely used in the MS-based global proteome quantification.[26]

### 1.2.2 ITRAQ

ICAT and dimethyl strategies are chemical labeling methods with the use of isotopic tags at different molecular masses. Alternatively, chemical labeling can be implemented with the use of isobaric tags, e.g., isobaric tag for relative and absolute quantification (ITRAQ).[27] As displayed in Figure 1.3B, this tag contains an amine-reactive NHS groups, a mass normalizer and a mass tag as the mass reporter. Unlike isotopic tags, which give rise to the mass difference of isotope-labeled analyte pairs, the mass-to-charge ratio of the corresponding peptide pair is constant after labeling with isobaric tags. With identical mass and chemical properties, each pair co-elutes during MS analysis. The mass tag is then cleaved through collision-induced dissociation for tandem mass spectrometry. Identification of a peptide is through analyzing the fragment ions of the peptide, whereas quantification result is obtained via the relative signal intensities of mass tags, known as reporter ions, derived concurrently from each sample.

The labeling strategy of ITRAQ is similar to the ICAT labeling, except that the labeling is performed at peptide level. To be specific, after cell lysis and tryptic digestion, the resulting peptides from two different samples are labeled separately with differential ITRAQ tags. The peptide mixtures are then combined and analyzed by MS without further enrichment.

The advantage of isobaric tags is its capability to perform multiplexed analysis with high throughput. For example, an amine-reactive, 10-plex tandem mass tag reagents is commercially available from Thermo, which enables simultaneous analysis of the

global proteome from 10 different samples, with the generation of reporter ion ranging from 126.1 to 131.1 Da after high-energy collision dissociation.[28]

For different chemical labeling strategies, stable isotope labeling is conducted during the late steps of the entire workflow, either at protein or peptide level after cell lysis. Thus, they are more error-prone due to variations in sample preparation and/or enzymatic digestions compared to metabolic labeling at early stage during cell culture or animal feeding.[29]

### 1.2.3 SILAC

Stable isotope labeling by amino acids in cell culture (SILAC) was introduced as a metabolic labeling method.[30] SILAC labeling is achieved through the addition of stable isotope-labeled essential amino acids, normally lysine and arginine, to the cell culture media.[31] Ideally the amino acids should be essential, such as lysine, thus the cells will take up these amino acids from the cell culture media for protein expression, which enables stable isotope labeling of the proteome.[32] In general, arginine is non-essential, however it is mainly acquired from diet for whole organisms, and is proved to be essential for the growth of some cell lines.[33] Given that trypsin cleaves the peptide bonds primarily at the carboxyl side of lysine and arginine, theoretically, all the resultant peptides, expect C-terminal peptides from some proteins, should possess the labeling.[34]

The labeling strategy of SILAC is distinct from above-mentioned chemical labeling.[35] After being cultured in the media containing stable isotope-labeled amino acids for more than 6-8 cell doublings, the cells will be completely labeled. Subsequently, differentially labeled cells with different physiological states will be

harvested and lysed. The resulting cell lysates are then mixed at one-to-one ratio in mass. After that, different options can be selected to perform downstream sample preparation steps, basically including detergent removal, reduction, alkylation, enzymatic digestion, further fractionation, purification and desalting, before MS analysis. Similar to the MS analysis for ICAT labeling, the identification is based on MS/MS, and quantification is based on MS.

The advantage of SILAC over previous chemical labeling is that since the labeling is achieved during cell culture, combination of SILAC-labeled cell lysates at early stage will prevent the downstream sample preparation, purification and digestion steps from introducing variations in protein quantification. However, as stated previously, the SILAC labeling strategy is expensive and has low efficiency for labeling clinical samples compared to ICAT labeling. Despite these disadvantages, SILAC has become the method of choice in cell biology for quantitative analysis of the global proteome of different cells from various species.[36] In addition, in some modified SILAC strategies, such as pulsed SILAC, cells are exposed to the SILAC media for a certain period of time, which enable analysis of protein turnover rates.[37]

### 1.2.4 Label-free quantification

Other than the above-mentioned chemical and metabolic labeling strategies, protein quantification can also be achieved through label-free quantification. It serves as a highly cost-effective alternative for rapid proteomic analysis. In the label-free quantification, samples are collected, prepared, digested and analyzed by MS separately. Subsequent peptide quantification is performed by the comparison of the signal intensity

in MS or spectra counts of MS/MS.[38] The overall accuracy of this approach is reasonable; however, since all the experimental procedures from cell culture to MS analysis are performed separately, many factors can contribute to the quantification variation, such as differences in digestion efficiency and mass spectrometric measurements. In addition, the accuracy of quantification associated with smaller peptide ratios is less precise than the ones with larger ratios, and the dynamic range is relatively small compared to other labeling strategies.[39]

### 1.3 Discovery-based proteomics

Generally speaking, there are two fundamental approaches for MS-based proteomic analysis, namely, discovery-based and targeted proteomics. Discovery-based proteomics, also known as shotgun proteomics, is primarily employed for systematic global proteome screening and comparison of the proteome between cells under different physiological states. Instead of focusing on the detection of a specific set of protein targets, the discovery-based proteomic study offers the opportunity for hypothesis-free and systems-wide analysis.[40] In this type of study, the number of proteins that can be identified and quantified with a broad dynamic range is an important indicator.

Shown in Figure 1.4 is the general workflow of discovery-based proteomics. The first step is sample preparation.[41] Generally, the entire process starts from metabolic labeling or protein extraction from cells, tissues or body fluids. For protein extraction, different cell lysis reagents can be used. Normally, the detergent-based approach yields better recovery of proteins, especially membrane proteins than chaotropic salts and organic solvents.[40, 42] However, some detergents, including sodium dodecyl sulfate

(SDS), 3-[(3-cholamidopropyl)dimethylammonio]-1-propanesulfonate (CHAPS) and nonyl phenoxypolyethoxylethanol (NP40), are not LC-MS-compatible; thus, detergent removal or purification step is performed before enzymatic digestion. This step can be achieved via dialysis, SDS-polyacrylamide gel electrophoresis (SDS-PAGE) or the filter-aided sample preparation.[42] Next, purified protein samples are reduced and alkylated by dithiothreitol and iodoacetamide, respectively. The purpose of these two steps are to break the disulfide bond, which may compromise and interfere with the digestion efficiency and MS analysis, and prevent it from reforming. Subsequently, the protein mixtures are digested with protease(s), including trypsin, Lys-C, Arg-C, Asp-N and Glu-C, either individually or in combination, for the sequential enzymatic digestion.[43] Resulting peptides are then fractionated by HPLC to reduce sample complexity; however, for in-gel digestion, protein fractionation is performed through cutting gel bands into different pieces.[41] After further desalting steps with centrifugal filters or chromatography media-fixed pipette tips, samples are ready for MS analysis. The data processing and pathway analysis are completed by using specific bioinformatic tools.[11b]

### 1.3.1 Sample preparation

Sample preparation mainly involves protein purification, chemical modification, buffer exchange and protein digestion. In addition, fractionation of samples into a few fractions for MS analysis can further help increasing the recovery of proteins by reducing sample complexity.

#### 1.3.1.1 In-gel digestion

Previously, the most widely used approach is through in-gel digestion.[44] For this method, after cell lysis with detergent, protein samples are separated by SDS-PAGE based on their molecular weight. After staining with sliver or Commassie bright blue, the gel is cut into 10-20 bands. Proteins in each band are then washed, reduced, alkylated and digested by protease in gel separately. The resulting peptides are then extracted from the gel.

Compared to gel-free method, this method enables fractionation of protein samples by SDS-PAGE and facilitates the removal of impurities, including detergents and buffer components.[41] Protein fractionation increases the dynamic range of protein analysis.[44b] However, some proteins such as membrane proteins, proteins with extreme hydrophobicity have limited solubility in SDS-PAGE.[45] In addition, incomplete peptide extraction could also give rise to sample loss, and compromise protein recovery.

#### 1.3.1.2 Detergent-free in-solution digestion

Alternatively, samples can be prepared through in-solution digestion.[46] Compared to in-gel digestion, this method is detergent-free, which uses strong chaotropic reagents for cell lysis. Such reagents include urea and thiourea at high concentration. After cell lysis, proteins are reduced and alkylated, followed by direct protein digestion with selected protease in solution under denaturing conditions. To increase protein recovery, subsequent peptide fractionation is frequently adopted.

In-solution digestion is a straightforward way to obtain peptides for MS analysis, which minimizes and simplifies sample handling. However, some proteins may be

incompletely dissolved, and digestion efficiency may be compromised by interfering substances.[45]

#### 1.3.1.3 FASP

As stated above, although sample preparation methods such as in-gel or in-solution digestion have been well established, there are still some disadvantages of these two approaches. For in-solution digestion, impurities may compromise the solubilization and digestion of proteins. For in-gel digestion, only proteins dissolved in SDS-PAGE gel can be analyzed. In this case, some important proteins, such as membrane proteins that serve as cell signal transduction components, may not be detected.[47]

To solve this problem, the filter-aided sample preparation (FASP) method was introduced.[48] In this approach, the filter unit is used as the proteomics reactor for all steps of sample preparation. The general principle is that filters with selected pore size can retain proteins, while allow small molecules, such as detergent, impurities and buffer component, flow through by centrifugation. Theoretically this allows the capture of all proteins, including membrane proteins.

Figure 1.5 depicts the workflow for FASP.[48] Initially, samples are solubilized in 4% SDS, followed by sonication to reduce the viscosity introduced by DNA. Urea (8 M) is then added to facilitate the removal of SDS. Subsequently the urea-containing samples are loaded onto the filters, which contain membrane with molecular weight cutoff of 3000 or 10000 Da. With additional washing with 8 M urea buffer, low-molecular weight components are depleted. Next, protein reduction and alkylation buffer is added to the filter unit successively, for carbamidomethylation of thiol groups on the cysteine residues

to prevent disulfide bond formation. All reagents and buffers are removed through centrifugation at room temperature to prevent decomposition of urea at high temperature and precipitation of SDS at low temperature. Afterwards, trypsin is added to the purified and chemically modified protein mixture retained in the filter. To improve protein coverage, other protease(s) can be added to the filter unit after tryptic digestion, for example Glu-C, to achieve sequential digestion of proteins.[43b] After digestion, the proteolytic peptides can be collected by centrifugation.

SDS is predominantly used as a detergent for solubilizing cells and tissues with high efficiency. However, failure to completely remove SDS, not even with a small amount left, will hinder the proteolytic process and influence the MS analysis by dominating the mass spectra. In the FASP protocol, a relatively high percentage of SDS can be totally removed when mixed with 8 M urea owing to the centrifugal filters. Besides, addition of highly concentrated urea buffer can facilitate the recovery of membrane proteins and allow them to be analyzed as efficiently as soluble proteins.[49] Thus, FASP successfully combines the in-gel and in-solution digestion methods and overcomes their disadvantages, which has the capability of accommodating a wider range of digestion conditions with deeper proteome coverage. In addition, it simplifies the sample preparation process and increases the overall throughput of the sample preparation process.

### 1.3.2 Peptide fractionation

To further increase protein coverage and reduce sample complexity, subsequent high-resolution fractionation of peptides prior to LC-MS/MS analysis is often necessary for both in-solution digestion and FASP methods.[50] High performance liquid chromatography (HPLC) separation is commonly used for this purpose to narrow the dynamic range of components within the fraction and increase MS analysis efficiency.[51] Generally, different HPLC separation methods are combined to achieve orthogonal 2D LC fractionation, where low-pH reversed phase LC (RPLC) is commonly used as the second dimension prior to MS analysis.[52] For the first dimension, several approaches can be utilized, including strong cation exchange (SCX), strong anion exchange (SAX) and high-pH RPLC separation.[53]

#### 1.3.2.1 SCX

With comparatively higher orthogonality to the second dimension of RPLC than other methods, SCX has become the method of choice as the first dimension of the 2D fractionation.[54] Due to the basicities of lysine, arginine and histidine, peptides containing these residues tend to be positively charged. In the aqueous solution, positively charged analytes bind to the negatively charged stationary phase of the SCX resin, which usually contains the aliphatic sulfonic acid group. Separation by SCX is achieved by using salt-containing buffer to differentially exchange cations from the resin. With increasing salt concentration, cations with increasing binding affinity will be sequentially eluted.

The SCX fractionation is performed on HPLC system, starting with equilibration of the SCX column for optimized binding of analytes.[35] Proteolytic peptides are then reconstituted in 0.1% FA and loaded onto the SCX column, followed by washing to remove impurities. The analytes are then eluted with a linear gradient of 0-500 mM ammonium acetate in 0.1% FA, and collected into 10-20 fractions. Each fraction is then desalted and injected for online LC-MS analysis.

SAX is an inverse method to SCX. The functional group on the resin is tertiary amine, which reversibly binds to negatively charged analytes. Both SCX and SAX are also utilized for phosphopeptide fractionation.[55]

**1.3.2.2 High-pH RPLC**

SCX fractionation provides satisfactory orthogonality to the subsequent RPLC separation; however, the eluate often has high concentration of salts, and further desalting step is needed, which may reduce protein recovery. In addition, its limited capability in resolving peptides compared to RPLC may lead to sample overlapping between different fractions. Therefore, RPLC may be a better choice as the first dimension of 2D fractionation.

RPLC uses hydrophobic stationary phase with alkyl chains, and the separation is based on the reversible binding of analytes.[56] For the elution of bound peptides, organic solvent such as methanol or acetonitrile is utilized as mobile phase. Hydrophilic molecules will be washed out immediately. However, molecules with higher hydrophobicity will be gradually eluted out with the increase of organic solvent in the composition of the mobile phase.

For samples containing ionizable compounds, the pH of mobile phases will affect the retention of analytes in the RPLC separation.[57] To increase the orthogonality, high-pH RPLC is used prior to secondary low-pH RPLC separation.[58]

For low-pH RPLC, distilled water and 90% acetonitrile in 0.1% FA with a pH around 4 are employed as mobile phases A and B for the separation, respectively. To achieve high-pH RPLC fractionation, 10 mM ammonium formate is added to both mobile phases for adjusting the pH to be around 10.[53] During the HPLC separation, samples are collected concatenately into 10-20 fractions.

High-pH RPLC achieves better performance than the SCX approach with larger number of peptides and proteins being recovered as well as increasing protein sequence coverage.[53] The concatenating strategy of combining early, middle and late fractions with minimum overlap into one sample, improves analysis coverage while retaining high throughput.[53] In addition, the use of low salt or MS-compatible salt in mobile phases yields cleaner samples that are amenable to direct MS analysis requiring no additional desalting steps. By this means, sample loss is reduced and sample handling is simplified.[58a]

It worth noting that, silica-based columns usually work in a pH range of 2-8. With pH higher than 8, the silica backbone tends to be soluble and thus is detrimental to most columns. Therefore, specialized columns that tolerant of high pH condition should be selected.

### 1.3.3 Mass spectrometry analysis

With the development and advancement of mass spectrometers, especially those with faster scan speed, higher resolution and higher mass accuracy, researchers nowadays can achieve identification and quantification of thousands of proteins.[43b] This ultra high coverage of the entire proteome provides us with a complete picture of cellular changes under different physiological conditions.

#### 1.3.3.1 Instrumentation

The general workflow for mass spectrometry analysis is sample introduction, ionization, mass analysis and detection. The mass spectrum contains information about the composition of sample, mass-to-charge ratio of each component and abundance of each species. Different types of mass spectrometers have been utilized for the discovery-based proteomic analysis, such as linear quadrupole ion trap, time-of-flight and Orbitrap mass analyzers.[59]

The linear ion trap can be used for both inducing fragmentation and detection of ions in a two-dimensional quadrupole field.[60] The time-of-flight mass analyzer, on the other hand, detects ions based on their movement in the electric field. By their velocity, m/z of each ion is determined.[61]

Orbitrap was invented in the most recent decade and has been used predominantly for the global proteome quantification.[62] The core of Orbitrap is similar to Fourier-transform ion cyclotron resonance mass analyzer, which traps ions in the orbit around the central electrode. Mass spectrum is acquired by Fourier transformation of the image current generated by oscillation of ions along the electrode, thus determining the m/z of

each ion. Compared to conventional instrumentation, Orbitrap possesses higher mass accuracy and sensitivity.

#### 1.3.3.2 Analysis principle

For discovery-based proteomics, data-dependent analysis (DDA) is prevalent. In the DDA mode (Figure 1.6), the mass spectrometer will first acquire one full-scan MS, from which 10-20 most abundant ions are selected and fragmented for tandem mass spectrometry analysis.[63] From the analysis, the m/z values of the analyte and its fragments are determined. After mapping the fragments on MS/MS against relevant database, peptide identification can be achieved. In the meanwhile, peptide quantification is calculated based on the relative abundance of each precursor ion in MS.

## 1.4 Targeted proteomics

As mentioned above, in the data-dependent analysis, the fragmentation and measurement of an ion is based on its signal intensity in the full-MS scan. In this case, the chance for detecting abundant proteins is higher.[64] Some important proteins such as kinases and membrane proteins, which are relevantly low in abundance compared to the entire proteome, may not be readily detected. Additional, considering the complexity of the entire proteome, the space for the MS to analyze is quite huge. During every analysis, the MS may lead to the detection of a slightly different list of proteins.[65] For hypothesis-driven analysis, reproducible answers for changes in expression of selected protein targets are needed.[66]

To solve this problem, targeted approach for proteomic analysis has been introduced, which is dominated by the multiple reaction monitoring (MRM) technology.

Instead of the abundance-based selection of ions, each pair of precursor and product ions to be monitored in the MRM mode is predetermined.[64] The pair of product ion and its corresponding precursor ion is considered a "transition". For the reliable quantification of each proteolytic peptide, several representative transitions are selected and monitored in MRM analysis. Compared to discovery-based proteomics, the targeted approach offers superior sensitivity, reproducibility and quantitative accuracy.[64]

The general workflow for MRM analysis is shown in Figure 1.7. The MRM assay is developed via upstream determination of the m/z values for precursor and product ions in each transition, which is mainly completed by the mass spectrum acquired from precedent data-dependant analysis.[67] Once the method is established, the MRM analysis is relatively straightforward with high throughput. The sample preparation steps are similar as those for discovery-based proteomic analysis. To increase the detection sensitivity, especially for proteins of low abundance, affinity enrichment of targeted proteolytic peptides is required. After LC-MRM analysis, the identification and quantification results are obtained by specific bioinformatic tools.

### 1.4.1 Affinity purification

To reduce sample complexity for the analysis and to increase detection sensitivity, enrichment of targeted proteins prior to the LC-MS analysis is favorable. Optimized enrichment with different probes can be achieved based on their differential binding chemistry. These probes normally contain a purification and enrichment moiety, such as biotin, a linker, as well as a binding moiety for binding protein and peptide targets.

Different reagents have been utilized as the binding moiety for the affinity purification of targeted proteins or proteolytic peptides through chemical crosslinking. This crosslinking involves formation of covalent bonds between the two components, which depends on the compatibility of specific reagents with the selected functional groups in proteins or peptides. The binding could be affected by the binding affinity, protein structure and probe stability. The most commonly used target functional groups contains primary amines on the N-termini and lysine side chain, carboxylic acids on the C-termini and asparatate and glutamate side chain, sulfhydryls on the cysteine side chain, as well as aldehydes generated through oxidation of carbohydrate groups in glycoproteins.[68] For different targets, different probes with relevant reactive groups have been developed.

**1.4.1.1 NHS ester**

Primary amines on the N-termini and lysine side chain are widely present in the tryptic peptides. The major amine-reactive group in use is the N-hydroxysuccinimide (NHS) ester.[69] As shown in Figure 1.8A, primary amines on proteins or peptides will attack and bind the carbon in the carboxyl group and form covalent amide bond under pH 7.2 to 8.5. To increase the solubility of this reagent, a modified version of sulfo-NHS can be used without changing the conjugation chemistry.

There is at least one primary amine existing in every trypic peptide, and lysine is ubiquitously present in proteins. In addition, since lysine is positively charged and thus exists primarily on the outside of tertiary structure of proteins under physiologic pH, the primary amine is an ideal target with high accessibility to the crosslinking reagents.[70]

#### 1.4.1.2 Acyl phosphate

Similar to the NHS group, acyl phosphate group can also bind primary amines via nucleophilic substitution (Figure 1.8B). Although the binding affinity is not as good as NHS group, the use of such binding moiety facilitates specialized enrichment of ATP- or GTP-binding proteins which are critical for the functional study of global kinome and cell signaling pathways. Moreover, binding of the acyl phosphate group requires precedent binding of the ATP and GTP molecules in the binding moiety with the active ATP or GTP binding pockets of proteins, thus prevents non-specific binding of the probe.

Apart from the above-mentioned reagents, there are other crosslinkers for targeting different functional groups. These include carbodiimide and hydrozide, which are utilized for including crosslinking with carboxyl and aldehyde groups, respectively.[68, 71]

### 1.4.2 MRM detection platform with scheduled analysis strategy

For the reliable quantification of a peptide, at least three transitions are typically monitored in the MRM analysis for targeted proteomic study.[72] Thus, the total number of transitions could add up to several thousand. For each cycle, only around 170 transitions can be monitored simultaneously with adequate sensitivity. To increase the robustness and throughput of the targeted analysis, scheduled MRM is often the method of choice with the help of bioinformatic tools.[73] For scheduled MRM, each transition is monitored within a short-period time frame, known as the retention time window. Therefore, the accuracy in predicting retention time window controls the successful detection of each transition.

#### 1.4.2.1 Instrumentation and detection principle

The MS for achieving this task is triple quadruple mass spectrometers (Figure 1.9).[74] As its name implies, the MS consists of three quadruples, the first and third quadruple serve as mass filters for the selection and detection of ions and the second quadruple is for induction of fragmentation. To be specific, during MRM analysis, complex peptide samples are injected; in the first quadrupole (Q1) only the preselected parent ion derived from protein of interest is allowed to enter to the second quadrupole (Q2). The selected parent ion is then fragmented via CID in Q2. Subsequently, only product ions monitored as transitions for the quantification of the parent ion are detected in the third quadrupole (Q3). Quantification of each peptide is calculated based on the signal intensity of each monitored transition.

#### 1.4.2.2 Method development

Unlike discovery-based proteomic study, MRM analysis necessitates prior method development. Normally, this process combines MS-based shotgun proteomic study of the targeted proteins with processing by specialized bioinformatic tools, such as Skyline.[75] For method development, knowledge of protein targets and transition pairs is required, such as the m/z value and retention time.

To illustrate, for the global kinome study, a kinome library containing tandem mass spectra and retention time information has been constructed.[67] To this end, kinases from whole cell lysates of different human cell lines have been enriched with an ATP affinity probe.[76] The probe consists of a biotin purification and enrichment group, as well as a stable isotope-labeled linker and an ATP binding moiety that are joined together by

an acyl phosphate group. The acyl phosphate group enables chemical crosslinking of the probe with primary amine groups on the lysine residue after binding with active ATP binding proteins. After tryptic digestion, the biotin-labeled peptides can then be analyzed by shotgun proteomics method in DDA mode.

For library construction, tandem mass spectrum of each biotin-tagged peptide is extracted and analyzed by Skyline. After further peptide selection, 3-4 most-abundant y ions are chosen as targeted transitions for the quantification of each peptide. MRM analysis methods with the m/z, collision energy and retention time window of all transitions are determined by Skyline. Based on the developed method, MRM analysis of samples is performed on the triple quadrupole mass spectrometer as described above. Since different transitions derived from the same peptide occur in the time window during the MRM analysis, peptide identification and quantification can be determined based on the MRM spectrum.

**1.4.2.3 Retention time prediction**

As stated above, the efficiency of MRM analysis is limited by the number of peptides that can be monitored in an LC-MS/MS run. Through scheduled acquisition, the number can be dramatically increased; however, precise retention time prediction is essential.[77]

Previously, the prediction of retention time in the scheduled MRM analysis is based on the intrinsic property of the peptide, such as hydrophobicity.[78] SSRCalc scale is utilized for this purpose.[79] This scale is derived from the summation of the retention coefficients for every amino acid in a peptide with additional adjustment according to the

retention coefficients of residues on the N-termini. The linear dependence of retention time on SSRCalc scale can be utilized for the retention time prediction in scheduled MRM analysis.

In actual analysis, the accuracy of retention time prediction by SSRCalc scale is often compromised by different factors related to the intrinsic property of peptide towards different resins and mobile phases.[80] In addition, differential chromatographic setup and residual variance will also compromise the accuracy for retention time prediction by SSRCalc scale. Along this line, a novel scale named iRT, which is an empirically determined retention time scale for peptides, has been introduced.[77]

The iRT scale is empirically determined and normalized to the assigned iRT scores of reference peptides. These reference peptides should have relative high signal intensities that can be readily detected by mass spectrometers. In addition, absence in modification-prone amino acids, as well as broad distribution along the gradient is required. Moreover, the reference peptides should be different from natural protein sequences, thereby preventing interference of peptide quantification.

The calculation of iRT is depicted in Figure 1.10. Cell lysates containing the protein targets are combined with the reference peptides for MS analysis. iRT is determined by the retention time of each peptide from the full-MS scan. The first and last eluted reference peptides are assigned an iRT of 0 and 100, respectively; thus, the linear fit of measured retention time versus iRT is determined by these two points. The iRT values of all other peptides are then calculated by the equation of this linear regression based on their measured retention time. For the scheduled MRM analysis,

only reference peptides need to be analyzed in advance to acquire the slope and intercept of the linear regression on the current instrument. Predicted retention time of all targeted peptides can be transformed from their iRT scores using linear regression.

Unlike the conventional hydrophobicity-dependant SSRCalc scale, which is based on the theoretical retention factor of amino acid composition of the peptide sequence and subjected to the chromatographic variance, the iRT of each peptide is a fixed number relative to the iRTs of a selected set of reference peptides and is more robust. Thus, the scale can be easily transferrable on different instruments with diverse chromatographic setup among different laboratories. In addition, retention time prediction based on the iRT scale is more accurate than the SSRCalc scale based on the hydrophobicity of the peptides.[77] The increased prediction accuracy not only allows for shorter retention time window duration, but also increases the accuracy of quantification.

**1.4.2.4 On-the-fly retention time recalibration**

Although the elution of each peptide follows the exact same order as indicated by the iRT, systematic shift in retention time is unavoidable. This could stem from the change of mobile phase flow rate or discrepancy in sample loading. To be able to correct for this unpredictable systematic retention time shift, researches have brought in the on-the-fly retention time recalibration, which is now implemented in the mass spectrometer operating software.[81] To be specific, during the MRM run, retention times for the reference peptides are recorded for the assessment of the systematic retention time shift. The RTs of two successive reference peptides are used for the generation of a linear regression, and the retention time window for all the following peptides are adjusted

according to the linear fit in real time. Only regression of the two most recently eluted peptides are used for the dynamic adjustment of retention time shift.

This method allows real-time monitoring and adjustment of retention time shift, thus reduces failure in transition capture caused by changes in LC performance. Additionally, this approach further increases the accuracy for retention time prediction and allows shorter retention time window duration. Given that more transitions can be accommodated, the throughput of the scheduled MRM analysis is increased.

**1.5 Scope of the dissertation**

Compared to conventional proteomic approaches, mass spectrometry-based approach has its own advantages in achieving the proteomic analysis with better reproducibility, higher sensitivity and superior quantitative accuracy. In this dissertation, we reported the application of these approaches for comparative analysis of global proteome and kinome expression profile under different physiological conditions induced by environment toxicant treatment and disease-related changes.

In Chapter 2, we studied hexavalent chromium-induced alteration of proteomic landscape in human skin fibroblast cells. Hexavalent chromium [Cr(VI)] generated during industrial processes is carcinogenic. Although much is known about the deleterious effects caused by reactive oxygen species generated during the reduction of Cr(VI) after its absorption by biological systems, the precise mechanisms underlying Cr(VI) cytotoxicity remain poorly defined. Here, we analyzed, at the global proteome scale, the perturbation of protein expression in GM00637 human skin fibroblast cells upon exposure to potassium dichromate ($K_2Cr_2O_7$). We were able to quantify ~ 4600

unique proteins, among which ~ 400 exhibited significant alterations in expression levels upon a 24-hr treatment with 0.5 μM $K_2Cr_2O_7$. Pathway analysis revealed the Cr(VI)-induced perturbation of cholesterol biosynthesis, G-protein signaling, inflammatory response, and selenoprotein pathways. In particular, we discovered that the $K_2Cr_2O_7$ treatment led to pronouncedly elevated expression of a large number of enzymes involved in *de novo* cholesterol biosynthesis. Real-time PCR analysis revealed the increased mRNA expression of selected genes involved in cholesterol biosynthesis. Consistently, $K_2Cr_2O_7$ treatment resulted in marked increases in cellular cholesterol level in multiple cell lines. Moreover, the Cr(VI)-induced growth inhibition of cultured human cells could be rescued by a cholesterol-lowering drug, lovastatin. Together, we demonstrated, for the first time, that Cr(VI) may exert its cytotoxic effect, at least partly, through the up-regulation of enzymes involved in *de novo* cholesterol biosynthesis and the resultant increase of cholesterol level in cells.

In Chapter 3, we demonstrated monomethylarsonous acid inhibited endogenous cholesterol biosynthesis in human skin fibroblasts. Human exposure to arsenic in drinking water is a widespread public health concern, and such exposure is known to be associated with many human diseases. The detailed molecular mechanisms about how arsenic species contribute to the adverse human health effects, however, remain incompletely understood. Monomethylarsonous acid [MMA(III)] is a highly toxic and stable metabolite of inorganic arsenic. To exploit the mechanisms through which MMA(III) exerts its cytotoxic effect, we adopted a quantitative proteomic approach, by coupling stable isotope labeling by amino acids in cell culture (SILAC) with LC-MS/MS

analysis, to examine the variation in the entire proteome of GM00637 human skin fibroblasts following acute MMA(III) exposure. Among the ~6500 unique proteins quantified, ~300 displayed significant changes in expression after exposure with 2 μM MMA(III) for 24 h. Subsequent analysis revealed the perturbation of *de novo* cholesterol biosynthesis, selenoprotein synthesis and Nrf2 pathways evoked by MMA(III) exposure. Particularly, MMA(III) treatment resulted in considerable down-regulation of several enzymes involved in cholesterol biosynthesis. In addition, real-time PCR analysis showed reduced mRNA levels of select genes in this pathway. Furthermore, MMA(III) exposure contributed to a distinct decline in cellular cholesterol content and significant growth inhibition of multiple cell lines, both of which could be restored by supplementation of cholesterol to the culture media. Collectively, the present study demonstrated that the cytotoxicity of MMA(III) may arise, at least in part, from the down-regulation of cholesterol biosynthesis enzymes and the resultant decrease of cellular cholesterol content.

In Chapter 4, we applied ATP affinity probe and scheduled multiple-reaction monitoring analysis for profiling global kinome in human cells in response to arsenite treatment. Phosphorylation of cellular components catalyzed by kinases plays important roles in cell signaling and proliferation. Quantitative assessment of perturbation in global kinome may provide crucial knowledge for elucidating the mechanisms underlying the cytotoxic effects of environmental toxicants. Here, we utilized an ATP affinity probe coupled with SILAC to assess quantitatively the arsenite-induced alteration of global kinome in human cells. We constructed a SILAC-compatible kinome library for

scheduled MRM analysis and adopted on-the-fly recalibration of retention time shift, which provided better throughput of the analytical method and enabled the simultaneous quantification of the expression of ~300 kinases in two LC-MRM runs. With this improved analytical method, we conducted an in-depth quantitative analysis of the perturbation of kinome of GM00637 human skin fibroblast cells induced by arsenite exposure. Several kinases involved in cell cycle progression, including cyclin-dependent kinases (CDK1 and CDK4) and Aurora kinases A, B, and C, were found to be hyperactivated, and the altered expression of CDK1 was further validated by Western analysis. In addition, treatment with a CDK inhibitor, flavopiridol, partially restored the arsenite-induced growth inhibition of human skin fibroblast cells. Thus, sodium arsenite may confer its cytotoxic effect partly through the aberrant activation of CDKs and the resultant perturbation of cell cycle progression. Together, we developed a high-throughput, SILAC-compatible, and MRM-based kinome profiling method and demonstrated that the method is powerful in deciphering the molecular modes of action of a widespread environmental toxicant. The method should be generally applicable for uncovering the cellular pathways triggered by other extracellular stimuli.

In Chapter 5, we profiled global kinome signatures of the radioresistant MCF-7/C6 breast cancer cells using MRM-based targeted proteomics. Ionizing radiation is widely used in cancer therapy; however, cancer cells often develop radioresistance, which compromises the efficacy of cancer radiation therapy. Quantitative assessment of the alteration of the entire kinome in radioresistant cancer cells relative to their radiosensitive counterparts may provide important knowledge to define the mechanism(s)

underlying tumor adaptive radioresistance and uncover novel target(s) for effective prevention and treatment of tumor radioresistance. By employing a scheduled multiple-reaction monitoring analysis in conjunction with isotope-coded ATP affinity probes, we assessed the global kinome of radioresistant MCF-7/C6 cells and their parental MCF-7 human breast cancer cells. We rigorously quantified 120 kinases, of which $^{1}/_{3}$ exhibited significant differences in expression levels or ATP binding affinities. Several kinases involved in cell cycle progression and DNA damage response were found to be overexpressed or hyperactivated, including checkpoint kinase 1 (CHK1), cyclin-dependent kinases 1 and 2 (CDK1 and CDK2), and the catalytic subunit of DNA-dependent protein kinase. The elevated expression of CHK1, CDK1, and CDK2 in MCF-7/C6 cells was further validated by Western blot analysis. Thus, the altered kinome profile of radioresistant MCF-7/C6 cells suggests the involvement of kinases on cell cycle progression and DNA repair in tumor adaptive radioresistance. The unique kinome profiling results also afforded potential effective targets for resensitizing radioresistant cancer cells and counteracting deleterious effects of ionizing radiation exposure.

## References


1. Crick, F., Central dogma of molecular biology. *Nature* **1970,** *227* (5258), 561-3.

2. (a) Ipsaro, J. J.; Joshua-Tor, L., From guide to target: molecular insights into eukaryotic RNA-interference machinery. *Nat. Struct. Mol. Biol.* **2015,** *22* (1), 20-28; (b) Gomez-Escoda, B.; Wu, P. Y., The programme of DNA replication: beyond genome duplication. *Biochem. Soc. Trans.* **2013,** *41* (6), 1720-5.

3. Lopez-Mejia, I. C.; Fajas, L., Cell cycle regulation of mitochondrial function. *Curr. Opin. Cell Biol.* **2014,** *33C*, 19-25.

4. Masuda, M.; Yamada, T., Signaling pathway profiling by reverse-phase protein array for personalized cancer medicine. *Biochim. Biophys. Acta.* **2014**.

5. Cox, J.; Mann, M., Quantitative, high-resolution proteomics for data-driven systems biology. *Annu. Rev. Biochem.* **2011,** *80*, 273-99.

6. Kenyon, G. L.; DeMarini, D. M.; Fuchs, E.; Galas, D. J.; Kirsch, J. F.; Leyh, T. S.; Moos, W. H.; Petsko, G. A.; Ringe, D.; Rubin, G. M.; Sheahan, L. C., Defining the mandate of proteomics in the post-genomics era: workshop report. *Mol. Cell. Proteomics* **2002,** *1* (10), 763-80.

7. Phizicky, E.; Bastiaens, P. I. H.; Zhu, H.; Snyder, M.; Fields, S., Protein analysis on a proteomic scale. *Nature* **2003,** *422* (6928), 208-215.

8. O'Farrell, P. H., High resolution two-dimensional electrophoresis of proteins. *J. Biol. Chem.* **1975,** *250* (10), 4007-21.

9. Rabilloud, T.; Chevallet, M.; Luche, S.; Lelong, C., Two-dimensional gel electrophoresis in proteomics: Past, present and future. *J. Proteomics* **2010,** *73* (11), 2064-77.

10. (a) Switzer Iii, R. C.; Merril, C. R.; Shifrin, S., A highly sensitive silver stain for detecting proteins and peptides in polyacrylamide gels. *Anal. Biochem.* **1979,** *98* (1), 231-237; (b) Berth, M.; Moser, F. M.; Kolbe, M.; Bernhardt, J., The state of the art in the analysis of two-dimensional gel electrophoresis images. *Appl. Microbiol. Biotechnol.* **2007,** *76* (6), 1223-43.

11. (a) Mann, M., Functional and quantitative proteomics using SILAC. *Nat. Rev. Mol. Cell Biol.* **2006,** *7* (12), 952-8; (b) Tyanova, S.; Mann, M.; Cox, J., MaxQuant for in-depth analysis of large SILAC datasets. *Methods Mol. Biol.* **2014,** *1188*, 351-64.

12. Aebersold, R.; Mann, M., Mass spectrometry-based proteomics. *Nature* **2003,** *422* (6928), 198-207.

13. Gstaiger, M.; Aebersold, R., Applying mass spectrometry-based proteomics to genetics, genomics and network biology. *Nat. Rev. Genet.* **2009,** *10* (9), 617-627.

14. Gregorich, Z. R.; Ge, Y., Top-down proteomics in health and disease: challenges and opportunities. *Proteomics* **2014,** *14* (10), 1195-210.

15. Chait, B. T., Chemistry. Mass spectrometry: bottom-up or top-down? *Science* **2006,** *314* (5796), 65-6.

16. Kaake, R. M.; Wang, X.; Huang, L., Profiling of protein interaction networks of protein complexes using affinity purification and quantitative mass spectrometry. *Mol. Cell. Proteomics* **2010,** *9* (8), 1650-65.

17. Zeiler, M.; Straube, W. L.; Lundberg, E.; Uhlen, M.; Mann, M., A protein epitope signature tag (PrEST) library allows SILAC-based absolute quantification and multiplexed determination of protein copy numbers in cell lines. *Mol. Cell. Proteomics* **2012,** *11* (3), O111.009613.

18. Zhu, W.; Smith, J. W.; Huang, C. M., Mass spectrometry-based label-free quantitative proteomics. *J. Biomed. Biotechnol.* **2010,** *2010*, 840518.

19. Bantscheff, M.; Schirle, M.; Sweetman, G.; Rick, J.; Kuster, B., Quantitative mass spectrometry in proteomics: a critical review. *Anal. Bioanal. Chem.* **2007,** *389* (4), 1017-31.

20. Dahal, U. P.; Jones, J. P.; Davis, J. A.; Rock, D. A., Small molecule quantification by liquid chromatography-mass spectrometry for metabolites of drugs and drug candidates. *Drug Metab. Dispos.* **2011,** *39* (12), 2355-60.

21. Shiio, Y.; Aebersold, R., Quantitative proteome analysis using isotope-coded affinity tags and mass spectrometry. *Nat. Protoc.* **2006,** *1* (1), 139-45.

22. (a) Fu, C.; Hu, J.; Liu, T.; Ago, T.; Sadoshima, J.; Li, H., Quantitative analysis of redox-sensitive proteome with DIGE and ICAT. *J. Proteome Res.* **2008,** *7* (9), 3789-3802; (b) Tam, E. M.; Morrison, C. J.; Wu, Y. I.; Stack, M. S.; Overall, C. M., Membrane protease proteomics: Isotope-coded affinity tag MS identification of undescribed MT1-matrix metalloproteinase substrates. *Proc. Natl. Acad. Sci. U. S. A.* **2004,** *101* (18), 6917-22.

23. Li, C.; Hong, Y.; Tan, Y. X.; Zhou, H.; Ai, J. H.; Li, S. J.; Zhang, L.; Xia, Q. C.; Wu, J. R.; Wang, H. Y.; Zeng, R., Accurate qualitative and quantitative proteomic analysis of clinical hepatocellular carcinoma using laser capture microdissection coupled with isotope-coded affinity tag and two-dimensional liquid chromatography mass spectrometry. *Mol. Cell. Proteomics* **2004,** *3* (4), 399-409.

24. Zhang, H.; Yan, W.; Aebersold, R., Chemical probes and tandem mass spectrometry: a strategy for the quantitative analysis of proteomes and subproteomes. *Curr. Opin. Chem. Biol.* **2004,** *8* (1), 66-75.

25. Kovanich, D.; Cappadona, S.; Raijmakers, R.; Mohammed, S.; Scholten, A.; Heck, A. J., Applications of stable isotope dimethyl labeling in quantitative proteomics. *Anal. Bioanal. Chem.* **2012,** *404* (4), 991-1009.

26. Pan, Y.; Cheng, K.; Mao, J.; Liu, F.; Liu, J.; Ye, M.; Zou, H., Quantitative proteomics reveals the kinetics of trypsin-catalyzed protein digestion. *Anal. Bioanal. Chem.* **2014,** *406* (25), 6247-56.

27. Wiese, S.; Reidegeld, K. A.; Meyer, H. E.; Warscheid, B., Protein labeling by iTRAQ: a new tool for quantitative mass spectrometry in proteome research. *Proteomics* **2007,** *7* (3), 340-50.

28. Werner, T.; Sweetman, G.; Savitski, M. F.; Mathieson, T.; Bantscheff, M.; Savitski, M. M., Ion coalescence of neutron encoded TMT 10-plex reporter ions. *Anal. Chem.* **2014,** *86* (7), 3594-601.

29. Oda, Y.; Huang, K.; Cross, F. R.; Cowburn, D.; Chait, B. T., Accurate quantitation of protein expression and site-specific phosphorylation. *Proc. Natl. Acad. Sci. U. S. A.* **1999,** *96* (12), 6591-6.

30. Ong, S. E.; Blagoev, B.; Kratchmarova, I.; Kristensen, D. B.; Steen, H.; Pandey, A.; Mann, M., Stable isotope labeling by amino acids in cell culture, SILAC, as a simple and accurate approach to expression proteomics. *Mol. Cell. Proteomics* **2002,** *1* (5), 376-86.

31. Ong, S. E.; Kratchmarova, I.; Mann, M., Properties of 13C-substituted arginine in stable isotope labeling by amino acids in cell culture (SILAC). *J. Proteome Res.* **2003,** *2* (2), 173-81.

32. Ong, S.-E.; Mann, M., A practical recipe for stable isotope labeling by amino acids in cell culture (SILAC). *Nat. Protocols* **2007,** *1* (6), 2650-2660.

33. Scott, L.; Lamb, J.; Smith, S.; Wheatley, D. N., Single amino acid (arginine) deprivation: rapid and selective death of cultured transformed and malignant cells. *Br. J. Cancer* **2000,** *83* (6), 800-10.

34. Biringer, R. G.; Amato, H.; Harrington, M. G.; Fonteh, A. N.; Riggins, J. N.; Huhmer, A. F., Enhanced sequence coverage of proteins in human cerebrospinal fluid using multiple enzymatic digestion and linear ion trap LC-MS/MS. *Brief. Funct. Genomic. Proteomic.* **2006,** *5* (2), 144-53.

35. Guo, L.; Xiao, Y.; Wang, Y., Monomethylarsonous acid inhibited endogenous cholesterol biosynthesis in human skin fibroblasts. *Toxicol. Appl. Pharmacol.* **2014,** *277* (1), 21-9.

36. (a) Blagoev, B.; Kratchmarova, I.; Ong, S. E.; Nielsen, M.; Foster, L. J.; Mann, M., A proteomics strategy to elucidate functional protein-protein interactions applied to EGF signaling. *Nat. Biotechnol.* **2003,** *21* (3), 315-8; (b) Everley, P. A.; Krijgsveld, J.; Zetter, B. R.; Gygi, S. P., Quantitative cancer proteomics: stable isotope labeling with amino acids in cell culture (SILAC) as a tool for prostate cancer research. *Mol. Cell. Proteomics* **2004,** *3* (7), 729-35.

37. Schwanhausser, B.; Gossen, M.; Dittmar, G.; Selbach, M., Global analysis of cellular protein translation by pulsed SILAC. *Proteomics* **2009,** *9* (1), 205-9.

38. (a) Liu, H.; Sadygov, R. G.; Yates, J. R., 3rd, A model for random sampling and estimation of relative protein abundance in shotgun proteomics. *Anal. Chem.* **2004,** *76* (14), 4193-201; (b) Florens, L.; Carozza, M. J.; Swanson, S. K.; Fournier, M.; Coleman, M. K.; Workman, J. L.; Washburn, M. P., Analyzing chromatin remodeling complexes using shotgun proteomics and normalized spectral abundance factors. *Methods* **2006,** *40* (4), 303-11.

39. Old, W. M.; Meyer-Arendt, K.; Aveline-Wolf, L.; Pierce, K. G.; Mendoza, A.; Sevinsky, J. R.; Resing, K. A.; Ahn, N. G., Comparison of label-free methods for quantifying human proteins by shotgun proteomics. *Mol. Cell. Proteomics* **2005,** *4* (10), 1487-502.

40. Meissner, F.; Mann, M., Quantitative shotgun proteomics: considerations for a high-quality workflow in immunology. *Nat. Immunol.* **2014,** *15* (2), 112-117.

41. Zhang, Y.; Fonslow, B. R.; Shan, B.; Baek, M. C.; Yates, J. R., 3rd, Protein analysis by shotgun/bottom-up proteomics. *Chem. Rev.* **2013,** *113* (4), 2343-94.

42. Arnold, T.; Linke, D., The use of detergents to purify membrane proteins. *Curr. Protoc. Protein Sci.* **2008,** *Chapter 4*, Unit 4 8 1-4 8 30.

43. (a) Swaney, D. L.; Wenger, C. D.; Coon, J. J., The value of using multiple proteases for large-scale mass spectrometry-based proteomics. *J. Proteome Res.* **2010,** *9* (3), 1323-1329; (b) Nagaraj, N.; Wisniewski, J. R.; Geiger, T.; Cox, J.; Kircher, M.; Kelso, J.; Pääbo, S.; Mann, M., Deep proteome and transcriptome mapping of a human cancer cell line. *Mol. Syst. Biol.* **2011,** *7*, 548-548.

44. (a) Shevchenko, A.; Wilm, M.; Vorm, O.; Mann, M., Mass spectrometric sequencing of proteins silver-stained polyacrylamide gels. *Anal. Chem.* **1996,** *68* (5), 850-8; (b) Shevchenko, A.; Tomas, H.; Havlis, J.; Olsen, J. V.; Mann, M., In-gel digestion for mass spectrometric characterization of proteins and proteomes. *Nat. Protocols* **2007,** *1* (6), 2856-2860.

45. Choksawangkarn, W.; Edwards, N.; Wang, Y.; Gutierrez, P.; Fenselau, C., Comparative study of workflows optimized for in-gel, in-solution, and on-filter proteolysis in the analysis of plasma membrane proteins. *J. Proteome Res.* **2012,** *11* (5), 3030-4.

46. Glatter, T.; Ludwig, C.; Ahrné, E.; Aebersold, R.; Heck, A. J. R.; Schmidt, A., Large-scale quantitative assessment of different in-solution protein digestion protocols reveals superior cleavage efficiency of tandem Lys-C/trypsin proteolysis over trypsin digestion. *J. Proteome Res.* **2012,** *11* (11), 5145-5156.

47. Cho, W.; Stahelin, R. V., Membrane-protein interactions in cell signaling and membrane trafficking. *Annu. Rev. Biophys. Biomol. Struct.* **2005,** *34*, 119-51.

48. Wisniewski, J. R.; Zougman, A.; Nagaraj, N.; Mann, M., Universal sample preparation method for proteome analysis. *Nat. Meth.* **2009,** *6* (5), 359-362.

49. Nagaraj, N.; Lu, A.; Mann, M.; Wisniewski, J. R., Detergent-based but gel-free method allows identification of several hundred membrane proteins in single LC-MS runs. *J. Proteome Res.* **2008,** *7* (11), 5028-32.

50. Wang, H.; Chang-Wong, T.; Tang, H. Y.; Speicher, D. W., Comparison of extensive protein fractionation and repetitive LC-MS/MS analyses on depth of analysis for complex proteomes. *J. Proteome Res.* **2010,** *9* (2), 1032-40.

51. Fournier, M. L.; Gilmore, J. M.; Martin-Brown, S. A.; Washburn, M. P., Multidimensional separations-based shotgun proteomics. *Chem. Rev.* **2007,** *107* (8), 3654-86.

52. Fang, Y.; Robinson, D. P.; Foster, L. J., Quantitative analysis of proteome coverage and recovery rates for upstream fractionation methods in proteomics. *J. Proteome Res.* **2010,** *9* (4), 1902-12.

53. Wang, Y.; Yang, F.; Gritsenko, M. A.; Wang, Y.; Clauss, T.; Liu, T.; Shen, Y.; Monroe, M. E.; Lopez-Ferrer, D.; Reno, T.; Moore, R. J.; Klemke, R. L.; Camp, D. G., 2nd; Smith, R. D., Reversed-phase chromatography with multiple fraction concatenation strategy for proteome profiling of human MCF10A cells. *Proteomics* **2011,** *11* (10), 2019-26.

54. Slebos, R. J.; Brock, J. W.; Winters, N. F.; Stuart, S. R.; Martinez, M. A.; Li, M.; Chambers, M. C.; Zimmerman, L. J.; Ham, A. J.; Tabb, D. L.; Liebler, D. C., Evaluation of strong cation exchange versus isoelectric focusing of peptides for multidimensional liquid chromatography-tandem mass spectrometry. *J. Proteome Res.* **2008,** *7* (12), 5286-94.

55. (a) Han, G.; Ye, M.; Zhou, H.; Jiang, X.; Feng, S.; Jiang, X.; Tian, R.; Wan, D.; Zou, H.; Gu, J., Large-scale phosphoproteome analysis of human liver tissue by enrichment and fractionation of phosphopeptides with strong anion exchange

chromatography. *Proteomics* **2008,** *8* (7), 1346-61; (b) Edelmann, M. J., Strong cation exchange chromatography in analysis of posttranslational modifications: innovations and perspectives. *J. Biomed. Biotechnol.* **2011,** *2011*, 7.

56. McNaught, A. D.; Wilkinson, A., *IUPAC. Compendium of Chemical Terminology, 2nd ed. (the "Gold Book")*. WileyBlackwell; 2nd Revised edition edition.

57. Gritti, F.; Guiochon, G., Critical contribution of nonlinear chromatography to the understanding of retention mechanism in reversed-phase liquid chromatography. *J. Chromatogr. A* **2005,** *1099* (1-2), 1-42.

58. (a) Yang, F.; Shen, Y.; Camp, D. G.; Smith, R. D., High pH reversed-phase chromatography with fraction concatenation as an alternative to strong-cation exchange chromatography for two-dimensional proteomic analysis. *Expert Rev. Proteom.* **2012,** *9* (2), 129-134; (b) Gilar, M.; Olivova, P.; Daly, A. E.; Gebler, J. C., Two-dimensional separation of peptides using RP-RP-HPLC system with different pH in first and second separation dimensions. *J. Sep. Sci.* **2005,** *28* (14), 1694-703.

59. (a) Qiu, H.; Wang, Y., Quantitative analysis of surface plasma membrane proteins of primary and metastatic melanoma cells. *J. Proteome Res.* **2008,** *7* (5), 1904-15; (b) Xiong, L.; Wang, Y., Quantitative proteomic analysis reveals the perturbation of multiple cellular pathways in HL-60 cells induced by arsenite treatment. *J. Proteome Res.* **2010,** *9* (2), 1129-37; (c) Dong, X.; Xiao, Y.; Jiang, X.; Wang, Y., Quantitative proteomic analysis revealed lovastatin-induced perturbation of cellular pathways in HL-60 cells. *J. Proteome Res.* **2011,** *10* (12), 5463-71.

60. Schwartz, J. C.; Senko, M. W.; Syka, J. E. P., A two-dimensional quadrupole ion trap mass spectrometer. *J. Am. Soc. .Mass Spectrom.* **2002,** *13* (6), 659-669.

61. Liu, Z. Y., An introduction to hybrid ion trap/time-of-flight mass spectrometry coupled with liquid chromatography applied to drug metabolism studies. *J. Mass Spectrom.* **2012,** *47* (12), 1627-42.

62. Hu, Q.; Noll, R. J.; Li, H.; Makarov, A.; Hardman, M.; Graham Cooks, R., The Orbitrap: a new mass spectrometer. *J. Mass Spectrom.* **2005,** *40* (4), 430-43.

63. Geromanos, S. J.; Vissers, J. P.; Silva, J. C.; Dorschel, C. A.; Li, G. Z.; Gorenstein, M. V.; Bateman, R. H.; Langridge, J. I., The detection, correlation, and comparison of peptide precursor and product ions from data independent LC-MS with data dependant LC-MS/MS. *Proteomics* **2009,** *9* (6), 1683-95.

64. Doerr, A., Mass spectrometry-based targeted proteomics. *Nat. Meth.* **2013,** *10* (1), 23-23.

65. Marx, V., Targeted proteomics. *Nat. Meth.* **2013,** *10* (1), 19-22.

66. Hause, R. J.; Kim, H. D.; Leung, K. K.; Jones, R. B., Targeted protein-omic methods are bridging the gap between proteomic and hypothesis-driven protein analysis approaches. *Expert Rev. Proteomics* **2011,** *8* (5), 565-75.

67. Xiao, Y.; Guo, L.; Wang, Y., A targeted quantitative proteomics strategy for global kinome profiling of cancer cells and tissues. *Mol. Cell. Proteomics* **2014,** *13* (4), 1065-75.

68. Nakajima, N.; Ikada, Y., Mechanism of amide formation by carbodiimide for bioconjugation in aqueous media. *Bioconjugate Chem.* **1995,** *6* (1), 123-130.

69. Madler, S.; Bich, C.; Touboul, D.; Zenobi, R., Chemical cross-linking with NHS esters: a systematic study on amino acid reactivities. *J. Mass Spectrom.* **2009,** *44* (5), 694-706.

70. Patil, U. S.; Qu, H.; Caruntu, D.; O'Connor, C. J.; Sharma, A.; Cai, Y.; Tarr, M. A., Labeling primary amine groups in peptides and proteins with N-hydroxysuccinimidyl ester modified Fe3O4@SiO2 nanoparticles containing cleavable disulfide-bond linkers. *Bioconjugate Chem.* **2013,** *24* (9), 1562-1569.

71. Zara, J. J.; Wood, R. D.; Boon, P.; Kim, C. H.; Pomato, N.; Bredehorst, R.; Vogel, C. W., A carbohydrate-directed heterobifunctional cross-linking reagent for the synthesis of immunoconjugates. *Anal. Biochem.* **1991,** *194* (1), 156-62.

72. Mani, D. R.; Abbatiello, S. E.; Carr, S. A., Statistical characterization of multiple-reaction monitoring mass spectrometry (MRM-MS) assays for quantitative proteomics. *BMC bioinformatics* **2012,** *13 Suppl 16*, S9.

73. Colangelo, C. M.; Chung, L.; Bruce, C.; Cheung, K.-H., Review of software tools for design and analysis of large scale MRM proteomic datasets. *Methods (San Diego, Calif.)* **2013,** *61* (3), 287-298.

74. Boja, E. S.; Rodriguez, H., Mass spectrometry-based targeted quantitative proteomics: achieving sensitive and reproducible detection of proteins. *Proteomics* **2012,** *12* (8), 1093-110.

75. MacLean, B.; Tomazela, D. M.; Shulman, N.; Chambers, M.; Finney, G. L.; Frewen, B.; Kern, R.; Tabb, D. L.; Liebler, D. C.; MacCoss, M. J., Skyline: an open source document editor for creating and analyzing targeted proteomics experiments. *Bioinformatics* **2010,** *26* (7), 966-8.

76. (a) Xiao, Y.; Guo, L.; Jiang, X.; Wang, Y., Proteome-wide discovery and characterizations of nucleotide-binding proteins with affinity-labeled chemical probes. *Anal. Chem.* **2013,** *85* (6), 3198-206; (b) Xiao, Y.; Guo, L.; Wang, Y., Isotope-coded ATP probe for quantitative affinity profiling of ATP-binding proteins. *Anal. Chem.* **2013,** *85* (15), 7478-86.

77. Escher, C.; Reiter, L.; MacLean, B.; Ossola, R.; Herzog, F.; Chilton, J.; MacCoss, M. J.; Rinner, O., Using iRT, a normalized retention time for more targeted measurement of peptides. *Proteomics* **2012,** *12* (8), 1111-21.

78. Baczek, T.; Kaliszan, R., Predictions of peptides' retention times in reversed-phase liquid chromatography as a new supportive tool to improve protein identification in proteomics. *Proteomics* **2009,** *9* (4), 835-47.

79. Krokhin, O. V.; Craig, R.; Spicer, V.; Ens, W.; Standing, K. G.; Beavis, R. C.; Wilkins, J. A., An improved model for prediction of retention times of tryptic peptides in ion pair reversed-phase HPLC: its application to protein peptide mapping by off-line HPLC-MALDI MS. *Mol. Cell. Proteomics* **2004,** *3* (9), 908-19.

80. Shibue, M.; Mant, C. T.; Hodges, R. S., Effect of anionic ion-pairing reagent hydrophobicity on selectivity of peptide separations by reversed-phase liquid chromatography. *J. Chromatogr. A* **2005,** *1080* (1), 68-75.

81. Kiyonami, R.; Schoen, A.; Zabrouskov, V., On-the-fly retention time shift correction for multiple targeted peptide quantification by LC-MS/MS. *Thermo Fisher Scientific* **2010,** *Application Note 503*.

**Figure 1.1** Development of proteomics (adopted from Patterson, S.D., et. al., *Nat. Genet.* 2003, 33:311-323).

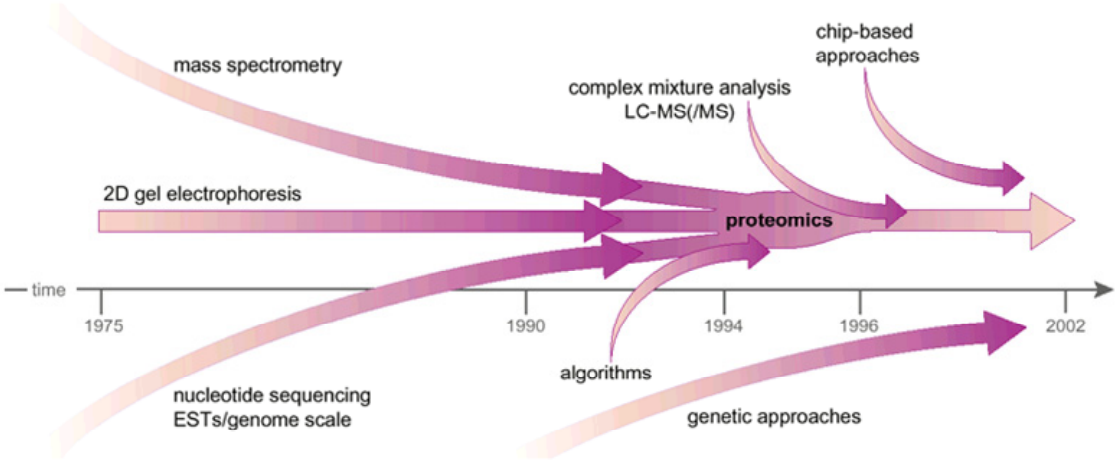

**Figure 1.2** Comparison of representative isotope labeling procedures. The blue and red asterisk indicates light and heavy stable isotope labeling, respectively.

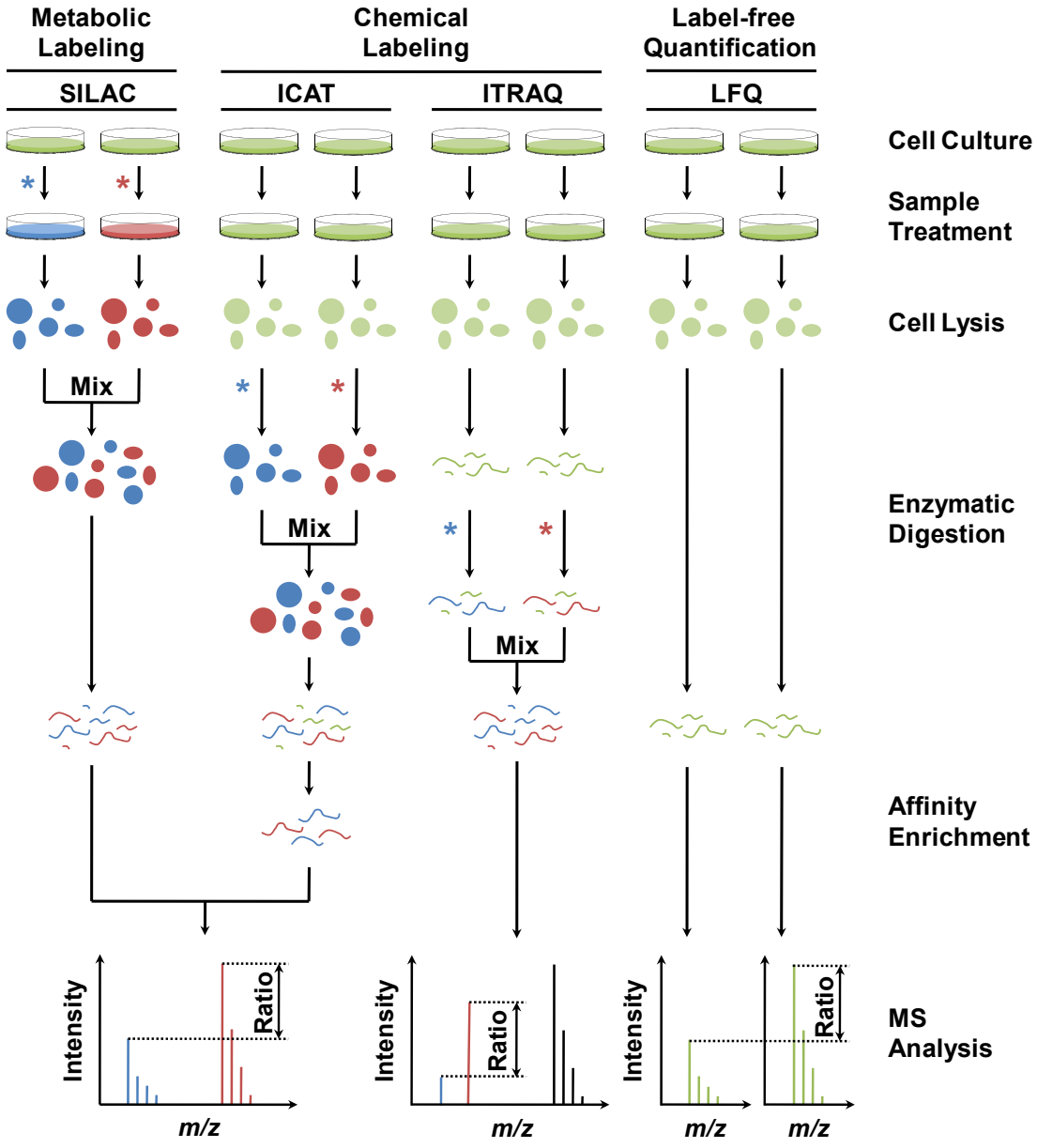

**Figure 1.3** The structures of common labeling reagents. The structures of ICAT (A) and ITRAQ (B) probes, as well as stable isotope-labeled lysine and arginine for SILAC labeling (C) (adopted from Thermo Fisher Scientific).

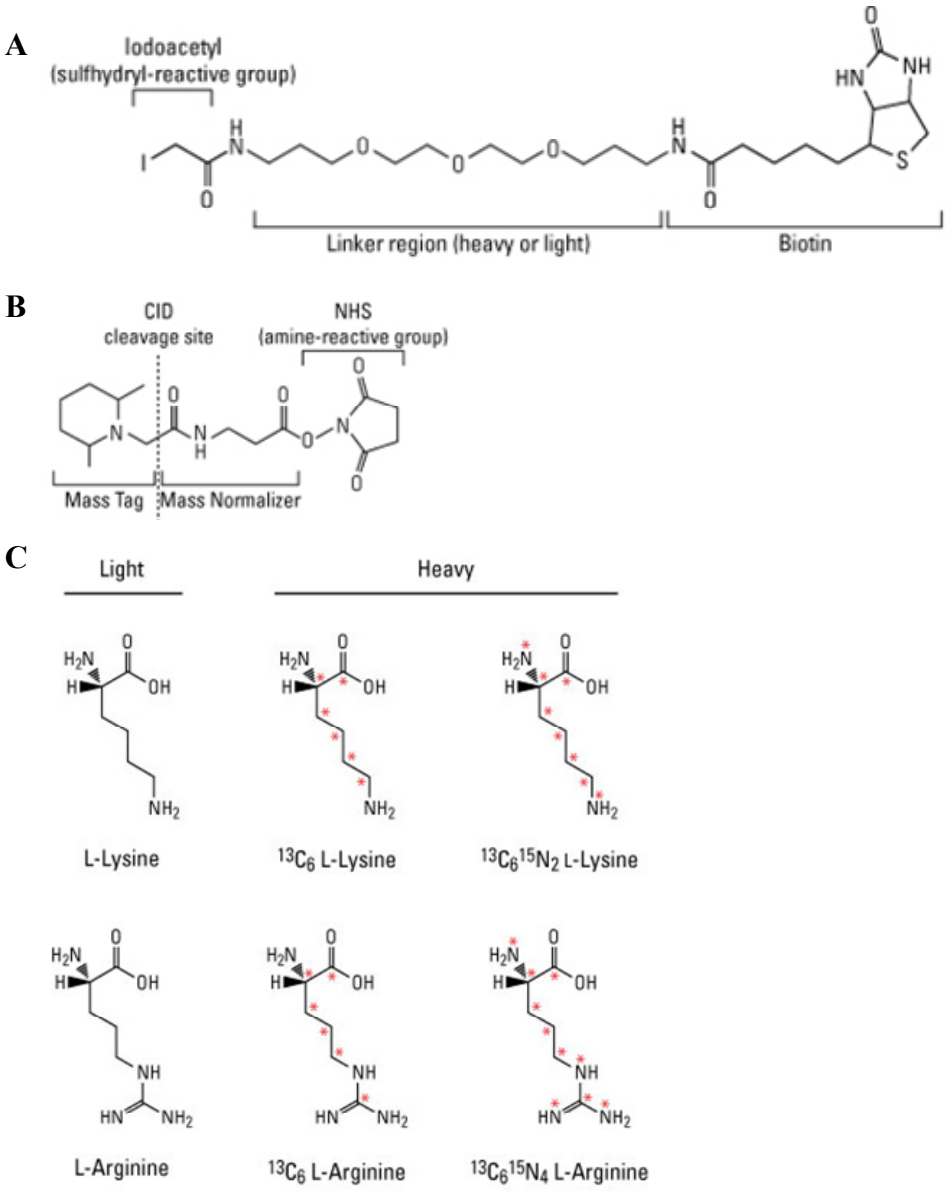

**Figure 1.4** General workflow of discovery-based proteomics studies in data-dependant acquisition mode.

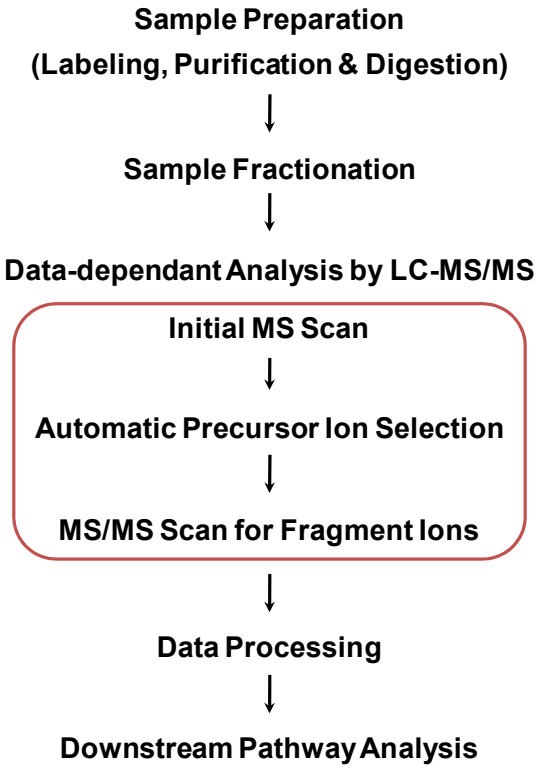

**Figure 1.5** Workflow for filter-aided sample preparation method.

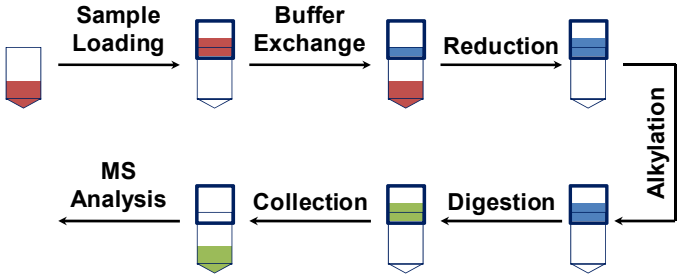

**Figure 1.6** Detection principle for data-dependant acquisition in discovery-based proteomics (adopted from Olsen, J. V., et al., *Mol. Cell. Proteomics* 2009, 8(12):2759-2769).

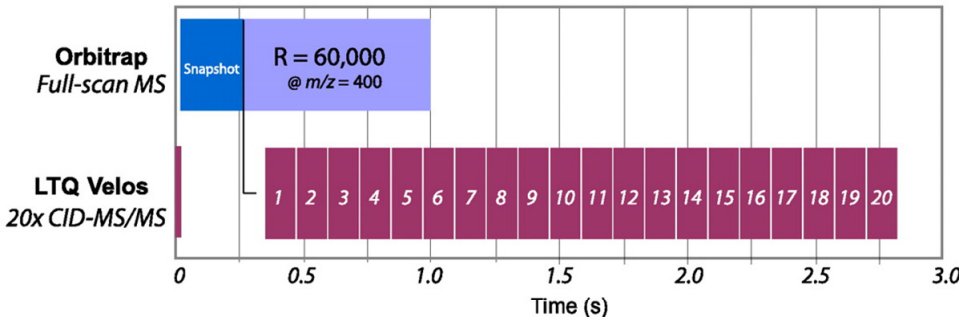

**Figure 1.7** General workflow for targeted proteomics with multiple reaction monitoring.

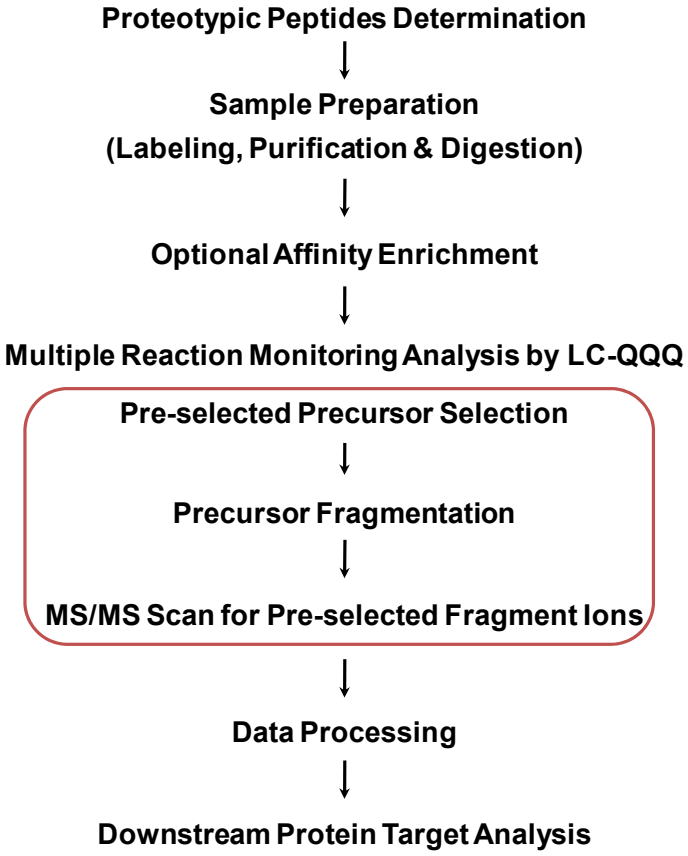

**Figure 1.8** Structures of chemical crosslinking reagents. N-hydroxysuccinimide (A), acyl phosphate (B), carbodiimide (C), and hydrazide (D) (adopted from Thermo Fisher Scientific and Xiao, Y., et al., *Anal. Chem.* 2013, 85(6):3198-3206).

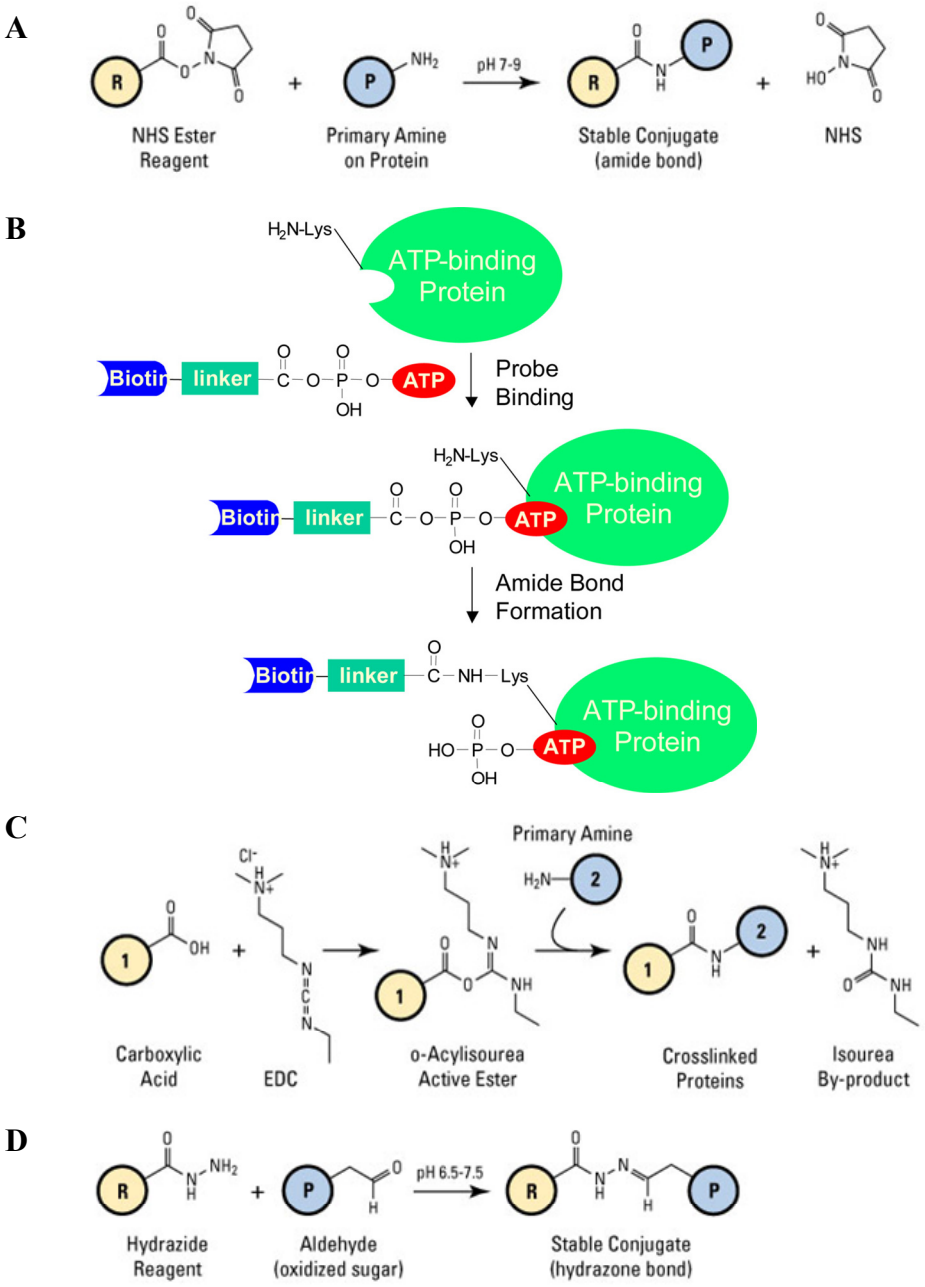

**Figure 1.9** Scheme of triple quadruple mass spectrometers (adapted from Boja, E. S., et. al., *Korean J. Lab Med.* 2011, 31(2):61-71).

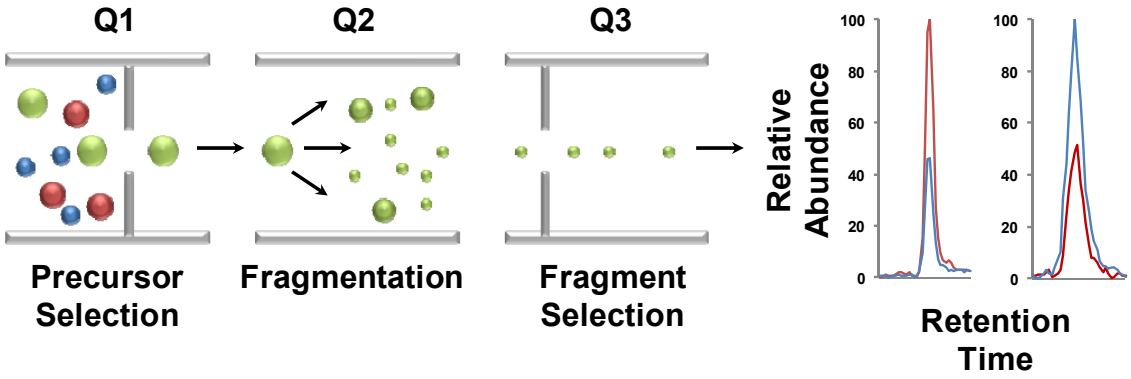

**Figure 1.10** A schematic illustration of empirical determination of iRT scale and conversion of retention times for targeted peptides into iRTs for scheduled multiple reaction monitoring.

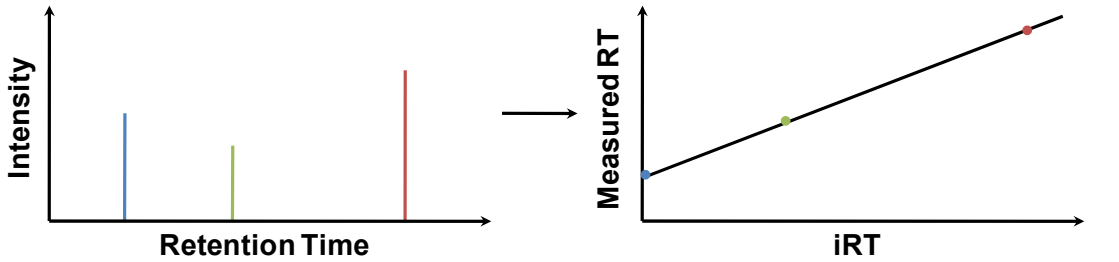

# Chapter 2

# Hexavalent Chromium-Induced Alteration of Proteomic Landscape in Human Skin Fibroblast Cells

## Introduction

Heavy metal toxication has become a leading aspect of environmental pollution over the past century. Generally speaking, heavy metals exert their cytotoxic effects mainly through imitating the action of essential elements and forming complexes or ligands with cellular components which cause malfunction and eventually death of the affected individual.[1] As a representative heavy metal, chromium is an indispensable source for metallurgical, chemical and refractory industries; however, it is also a well documented occupational and environmental health hazard.[2] Unlike other toxic heavy metals, such as lead, cadmium and arsenic, chromium toxicity depends on its oxidation state.[3] Among the different oxidation states, hexavalent chromium [Cr(VI)] is carcinogenic, although trivalent chromium [Cr(III)] in trace amounts is an essential dietary nutrient.[4] Exposure to Cr(VI) occurs primarily through inhalation, dermal contact and ingestion. Previous studies have shown that Cr(VI) species are more readily absorbed by biological systems than Cr(III), because Cr(VI) can be easily uptaken into cells through non-specific phosphate and sulfate ion transporters.[5]

Cr(VI) is an oxidizing agent, which undergoes facile reduction to yield Cr(III) in plasma and cells. This process appears to be somewhat paradoxical. On one hand, the reduction of Cr(VI) to Cr(III) is the first defense against Cr(VI) after exposure. For instance, inhaled Cr(VI) can be reduced to Cr(III) in the lower respiratory tract by the epithelial lining fluid and pulmonary alveolar macrophages, which minimizes the cellular uptake of chromium species.[6] On the other hand, Cr(VI) toxicity also arises mainly from its reduction, but this occurs intracellularly after it enters the cells. Under physiological conditions, Cr(VI) can be reduced by cellular reductants, including ascorbic acid, glutathione, and enzymes (e.g. glutathione reductase) to produce Cr(V), Cr(IV) and ultimately, Cr(III).[4] These reduction processes also generate other reactive intermediates including thiyl radicals and hydroxyl radicals.[4] The reactive oxygen species (ROS) generated during Cr(VI) reduction can modify DNA to form DNA-chromium complexes, DNA strand breaks, DNA-DNA cross-links and DNA-protein cross-links.[7] They can also attack proteins and membrane lipids resulting in the disruption of cellular integrity and functions.[8]

Although intracellular reduction of Cr(VI) is known to be important for its toxicity, more studies are needed to systematically explore the exact modes of action. DNA microarray has been used for exploring Cr(VI)-induced changes in gene expression by providing a quantitative measurement of gene transcription.[9] However, microarray analysis can only assess the elevated or depressed mRNA expression levels and it provides little information about changes in protein expression, considering that protein

expression is also affected by translational regulation and, more importantly, protein turnover.[10]

Recent advances in mass spectrometry instrumentation with improved mass accuracy and resolution render it possible to conduct rapid and high-throughput identification and quantification of proteins at the entire proteome scale.[11] Here we utilized a mass spectrometry-based quantitative proteomic technique using stable isotope labeling by amino acids in cell culture (SILAC)[12] to elucidate the cellular mechanisms targeted by Cr(VI) via interrogating the toxicant-induced perturbation of the whole proteome. With this method, we were able to quantify a total of 4607 unique proteins, among which 270 and 127 were significantly up- and down-regulated, respectively. Importantly, our study revealed that, apart from several other cellular pathways, Cr(VI) induced up-regulation of many enzymes involved in cholesterol biosynthesis. This unprecedented finding, confirmed by follow-up studies, allowed us to unveil that Cr(VI) may exert its cytotoxic effect, at least in part, by stimulating cholesterol biosynthesis.

## Materials and methods

### Cell culture

All reagents unless otherwise noted were purchased from Sigma-Aldrich (St. Louis, MO) and all culture medium unless otherwise stated were from ATCC (Manassas, VA). GM00637 and HCT-116 cells were generously provided by Profs. Gerd P. Pfeifer (the City of Hope) and Frances Sladek (University of California Riverside), respectively. HEK293T cells were obtained from ATCC. Control GM00637 and HEK293T cells were cultured in Dulbecco's Modified Eagle's Medium (DMEM, ATCC) supplemented with 10% fetal bovine serum (FBS, Invitrogen, Carlsbad, CA) and 100 IU/ml penicillin (ATCC). HCT-116 cells were cultured under the same conditions except that McCoy's 5a medium (ATCC) was used. Cells were maintained in a humidified atmosphere with 5% $CO_2$ at 37°C, with medium renewal at every 1-2 days depending on cell densities. MTT assay was performed using a kit from Roche (Basel, Switzerland) and absorbance reading was taken using a Victor 2 plate reader (Perkin Elmer, Waltham, MA, Figure 2.1).

DMEM medium without lysine or arginine (DMEM minus L-lysine and L-arginine) was purchased from Cambridge Isotope Laboratories (Andover, MA). The complete light and heavy DMEM medium were prepared by adding light or heavy ($[^{13}C_6, ^{15}N_2]$-L-lysine and $[^{13}C_6]$-L-arginine, Sigma) lysine and arginine to the above medium at amounts according to ATCC formulation. Cells were cultured in light or heavy DMEM medium containing dialyzed FBS (Invitrogen, Grand Island, NY) for at

least 10 days (more than 5 cell doublings) to ensure complete stable isotope incorporation.

**Potassium dichromate treatment and sample preparation**

GM00637 cells, at a density of ~ $5\times10^5$ cells/mL in light or heavy DMEM medium, were treated with 0.5 μM $K_2Cr_2O_7$ for 24 hrs. The cells were subsequently harvested by centrifugation at 300 g at 4°C for 5 min, washed for three times with ice-cold phosphate-buffered saline (PBS), and lysed with 2% SDS solution on ice with vortexing every other 5 min for a total of 30 min. The mixture was subsequently boiled for 5 min. The resulting cell lysate was centrifuged at 16,000 g at 4°C for 5 min and supernatant collected. The protein concentration in the cell lysate was measured using Bicinchoninic Acid Kit for Protein Determination (Sigma). In forward SILAC, the lysate of light labeled, $K_2Cr_2O_7$-treated cells and that of the heavy labeled, control cells were combined at 1:1 ratio (w/w), whereas the heavy labeled, $K_2Cr_2O_7$-treated cell lysate was mixed equally with the light labeled, control lysate in the reverse SILAC experiment (Figure 2.2A).

**SDS-PAGE separation and in-gel digestion**

The above equi-mass mixture of light and heavy lysates were denatured by heating to 95°C in Laemmli loading buffer and then separated on a 12% SDS-PAGE gel with a 4% stacking gel. The resulting gel was stained with Coomassie blue and equally cut into 20 slices. The proteins in each individual gel slices were reduced in-gel with dithiothreitol (DTT) and alkylated with iodoacetamide (IAA). The processed proteins were subsequently digested with trypsin (Promega, Madison, WI) at 37°C overnight.

Subsequently, peptides were extracted from gels with a solution containing 5% acetic acid in $H_2O$ and then $CH_3CN/H_2O$ (1:1, v/v).

**Desalting and purification**

The protein digests were desalted and purified using OMIX $C_{18}$ pipette tips (Agilent, Santa Clara, CA). Formic acid was added to the peptide samples until the solution pH reached ~4. The OMIX tips were hydrated in $CH_3CN/H_2O$ (1:1, v/v) and solvent discarded, followed by equilibration with 0.1% formic acid. Thereafter, pre-treated samples were aspirated and dispensed into OMIX tip. After rinsing the tip with 0.1% formic acid, bound peptides were eluted with $CH_3CN/H_2O$ (1:1, v/v). The resulting peptide solution was dried in SpeedVac concentrator and stored at −80°C until further analysis.

**LC-MS/MS for protein identification and quantification**

On-line LC-MS/MS analyses were conducted on an LTQ-Orbitrap Velos mass spectrometer equipped with a nanoelectrospray ionization source and coupled with an EASY n-LCII HPLC system (Thermo, San Jose, CA). HPLC separation was carried out automatically using a homemade trapping column (150 μm×50 mm) and a separation column (75 μm×200 mm, packed with ReproSil-Pur C18-AQ resin, 3 μm in particle size and 100 Å in pore size, Dr. Maisch HPLC GmbH, Germany). Initially, the peptide mixture was loaded onto the trapping column with a mobile phase of 0.1% formic acid in $H_2O$ at a flow rate of 3.0 μL/min. The peptides were then separated using a 120-min linear gradient of 2-40% $CH_3CN$ in 0.1% formic acid at a flow rate of 230 nL/min. The LTQ-Orbitrap Velos mass spectrometer was operated in the positive-ion mode, and the

spray voltage was set at 1.8 kV. All MS/MS spectra were acquired in a data-dependent scan mode, where one full-scan MS was followed with twenty MS/MS scans. The full-scan MS spectra (from *m/z* 350 to 2000) were acquired with a resolution of 60,000 at *m/z* 400 after accumulation to a target value of 500,000. The twenty most abundant ions detected in MS at a threshold above 500 counts were selected for further fragmentation by collision-induced dissociation at a normalized collision energy of 35%.

**Data processing**

The identification and quantification of global proteome were achieved by searching the LC-MS/MS data using Maxquant[13], Version 1.2.2.5 against the International Protein Index database, version 3.68 with 87,083 entries to which contaminants and reverse sequences were added. The maximum number of miss-cleavages for trypsin was set at two per peptide. Cysteine carbamidomethylation and methionine oxidation were included as fixed and variable modifications, respectively. The search was performed with the tolerances in mass accuracy of 10 ppm and 0.6 Da for MS and MS/MS, respectively. In addition, only proteins with at least two distinct peptides being discovered from LC-MS/MS analysis were considered reliably identified.

The normalized protein expression ratio reported in the present study was determined by Maxquant, with the assumption that the expression levels of the majority of proteins remained unchanged upon $K_2Cr_2O_7$ treatment. The required false positive rate was set to be 1% at both peptide and protein levels. The minimal required peptide length was set at six amino acids. The quantification was based on three independent SILAC and LC-MS/MS experiments, which included one forward and two reverse SILAC

labelings. The threshold of significant protein expression changes was determined by the corresponding significant A value for every protein ratio using Perseus 4.0 (Figure 2.3).[13] Only those proteins with alteration in expression levels being greater than 1.36 or less than 0.742 fold, as revealed by SILAC labeling experiments, were considered significantly changed. Subsequent pathway and GO analysis of significantly altered proteins was conducted using Gene Map Annotator and Pathway Profiler (GenMAPP-CS).[14]

**RNA extraction and quantitative real-time PCR analysis**

Total RNA was extracted using the RNeasy Mini Kit (QIAGEN, Valencia, CA) and reverse transcribed by employing M-MLV reverse transcriptase (Promega, Madison, WI) and a poly(dT) primer. Quantitative real-time PCR was performed with iQ SYBR Green Supermix kit (Bio-Rad, Hercules, CA) on a Bio-Rad MyiQ thermal cycler, and gene-specific primers are listed in Table 2.1. The comparative cycle threshold (*Ct*) method (*ΔΔCt*) was utilized for the relative quantification of gene expression level,[15] and *GAPDH* gene was used as internal control. The mRNA level of each gene was normalized to that of the internal control.

**Extraction and determination of the cellular cholesterol level**

Cells were collected and washed for 3 times with ice-cold PBS and extracted with chloroform:methanol:water (2:1.1:0.9, v/v/v), following previously published procedures.[16] The bottom chloroform layer was then washed three times with a methanol-water mixture (5:4, v/v), collected, and solvent removed using a SpeedVac. The cholesterol level was measured using HPLC as recently described.[17] Cholesterol

amount was normalized against the total protein content determined by the Bradford Assay (Bio-Rad).

## Results and discussion

### 1. Potassium dichromate treatment, protein identification, and quantification

It is generally believed that intracellular reduction of Cr(VI) to Cr(III) can give rise to ROS, which are capable of inducing DNA damage and triggering inflammatory response. However, it remains possible that Cr(VI) also exerts its cytotoxic effects by altering other cellular pathways. To explore this, we set out to employ an unbiased quantitative proteomic approach to assess the Cr(VI)-induced perturbation of the entire proteome of GM00637 human skin fibroblast cells. We first determined the optimal dose of $K_2Cr_2O_7$ by examining the dose-dependent survival rate of GM00637 cells. On the basis of MTT assay, we observed a less than 7% cell death after a 24-hr treatment with 0.5 μM $K_2Cr_2O_7$, whereas a significant reduction in cell viability (by ~30%) was induced by a 24-hr treatment with 2 μM $K_2Cr_2O_7$ (Figure 2.1). Thus, 0.5 μM $K_2Cr_2O_7$ was selected for the subsequent experiments to minimize the apoptosis-induced alteration in protein expression.

GM00637 cells were cultured in light or heavy medium for more than 5 cell doublings. After treatment with 0.5 μM $K_2Cr_2O_7$ for 24 hrs, the cells were lysed, and the lysates combined and subsequently fractionated with SDS-PAGE. After in-gel digestion, the proteins were identified and quantified using LC-MS/MS. To obtain reliable quantification results, we conducted SILAC experiments in triplicate, with one set of forward and two sets of reverse labelings (Figure 2.2A).

Protein identification and quantification were achieved by searching the mass spectrometric data using MaxQuant. Figure 2.4 depicts the representative LC-MS/MS

results of the peptide CIGHPEEFYNIVR from squalene synthase. The MS results, for both the forward and reverse SILAC labeling samples, revealed the significantly higher level of this peptide in $K_2Cr_2O_7$-treated cells than in control cells (Figure 2.4A and B), supporting the increased expression of the protein from which the peptide was derived. In addition, the MS/MS results supported unambiguously the identification of this peptide (Figure 2.4C and D).

The LC-MS and MS/MS results from the three SILAC labeling experiments enabled us to identify 5469 proteins, among which 4607 were quantified. Of these proteins, 2784, 798, and 933 could be quantified in all three SILAC labeling experiments, only in two labeling experiments, and only in one labeling experiment, respectively (Figure 2.2B).

**2. Pathway and GO analysis for significantly changed proteins upon potassium dichromate treatment**

The distribution of the changes in protein expression levels induced by $K_2Cr_2O_7$ treatment is shown in Figure 2.2C. The majority of the 4607 quantified proteins did not display significant alterations in expression levels. To screen for significantly changed proteins, we first used Perseus to calculate the significant A value for each protein ratio. As shown in Figure 2.3, the chart is plotted by significant A versus $\log_{10}$(Ratio). Proteins with significant A values of $< 0.05$ were considered significantly changed. By using this criterion, proteins exhibiting changes that are greater than 1.360- or less than 0.742-fold are considered significantly altered upon $K_2Cr_2O_7$ treatment, and a total of 270 and 127 proteins were significantly up- and down-regulated, respectively.

All significantly changed proteins were included for pathway analysis using GenMAPP. Among the perturbed pathways identified, only one was down-regulated and the rest up-regulated. We also used GenMAPP to analyze our data from the perspective of GO annotation, such as biological process, cellular component and molecular function (Tables 2.3 and 2.4). From the GenMAPP analysis results, we chose the top five significant pathways based on their importance and Z scores (Tables 2.3 and 2.4). Next we discuss further several pathways that are altered by Cr(VI) exposure.

**3. Potassium dichromate-induced perturbation of cholesterol biosynthesis**

GenMAPP pathway and GO analysis demonstrated that the cholesterol biosynthesis pathway was significantly perturbed following Cr(VI) exposure (Figure 2.5). In this vein, we were able to quantify 16 enzymes involved in the cholesterol biosynthesis pathway, 13 of which were significantly up-regulated (by 1.4-4.2 fold, Figure 2.5). Additionally, the level of low-density lipoprotein receptor, which mediates the cellular uptake of LDL cholesterol,[18] is also up-regulated by 3.2 fold.

Sterol regulatory element binding proteins (SREBPs) are the major known transcription factors responsible for regulating the above-mentioned enzymes associated with cholesterol biosynthesis.[19] Upon proteolytic maturation, the N-terminal domain of SREBPs is released and translocated to the nucleus, where it binds the promoter/enhancer regions of genes, like *HMGCS1* and *HMGCR*, involved in cholesterol biosynthesis and initiates their transcription.[20] To assess whether the up-regulation of the cholesterol biosynthesis enzymes occurred at the transcriptional level through SREBP activation, we performed qRT-PCR analysis of several key SREBP target genes, some of which are

involved in cholesterol biosynthesis. Our results revealed that the relative mRNA expression levels of all five genes tested (*HMGCS1*, *HMGCR*, *FDPS*, *FDFT1* and *DHCR7*) were significantly increased (by 1.5-3.5 fold, Figure 2.6A), supporting that the elevated expression of these enzymes at protein levels occurs mainly through a transcriptional mechanism via SREBP activation.

Previous studies suggested that oxidative stress could result in increased expression or enhanced activity of SREBPs. In this vein, Waris et al.[21] observed that viral infection-induced oxidative stress could stimulate the activation of SREBPs thereby augmenting cholesterol biosynthesis. These authors further demonstrated that oxidative stress induced by hepatitis C virus infection results in the activation of phosphatidylinositol 3-kinase-Akt (PI3K-Akt) pathway, which subsequently transactivates SREBPs.[21] Our quantitative proteomic data unveiled that phosphatidylinositol 3-kinase 85 kDa regulatory subunit beta and protein kinase B (Akt) were up-regulated by 1.52 and 1.49 fold, respectively (Table 2.2). Therefore, the Cr(VI)-induced up-regulation of enzymes involved in cholesterol biosynthesis likely arises from the Cr(VI)-induced oxidative stress, the subsequent activation of the PI3K-Akt pathway and the ensuing activation of SREBPs.

**4. Cr(VI) led to increased intracellular cholesterol level and Cr(VI)-induced inhibition of cell proliferation could be rescued by lovastatin**

Considering that a large number of enzymes involved in cholesterol biosynthesis were up-regulated, we reason that Cr(VI) may induce elevated cellular cholesterol production. To test this, we measured the cholesterol levels in GM00637 human skin

fibroblast, HEK293T human embryonic kidney epithelial cells, and HCT-116 human colon carcinoma cells with and without $K_2Cr_2O_7$ treatment. Our results showed that a 24-hr treatment with 0.5 μM $K_2Cr_2O_7$ led to statistically significant increase of the cellular cholesterol content (by 1.3-2.0 fold) in these three cell lines (Figure 2.6B). These results are in line with the Cr(VI)-induced up-regulation of enzymes involved in cholesterol biosynthesis, as revealed by quantitative proteomic experiment. Together, the above findings demonstrated that Cr(VI) stimulates endogenous cholesterol biosynthesis.

Cholesterol is an essential component for mammalian cell membrane and is required for proper membrane permeability, fluidity, protein function and organelle identity.[22] During cholesterol biosynthesis, a series of metabolites are produced and utilized in membrane assembly, cell signaling, protein synthesis and cell-cycle progression.[23] However, unregulated, especially high cholesterol level is known to be associated with cardiovascular disease and cancer promotion.[24]

We reasoned that the elevated production of cellular cholesterol may be one of the major factors contributing to the toxic effects of Cr(VI). To explore this possibility, we assessed the Cr(VI)-induced perturbation of cell growth and examined whether such perturbation can be rescued by a cholesterol-lowering drug. Thus, we used lovastatin to inhibit HMG-CoA reductase (*HMGCR*), which is a rate-limiting enzyme in cholesterol biosynthesis.[25] It turned out that exposure to Cr(VI) resulted in pronounced growth inhibition of GM00637 and HEK293T cells and this inhibition could indeed be rescued by the addition of lovastastin (Figure 2.7A and B). Along this line, the cellular cholesterol returned to a level that is similar to that of control cells after a 24-hr co-

treatment with 0.5 μM Cr(VI) and 1 μM lovastatin (Figure 2.7C). These results demonstrated that the Cr(VI)-induced growth inhibition of GM00637 and HEK293T cells could be mainly attributed to the elevated expression of enzymes involved in the cholesterol biosynthesis and the resultant over-production of endogenous cholesterol.

**5. Elevated G protein signaling pathway upon potassium dichromate treatment**

Pathway analysis also revealed that the guanine nucleotide binding protein (G proteins) signaling pathway is significantly up-regulated upon Cr(VI) treatment. G protein signaling is a pivotal transmembrane signaling pathway which is responsible for regulating a myriad of physiological responses.[26] Briefly, G protein signaling pathway starts with the activation of G protein-coupled receptors (GPCRs) through binding of extracellular signaling molecules. GPCR activation may trigger a multiple of downstream signal transduction pathways mediated by their membrane-bound partners, the G proteins.[27] One is through the activation of $G\alpha_s$ subunit, which triggers the activation of adenylate cyclase (AC) to produce cyclic-adenosine monophosphate (cAMP) and eventually the activation of the transcription factor of cAMP-responsive element-binding protein (CREBP). Another G protein, $G\alpha_q$, regulates the activity of its downstream effector phospholipase C-β, which is responsible for catalyzing the cleavage of phosphatidylinositol 4,5-bisphosphate into the second messengers inositol 1,4,5-trisphosphate (IP3) and diacylglycerol (DAG), thereby giving rise to protein kinase C (PKC) activation.[28] Along this line, our quantitative proteomic data showed that several proteins involved in the G protein signaling pathway, including CREBP1, PKC, and

mitogen-activated protein kinase 3, were significantly up-regulated by 1.43, 1.96 and 1.40 fold, respectively (Table 2.2).

Elevated GPCRs and relevant G protein signaling pathways after Cr(VI) treatment may result in malfunction of cells and promote aberrant cell proliferation through the crosstalk between GPCRs and growth factor receptors.[27] Thus, the stimulation of diverse downstream signal transduction pathways may lead to changes in gene expression, cell migration and proliferation, and ultimately, cancer progression.[28]

**6. Potassium dichromate-induced alteration of inflammatory response pathways and inhibition of selenoprotein expression**

Pathway analysis also showed that inflammatory response and interleukin 5 (IL-5) signaling pathways were up-regulated after Cr(VI) exposure (Table 2.3). Our quantitative proteomic results revealed the increased expression of several collagen proteins as well as kinases involved in IL-5 signaling. In the latter respect, the aforementioned phosphatidylinositol 3-kinase 85 kDa regulatory subunit beta and protein kinase B (Akt), as well as Janus kinase 1, mitogen-activated protein kinase 3, and protein kinase C beta were all up-regulated following $K_2Cr_2O_7$ treatment (Table 2.2). This finding is in accordance with a previous study demonstrating that Cr(VI) could activate the Akt, NF-κB and MAPK pathways in kerotinocytes, which is accompanied with the increased production of cytokines, including tumor necrosis factor-α (TNF-α) and IL-1α.[29] ROS are known to activate transcription factors, such as NF-κB and AP-1, which are responsible for regulating the expression levels of numerous inflammatory pathway

genes.[30] Thus, the Cr(VI)-induced activation of inflammatory response may reflect cellular ROS generation arising from Cr(VI) reduction.

GenMAPP analysis also revealed the down-regulation of two selenoproteins, i.e., 15kDa selenoprotein (Sep15, by 0.56 fold) and selenoprotein S (Sep S, by 0.59 fold, Table 2.2). Along this line, previous studies showed that exposure to silver nanoparticles or monomethylarsonous acid could lead to inhibition of selenoprotein synthesis.[31] Selenoproteins function to protect cells from oxidative damage and apoptosis by preventing the deleterious consequences of accumulation of misfolded proteins that has been linked to immune and inflammatory processes.[32] Thus, diminished expression of these two selenoproteins may exaggerate the cellular inflammatory response with increased release of cytokines like tumor necrosis factor-α (TNF-α) after Cr(VI) treatment.[33]

## Conclusions

Cr(VI) is a major heavy metal pollutant that is responsible for inducing different types of cancers among exposed population.[3] By using SILAC combined with LC-MS/MS analysis, we were able to achieve a quantitative assessment of the $K_2Cr_2O_7$-induced perturbation of the proteome of GM00637 cells. The quantitative information facilitated us to elucidate the mechanisms through which Cr(VI) exerts its deleterious effect. In the present study, we were able to identify 5469 proteins, with 4607 quantified from three sets of SILAC experiments. Among them, 270 and 127 proteins were significantly up- and down-regulated, respectively, upon a 24-hr treatment with 0.5 μM $K_2Cr_2O_7$. Particularly, we demonstrated, for the first time, that Cr(VI) may exert its cytotoxic effect, at least in part, through elevating endogenous cholesterol biosynthesis. Additionally, the stimulation of inflammatory response and GPCR signaling pathways, as well as the suppression of selenoproteins may also contribute to the cytotoxic effects of Cr(VI). The novel insight into the cytotoxicity of Cr(VI) provides the basis for the future development of effective approaches for the therapeutic intervention following Cr(VI) exposure.

**References**


1. Shanker, A. K., Mode of Action and Toxicity of Trace Elements. In *Trace Elements as Contaminants and Nutrients*, John Wiley & Sons, Inc.: 2008; pp 523-553.

2. WHO, Chromium (Environmental Health Criteria 61). *International Programme on Chemical Safety* **1990,** *Geneva, Switzerland*.

3. ATSDR, Toxicological Profile for Chromium. **2012**.

4. Ding, M.; Shi, X., Molecular mechanisms of Cr(VI)-induced carcinogenesis. *Mol. Cell. Biochem.* **2002,** *234-235* (1-2), 293-300.

5. Kerger, B. D.; Paustenbach, D. J.; Corbett, G. E.; Finley, B. L., Absorption and elimination of trivalent and hexavalent chromium in humans following ingestion of a bolus dose in drinking water. *Toxicol. Appl. Pharmacol.* **1996,** *141* (1), 145-58.

6. Dayan, A. D.; Paine, A. J., Mechanisms of chromium toxicity, carcinogenicity and allergenicity: review of the literature from 1985 to 2000. *Hum. Exp. Toxicol.* **2001,** *20* (9), 439-51.

7. Wise, S. S.; Holmes, A. L.; Wise, J. P., Sr., Hexavalent chromium-induced DNA damage and repair mechanisms. *Rev. Environ. Health* **2008,** *23* (1), 39-57.

8. De Mattia, G.; Bravi, M. C.; Laurenti, O.; De Luca, O.; Palmeri, A.; Sabatucci, A.; Mendico, G.; Ghiselli, A., Impairment of cell and plasma redox state in subjects professionally exposed to chromium. *Am. J. Ind. Med.* **2004,** *46* (2), 120-5.

9. Ye, J.; Shi, X., Gene expression profile in response to chromium-induced cell stress in A549 cells. *Mol. Cell. Biochem.* **2001,** *222* (1-2), 189-97.

10. Izzotti, A.; Bagnasco, M.; Cartiglia, C.; Longobardi, M.; De Flora, S., Proteomic analysis as related to transcriptome data in the lung of chromium(VI)-treated rats. *Int. J. Oncol.* **2004,** *24* (6), 1513-22.

11. Aebersold, R.; Mann, M., Mass spectrometry-based proteomics. *Nature* **2003,** *422* (6928), 198-207.

12. Ong, S.-E.; Blagoev, B.; Kratchmarova, I.; Kristensen, D. B.; Steen, H.; Pandey, A.; Mann, M., Stable Isotope Labeling by Amino Acids in Cell Culture, SILAC, as a Simple and Accurate Approach to Expression Proteomics. *Mol. Cell. Proteomics* **2002,** *1* (5), 376-386.

13. Cox, J.; Mann, M., MaxQuant enables high peptide identification rates, individualized p.p.b.-range mass accuracies and proteome-wide protein quantification. *Nat. Biotechnol.* **2008,** *26* (12), 1367-1372.

14. Salomonis, N.; Hanspers, K.; Zambon, A.; Vranizan, K.; Lawlor, S.; Dahlquist, K.; Doniger, S.; Stuart, J.; Conklin, B.; Pico, A., GenMAPP 2: new features and resources for pathway analysis. *BMC Bioinformatics* **2007,** *8* (1), 217.

15. Livak, K. J.; Schmittgen, T. D., Analysis of relative gene expression data using real-time quantitative PCR and the 2(-ΔΔCt) Method. *Methods* **2001,** *25* (4), 402-8.

16. Osada, K.; Ravandi, A.; Kuksis, A., Rapid analysis of oxidized cholesterol derivatives by high-performance liquid chromatography combined with diode-array ultraviolet and evaporative laser light-scattering detection. *J. Am. Oil Chem. Soc.* **1999,** *76* (7), 863-871.

17. Dong, X.; Xiong, L.; Jiang, X.; Wang, Y., Quantitative proteomic analysis reveals the perturbation of multiple cellular pathways in jurkat-T cells induced by doxorubicin. *J. Proteome. Res.* **2010,** *9* (11), 5943-51.

18. Defesche, J. C., Low-density lipoprotein receptor--its structure, function, and mutations. *Semin. Vasc. Med.* **2004,** *4* (1), 5-11.

19. Brown, M. S.; Goldstein, J. L., A proteolytic pathway that controls the cholesterol content of membranes, cells, and blood. *Proc. Natl. Acad. Sci. USA* **1999,** *96* (20), 11041-8.

20. Horton, J. D.; Goldstein, J. L.; Brown, M. S., SREBPs: activators of the complete program of cholesterol and fatty acid synthesis in the liver. *J. Clin. Invest.* **2002,** *109* (9), 1125-31.

21. Waris, G.; Felmlee, D. J.; Negro, F.; Siddiqui, A., Hepatitis C virus induces proteolytic cleavage of sterol regulatory element binding proteins and stimulates their phosphorylation via oxidative stress. *J. Virol.* **2007,** *81* (15), 8122-30.

22. Alberts B, J. A., Lewis J, et al., *Molecular Biology of the Cell. 4th edition.* New York: Garland Science: 2002.

23. Herold, G.; Jungwirth, R.; Rogler, G.; Geerling, I.; Stange, E. F., Influence of cholesterol supply on cell growth and differentiation in cultured enterocytes (CaCo-2). *Digestion* **1995,** *56* (1), 57-66.

24. Tete, S.; Nicoletti, M.; Saggini, A.; Maccauro, G.; Rosati, M.; Conti, F.; Cianchetti, E.; Tripodi, D.; Toniato, E.; Fulcheri, M.; Salini, V.; Caraffa, A.; Antinolfi, P.; Frydas, S.; Pandolfi, F.; Conti, P.; Potalivo, G.; Theoharides, T. C., Nutrition and cancer prevention. *Int. J. Immunopathol. Pharmacol.* **2012,** *25* (3), 573-81.

25. Wong, W. W.; Dimitroulakos, J.; Minden, M. D.; Penn, L. Z., HMG-CoA reductase inhibitors and the malignant cell: the statin family of drugs as triggers of tumor-specific apoptosis. *Leukemia* **2002,** *16* (4), 508-19.

26. Venkatakrishnan, A. J.; Deupi, X.; Lebon, G.; Tate, C. G.; Schertler, G. F.; Babu, M. M., Molecular signatures of G-protein-coupled receptors. *Nature* **2013,** *494* (7436), 185-94.

27. Lappano, R.; Maggiolini, M., G protein-coupled receptors: novel targets for drug discovery in cancer. *Nat. Rev. Drug Discov.* **2011,** *10* (1), 47-60.

28. Dorsam, R. T.; Gutkind, J. S., G-protein-coupled receptors and cancer. *Nat. Rev. Cancer* **2007,** *7* (2), 79-94.

29. Wang, B. J.; Sheu, H. M.; Guo, Y. L.; Lee, Y. H.; Lai, C. S.; Pan, M. H.; Wang, Y. J., Hexavalent chromium induced ROS formation, Akt, NF-kappaB, and MAPK activation, and TNF-alpha and IL-1alpha production in keratinocytes. *Toxicol. Lett.* **2010,** *198* (2), 216-24.

30. (a) Bubici, C.; Papa, S.; Dean, K.; Franzoso, G., Mutual cross-talk between reactive oxygen species and nuclear factor-kappa B: molecular basis and biological significance. *Oncogene* **2006,** *25* (51), 6731-48; (b) Reuter, S.; Gupta, S. C.; Chaturvedi, M. M.; Aggarwal, B. B., Oxidative stress, inflammation, and cancer: how are they linked? *Free radical biology & medicine* **2010,** *49* (11), 1603-16.

31. (a) Meno, S. R.; Nelson, R.; Hintze, K. J.; Self, W. T., Exposure to monomethylarsonous acid (MMAIII) leads to altered selenoprotein synthesis in a primary human lung cell model. *Toxicol. Appl. Pharmacol.* **2009,** *239* (2), 130-136; (b) Srivastava, M.; Singh, S.; Self, W. T., Exposure to silver nanoparticles inhibits selenoprotein synthesis and the activity of thioredoxin reductase. *Environ. Health Persp.* **2012,** *120* (1), 56-61.

32. Lu, J.; Holmgren, A., Selenoproteins. *J. Biol. Chem.* **2009,** *284* (2), 723-7.

33. Huang, Z.; Rose, A. H.; Hoffmann, P. R., The role of selenium in inflammation and immunity: from molecular mechanisms to therapeutic opportunities. *Antioxid. Redox. Signal.* **2012,** *16* (7), 705-43.

**Figure 2.1** Cell viability test with MTT assay of GM00637 cells after 24 hrs of treatment with 0, 0.125, 0.5, 1, 2 µM potassium dichromate.

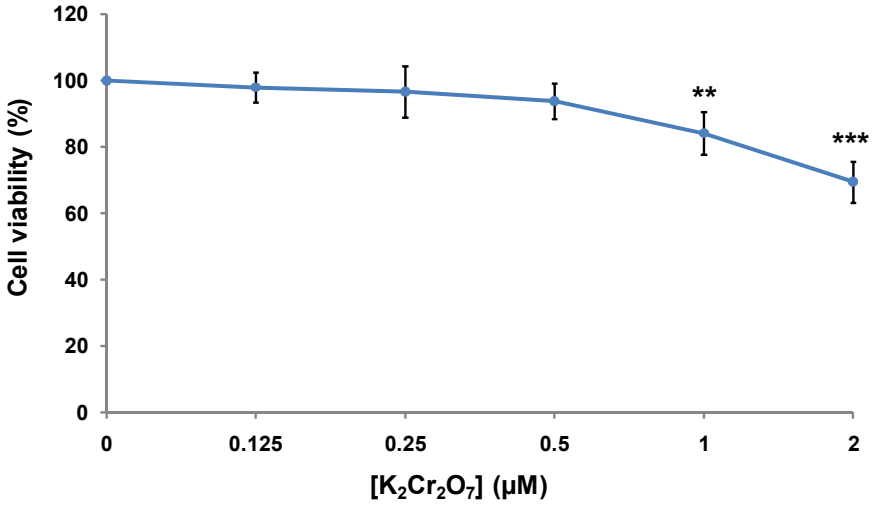

**Figure 2.2** An SILAC-based quantitative proteomics approach to reveal the potassium dichromate-induced perturbation of global protein expression. (A) A flowchart illustrating forward SILAC combined with LC-MS/MS for the comparative analysis of protein expression in GM00637 cells upon potassium dichromate treatment. (B) A summary of the number of proteins quantified from three independent SILAC experiments. (C) The distribution of expression ratios (treated/untreated) for proteins that were quantified in at least one set of SILAC experiment.

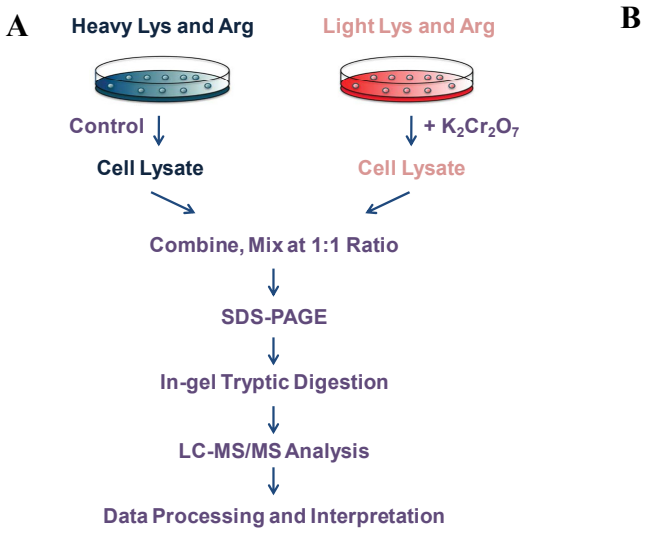


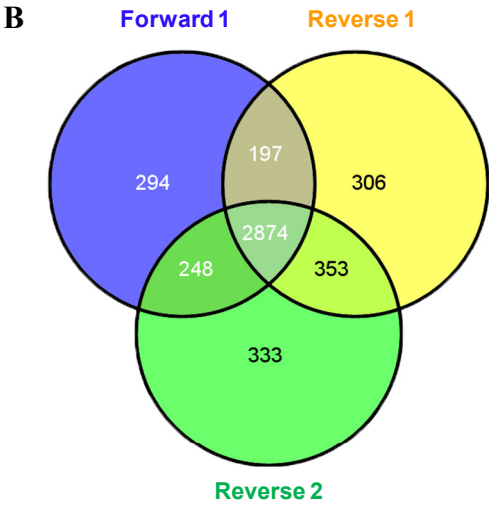


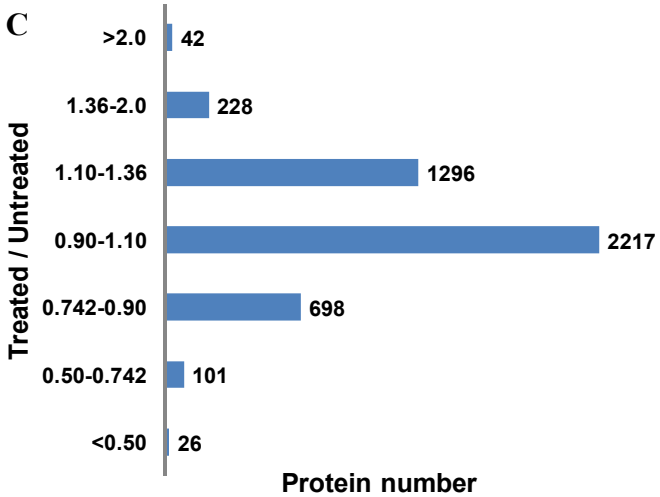

**Figure 2.3** Determination of the threshold value of significantly changed proteins by Perseus.

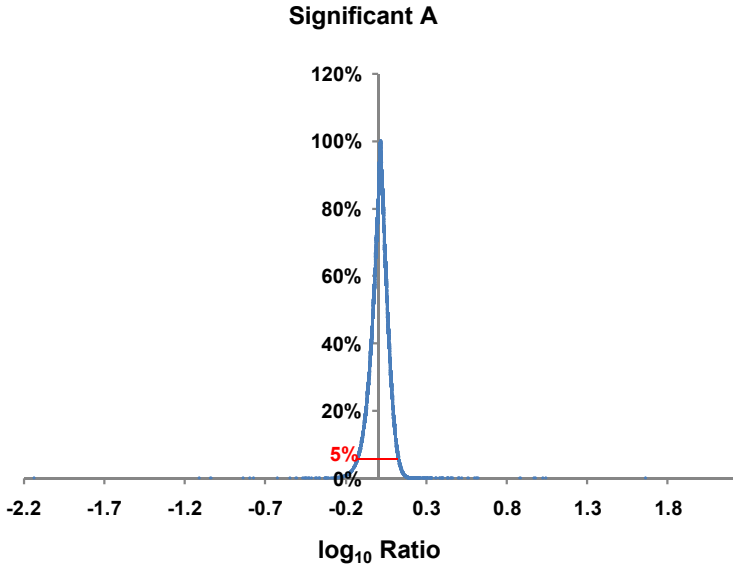

**Figure 2.4** Representative ESI-MS and MS/MS data revealing the Cr (VI) induced up regulation of squalene synthase. Shown are the MS for the $[M+2H]^{2+}$ ions of squalene synthase peptide C*IGHPEEFYNIVR and C*IGHPEEFYNIVR* ("C*" represents carbamidomethylated cysteine and "R*" designates the heavy labeled arginine) from the forward (A) and reverse (B) SILAC experiments. Depicted in (C) and (D) are the MS/MS for the $[M+2H]^{2+}$ ions of C*IGHPEEFYNIVR and C*IGHPEEFYNIVR*, respectively.

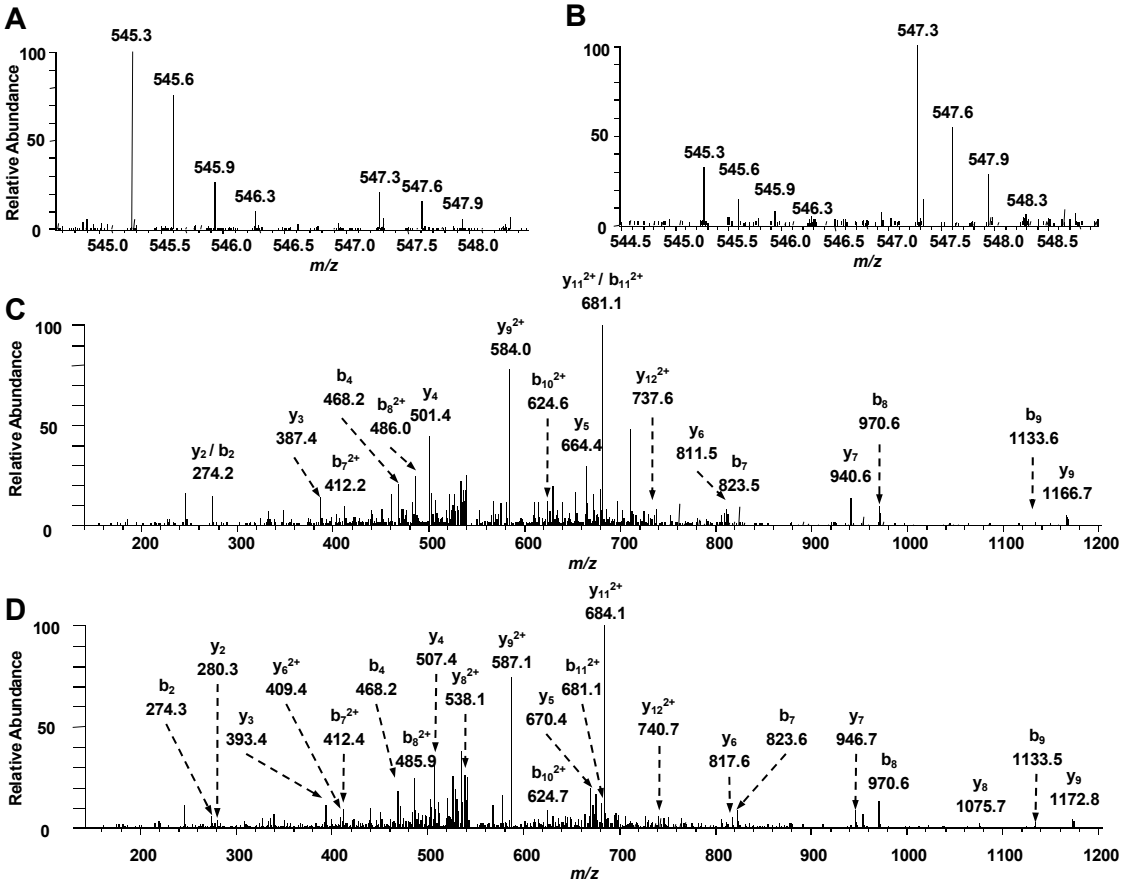

**Figure 2.5** The key intermediary steps in *de novo* cholesterol biosynthesis. The fold changes of quantified enzymes are shown. NA, not applicable; these enzymes were not quantified in any set of the SILAC experiments. The fold changes of mRNA expression level measured by real-time PCR are shown in the parenthesis, and the values represent mean of results obtained from three independent experiments.

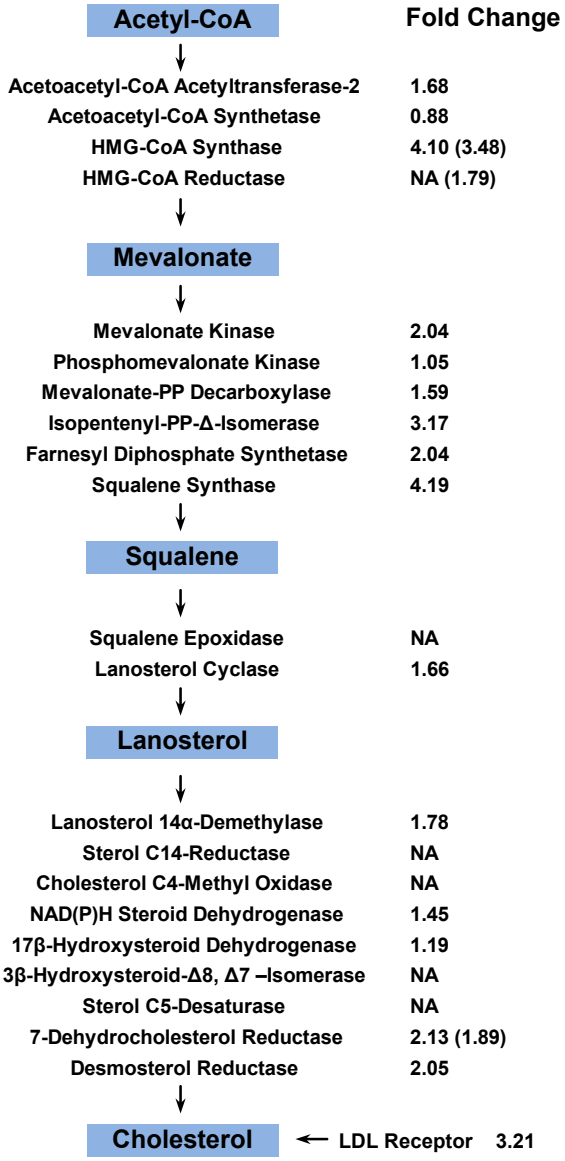

**Figure 2.6** Potassium dichromate perturbed *de novo* cholesterol biosynthesis. (A) Shown are the histograms of gene expression levels of proteins involved in cholesterol biosynthesis in GM00637 cells that were untreated or treated with 0.5 µM potassium dichromate for 24 hrs. (B) Effect of 24 hrs of potassium dichromate treatment on cholesterol content of GM00637, HEK293T and HCT-116 cell lines. Cholesterol content is expressed as fold change of the value from control. The values represent mean ± S.D. of results obtained from three independent experiments. '*', $p < 0.05$; '**', $p < 0.01$; '***', $p < 0.001$. The p values were calculated by using unpaired two-tailed t-test.

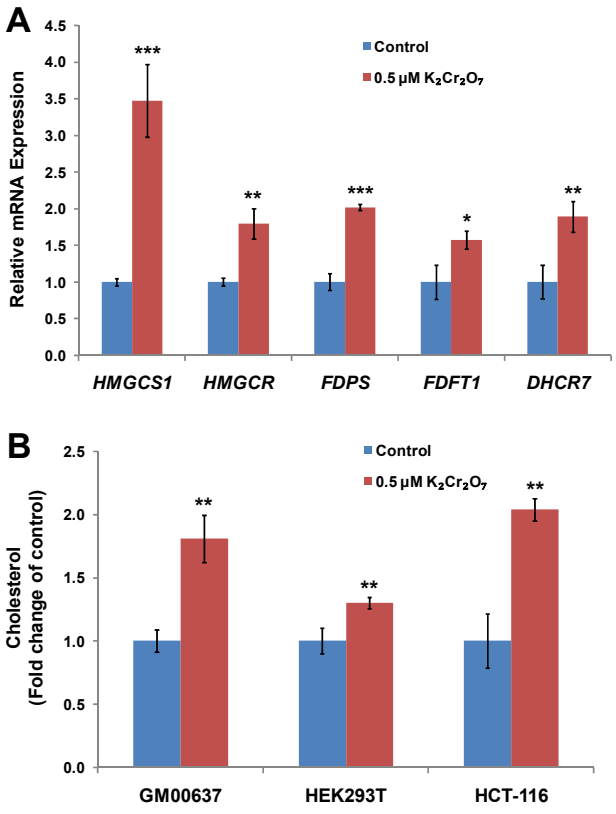

**Figure 2.7** Potassium dichromate-induced cell proliferation can be rescued by external addition of lovastatin. The cell viability of GM00637 (A) and HEK293T (B) determined by trypan blue exclusion assay after 12 and 24 hrs of treatment with 0 μM, 0.5 μM $K_2Cr_2O_7$ in the presence or absence of 1 μM lovastatin. (C) Shown are the cholesterol levels in GM00637 and HEK293T cells that were untreated or treated for 24 hrs with 0.5 μM potassium dichromate, alone or in combination with 1 μM lovastatin.

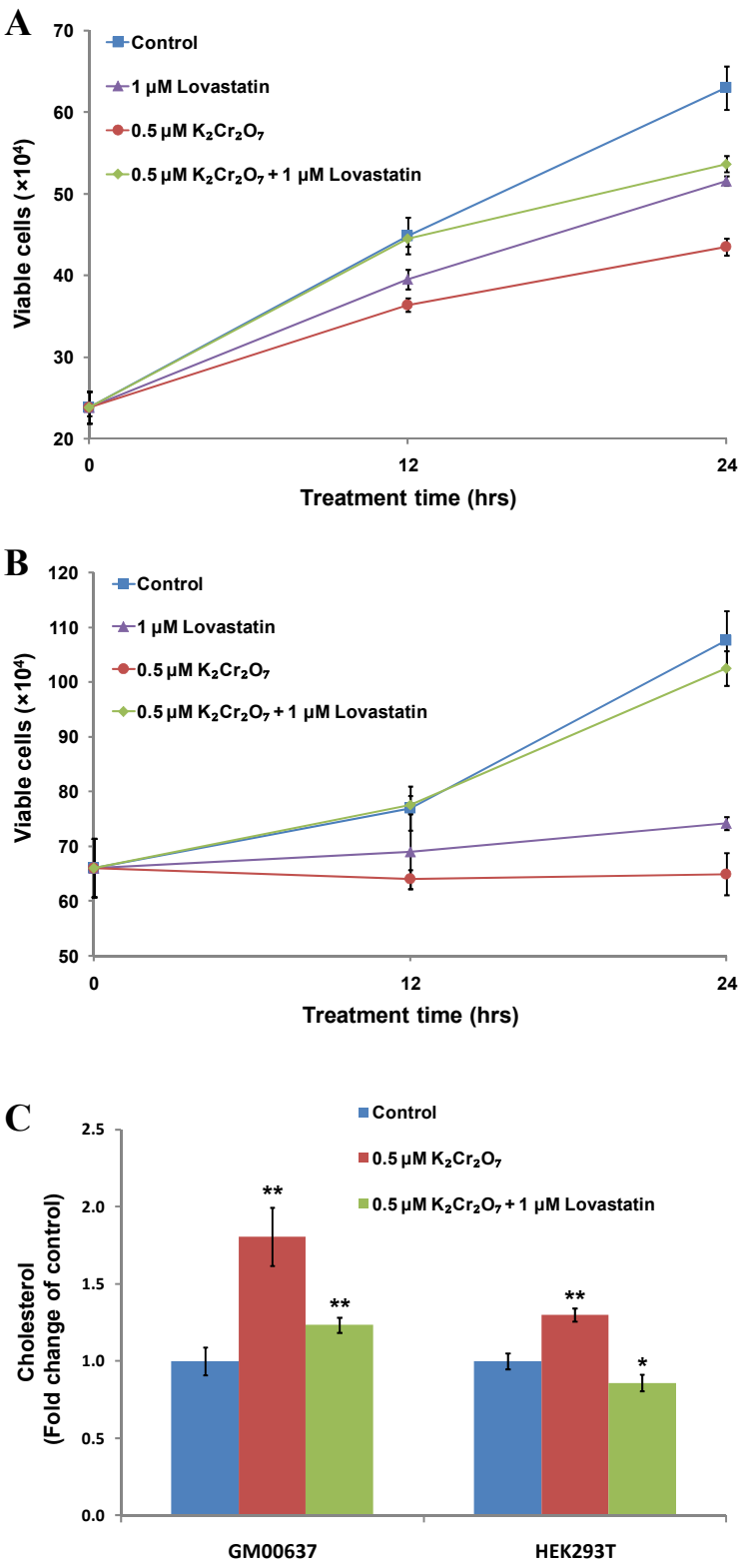
A
Control
1 μM Lovastatin
0.5 μM K2Cr2O7
0.5 μM K2Cr2O7 + 1 μM Lovastatin
Viable cells (×10⁴)
70
60
50
40
30
20
0
12
24
Treatment time (hrs)
B
Control
1 μM Lovastatin
0.5 μM K2Cr2O7
0.5 μM K2Cr2O7 + 1 μM Lovastatin
Viable cells (×10⁴)
120
110
100
90
80
70
60
50
0
12
24
Treatment time (hrs)
C
Control
0.5 μM K2Cr2O7
0.5 μM K2Cr2O7 + 1 μM Lovastatin
Cholesterol
(Fold change of control)
2.5
2.0
1.5
1.0
0.5
0.0
**
**
**
*
GM00637
HEK293T

**Table 2.1** List of primers used for real-time PCR as designed by Primer Premier 5.

| Genes | Forward Primer | Reverse Primer |
|---|---|---|
| *HMGCS1* | 5' - TGA AAA GCA CAG AAG AAC TTA CGC - 3' | 5' - TCT TGG CAG GGC TTG GAA TA - 3' |
| *HMGCR* | 5' - TGG GGA ATT GTC ACT TAT GG - 3' | 5' - GGG CTA TTC AGG CTG TCT TC - 3' |
| *FDPS* | 5' - CAA AAT TGG CAC TGA CAT CC - 3' | 5' - GCC ACT TTC TCA GCC TCC TT - 3' |
| *FDFT1* | 5' - CAA GCA GTG ACC CTG ATG AT - 3' | 5' - CTG AGT CGG GGA TTC TAT GA - 3' |
| *DHCR7* | 5' - TGC CTT ATC TTT ACA CGC TG - 3' | 5' - AAC AGG TCC TTC TGG TGG TT - 3' |

*HMGCS1*, 3-hydroxy-3-methylglutaryl-CoA synthase 1; *HMGCR*, 3-hydroxy-3-methylglutaryl-CoA reductase; *FDPS*, farnesyl diphosphate synthase; *FDFT1*, Squalene synthase ; *DHCR7*, 7-dehydrocholesterol reductase.

**Table 2.2** List of proteins whose expression was significantly changed upon $K_2Cr_2O_7$ treatment. The ratio is expressed as the average ratio in $K_2Cr_2O_7$-treated cells versus control untreated cells. ("S.D." represents standard deviation).

| IPI NO. | Protein Names | Ratio | S.D. |
|---|---|---|---|
| | **Up-regulated** | | |
| IPI00945846 | Trypsin 1 | 46.16 | 79.91 |
| IPI00022990 | Statherin | 11.11 | |
| IPI00027462 | Calgranulin-B | 10.60 | |
| IPI00302030 | Ras-related protein Rab-30 | 9.58 | |
| IPI00296909 | 193 kDa vault protein | 9.37 | |
| IPI00747077 | RUN and TBC1 domain-containing protein 2 | 7.68 | |
| IPI00020944 | Squalene synthase | 4.19 | 0.67 |
| IPI00008475 | HMG-CoA synthase | 4.10 | 0.86 |
| IPI00220327 | 67 kDa cytokeratin | 4.01 | 6.75 |
| IPI00290110 | Neoplastic transformation inhibitor protein | 3.64 | 0.39 |
| IPI00176193 | Collagen alpha-1(XIV) chain | 3.33 | 4.49 |
| IPI00000070 | Low-density lipoprotein receptor | 3.21 | 0.90 |
| IPI00220014 | Isopentenyl-PP-delta-isomerase | 3.17 | 0.36 |
| IPI00295601 | BM88 antigen | 2.91 | |
| IPI00016014 | Cerebral protein 14 | 2.87 | |
| IPI00300725 | Cytokeratin-6A | 2.84 | |
| IPI00030362 | Differentiation-dependent protein A4 | 2.74 | |
| IPI00477802 | Nuclear phosphoprotein p21/SIIR | 2.74 | 1.96 |
| IPI00477526 | UPF0550 protein C7orf28 | 2.71 | |
| IPI00914045 | Small integral membrane protein 13 | 2.55 | |
| IPI00103145 | Class A basic helix-loop-helix protein 39 | 2.54 | |
| IPI00006442 | Coilin | 2.51 | 2.37 |
| IPI00296999 | ATP synthase mitochondrial F1 complex assembly factor 2 | 2.50 | |
| IPI00410297 | Endo-glucoronidase | 2.45 | |
| IPI00300333 | Pancreatic differentiation protein 2 | 2.42 | 2.40 |
| IPI00019355 | Cerebral protein 2 | 2.31 | |
| IPI00016441 | Pro-rich, PH and SH2 domain-containing signaling mediator | 2.29 | |
| IPI00107831 | Leukocyte common antigen related | 2.18 | |
| IPI00045914 | Msx2-interacting protein | 2.15 | 1.76 |
| IPI00007956 | Thioredoxin-binding protein 2 | 2.15 | |
| IPI00909366 | cDNA FLJ60058, highly similar to Myosin light chain 1, slow-twitch muscle A isoform | 2.14 | 1.79 |
| IPI00332493 | Pleckstrin homology domain-containing family O member 2 | 2.14 | 1.39 |
| IPI00021033 | Collagen alpha-1(III) chain | 2.14 | 0.50 |

| IPI NO. | Protein Names | Ratio | S.D. |
|---|---|---|---|
| IPI00465261 | Endoplasmic reticulum aminopeptidase 2 | 2.13 | |
| IPI00294501 | 7-dehydrocholesterol reductase | 2.13 | 0.09 |
| IPI00847793 | Dermcidin isoform 2 | 2.12 | 3.46 |
| IPI00954460 | MHC class I antigen | 2.09 | 1.15 |
| IPI00016703 | Desmosterol reductase | 2.05 | 0.56 |
| IPI00010717 | Mevalonate kinase | 2.04 | |
| IPI00914566 | Farnesyl diphosphate synthetase | 2.04 | 0.11 |
| IPI00395596 | Amino-terminal enhancer of split | 2.03 | |
| IPI00014172 | Golgi 4-transmembrane-spanning transporter MTP | 2.01 | |
| IPI00219783 | Ubiquitin-conjugating enzyme E2G 1 | 1.99 | 1.61 |
| IPI00299033 | Importin alpha Q2 | 1.98 | 1.54 |
| IPI00872929 | Apolipoprotein B mRNA editing enzyme, catalytic polypeptide-like 3C variant | 1.96 | |
| IPI00219628 | Protein kinase C beta type | 1.96 | |
| IPI00027240 | Guanine nucleotide-binding protein G(I)/G(S)/G(O) subunit gamma-5 | 1.93 | 0.01 |
| IPI00402657 | RNA polymerase II-associated protein 1 | 1.93 | |
| IPI00398625 | Hornerin | 1.92 | 3.15 |
| IPI00922513 | cDNA FLJ57872, highly similar to Mevalonate kinase (EC 2.7.1.36) | 1.90 | 0.22 |
| IPI00645782 | cDNA FLJ58300, highly similar to Seryl-tRNA synthetase, mitochondrial (EC 6.1.1.11) | 1.88 | 0.95 |
| IPI00163361 | T-box transcription factor TBX14 | 1.84 | |
| IPI00003817 | Rho GDP dissociation inhibitor (GDI) beta | 1.84 | |
| IPI00304227 | Cadherin-11 | 1.83 | |
| IPI00386516 | cDNA FLJ32696 fis, clone TESTI2000358 | 1.83 | 0.84 |
| IPI00896498 | cDNA, FLJ93047, highly similar to Homo sapiens matrix metallopeptidase 14 (membrane-inserted) (MMP14), mRNA | 1.82 | 0.25 |
| IPI00299086 | Melanoma differentiation-associated protein 9 | 1.80 | 0.22 |
| IPI00303297 | DnaJ homolog subfamily C member 25 | 1.80 | |
| IPI00554560 | Lysine-rich nucleolar protein 1 | 1.80 | 0.99 |
| IPI00018801 | Eva-1 homolog B | 1.79 | 0.38 |
| IPI00942417 | Nik-related protein kinase | 1.79 | |
| IPI00299738 | Procollagen C-endopeptidase enhancer 1 | 1.78 | 0.16 |
| IPI00295772 | Lanosterol 14 alpha-demethylase | 1.78 | 0.06 |
| IPI00332106 | Hematopoietic PBX-interacting protein | 1.76 | 0.26 |
| IPI00514832 | RING finger protein 109 | 1.76 | |
| IPI00009111 | 5T4 oncofetal antigen | 1.75 | 0.12 |
| IPI00009634 | Sulfide:quinone oxidoreductase, mitochondrial | 1.74 | |
| IPI00015285 | CTP:phosphoethanolamine cytidylyltransferase | 1.72 | 0.20 |
| IPI00289547 | Transcription factor jun-D | 1.71 | 0.45 |
| IPI00011528 | CF-1 50 kDa subunit | 1.71 | 1.33 |
| IPI00651738 | 1,2-dihydroxy-3-keto-5-methylthiopentene dioxygenase | 1.71 | 0.40 |
| IPI00761160 | Calpain inhibitor | 1.70 | |
| IPI00645849 | Extracellular matrix protein 1 | 1.70 | 0.20 |
| IPI00465176 | 39S ribosomal protein L28, mitochondrial | 1.69 | 0.97 |
| IPI00041127 | Anti-silencing function protein 1 homolog B | 1.69 | 0.15 |

| IPI NO. | Protein Names | Ratio | S.D. |
|---|---|---|---|
| IPI00180675 | Alpha-tubulin 3 | 1.68 | 0.24 |
| IPI00100213 | p53-inducible ribonucleotide reductase small subunit 2-like protein | 1.68 | 0.49 |
| IPI00291419 | Acetoacetyl-CoA acetyltransferase-2 | 1.68 | 0.12 |
| IPI00019551 | Beckwith-Wiedemann syndrome chromosomal region 1 candidate gene C protein | 1.67 | |
| IPI00157734 | Exocyst complex component 3 | 1.67 | |
| IPI00784739 | Uncharacterized protein C14orf43 | 1.67 | 0.12 |
| IPI00011676 | Neural Wiskott-Aldrich syndrome protein | 1.67 | 0.60 |
| IPI00413817 | Serine incorporator 1 | 1.66 | |
| IPI00009747 | Lanosterol cyclase | 1.66 | 0.03 |
| IPI00183642 | Suppressor of hairy wing homolog 3 | 1.66 | |
| IPI00022078 | Differentiation-related gene 1 protein | 1.65 | 0.19 |
| IPI00739099 | Collagen alpha-2(V) chain | 1.65 | 0.64 |
| IPI00219344 | Calcium-binding protein BDR-1 | 1.65 | 0.28 |
| IPI00328243 | Choline phosphatase 3 | 1.65 | 0.14 |
| IPI00247063 | Atriopeptidase | 1.64 | 0.33 |
| IPI00642259 | 230 kDa bullous pemphigoid antigen | 1.64 | 0.97 |
| IPI00911050 | cDNA FLJ53329, highly similar to NADPH:adrenodoxin oxidoreductase, mitochondrial (EC 1.18.1.2) | 1.64 | |
| IPI00024307 | Ephrin-B1 | 1.63 | |
| IPI00184871 | Uncharacterized protein C6orf130 | 1.63 | |
| IPI00880117 | Apolipoprotein B mRNA editing enzyme, catalytic polypeptide-like 3B | 1.63 | 0.89 |
| IPI00290614 | Endonuclease G, mitochondrial | 1.62 | |
| IPI00022629 | Protein regulator of cytokinesis 1 | 1.61 | 0.42 |
| IPI00657752 | Putative uncharacterized protein CD81 | 1.61 | 0.42 |
| IPI00000398 | Nucleolar and spindle-associated protein 1 | 1.60 | 0.20 |
| IPI00102660 | Progressive external ophthalmoplegia 1 protein | 1.60 | |
| IPI00061111 | BLM-associated protein of 18 kDa | 1.60 | 0.06 |
| IPI00027223 | Cytosolic NADP-isocitrate dehydrogenase | 1.60 | 0.15 |
| IPI00257932 | Transcription elongation factor A protein-like 5 | 1.60 | |
| IPI00375462 | Serine/arginine-rich-splicing regulatory protein 86 | 1.59 | 0.08 |
| IPI00022745 | Mevalonate-PP decarboxylase | 1.59 | 0.28 |
| IPI00465431 | 35 kDa lectin | 1.59 | 0.07 |
| IPI00743663 | E3 ubiquitin-protein ligase TRAF6 | 1.59 | 0.51 |
| IPI00549564 | Acetoacetyl-CoA synthetase | 1.58 | |
| IPI00401829 | Uncharacterized protein C14orf38 | 1.58 | 0.82 |
| IPI00478390 | Cyclin-dependent kinase inhibitor 2A, isoform 4 | 1.58 | |
| IPI00304483 | Polyadenylate-binding protein-interacting protein 2 | 1.57 | |
| IPI00329598 | 17-beta-hydroxysteroid dehydrogenase 11 | 1.56 | 0.14 |
| IPI00788747 | TIMP metallopeptidase inhibitor 2 | 1.56 | |
| IPI00954084 | MHC class I antigen | 1.55 | 0.31 |
| IPI00004758 | Autosomal recessive hypercholesterolemia protein | 1.55 | |
| IPI00005036 | RNA binding motif protein 5 | 1.55 | 0.34 |
| IPI00098524 | Enzyme-like protein PIT13 | 1.55 | |
| IPI00479018 | Melanoma differentiation-associated protein 9 | 1.54 | 0.25 |

| IPI NO. | Protein Names | Ratio | S.D. |
|---|---|---|---|
| IPI00641384 | Protein transport protein Sec16A | 1.54 | |
| IPI00018404 | Elongin 110 kDa subunit | 1.54 | |
| IPI00063213 | Mediator complex subunit 30 | 1.54 | 0.06 |
| IPI00099497 | Transcription factor MafF | 1.53 | 0.32 |
| IPI00647163 | Transcription elongation factor A protein-like 4 | 1.53 | 0.38 |
| IPI00103521 | Stoned B | 1.53 | 1.04 |
| IPI00022145 | Nuclear ubiquitous casein and cyclin-dependent kinases substrate | 1.53 | 0.02 |
| IPI00514926 | Guanylate kinase 1 | 1.53 | 0.58 |
| IPI00166066 | ORM1-like protein 3 | 1.53 | |
| IPI00016542 | WD repeat-containing protein 76 | 1.53 | |
| IPI00011736 | Phosphatidylinositol 3-kinase 85 kDa regulatory subunit beta | 1.52 | 0.39 |
| IPI00828172 | Protein FAM114A2 | 1.52 | 0.30 |
| IPI00029144 | PP2A subunit B isoform PR72/PR130 | 1.52 | |
| IPI00017373 | Replication factor A protein 3 | 1.52 | 0.38 |
| IPI00215610 | 55 kDa erythrocyte membrane protein | 1.52 | 0.67 |
| IPI00873459 | Septin-10 | 1.52 | |
| IPI00329784 | Brain ryanodine receptor-calcium release channel | 1.52 | |
| IPI00028419 | Adenovirus E1B19K-binding protein B5 | 1.51 | 0.03 |
| IPI00016807 | NAD-dependent deacetylase sirtuin-5 | 1.51 | |
| IPI00029656 | Inversely correlated with estrogen receptor expression 1 | 1.51 | |
| IPI00027166 | TIMP metallopeptidase inhibitor 2 | 1.51 | 0.36 |
| IPI00006971 | Endosialin | 1.51 | |
| IPI00552452 | Ubiquitin-like modifier activating enzyme 1 | 1.50 | 0.41 |
| IPI00464999 | Amplified in breast cancer protein 1 | 1.50 | |
| IPI00607861 | 6-phosphogluconolactonase | 1.50 | |
| IPI00043622 | FERM domain-containing protein 6 | 1.50 | |
| IPI00220578 | G(i) alpha-3 | 1.49 | 0.27 |
| IPI00940950 | Ribosomal protein L10 | 1.49 | 1.01 |
| IPI00216088 | Cellular retinoic acid-binding protein 2 | 1.49 | 0.05 |
| IPI00295940 | cDNA FLJ55508, highly similar to Sad1/unc-84-like protein 2 | 1.49 | 0.20 |
| IPI00012866 | Protein kinase B | 1.49 | 0.18 |
| IPI00012069 | Azoreductase | 1.49 | 0.61 |
| IPI00100980 | EH domain-containing protein 2 | 1.48 | 0.19 |
| IPI00017344 | Ras-related protein Rab-5B | 1.48 | 0.07 |
| IPI00921909 | Zinc finger protein 185 variant 721 | 1.48 | |
| IPI00852806 | cDNA FLJ13729 fis, clone PLACE3000121, weakly similar to VESICULAR TRAFFIC CONTROL PROTEIN SEC15 | 1.48 | 0.65 |
| IPI00216730 | Histone H2A type 2-B | 1.48 | |
| IPI00551024 | ATP-dependent dihydroxyacetone kinase | 1.48 | 0.11 |
| IPI00298946 | Down syndrome critical region protein 3 | 1.48 | 0.35 |
| IPI00215997 | CD9 antigen | 1.48 | 0.31 |
| IPI00306400 | Kinesin-like protein 2 | 1.48 | 0.31 |
| IPI00001690 | Cullin-7 | 1.48 | 0.42 |
| IPI00001883 | SH3 and PX domain-containing protein 1 | 1.48 | |

| IPI NO. | Protein Names | Ratio | S.D. |
|---|---|---|---|
| IPI00042099 | Pygopus homolog 2 | 1.47 | 0.20 |
| IPI00306046 | Developmentally-regulated endothelial cell locus 1 protein | 1.47 | 0.71 |
| IPI00000155 | 3-hydroxyisobutyrate dehydrogenase-like protein | 1.47 | 0.09 |
| IPI00178899 | Cyclin-A/CDK2-associated protein p45 | 1.47 | |
| IPI00218803 | Fibulin-1 | 1.47 | |
| IPI00301579 | cDNA FLJ59142, highly similar to Epididymal secretory protein E1 | 1.47 | 0.10 |
| IPI00029665 | Cob(I)alamin adenosyltransferase | 1.46 | 0.06 |
| IPI00401002 | OriLyt TD-element-binding protein 7 | 1.46 | 0.28 |
| IPI00009737 | Ras-related GTP-binding protein D | 1.46 | |
| IPI00016891 | Ras-related protein Rab-6B | 1.46 | 0.41 |
| IPI00641124 | cDNA FLJ55777, highly similar to DCN1-like protein 4 | 1.46 | |
| IPI00008943 | ATP-dependent RNA helicase DDX19B | 1.46 | 0.06 |
| IPI00027463 | Calcyclin | 1.46 | |
| IPI00019407 | NAD(P)H steroid dehydrogenase | 1.45 | 0.09 |
| IPI00029605 | Chondroitinsulfatase | 1.45 | 0.16 |
| IPI00304875 | HIRA-interacting protein 3 | 1.45 | |
| IPI00043565 | Coiled-coil domain-containing protein 16 | 1.45 | 0.18 |
| IPI00893949 | MHC class I antigen | 1.45 | 0.32 |
| IPI00921172 | Peroxisomal carnitine O-octanoyltransferase | 1.45 | |
| IPI00289831 | Receptor-type tyrosine-protein phosphatase S | 1.44 | 0.71 |
| IPI00166955 | Protein canopy homolog 4 | 1.44 | 0.12 |
| IPI00550854 | Limitrin | 1.44 | |
| IPI00296772 | ADP-ribosylation factor-binding protein GGA2 | 1.44 | 0.12 |
| IPI00031680 | Acyl-CoA-binding domain-containing protein 6 | 1.44 | 0.35 |
| IPI00009726 | Nicotinamide mononucleotide adenylyltransferase 1 | 1.44 | |
| IPI00026314 | Actin-depolymerizing factor | 1.44 | 0.12 |
| IPI00160901 | Putative uncharacterized protein GTSE1 | 1.44 | 0.60 |
| IPI00792422 | WASH complex subunit FAM21A | 1.43 | 0.11 |
| IPI00022865 | Cyclin-A2 | 1.43 | |
| IPI00479217 | Heterogeneous nuclear ribonucleoprotein U | 1.43 | |
| IPI00027713 | Cyclic AMP-responsive element-binding protein 1 | 1.43 | |
| IPI00014264 | Arf-GAP with coiled-coil, ANK repeat and PH domain-containing protein 2 | 1.43 | |
| IPI00217950 | High mobility group nucleosome-binding domain-containing protein 2 | 1.43 | 0.23 |
| IPI00303954 | Cytochrome b5 outer mitochondrial membrane isoform | 1.43 | 0.06 |
| IPI00551002 | cDNA FLJ55173, highly similar to Nuclear distribution protein nudE-like 1 | 1.43 | |
| IPI00402231 | Cysteine string protein | 1.43 | 0.12 |
| IPI00419721 | EPM2A-interacting protein 1 | 1.43 | 0.67 |
| IPI00395768 | Syntaxin-3 | 1.43 | 0.02 |
| IPI00027444 | Leukocyte elastase inhibitor | 1.42 | 0.02 |
| IPI00216952 | 70 kDa lamin | 1.42 | 0.41 |
| IPI00257508 | Collapsin response mediator protein 2 | 1.42 | 0.06 |
| IPI00026781 | [Acyl-carrier-protein] S-acetyltransferase | 1.42 | 0.18 |
| IPI00011118 | Putative uncharacterized protein RRM2 | 1.42 | 0.27 |

| IPI NO. | Protein Names | Ratio | S.D. |
|---|---|---|---|
| IPI00644290 | NDRG family member 3 | 1.42 | 0.05 |
| IPI00395488 | Protein slit-like 2 | 1.42 | 0.42 |
| IPI00307257 | TBC1 domain family member 9B | 1.42 | 0.38 |
| IPI00000105 | Lung resistance-related protein | 1.42 | 0.07 |
| IPI00936141 | AKT-interacting protein | 1.41 | |
| IPI00028122 | CLL-associated antigen KW-7 | 1.41 | 0.18 |
| IPI00021924 | Histone H1x | 1.41 | 0.18 |
| IPI00032293 | Cystatin-3 | 1.41 | 0.28 |
| IPI00023191 | cDNA FLJ54710, highly similar to Target of Myb protein 1 | 1.41 | 0.26 |
| IPI00816474 | Mammalian retrotransposon derived protein 8C | 1.41 | 0.49 |
| IPI00005658 | Ubiquitin-like protein 4A | 1.41 | |
| IPI00299463 | Cell cycle regulatory protein p95 | 1.40 | |
| IPI00925205 | SH3-domain GRB2-like endophilin B2 | 1.40 | |
| IPI00784013 | Janus kinase 1 | 1.40 | 0.09 |
| IPI00018195 | Mitogen-activated protein kinase 3 | 1.40 | 0.15 |
| IPI00328350 | Cell growth-inhibiting gene 39 protein | 1.40 | 0.23 |
| IPI00470559 | Ankyrin repeat domain-containing protein 25 | 1.40 | 0.43 |
| IPI00007941 | Cardiac lineage protein 1 | 1.40 | 0.11 |
| IPI00657692 | cDNA FLJ39535 fis, clone PUAEN2005502, highly similar to Goodpasture antigen-binding protein (EC 2.7.11.9) | 1.40 | |
| IPI00478127 | Transcription elongation factor A protein-like 3 | 1.40 | |
| IPI00003527 | Ezrin-radixin-moesin-binding phosphoprotein 50 | 1.40 | 0.34 |
| IPI00031397 | Long-chain acyl-CoA synthetase 3 | 1.40 | 0.12 |
| IPI00304962 | Alpha-2 type I collagen | 1.39 | 0.14 |
| IPI00384280 | Prenylcysteine lyase | 1.39 | 0.13 |
| IPI00221172 | N-recognin-7 | 1.39 | 0.19 |
| IPI00299214 | Thymidine kinase, cytosolic | 1.39 | 0.39 |
| IPI00084828 | Syntaxin binding protein 1 | 1.39 | |
| IPI00103090 | Replicative senescence down-regulated leo1-like protein | 1.39 | |
| IPI00848090 | cDNA, FLJ94534, highly similar to Homo sapiens capping protein (actin filament), gelsolin-like(CAPG), mRNA | 1.39 | 0.55 |
| IPI00003348 | G protein subunit beta-2 | 1.39 | 0.19 |
| IPI00002478 | Endothelin-converting enzyme 1 | 1.39 | 0.43 |
| IPI00023832 | Adapter protein HOFI | 1.39 | 0.07 |
| IPI00642238 | Heterochromatin protein 1-binding protein 3 | 1.39 | 0.10 |
| IPI00414657 | Chromosome transmission fidelity factor 18 homolog | 1.39 | 0.11 |
| IPI00297646 | Alpha-1 type I collagen | 1.39 | 0.11 |
| IPI00010388 | Centromere protein B | 1.38 | 0.01 |
| IPI00879287 | Putative uncharacterized protein CDCA5 | 1.38 | 0.25 |
| IPI00410717 | Pogo transposable element with ZNF domain | 1.38 | 0.00 |
| IPI00902843 | cDNA FLJ16129 fis, clone BRACE2039823, highly similar to CDP-diacylglycerol--inositol3-phosphatidyltransferase (EC 2.7.8.11) | 1.38 | |
| IPI00152303 | Phosphatidylinositol-5-phosphate 4-kinase type II gamma | 1.38 | 0.08 |
| IPI00942981 | DDRGK domain-containing protein 1 | 1.38 | |
| IPI00382990 | Dermal papilla derived protein 12 | 1.38 | 1.05 |

| IPI NO. | Protein Names | Ratio | S.D. |
|---|---|---|---|
| IPI00028911 | Alpha-dystroglycan | 1.38 | |
| IPI00644697 | Heme-binding protein 2 | 1.38 | 0.34 |
| IPI00848174 | cDNA FLJ34950 fis, clone NT2RP7017284, highly similar to Casein kinase I isoform epsilon (EC 2.7.11.1) | 1.38 | |
| IPI00844090 | Collagen alpha-1(V) chain | 1.38 | 0.35 |
| IPI00008726 | Iron regulatory protein 2 | 1.38 | |
| IPI00301609 | Nercc1 kinase | 1.38 | 0.22 |
| IPI00447051 | B-cell CLL/lymphoma 7 protein family member C | 1.37 | |
| IPI00026268 | Guanine nucleotide-binding protein G(I)/G(S)/G(T) subunit beta-1 | 1.37 | 0.17 |
| IPI00175029 | Transmembrane protein 55A | 1.37 | 0.28 |
| IPI00004312 | Signal transducer and activator of transcription 2 | 1.37 | 0.30 |
| IPI00102182 | Zinc finger FYVE domain-containing protein 21 | 1.37 | |
| IPI00029015 | 3-dehydrosphinganine reductase | 1.37 | |
| IPI00219718 | cDNA FLJ76382, highly similar to Homo sapiens retinol binding protein 1, cellular (RBP1), mRNA | 1.37 | |
| IPI00337648 | Fas-associated protein-tyrosine phosphatase 1 | 1.37 | |
| IPI00217541 | ATP-dependent RNA helicase DDX51 | 1.37 | 1.09 |
| IPI00647389 | EH domain-binding mitotic phosphoprotein | 1.37 | 0.49 |
| IPI00018311 | Neuroplastin | 1.37 | 0.23 |
| IPI00156984 | Charged multivesicular body protein 1b | 1.37 | 0.07 |
| IPI00060521 | FLYWCH family member 2 | 1.37 | 0.25 |
| IPI00792186 | ATP-binding cassette sub-family F member 1 | 1.37 | 0.20 |
| IPI00016457 | Carnitine acetyltransferase | 1.36 | |
| IPI00008599 | 3-beta-hydroxysteroid-delta(8),delta(7)-isomerase | 1.36 | |
| IPI00550781 | PRKR-interacting protein 1 | 1.36 | 0.24 |
| IPI00168336 | LEM domain-containing protein 2 | 1.36 | 0.16 |
| | **Down-regulated** | | |
| IPI00514027 | Heat shock protein 90kDa alpha (Cytosolic), class B member 1 | 0.01 | |
| IPI00413517 | Rho guanine nucleotide exchange factor 10 | 0.08 | |
| IPI00796114 | cDNA FLJ11889 fis, clone HEMBA1007251, weakly similar to Homo sapiens F-box protein FBX29 (FBX29) mRNA | 0.09 | |
| IPI00740545 | POTE ankyrin domain family, member I | 0.15 | 0.11 |
| IPI00409761 | CHETK-alpha | 0.16 | |
| IPI00069084 | 350/400 kDa PCAF-associated factor | 0.17 | |
| IPI00163172 | Putative uncharacterized protein SKP2 | 0.24 | |
| IPI00299145 | Cytokeratin-6C | 0.29 | |
| IPI00029728 | Basic transcription factor 2 80 kDa subunit | 0.31 | |
| IPI00028980 | Unhealthy ribosome biogenesis protein 2 homolog | 0.34 | |
| IPI00299635 | Baculoviral IAP repeat-containing protein 6 | 0.35 | 0.31 |
| IPI00023020 | Alpha-inhibin-31 | 0.36 | |
| IPI00293307 | Adipophilin | 0.36 | 0.15 |
| IPI00022628 | cDNA, FLJ93207, highly similar to Homo sapiens microtubule-associated protein 7 (MAP7), mRNA | 0.37 | |
| IPI00927606 | Cellular glutathione peroxidase | 0.38 | |

| IPI NO. | Protein Names | Ratio | S.D. |
|---|---|---|---|
| IPI00783004 | 1-phosphatidylinositol-4,5-bisphosphate phosphodiesterase beta-4 | 0.39 | 0.37 |
| IPI00007118 | Endothelial plasminogen activator inhibitor | 0.41 | 0.05 |
| IPI00016334 | Cell surface glycoprotein MUC18 | 0.42 | |
| IPI00007253 | Protein TRS85 homolog | 0.43 | |
| IPI00293665 | Cytokeratin-6B | 0.44 | |
| IPI00012215 | UPF0184 protein C9orf16 | 0.47 | |
| IPI00021685 | ADP-ribosylation factor-like protein 6 | 0.47 | |
| IPI00333913 | Neuroblastoma-amplified gene protein | 0.48 | |
| IPI00942405 | LSM7 homolog, U6 small nuclear RNA associated | 0.48 | |
| IPI00010676 | Monocyte activation antigen Mo3 | 0.49 | 0.01 |
| IPI00747787 | Condensin-2 complex subunit D3 | 0.50 | |
| IPI00018219 | Kerato-epithelin | 0.51 | 0.18 |
| IPI00022498 | Metallothionein-2 | 0.53 | |
| IPI00166861 | Uncharacterized protein C12orf45 | 0.53 | |
| IPI00550977 | Coiled-coil domain-containing protein 21 | 0.55 | |
| IPI00025050 | Tryptophanyl tRNA synthetase 2, mitochondrial | 0.55 | 0.51 |
| IPI00004436 | Cancer-associated Sm-like | 0.55 | |
| IPI00377050 | 13S Golgi transport complex 90 kDa subunit | 0.55 | 0.45 |
| IPI00027693 | Nuclear body protein SP140-like protein | 0.55 | 0.00 |
| IPI00396967 | Four and a half LIM-domain protein 2 | 0.55 | 0.11 |
| IPI00030877 | 15 kDa selenoprotein | 0.56 | 0.02 |
| IPI00060148 | Coiled-coil domain-containing protein 127 | 0.57 | |
| IPI00150963 | RNA pseudouridylate synthase domain-containing protein 2 | 0.58 | |
| IPI00297617 | PH domain leucine-rich repeat-containing protein phosphatase 1 | 0.58 | |
| IPI00299219 | CCN family member 1 | 0.58 | 0.10 |
| IPI00900386 | Putative uncharacterized protein GTPBP3 | 0.58 | |
| IPI00297357 | Liver-related putative tumor suppressor | 0.58 | |
| IPI00004962 | Golgi integral membrane protein 4 | 0.59 | 0.04 |
| IPI00015713 | CDK5 regulatory subunit-associated protein 1-like 1 | 0.59 | 0.23 |
| IPI00793181 | Selenoprotein S | 0.59 | 0.22 |
| IPI00815672 | Axonal transporter of synaptic vesicles | 0.60 | |
| IPI00013735 | FAST kinase domain-containing protein 2 | 0.60 | 0.35 |
| IPI00747478 | Methylmalonic aciduria and homocystinuria type D protein, mitochondrial | 0.61 | |
| IPI00917041 | Putative uncharacterized protein METTL5 | 0.61 | 0.04 |
| IPI00295849 | Geranylgeranyl transferase type II subunit beta | 0.61 | |
| IPI00414717 | Golgi glycoprotein 1 | 0.61 | 0.10 |
| IPI00023529 | Cell division protein kinase 6 | 0.61 | 0.12 |
| IPI00016046 | Protein MGR2 homolog | 0.62 | |
| IPI00004459 | 18S rRNA dimethylase | 0.62 | 0.09 |
| IPI00008752 | Metallothionein-1G | 0.62 | 0.00 |
| IPI00844311 | Uridine-cytidine kinase-like 1 | 0.62 | |
| IPI00025257 | Semaphorin 7A | 0.62 | |
| IPI00218696 | Caldesmon | 0.62 | |

| IPI NO. | Protein Names | Ratio | S.D. |
|---|---|---|---|
| IPI00178314 | Amisyn | 0.63 | 0.04 |
| IPI00884192 | Glutathione peroxidase 4 | 0.64 | 0.20 |
| IPI00329625 | cDNA FLJ56153, highly similar to Homo sapiens transforming growth factor beta regulator 4 (TBRG4), transcript variant 1, mRNA | 0.64 | 0.04 |
| IPI00216135 | Alpha-tropomyosin | 0.64 | 0.10 |
| IPI00941549 | cDNA FLJ75843, highly similar to Homo sapiens pleckstrin homology domain containing, family A (phosphoinositide binding specific) member 2 (PLEKHA2), mRNA | 0.65 | |
| IPI00412787 | ADP-ribosylation factor-like protein 5A | 0.65 | |
| IPI00556494 | Activator-recruited cofactor 36 kDa component | 0.66 | |
| IPI00008750 | Metallothionein-0 | 0.66 | 0.01 |
| IPI00384180 | Dopamine receptor-interacting protein 3 | 0.66 | 0.08 |
| IPI00797887 | cDNA FLJ58199, highly similar to Fragile X mental retardation syndrome-related protein 1 | 0.66 | |
| IPI00855785 | Anastellin | 0.66 | |
| IPI00553067 | Coiled-coil domain-containing protein 132 | 0.66 | |
| IPI00414037 | Uncharacterized protein C9orf93 | 0.67 | |
| IPI00480103 | Protein FAM83D | 0.67 | 0.46 |
| IPI00478838 | Fatty acyl-CoA reductase 1 | 0.67 | 0.00 |
| IPI00006142 | ARM protein lost in epithelial cancers on chromosome X 2 | 0.67 | |
| IPI00946154 | Basic fibroblast growth factor | 0.67 | 0.05 |
| IPI00419084 | DENN domain-containing protein 5B | 0.68 | |
| IPI00008711 | Wolframin | 0.68 | |
| IPI00015953 | DEAD box protein 21 | 0.68 | 0.04 |
| IPI00294744 | Deadenylating nuclease | 0.68 | |
| IPI00153032 | Protein LTV1 homolog | 0.68 | 0.04 |
| IPI00304181 | Eukaryotic translation initiation factor 2C 3 | 0.69 | |
| IPI00794278 | Anaphase-promoting complex subunit 3 | 0.69 | 0.71 |
| IPI00456429 | 60S ribosomal protein L40 | 0.69 | |
| IPI00929268 | cDNA FLJ57057, highly similar to Small subunit processome component 20 homolog | 0.69 | 0.09 |
| IPI00014310 | Cullin-1 | 0.69 | 0.45 |
| IPI00604527 | Threonine--tRNA ligase | 0.69 | 0.01 |
| IPI00010130 | Glutamate decarboxylase | 0.70 | 0.19 |
| IPI00646899 | Putative uncharacterized protein RPL10 | 0.70 | |
| IPI00009365 | Cytochrome c oxidase assembly protein COX16 homolog, mitochondrial | 0.70 | 0.09 |
| IPI00646748 | Tropomyosin 2 (Beta) | 0.70 | |
| IPI00011307 | Bifunctional methylenetetrahydrofolate dehydrogenase/cyclohydrolase, mitochondrial | 0.71 | 0.04 |
| IPI00001541 | Mitochondrial import inner membrane translocase subunit Tim9 | 0.71 | 0.12 |
| IPI00470498 | PAI1 RNA-binding protein 1 | 0.71 | 0.12 |
| IPI00217630 | DEAH box protein 37 | 0.71 | |
| IPI00019004 | Translocation protein 1 | 0.72 | 0.11 |
| IPI00024579 | E3 ubiquitin-protein ligase RAD18 | 0.72 | 0.16 |
| IPI00514399 | Putative uncharacterized protein RPS27 | 0.72 | 0.10 |
| IPI00829835 | G patch domain-containing protein 4 | 0.72 | |

| IPI NO. | Protein Names | Ratio | S.D. |
|---|---|---|---|
| IPI00554777 | Asparagine synthetase [glutamine-hydrolyzing] | 0.72 | 0.06 |
| IPI00152708 | U3 small nucleolar RNA-associated protein 15 homolog | 0.72 | 0.03 |
| IPI00009335 | Brain protein 16 | 0.72 | 0.02 |
| IPI00657953 | PTPRF-interacting protein | 0.72 | |
| IPI00873982 | Myosin heavy chain 11 smooth muscle isoform | 0.72 | |
| IPI00871704 | Putative uncharacterized protein DIAPH3 | 0.72 | 0.12 |
| IPI00015916 | Bone-derived growth factor | 0.73 | |
| IPI00003310 | RPB11a protein | 0.73 | |
| IPI00791720 | Protein Smaug homolog 2 | 0.73 | |
| IPI00291646 | Methylenetetrahydrofolate dehydrogenase (NADP+ dependent) 1-like | 0.73 | 0.03 |
| IPI00446294 | Target of Myb-like protein 2 | 0.73 | |
| IPI00759776 | Alpha actin 1 | 0.73 | |
| IPI00024425 | Putative uncharacterized protein KIAA0664 | 0.73 | |
| IPI00384471 | Bromodomain containing 1 | 0.73 | |
| IPI00016207 | Inner membrane preprotein translocase Tim17a | 0.73 | |
| IPI00216674 | Apoptotic protease Mch-3 | 0.73 | |
| IPI00794521 | Putative uncharacterized protein DKFZp434J046 | 0.73 | |
| IPI00014516 | Caldesmon | 0.73 | 0.06 |
| IPI00396329 | Brix domain-containing protein 1 | 0.73 | 0.02 |
| IPI00456899 | RING finger protein 169 | 0.74 | |
| IPI00298928 | Leucine-rich repeat protein SHOC-2 | 0.74 | |
| IPI00065671 | Cytidine monophosphokinase 2 | 0.74 | 0.13 |
| IPI00219153 | 60S ribosomal protein L22 | 0.74 | 0.20 |
| IPI00909247 | cDNA FLJ51655, highly similar to Actin-like protein 2 | 0.74 | |
| IPI00006050 | Family with sequence similarity 115, member A | 0.74 | |
| IPI00009943 | Tumor protein, translationally-controlled 1 | 0.74 | 0.02 |
| IPI00642369 | cDNA FLJ60364, highly similar to Stat3-interacting protein | 0.74 | |
| IPI00829741 | Ankyrin repeat and LEM domain-containing protein 2 | 0.74 | |
| IPI00019835 | Bcl-2-like protein 12 | 0.74 | 0.14 |

**Table 2.3** Pathways perturbed by potassium dichromate treatment, as identified by GenMAPP analysis. (A) Summary of significantly perturbed pathways. (B) List of proteins involved in the perturbed pathways.

(A)

| MAPP Name | Number Changed | Number Measured | Number on MAPP | Percent Changed | Percent Present | Z Score |
|---|---|---|---|---|---|---|
| **Down-regulated Pathway** | | | | | | |
| Selenium Pathway | 3 | 24 | 87 | 12.5 | 27.6 | 3.0 |
| **Up-regulated Pathway** | | | | | | |
| Cholesterol Biosynthesis | 13 | 16 | 21 | 81.3 | 76.2 | 11.1 |
| Signal Transduction of S1P Receptor | 3 | 7 | 24 | 42.9 | 29.2 | 3.8 |
| Inflammatory Response Pathway | 3 | 8 | 32 | 37.5 | 25.0 | 3.4 |
| IL-5 Signaling Pathway | 6 | 29 | 70 | 20.7 | 41.4 | 3.0 |
| estrogen signalling | 3 | 10 | 23 | 30.0 | 43.5 | 2.9 |
| G Protein Signaling Pathways | 6 | 32 | 94 | 18.8 | 34.0 | 2.7 |

(B)

| IPI NO. | Symbol | Protein Name | Ratio |
|---|---|---|---|
| **Down-regulate Pathway** | | | |
| **Selenium Pathway** | | | |
| IPI00030877 | RP4-604K5.1 | 15 kDa selenoprotein | 0.56±0.02 |
| IPI00007118 | SERPINE1 | Endothelial plasminogen activator inhibitor | 0.41±0.05 |
| IPI00793181 | AC023024.1 | Selenoprotein S | 0.59±0.22 |
| **Up-regulated Pathway** | | | |
| **Cholesterol Biosynthesis** | | | |
| IPI00019407 | NSDHL | NAD(P)H steroid dehydrogenase | 1.45±0.09 |
| IPI00914566 | FDPS | Farnesyl diphosphate synthetase | 2.04±0.11 |
| IPI00022745 | MVD | Mevalonate-PP decarboxylase | 1.59±0.28 |
| IPI00009747 | LSS | Lanosterol cyclase | 1.66±0.03 |
| IPI00008599 | EBP | 3-beta-hydroxysteroid-delta(8),delta(7)-isomerase | 1.36 |

| IPI NO. | Symbol | Protein Name | Ratio |
|---|---|---|---|
| IPI00008475 | HMGCS1 | HMG-CoA synthase | 4.10±0.86 |
| IPI00295772 | CYP51A1 | Lanosterol 14 alpha-demethylase | 1.78±0.06 |
| IPI00020944 | FDFT1 | Squalene synthase | 4.19±0.67 |
| IPI00294501 | DHCR7 | 7-dehydrocholesterol reductase | 2.13±0.09 |
| IPI00010717 | MVK | Mevalonate kinase | 2.04 |
| IPI00220014 | IDI1 | Isopentenyl-PP-delta-isomerase | 3.17±0.36 |
| IPI00291419 | ACAT2 | Acetoacetyl-CoA acetyltransferase-2 | 1.68±0.12 |
| IPI00016703 | DHCR24 | Desmosterol reductase | 2.05±0.56 |
| | | **Signal Transduction of S1P Receptor** | |
| IPI00018195 | MAPK3 | Mitogen-activated protein kinase 3 | 1.40±0.15 |
| IPI00012866 | AKT1 | Protein kinase B | 1.49±0.18 |
| IPI00220578 | GNAI3 | G(i) alpha-3 | 1.49±0.27 |
| | | **Inflammatory Response Pathway** | |
| IPI00021033 | COL3A1 | Collagen alpha-1(III) chain | 2.14±0.50 |
| IPI00297646 | COL1A1 | Alpha-1 type I collagen | 1.39±0.11 |
| IPI00304962 | COL1A2 | Alpha-2 type I collagen | 1.39±0.14 |
| | | **IL-5 Signaling Pathway** | |
| IPI00784013 | JAK1 | Janus kinase 1 | 1.40±0.09 |
| IPI00011736 | PIK3R2 | Phosphatidylinositol 3-kinase 85 kDa regulatory subunit beta | 1.52±0.39 |
| IPI00012866 | AKT1 | Protein kinase B | 1.49±0.18 |
| IPI00219628 | PRKCB | Protein kinase C beta type | 1.96 |
| IPI00299086 | SDCBP | Melanoma differentiation-associated protein 9 | 1.80±0.22 |
| IPI00018195 | MAPK3 | Mitogen-activated protein kinase 3 | 1.40±0.15 |
| | | **Estrogen Signalling** | |
| IPI00027713 | CREB1 | Cyclic AMP-responsive element-binding protein 1 | 1.43 |
| IPI00026268 | GNB1 | Guanine nucleotide-binding protein G(I)/G(S)/G(T) subunit beta-1 | 1.37±0.17 |
| IPI00012866 | AKT1 | Protein kinase B | 1.49±0.18 |
| | | **G Protein Signaling Pathways** | |
| IPI00027240 | GNG5 | Guanine nucleotide-binding protein G(I)/G(S)/G(O) subunit gamma-5 | 1.93±0.01 |
| IPI00220578 | GNAI3 | G(i) alpha-3 | 1.49±0.27 |
| IPI00303297 | DNAJC25 | DnaJ homolog subfamily C member 25 | 1.80 |
| IPI00026268 | GNB1 | Guanine nucleotide-binding protein G(I)/G(S)/G(T) subunit beta-1 | 1.37±0.17 |
| IPI00003348 | GNB2 | G protein subunit beta-2 | 1.39±0.19 |
| IPI00219628 | PRKCB | Protein kinase C beta type | 1.96 |

**Table 2.4** GO annotation of significantly changed proteins by potassium dichromate treatment, as identified by GenMAPP analysis. (A) Summary of GO types. (B) List of proteins involved in different GO types.

(A)

| GO Name | Number Changed | Number Measured | Number in GO | Percent Changed | Percent Present | Z Score |
|---|---|---|---|---|---|---|
| **Down-regulated GO Type** | | | | | | |
| **Biological Process** | | | | | | |
| tissue regeneration | 3 | 9 | 35 | 33.3 | 25.7 | 5.8 |
| regulation of inflammatory response | 4 | 16 | 135 | 25.0 | 11.9 | 5.6 |
| cellular divalent inorganic cation homeostasis | 5 | 24 | 208 | 20.8 | 11.5 | 5.6 |
| regulation of cell-matrix adhesion | 3 | 11 | 43 | 27.3 | 25.6 | 5.1 |
| wound healing | 4 | 19 | 70 | 21.1 | 27.1 | 5.0 |
| muscle cell development | 3 | 12 | 40 | 25.0 | 30.0 | 4.9 |
| **Cellular Component** | | | | | | |
| contractile fiber | 3 | 9 | 40 | 33.3 | 22.5 | 5.8 |
| platelet alpha granule lumen | 3 | 10 | 48 | 30.0 | 20.8 | 5.4 |
| contractile fiber part | 5 | 37 | 125 | 13.5 | 29.6 | 4.2 |
| actin filament bundle | 3 | 25 | 39 | 12.0 | 64.1 | 2.9 |
| extracellular region | 10 | 160 | 2036 | 6.3 | 7.9 | 2.9 |
| **Molecular Function** | | | | | | |
| heparin binding | 4 | 16 | 126 | 25.0 | 12.7 | 5.6 |
| extracellular matrix binding | 3 | 13 | 39 | 23.1 | 33.3 | 4.6 |
| structural constituent of muscle | 3 | 14 | 45 | 21.4 | 31.1 | 4.4 |
| integrin binding | 4 | 26 | 78 | 15.4 | 33.3 | 4.1 |
| antioxidant activity | 3 | 22 | 57 | 13.6 | 38.6 | 3.2 |

| GO Name | Number Changed | Number Measured | Number in GO | Percent Changed | Percent Present | Z Score |
|---|---|---|---|---|---|---|
| **Up-regulated GO Type** | | | | | | |
| **Biological Process** | | | | | | |
| cholesterol biosynthetic process | 13 | 18 | 33 | 72.2 | 54.5 | 10.8 |
| epidermis development | 9 | 27 | 152 | 33.3 | 17.8 | 5.9 |
| skeletal system development | 9 | 30 | 175 | 30.0 | 17.1 | 5.5 |
| cell-cell signaling | 13 | 73 | 637 | 17.8 | 11.5 | 4.2 |
| digestive system process | 3 | 7 | 38 | 42.9 | 18.4 | 4.1 |
| homophilic cell adhesion | 3 | 7 | 137 | 42.9 | 5.1 | 4.1 |
| G-protein coupled receptor protein signaling pathway | 6 | 33 | 1127 | 18.2 | 2.9 | 2.9 |
| **Cellular Component** | | | | | | |
| fibrillar collagen | 5 | 6 | 12 | 83.3 | 50.0 | 7.9 |
| extrinsic to internal side of plasma membrane | 6 | 14 | 50 | 42.9 | 28.0 | 5.8 |
| extracellular matrix | 12 | 50 | 330 | 24.0 | 15.2 | 5.3 |
| basement membrane | 6 | 22 | 78 | 27.3 | 28.2 | 4.2 |
| extracellular region | 22 | 160 | 2036 | 13.8 | 7.9 | 4.1 |
| G-protein-coupled receptor binding | 46 | 481 | 3659 | 9.6 | 13.1 | 3.4 |
| **Molecular Function** | | | | | | |
| platelet-derived growth factor binding | 4 | 6 | 11 | 66.7 | 54.5 | 6.2 |
| extracellular matrix structural constituent | 8 | 22 | 87 | 36.4 | 25.3 | 5.9 |
| beta-amyloid binding | 3 | 5 | 22 | 60.0 | 22.7 | 5.0 |
| calcium ion binding | 18 | 128 | 764 | 14.1 | 16.8 | 3.8 |
| integrin binding | 6 | 26 | 78 | 23.1 | 33.3 | 3.6 |

(B)

| IPI NO. | Symbol | Protein Name | Ratio |
|---|---|---|---|
| | | **Down-regulated GO Type** | |
| | | **Biological Process** | |
| | | **Tissue Regeneration** | |
| IPI00010676 | PLAUR | Monocyte activation antigen Mo3 | 0.49±0.01 |
| IPI00007118 | SERPINE1 | Endothelial plasminogen activator inhibitor | 0.41±0.05 |
| IPI00927606 | GPX1 | Cellular glutathione peroxidase | 0.38 |
| | | **Regulation of Inflammatory Response** | |
| IPI00793181 | AC023024.1 | Selenoprotein S | 0.59±0.22 |
| IPI00025257 | SEMA7A | Semaphorin 7A | 0.62 |
| IPI00007118 | SERPINE1 | Endothelial plasminogen activator inhibitor | 0.41±0.05 |
| IPI00927606 | GPX1 | Cellular glutathione peroxidase | 0.38 |
| | | **Cellular Divalent Inorganic Cation Homeostasis** | |
| IPI00009943 | TPT1 | Tumor protein, translationally-controlled 1 | 0.74±0.02 |
| IPI00008750 | MT1H | Metallothionein-0 | 0.66±0.01 |
| IPI00022498 | MT2A | Metallothionein-2 | 0.53 |
| IPI00008711 | WFS1 | Wolframin | 0.68 |
| IPI00946154 | FGF2 | Basic fibroblast growth factor | 0.67±0.05 |
| | | **Regulation of Cell-matrix Adhesion** | |
| IPI00023529 | CDK6 | Cell division protein kinase 6 | 0.61±0.12 |
| IPI00007118 | SERPINE1 | Endothelial plasminogen activator inhibitor | 0.41±0.05 |
| IPI00941549 | PLEKHA2 | cDNA FLJ75843, highly similar to Homo sapiens pleckstrin homology domain containing, family A (phosphoinositide binding specific) member 2 (PLEKHA2), mRNA | 0.65 |
| | | **Wound Healing** | |
| IPI00855785 | FN1 | Anastellin | 0.66 |
| IPI00007118 | SERPINE1 | Endothelial plasminogen activator inhibitor | 0.41±0.05 |
| IPI00216135 | TPM1 | Alpha-tropomyosin | 0.64±0.10 |
| IPI00946154 | FGF2 | Basic fibroblast growth factor | 0.67±0.05 |
| | | **Muscle Cell Development** | |
| IPI00396967 | FHL2 | Four and a half LIM-domain protein 2 | 0.55±0.11 |
| IPI00873982 | MYH11 | Myosin heavy chain 11 smooth muscle isoform | 0.72 |
| IPI00927606 | GPX1 | Cellular glutathione peroxidase | 0.38 |

| IPI NO. | Symbol | Protein Name | Ratio |
|---|---|---|---|
| | | **Cellular Component** | |
| | | **Contractile Fiber** | |
| IPI00014516 | CALD1 | Caldesmon | 0.73±0.06 |
| IPI00216135 | TPM1 | Alpha-tropomyosin | 0.64±0.10 |
| IPI00873982 | MYH11 | Myosin heavy chain 11 smooth muscle isoform | 0.72 |
| | | **Platelet Alpha Granule Lumen** | |
| IPI00855785 | FN1 | Anastellin | 0.66 |
| IPI00007118 | SERPINE1 | Endothelial plasminogen activator inhibitor | 0.41±0.05 |
| IPI00759776 | ACTN1 | Alpha actin 1 | 0.73 |
| | | **Contractile Fiber Part** | |
| IPI00396967 | FHL2 | Four and a half LIM-domain protein 2 | 0.55±0.11 |
| IPI00646748 | TPM2 | Tropomyosin 2 (Beta) | 0.70 |
| IPI00216135 | TPM1 | Alpha-tropomyosin | 0.64±0.10 |
| IPI00873982 | MYH11 | Myosin heavy chain 11 smooth muscle isoform | 0.72 |
| IPI00759776 | ACTN1 | Alpha actin 1 | 0.73 |
| | | **Actin Filament Bundle** | |
| IPI00216135 | TPM1 | Alpha-tropomyosin | 0.64±0.10 |
| IPI00873982 | MYH11 | Myosin heavy chain 11 smooth muscle isoform | 0.72 |
| IPI00759776 | ACTN1 | Alpha actin 1 | 0.73 |
| | | **Extracellular Region** | |
| IPI00855785 | FN1 | Anastellin | 0.66 |
| IPI00018219 | TGFBI | Kerato-epithelin | 0.51±0.18 |
| IPI00010676 | PLAUR | Monocyte activation antigen Mo3 | 0.49±0.01 |
| IPI00299219 | CYR61 | CCN family member 1 | 0.58±0.10 |
| IPI00023020 | SEMG1 | Alpha-inhibin-31 | 0.36 |
| IPI00293307 | PLIN2 | Adipophilin | 0.36±0.15 |
| IPI00946154 | FGF2 | Basic fibroblast growth factor | 0.67±0.05 |
| IPI00740545 | POTEI | POTE ankyrin domain family, member I | 0.15±0.11 |
| IPI00007118 | SERPINE1 | Endothelial plasminogen activator inhibitor | 0.41±0.05 |
| IPI00759776 | ACTN1 | Alpha actin 1 | 0.73 |
| | | **Molecular Function** | |
| | | **Heparin Binding** | |
| IPI00855785 | FN1 | Anastellin | 0.66 |
| IPI00299219 | CYR61 | CCN family member 1 | 0.58±0.10 |
| IPI00946154 | FGF2 | Basic fibroblast growth factor | 0.67±0.05 |
| IPI00219153 | RPL22 | 60S ribosomal protein L22 | 0.74±0.20 |

| IPI NO. | Symbol | Protein Name | Ratio |
|---|---|---|---|
| | | **Extracellular Matrix Binding** | |
| IPI00018219 | TGFBI | Kerato-epithelin | 0.51±0.18 |
| IPI00299219 | CYR61 | CCN family member 1 | 0.58±0.10 |
| IPI00941549 | PLEKHA2 | cDNA FLJ75843, highly similar to Homo sapiens pleckstrin homology domain containing, family A (phosphoinositide binding specific) member 2 (PLEKHA2), mRNA | 0.65 |
| | | **Structural Constituent of Muscle** | |
| IPI00646748 | TPM2 | Tropomyosin 2 (Beta) | 0.70 |
| IPI00216135 | TPM1 | Alpha-tropomyosin | 0.64±0.10 |
| IPI00873982 | MYH11 | Myosin heavy chain 11 smooth muscle isoform | 0.72 |
| | | **Integrin Binding** | |
| IPI00018219 | TGFBI | Kerato-epithelin | 0.51±0.18 |
| IPI00025257 | SEMA7A | Semaphorin 7A | 0.62 |
| IPI00299219 | CYR61 | CCN family member 1 | 0.58±0.10 |
| IPI00759776 | ACTN1 | Alpha actin 1 | 0.73 |
| | | **Antioxidant Activity** | |
| IPI00793181 | AC023024.1 | Selenoprotein S | 0.59±0.22 |
| IPI00030877 | RP4-604K5.1 | 15 kDa selenoprotein | 0.56±0.02 |
| IPI00927606 | GPX1 | Cellular glutathione peroxidase | 0.38 |
| | | **Up-regulated GO Type** | |
| | | **Biological Process** | |
| | | **Cholesterol Biosynthetic Process** | |
| IPI00019407 | NSDHL | NAD(P)H steroid dehydrogenase | 1.45±0.09 |
| IPI00914566 | FDPS | Farnesyl diphosphate synthetase | 2.04±0.11 |
| IPI00008475 | HMGCS1 | HMG-CoA synthase | 4.10±0.86 |
| IPI00022745 | MVD | Mevalonate-PP decarboxylase | 1.59±0.28 |
| IPI00009747 | LSS | Lanosterol cyclase | 1.66±0.03 |
| IPI00008599 | EBP | 3-beta-hydroxysteroid-delta(8),delta(7)-isomerase | 1.36 |
| IPI00016703 | DHCR24 | Desmosterol reductase | 2.05±0.56 |
| IPI00295772 | CYP51A1 | Lanosterol 14 alpha-demethylase | 1.78±0.06 |
| IPI00020944 | FDFT1 | Squalene synthase | 4.19±0.67 |
| IPI00294501 | DHCR7 | 7-dehydrocholesterol reductase | 2.13±0.09 |
| IPI00010717 | MVK | Mevalonate kinase | 2.04 |
| IPI00291419 | ACAT2 | Acetoacetyl-CoA acetyltransferase-2 | 1.68±0.12 |
| IPI00220014 | IDI1 | Isopentenyl-PP-delta-isomerase | 3.17±0.36 |

| IPI NO. | Symbol | Protein Name | Ratio |
|---|---|---|---|
| | | **Epidermis Development** | |
| IPI00019407 | NSDHL | NAD(P)H steroid dehydrogenase | 1.45±0.09 |
| IPI00220327 | KRT1 | 67 kDa cytokeratin | 4.01±6.75 |
| IPI00016703 | DHCR24 | Desmosterol reductase | 2.05±0.56 |
| IPI00478390 | CDKN2A | Cyclin-dependent kinase inhibitor 2A, isoform 4 | 1.58 |
| IPI00216088 | CRABP2 | Cellular retinoic acid-binding protein 2 | 1.49±0.05 |
| IPI00739099 | COL5A2 | Collagen alpha-2(V) chain | 1.65±0.64 |
| IPI00021033 | COL3A1 | Collagen alpha-1(III) chain | 2.14±0.50 |
| IPI00297646 | COL1A1 | Alpha-1 type I collagen | 1.39±0.11 |
| IPI00844090 | COL5A1 | Collagen alpha-1(V) chain | 1.38±0.35 |
| | | **Skeletal System Development** | |
| IPI00739099 | COL5A2 | Collagen alpha-2(V) chain | 1.65±0.64 |
| IPI00008599 | EBP | 3-beta-hydroxysteroid-delta(8),delta(7)-isomerase | 1.36 |
| IPI00395596 | AES | Amino-terminal enhancer of split | 2.03 |
| IPI00023832 | SH3PXD2B | Adapter protein HOFI | 1.39±0.07 |
| IPI00021033 | COL3A1 | Collagen alpha-1(III) chain | 2.14±0.50 |
| IPI00465431 | LGALS3 | 35 kDa lectin | 1.59±0.07 |
| IPI00304227 | CDH11 | Cadherin-11 | 1.83 |
| IPI00304962 | COL1A2 | Alpha-2 type I collagen | 1.39±0.14 |
| IPI00297646 | COL1A1 | Alpha-1 type I collagen | 1.39±0.11 |
| | | **Cell-cell Signaling** | |
| IPI00024307 | EFNB1 | Ephrin-B1 | 1.63 |
| IPI00027240 | GNG5 | Guanine nucleotide-binding protein G(I)/G(S)/G(O) subunit gamma-5 | 1.93±0.01 |
| IPI00220578 | GNAI3 | G(i) alpha-3 | 1.49±0.27 |
| IPI00027713 | CREB1 | Cyclic AMP-responsive element-binding protein 1 | 1.43 |
| IPI00026268 | GNB1 | Guanine nucleotide-binding protein G(I)/G(S)/G(T) subunit beta-1 | 1.37±0.17 |
| IPI00003348 | GNB2 | G protein subunit beta-2 | 1.39±0.19 |
| IPI00247063 | MME | Atriopeptidase | 1.64±0.33 |
| IPI00084828 | STXBP1 | Syntaxin binding protein 1 | 1.39 |
| IPI00219628 | PRKCB | Protein kinase C beta type | 1.96 |
| IPI00299086 | SDCBP | Melanoma differentiation-associated protein 9 | 1.80±0.22 |
| IPI00027462 | S100A9 | Calgranulin-B | 10.60 |
| IPI00012069 | NQO1 | Azoreductase | 1.49±0.61 |
| IPI00402231 | DNAJC5 | Cysteine string protein | 1.43±0.12 |
| | | **Digestive System Process** | |
| IPI00000070 | LDLR | Low-density lipoprotein receptor | 3.21±0.90 |
| IPI00008726 | IREB2 | Iron regulatory protein 2 | 1.38 |
| IPI00022990 | STATH | Statherin | 11.11 |

| IPI NO. | Symbol | Protein Name | Ratio |
|---|---|---|---|
| | | **Homophilic Cell Adhesion** | |
| IPI00304227 | CDH11 | Cadherin-11 | 1.83 |
| IPI00107831 | PTPRF | Leukocyte common antigen related | 2.18 |
| IPI00018311 | NPTN | Neuroplastin | 1.37±0.23 |
| | | **G-protein coupled receptor protein signaling pathway** | |
| IPI00027240 | GNG5 | Guanine nucleotide-binding protein G(I)/G(S)/G(O) subunit gamma-5 | 1.93±0.01 |
| IPI00220578 | GNAI3 | G(i) alpha-3 | 1.49±0.27 |
| IPI00303297 | DNAJC25 | DnaJ homolog subfamily C member 25 | 1.80 |
| IPI00026268 | GNB1 | Guanine nucleotide-binding protein G(I)/G(S)/G(T) subunit beta-1 | 1.37±0.17 |
| IPI00012866 | AKT1 | Protein kinase B | 1.49±0.18 |
| IPI00003348 | GNB2 | G protein subunit beta-2 | 1.39±0.19 |
| | | **Cellular Component** | |
| | | **Fibrillar Collagen** | |
| IPI00844090 | COL5A1 | Collagen alpha-1(V) chain | 1.38±0.35 |
| IPI00021033 | COL3A1 | Collagen alpha-1(III) chain | 2.14±0.50 |
| IPI00739099 | COL5A2 | Collagen alpha-2(V) chain | 1.65±0.64 |
| IPI00304962 | COL1A2 | Alpha-2 type I collagen | 1.39±0.14 |
| IPI00297646 | COL1A1 | Alpha-1 type I collagen | 1.39±0.11 |
| | | **Extrinsic to Internal Side of Plasma Membrane** | |
| IPI00027240 | GNG5 | Guanine nucleotide-binding protein G(I)/G(S)/G(O) subunit gamma-5 | 1.93±0.01 |
| IPI00220578 | GNAI3 | G(i) alpha-3 | 1.49±0.27 |
| IPI00303297 | DNAJC25 | DnaJ homolog subfamily C member 25 | 1.80 |
| IPI00026268 | GNB1 | Guanine nucleotide-binding protein G(I)/G(S)/G(T) subunit beta-1 | 1.37±0.17 |
| IPI00027463 | S100A6 | Calcyclin | 1.46 |
| IPI00303297 | DNAJC25 | DnaJ homolog subfamily C member 25 | 1.80 |
| IPI00001883 | SNX9 | SH3 and PX domain-containing protein 1 | 1.48 |
| | | **Extracellular Matrix** | |
| IPI00006971 | CD248 | Endosialin | 1.51 |
| IPI00299738 | PCOLCE | Procollagen C-endopeptidase enhancer 1 | 1.78±0.16 |
| IPI00218803 | FBLN1 | Fibulin-1 | 1.47 |
| IPI00645849 | ECM1 | Extracellular matrix protein 1 | 1.70±0.20 |
| IPI00844090 | COL5A1 | Collagen alpha-1(V) chain | 1.38±0.35 |
| IPI00739099 | COL5A2 | Collagen alpha-2(V) chain | 1.65±0.64 |
| IPI00027166 | TIMP2 | TIMP metallopeptidase inhibitor 2 | 1.51±0.36 |
| IPI00021033 | COL3A1 | Collagen alpha-1(III) chain | 2.14±0.50 |
| IPI00465431 | LGALS3 | 35 kDa lectin | 1.59±0.07 |
| IPI00297646 | COL1A1 | Alpha-1 type I collagen | 1.39±0.11 |
| IPI00176193 | COL14A1 | Collagen alpha-1(XIV) chain | 3.33±4.49 |
| IPI00304962 | COL1A2 | Alpha-2 type I collagen | 1.39±0.14 |

| IPI NO. | Symbol | Protein Name | Ratio |
|---|---|---|---|
| | | **Basement Membrane** | |
| IPI00028911 | DAG1 | Alpha-dystroglycan | 1.38 |
| IPI00218803 | FBLN1 | Fibulin-1 | 1.47 |
| IPI00027166 | TIMP2 | TIMP metallopeptidase inhibitor 2 | 1.51±0.36 |
| IPI00844090 | COL5A1 | Collagen alpha-1(V) chain | 1.38±0.35 |
| IPI00642259 | DST | 230 kDa bullous pemphigoid antigen | 1.64±0.97 |
| IPI00032293 | CST3 | Cystatin-3 | 1.41±0.28 |
| | | **Extracellular Region** | |
| IPI00028911 | DAG1 | Alpha-dystroglycan | 1.38 |
| IPI00299738 | PCOLCE | Procollagen C-endopeptidase enhancer 1 | 1.78±0.16 |
| IPI00410297 | HPSE | Endo-glucoronidase | 2.45 |
| IPI00329598 | HSD17B11 | 17-beta-hydroxysteroid dehydrogenase 11 | 1.56±0.14 |
| IPI00022990 | STATH | Statherin | 11.11 |
| IPI00739099 | COL5A2 | Collagen alpha-2(V) chain | 1.65±0.64 |
| IPI00026314 | GSN | Actin-depolymerizing factor | 1.44±0.12 |
| IPI00847793 | DCD | Dermcidin isoform 2 | 2.12±3.46 |
| IPI00844090 | COL5A1 | Collagen alpha-1(V) chain | 1.38±0.35 |
| IPI00301579 | NPC2 | cDNA FLJ59142, highly similar to Epididymal secretory protein E1 | 1.47±0.10 |
| IPI00176193 | COL14A1 | Collagen alpha-1(XIV) chain | 3.33±4.49 |
| IPI00027462 | S100A9 | Calgranulin-B | 10.60 |
| IPI00945846 | PRSS1 | Alpha-trypsin chain 1 | 46.16±79.91 |
| IPI00306046 | EDIL3 | Developmentally-regulated endothelial cell locus 1 protein | 1.47±0.71 |
| IPI00218803 | FBLN1 | Fibulin-1 | 1.47 |
| IPI00645849 | ECM1 | Extracellular matrix protein 1 | 1.70±0.20 |
| IPI00395488 | VASN | Protein slit-like 2 | 1.42±0.42 |
| IPI00027166 | TIMP2 | TIMP metallopeptidase inhibitor 2 | 1.51±0.36 |
| IPI00021033 | COL3A1 | Collagen alpha-1(III) chain | 2.14±0.50 |
| IPI00297646 | COL1A1 | Alpha-1 type I collagen | 1.39±0.11 |
| IPI00304962 | COL1A2 | Alpha-2 type I collagen | 1.39±0.14 |
| IPI00032293 | CST3 | Cystatin-3 | 1.41±0.28 |
| | | **G-protein coupled receptor binding** | |
| IPI00026268 | GNB1 | Guanine nucleotide-binding protein G(I)/G(S)/G(T) subunit beta-1 | 1.37±0.17 |
| IPI00220578 | GNAI3 | G(i) alpha-3 | 1.49±0.27 |
| IPI00299086 | SDCBP | Melanoma differentiation-associated protein 9 | 1.80±0.22 |
| IPI00003527 | SLC9A3R1 | Ezrin-radixin-moesin-binding phosphoprotein 50 | 1.40±0.34 |

| IPI NO. | Symbol | Protein Name | Ratio |
|---|---|---|---|
| | | **Molecular Function** | |
| | | **Platelet-derived Growth Factor Binding** | |
| IPI00844090 | COL5A1 | Collagen alpha-1(V) chain | 1.38±0.35 |
| IPI00021033 | COL3A1 | Collagen alpha-1(III) chain | 2.14±0.50 |
| IPI00297646 | COL1A1 | Alpha-1 type I collagen | 1.39±0.11 |
| IPI00304962 | COL1A2 | Alpha-2 type I collagen | 1.39±0.14 |
| | | **Extracellular Matrix Structural Constituent** | |
| IPI00218803 | FBLN1 | Fibulin-1 | 1.47 |
| IPI00022990 | STATH | Statherin | 11.11 |
| IPI00844090 | COL5A1 | Collagen alpha-1(V) chain | 1.38±0.35 |
| IPI00739099 | COL5A2 | Collagen alpha-2(V) chain | 1.65±0.64 |
| IPI00021033 | COL3A1 | Collagen alpha-1(III) chain | 2.14±0.50 |
| IPI00297646 | COL1A1 | Alpha-1 type I collagen | 1.39±0.11 |
| IPI00176193 | COL14A1 | Collagen alpha-1(XIV) chain | 3.33±4.49 |
| IPI00304962 | COL1A2 | Alpha-2 type I collagen | 1.39±0.14 |
| | | **Beta-amyloid Binding** | |
| IPI00016014 | ITM2C | Cerebral protein 14 | 2.87 |
| IPI00032293 | CST3 | Cystatin-3 | 1.41±0.28 |
| IPI00004758 | LDLRAP1 | Autosomal recessive hypercholesterolemia protein | 1.55 |
| | | **Calcium Ion Binding** | |
| IPI00027462 | S100A9 | Calgranulin-B | 10.60 |
| IPI00006971 | CD248 | Endosialin | 1.51 |
| IPI00329784 | RYR3 | Brain ryanodine receptor-calcium release channel | 1.52 |
| IPI00219344 | HPCAL1 | Calcium-binding protein BDR-1 | 1.65±0.28 |
| IPI00004312 | STAT2 | Signal transducer and activator of transcription 2 | 1.37±0.30 |
| IPI00307257 | TBC1D9B | TBC1 domain family member 9B | 1.42±0.38 |
| IPI00000070 | LDLR | Low-density lipoprotein receptor | 3.21±0.90 |
| IPI00218803 | FBLN1 | Fibulin-1 | 1.47 |
| IPI00027463 | S100A6 | Calcyclin | 1.46 |
| IPI00909366 | MYL6B | cDNA FLJ60058, highly similar to Myosin light chain 1, slow-twitch muscle A isoform | 2.14±1.79 |
| IPI00100980 | EHD2 | EH domain-containing protein 2 | 1.48±0.19 |
| IPI00398625 | HRNR | Hornerin | 1.92±3.15 |
| IPI00026314 | GSN | Actin-depolymerizing factor | 1.44±0.12 |
| IPI00642259 | DST | 230 kDa bullous pemphigoid antigen | 1.64±0.97 |
| IPI00304227 | CDH11 | Cadherin-11 | 1.83 |
| IPI00306046 | EDIL3 | Developmentally-regulated endothelial cell locus 1 protein | 1.47±0.71 |
| IPI00029144 | PPP2R3A | PP2A subunit B isoform PR72/PR130 | 1.52 |
| IPI00028911 | DAG1 | Alpha-dystroglycan | 1.38 |

| IPI NO. | Symbol | Protein Name | Ratio |
|---|---|---|---|
| | | **Integrin Binding** | |
| IPI00215997 | CD9 | CD9 antigen | 1.48±0.31 |
| IPI00306046 | EDIL3 | Developmentally-regulated endothelial cell locus 1 protein | 1.47±0.71 |
| IPI00844090 | COL5A1 | Collagen alpha-1(V) chain | 1.38±0.35 |
| IPI00027166 | TIMP2 | TIMP metallopeptidase inhibitor 2 | 1.51±0.36 |
| IPI00021033 | COL3A1 | Collagen alpha-1(III) chain | 2.14±0.50 |
| IPI00642259 | DST | 230 kDa bullous pemphigoid antigen | 1.64±0.97 |

# Chapter 3

# Monomethylarsonous Acid Inhibited Endogenous Cholesterol Biosynthesis in Human Skin Fibroblasts

## Introduction

Arsenic compounds are well-known human carcinogens. As an abundant element in the earth crust, the presence of high levels of arsenic in naturally contaminated drinking water poses a widespread public health problem worldwide [1]. In addition, anthropogenic activities involving the use of arsenicals as pesticides, rodenticides, and fungicides further exacerbate the situation [2]. Arsenic exposure was found to be associated with the development of skin, kidney, bladder, liver and lung cancers, as well as neurological and cardiovascular diseases [3]. Many mechanisms have been proposed to account for the carcinogenic effects of arsenic species [4]. In one mechanism, binding of As(III) with protein thiols is thought to disable critical proteins for regulating cell proliferation and metabolism [5]. Additionally, arsenic was proposed to elicit its cytotoxic and carcinogenic effects through the induction of oxidative stress [4, 6].

Among the different arsenic species, monomethylarsonous acid [MMA(III)], a metabolite of inorganic arsenic, possesses the highest degree of toxicity. Biomethylation is the major mechanism for the metabolism of inorganic arsenic to produce MMA(III), though the role of this transformation in arsenic toxicity is under debate. Traditionally, methylation is viewed as the primary detoxification process since organic arsenic

compounds can be detected in the urinary excretion [7]. This, however, becomes questionable, as mounting evidence supports that organic arsenic compounds are more toxic than their inorganic counterparts both *in vitro* [8] and *in vivo* [9]. Thus, a deep understanding of the modes of action for MMA(III) toxicity will help define the actual role of biomethylation in the toxification and detoxification of arsenic species.

Previous research about arsenic has focused on issues ranging from the detection and speciation of arsenic compounds to the interpretation of arsenic transport, metabolism, and toxicity [1, 10]. Genome-wide microarray analysis of human urothelial cells exposed with MMA(III) unveiled alterations of several biological processes and pathways including response to oxidative stress, enhanced cellular proliferation, anti-apoptosis, MAPK signaling, as well as inflammation [11]. Recent advances in mass spectrometry instrumentation and sample preparation methods provide the opportunity for conducting high-throughput and in-depth analysis of the alteration of the whole proteome [12]. Therefore, we reason that assessing the changes in global protein expression upon MMA(III) exposure may offer a more complete picture about the mechanisms of its toxicity [13].

In this study, we employed liquid chromatography-tandem mass spectrometry (LC-MS/MS), together with stable isotope labeling by amino acids in cell culture (SILAC) [14] and filter-aided sample preparation (FASP) [15], to examine the perturbation of cellular pathways induced by MMA(III) exposure. In total, we quantified approximately 6500 unique proteins, among which 198 and 105 were substantially increased and decreased, respectively, upon MMA(III) treatment. Notably, this study demonstrated, for

the first time, that MMA(III) exposure resulted in down-regulation of multiple enzymes engaged in *de novo* cholesterol biosynthesis. This finding, in combination with other experiments, supports that MMA(III) may exert its cytotoxic effect partly by inhibiting *de novo* cholesterol biosynthesis.

## Materials and methods

### Cell culture

All reagents unless otherwise stated were obtained from Sigma-Aldrich (St. Louis, MO), and all cell lines and cell culture reagents unless otherwise noted were from ATCC (Manassas, VA). MMA(III) and GM00637 cells were generously provided by Profs. X. Chris Le (University of Alberta) and Gerd P. Pfeifer (the City of Hope), respectively. GM00637 and HEK293T cells were cultured in Dulbecco's Modified Eagle's Medium (DMEM, ATCC) supplemented with 10% fetal bovine serum (FBS, Life Technologies, Grand Island, NY) and 100 IU/mL penicillin (ATCC). WM-266-4 cells were maintained under the above-mentioned conditions except that Eagle's Minimum Essential Medium (EMEM, ATCC) was used. Cells were cultured in a humidified atmosphere with 5% $CO_2$ at 37°C, with subculture at every 1-2 days.

MTT assay of dose-dependent cell viability was conducted using Cell Proliferation Kit 1 (Roche, Basel, Switzerland) and absorbance was recorded by Victor 2 plate reader (Perkin Elmer, Waltham, MA, Figure 3.1). Caspase 3 activity was examined by Western blot using caspase 3 antibody (Cell Signaling, Boston, MA) that detects the endogenous levels of full-length (35 kDa) and large fragments (17/19 kDa) of caspase-3 after cleavage at aspartic acid 175.

For SILAC labeling experiments, light lysine and arginine, or their stable isotope-labeled heavy counterparts ([$^{13}C_6$,$^{15}N_2$]-L-lysine and [$^{13}C_6$]-L-arginine, Sigma), were added to the DMEM medium without L-lysine and L-arginine (Thermo Scientific, Rockford, IL) at concentrations following ATCC formulation to give the complete light

and heavy DMEM media, respectively. GM00637 cells were maintained in the complete light or heavy DMEM medium with dialyzed FBS (Life Technologies, Grand Island, NY) for more than 10 days, corresponding to 5 cell doublings, to enable complete stable isotope incorporation into cells.

**Monomethylarsonous acid treatment and sample preparation**

GM00637 cells, at a density of ~ $5\times10^5$ cells/mL in the light or, after complete heavy isotope incorporation, the heavy DMEM medium without dialyzed FBS, were exposed with 2 μM MMA(III) for 24 h. Cells were harvested by centrifugation at 300× *g* at 4°C for 5 min, washed with ice-cold phosphate-buffered saline (PBS) for three times, and lysed with 4% sodium dodecyl sulfate (SDS). Subsequently, the mixture was heated at 95°C for 5 min and centrifuged at 16,000× *g* at 4°C for 5 min with supernatant collected. The total protein concentration was measured by Bicinchoninic Acid Kit for Protein Determination (Sigma). For the forward SILAC experiment, the light labeled, MMA(III)-treated cell lysate was mixed at 1:1 ratio (w/w) with the heavy labeled, control cell lysate (Figure 3.2A), whereas the labeling and MMA(III) treatment were reversed in the reverse SILAC experiment.

**Filter-aided sample preparation**

The above equi-mass mixture of light and heavy lysates were reduced with dithiothreitol (DTT) and processed with the FASP procedure [15] for the removal of detergents (SDS) and tryptic digestion, where 30 kDa Microcon filtration devices were used (Millipore, Billerica, MA). Briefly, 400 μg lysate was loaded onto the filtration devices, washed with 8 M urea twice, and centrifuged at 14000× *g* for 15 min. After the

centrifugation, the concentrates of proteins were alkylated with iodoacetamide (IAA), digested with trypsin (Promega, Madison, WI) at 37°C overnight, and the resulting peptides were collected by centrifugation of the filter units at 14000× *g* for 20 min.

**Off-line strong cation exchange (SCX) fractionation and desalting**

The above protein digest was reconstituted in 0.1% formic acid (FA) and loaded onto a PolySulfoethyl A SCX column (9.4 × 200 mm, 5 μm, 200 Å, PolyLC, Columbia, MD). Peptides were eluted with a linear gradient of 0-500 mM ammonium acetate in 0.1% FA over 90 min, and collected every 4.5 min for a total of 20 fractions. Each fraction of the above protein digest was desalted and purified by the OMIX $C_{18}$ pipette tips (Agilent, Santa Clara, CA). Formic acid solution (0.1%) was added until the solution pH of the peptide sample reached ~ 4. Initially, the OMIX $C_{18}$ tips were hydrated with $CH_3CN/H_2O$ (1:1, v/v), followed by equilibration with 0.1% formic acid. Subsequently, peptide samples were loaded onto the $C_{18}$ tip. After washing with 0.1% formic acid, bound peptides were eluted with $CH_3CN/H_2O$ (1:1, v/v).

**LC-MS and MS/MS**

An LTQ-Orbitrap Velos mass spectrometer was utilized for the on-line LC-MS/MS analysis, which was equipped with a nanoelectrospray ionization source and coupled to an EASY n-LCII HPLC system (Thermo, San Jose, CA). The experimental conditions were the same as those described elsewhere [16].

**Database search and pathway analysis**

Database search was conducted as previously published [16]. Briefly, the protein identification and quantification were performed using Maxquant [17], Version 1.2.2.5

based on the International Protein Index database, version 3.68. To obtain reliable results, the quantification of the protein expression ratio was based on three independent SILAC labeling experiments, which contained two forward and one reverse SILAC labelings. The threshold to define significantly changed proteins was calculated using Perseus 4.0 based on the corresponding significant A values (Figure 3.3) [17], where only those proteins with ratios being greater than 1.30 or less than 0.70 fold were considered significantly altered. Follow-up pathway analysis of significantly changed proteins was carried out with the use of Gene Map Annotator and Pathway Profiler (GenMAPP-CS) [18].

**RNA extraction and quantitative real-time PCR analysis**

Total RNA extraction of MMA(III)-treated and control GM00637 cells was performed using the Total RNA Kit 1 (VWR, Randor, PA), and reverse transcription using M-MLV reverse transcriptase (Promega, Madison, WI) and a poly(dT) primer. Subsequent qRT-PCR was conducted using iQ SYBR Green Supermix kit (Bio-Rad, Hercules, CA) and a Bio-Rad MyiQ thermal cycler. Gene-specific primers used for the analysis are listed in Table 3.1. Quantification of gene expression was performed with the comparative cycle threshold (*Ct*) method ($\Delta\Delta Ct$) [19], and the mRNA level of each gene was normalized to that of the *GAPDH* gene, which served as an internal control.

**Exogenous cholesterol addition and cell proliferation assay**

The cholesterol-BSA complex was prepared for cholesterol incorporation into living cells as previously published [20]. Briefly, 1% cholesterol in ethanol was mixed with water (1:1, v/v), which was then centrifuged at 2000× *g* for 10 min. Subsequently, the pellet was resuspended in an aqueous solution containing 0.25 M sucrose in 1 mM EDTA (pH 7.3), followed by a slow addition of 4 g bovine serum albumin (BSA, Sigma). The pH of the resultant solution was adjusted to 7.3 with Tris. After centrifugation at 12000× *g* for 10 min at 4°C, the supernatant was utilized for cholesterol rescue experiments.

GM00637, WM-266-4, and HEK293T cells were seeded in 24-well plates at a density of 1-1.5×$10^5$ cells/mL. After a 12- or 24-h treatment with or without MMA(III) in the presence of 0, 30 or 60 mg/L cholesterol, or selected intermediates of cholesterol biosynthesis pathway, cells were stained with trypan blue and viable cells counted on a hemocytometer.

**Extraction and determination of the cellular cholesterol level**

Cells were lysed with CelLytic M buffer (Sigma), and total protein content was determined using Bradford Assay (Bio-Rad). Subsequently, cholesterol was extracted with chloroform:methanol:water (2:1.1:0.9, v/v/v) as previously published [21]. After centrifugation, the bottom chloroform layer was washed with a methanol-water mixture (5:4, v/v) for three times and collected. Total cholesterol level was determined by HPLC and normalized against the corresponding total protein content, as described previously.[16]

## Results and discussion

### 1. MMA(III) treatment, sample preparation, protein identification, and quantification

The toxic modes of action of arsenic, including MMA(III), have been extensively studied. Arsenic may exert its cytotoxic effect through binding with protein thiols to induce malfunction of critical proteins [5]. In addition, exposure to MMA(III) may give rise to reactive oxygen species (ROS) in cells, which are capable of inducing DNA damage and triggering inflammatory response [4, 6]. However, MMA(III) may also act through other mechanisms. To investigate this, we utilized a quantitative proteomic technology to evaluate the MMA(III)-induced alteration of the global proteome in GM00637 human skin fibroblast cells. Initially, we determined the optimal dose of MMA(III) exposure by using a dose-dependent cell viability assay. From MTT assay, a less than 9% cell death was observed for GM00637 cells following exposure to 2 μM MMA(III) for 24 h. By contrast, a pronounced decline in cell survival (by ~30%) was induced by 8 μM MMA(III) (Figure 3.1). This result is consistent with previous findings with other mammalian cells treated with MMA(III) [8, 22]. In addition, treatment of 2 μM MMA(III) did not induce apparent apoptosis, as revealed by lack of caspase 3 activation (See Western blot result in Figure 3.3). Therefore, we chose 2 μM MMA(III) for the exposure experiment to minimize the apoptosis-induced perturbation of protein expression.

Upon complete SILAC labeling, GM00637 cells were treated with 2 μM MMA(III) for 24 h and lysed with SDS. The light and heavy cell lysates were combined

in equal mass, and subsequently purified and digested using the FASP protocol. After SCX fractionation, the resulting peptide mixtures were subjected to LC-MS/MS analysis.

Identification and quantification of the entire proteome were conducted using MaxQuant. Figure 3.4 shows the LC-MS/MS results of the peptide MLLNDFLNDQNR from 3-hydroxy-3-methylglutaryl-CoA synthase. The substantial decrease of this peptide in MMA(III)-exposed cells relative to control cells is evident from the MS results of samples obtained from both forward and reverse SILAC labeling experiments (Figure 3.4A and B), supporting the down-regulation of 3-hydroxy-3-methylglutaryl-CoA synthase. Additionally, the MS/MS results revealed the reliable identification of the corresponding light and heavy forms of the peptide (Figure 3.4C and D). In total, we were able to identify and quantify 7538 and 6543 proteins, respectively. Among them, 4220, 1074, and 1249 could be quantified in all three, only two, and only one SILAC labeling experiment, respectively (Figure 3.2B).

**2. Pathway analysis for significantly altered proteins upon MMA(III) exposure**

Figure 3.2C depicts the distribution of protein ratios representing alteration in protein expression triggered by MMA(III) exposure. The results showed that the expression of the majority of the quantified proteins (95.5%) was largely unchanged. To determine the threshold for screening significantly altered proteins, we utilized Perseus for the calculation of the significant A value for each protein [17], where significant A is plotted versus $\log_{10}$(Ratio) (Figure 3.5). From this plot, proteins with ratios $\leq$ 0.70- or $\geq$ 1.30-fold (Benjamini Hochberg FDR < 0.05) are categorized as significantly changed upon MMA(III) exposure; by using this criterion, we found that 105 and 198 proteins

were significantly down- and up-regulated, respectively (Table 3.2). All these proteins were analyzed in GenMAPP for pathway analysis, which revealed the down- and up-regulation of two and one pathways, respectively (Table 3.3).

**3. MMA(III)-inhibited *de novo* cholesterol biosynthesis**

Pathway analysis revealed that cholesterol biosynthesis was significantly inhibited upon MMA(III) treatment (Figure 3.6). Particularly, we quantified 18 enzymes in this pathway, 8 of which were substantially (by 0.56-0.70 fold, Figure 3.6), and 6 modestly (by 0.71-0.83 fold), down-regulated. In addition, the expression of low-density lipoprotein receptor (LDL receptor), a protein involved in the cellular uptake of LDL cholesterol [23], was reduced by 0.66 fold.

To exploit if the diminished expression of the cholesterol biosynthesis enzymes arises from decreased mRNA expression of the corresponding genes, we performed real-time PCR analysis of five select genes (*HMGCS1*, *HMGCR*, *FDPS*, *FDFT1* and *DHCR7*) involved in this pathway. It turned out that the mRNA expression levels of all the measured genes were substantially decreased (by 0.61-0.79 fold, Figure 3.7), demonstrating that the reduced expression of these enzymes at the protein level stems primarily from transcriptional regulation.

Sterol regulatory element binding proteins (SREBPs) are the common transcription factors for the transcriptional activation of genes involved in cholesterol biosynthesis, including *HMGCS1* and *HMGCR* [24]. The abundance of SREBPs is regulated, in part, by the liver X receptor (LXR) and retinoid X receptor (RXR) heterodimers [25]. It was reported previously that arsenic trioxide can inhibit LXR/RXR

via phosphorylation of RXR, thereby disrupting the nuclear receptor function of its binding partner [26]. Therefore, MMA(III) may deactivate the LXR/RXR heterodimer, thereby resulting in diminished SREBP synthesis, which subsequently gives rise to the down-regulation of genes involved in cholesterol biosynthesis.

**4. MMA(III)-induced reduction of intracellular cholesterol level and growth inhibition could be rescued by exogenous addition of cholesterol**

Given that several enzymes catalyzing cholesterol biosynthesis were down-regulated, we hypothesized that MMA(III) exposure may result in diminished production of cellular cholesterol. To explore this possibility, we measured the total cholesterol levels in GM00637 human skin fibroblast, WM-266-4 human melanoma, and HEK293T human embryonic kidney epithelial cells with or without MMA(III) exposure. Our results revealed substantial declines of the cholesterol level (by 0.58-0.70 fold) in all the three cell lines following a 24-h exposure with 2 μM MMA(III) (Figure 3.7B). This finding is in agreement with the MMA(III)-induced decreases, at both the mRNA and protein levels, of enzymes involved in the cholesterol biosynthesis. Thus, we conclude that MMA(III) inhibits *de novo* cholesterol biosynthesis.

On the basis of the above observations, we reasoned that the reduced endogenous cholesterol production may contribute to the cytotoxic effects of MMA(III). To test this, we assessed the MMA(III)-induced growth inhibition of cells and whether the inhibited cell proliferation could be abolished by the addition of exogenous cholesterol. Our results indeed showed that MMA(III) treatment caused substantial inhibition of proliferation of GM00637, WM-266-4 and HEK293T cells and this inhibition could be

restored by supplementation of cholesterol to the culture medium (Figure 3.8A-C). Consistently, the total cholesterol level returned to a comparable level as in control cells after a 24-h co-exposure with 2 μM MMA(III) and 60 mg/L cholesterol (Figure 3.7B). Therefore, growth inhibition caused by MMA(III) exposure of these cells may emanate primarily from the suppression of enzymes in cholesterol biosynthesis and the ensuing diminished *de novo* cholesterol production.

As a pivotal component of mammalian cell membrane, cholesterol plays a fundamental role in the maintenance of membrane permeability, fluidity, and membrane protein functions [24]. In addition, isoprenoid intermediates produced during cholesterol biosynthesis serve as lipid attachments for a variety of intracellular signaling molecules [27]. Thus, maintaining homeostasis in cholesterol biosynthesis is of utmost importance in cell proliferation, differentiation and apoptosis. In this vein, aberrant cellular cholesterol level has been reported as the primary cause of cytotoxicity induced by Cr(VI) [16] and some anti-cancer drugs [28].

Aside from cholesterol, several important intermediates, including mevalonic acid (MVA), farnesyl pyrophosphate (FPP) and geranylgeranyl pyrophosphate (GGPP), are known to play pivotal roles in cell signaling and proliferation. Inhibition of such intermediates alone may induce cell death through pathways such as non-canonical activation of RhoA and Rac1 GTPases [29]. Thus, there is some possibility that MMA(III), apart from perturbing intracellular cholesterol level, may also act through other pathways by inhibition of the aforementioned intermediates. However, supplementation with MVA, FPP or GGPP could not rescue the decreased cholesterol content or the growth

inhibition arising from MMA(III) treatment (Figure 3.9). Therefore, we conclude that the MMA(III)-induced cytotoxicity emanates primarily from the depletion of cholesterol, the final product of the cholesterol biosynthesis pathway, rather than the reduced formation of intermediates produced in this pathway.

**5. MMA(III)-induced perturbation of selenoprotein synthesis**

From the pathway analysis, we also observed the MMA(III)-induced perturbation of selenoproteins. In particular, MMA(III) treatment led to an increase of cytosolic thioredoxin reductase (TrxR1), but a decrease of selenoprotein M (Sel M). This finding is reminiscent of a previous study showing that exposure of human keratinocytes to MMA(III) could induce increase of TrxR1 and decrease of other small selenoproteins at both mRNA and protein levels [30]. Furthermore, several other studies have demonstrated the drop in activity of TrxR1 following MMA(III) exposure despite the overexpression of TrxR1, suggesting the strong inhibitory effect of MMA(III) on TrxR1 [31].

Selenoproteins possess critical functions in antioxidant defense [32]. For instance, it has been demonstrated that Sel M functions in reducing cellular ROS level and ROS-induced apoptotic cell death, as well as in maintaining cytosolic calcium level [33]. Aberrant selenoprotein synthesis is known to be associated with damage of DNA, protein and lipids, which can ultimately lead to apoptosis or carcinogenesis [32]. In this scenario, the decreased expression and/or activity of selenoprotein may result in a significant decline in the cells' ability to remove the ROS induced by MMA(III).

**6. MMA(III)-induced transcriptional activation of Nrf2 target genes**

In our quantitative proteomic experiment, we also found that the expression of multiple Nrf2 downstream genes was elevated following MMA(III) exposure. Nrf2 is a transcription factor known to mount a cellular response to defend cells against the deleterious effects of environmental toxicants [34]. Natural Nrf2 activators, such as *tert*-butylhydroquinone and sulforaphane, act through the canonical Keap1-cysteine residue 151 (C151)-dependent mechanism [35], and these activators have been suggested for the therapeutic and dietary interventions against the adverse effects of arsenic [36]. Paradoxically, the activation of Nrf2 is also implicated in cancer promotion [37]. Along this line, distinct from the aforementioned natural Nrf2 activators, trivalent arsenic, including arsenite and MMA(III), may trigger Nrf2 activation through a distinct mechanism that is independent of C151 in Keap1 [38]. Particularly, arsenic-induced activation of Nrf2 antioxidant pathway was found to involve the accumulation of p62, which induces the dysregulation of autophagy and ultimately results in the sequestration of Keap1, thereby hindering the Keap1-Cullin 3 E3 ubiquitin ligase complex from functioning properly to ubiquitinate Nrf2 [39]. This sustained activation has the potential to evoke arsenic toxicity and carcinogenicity instead of conferring protection.

We observed that several Nrf2 downstream targets, including glutamate-cysteine ligase and heme oxygenase-1, which are intracellular proteins involved in antioxidant defense, as well as NAD(P)H dehydrogenase [quinone] 1 (a.k.a. NAD(P)H:quinone oxidoreductase 1), which is a phase-II detoxifying enzyme, were up-regulated in human skin fibroblast cells upon MMA(III) treatment. This finding is in line with previous

results showing that both inorganic As(III) and MMA(III) could trigger the Nrf2-dependent response in human bladder urothelial cells [38]. Thus, our results suggest that the previously reported As(III)-induced Nrf2 activation is not restricted to a particular cell type.

## Conclusions

Human exposure to arsenic in drinking water is known to be correlated with the development of cancer and other human diseases [40]. MMA(III) is a toxic and stable arsenic metabolite, though the molecular mechanisms contributing to MMA(III) toxicity are not well understood. In the present study, we utilized an unbiased quantitative proteomic approach to evaluate the MMA(III)-induced perturbation of the entire proteome of GM00637 cells. Results from three independent sets of SILAC labeling experiments led to the quantification of 6543 unique proteins. Among them, 105 and 198 proteins were substantially down- and up-regulated, respectively, following a 24-h exposure to 2 μM MMA(III). Specifically, our study revealed that the cytotoxcity of MMA(III) may arise partly from the suppression of *de novo* cholesterol biosynthesis. In addition, the perturbation in selenoprotein synthesis and the activation of Nrf2 pathway may also lead to the adverse effect of MMA(III). Together, the results from the present study provide important new knowledge for the future clinical intervention towards MMA(III) exposure and, perhaps in general, arsenic exposure.

**References**


1. Mandal, B. K.; Suzuki, K. T., Arsenic round the world: a review. *Talanta* **2002,** *58* (1), 201-35.

2. Collotta, M.; Bertazzi, P. A.; Bollati, V., Epigenetics and pesticides. *Toxicology* **2013,** *307*, 35-41.

3. Bhattacharjee, P.; Banerjee, M.; Giri, A. K., Role of genomic instability in arsenic-induced carcinogenicity. A review. *Environ. Int.* **2013,** *53* (0), 29-40.

4. Kitchin, K. T., Recent advances in arsenic carcinogenesis: modes of action, animal model systems, and methylated arsenic metabolites. *Toxicol. Appl. Pharmacol.* **2001,** *172* (3), 249-61.

5. (a) Kitchin, K. T.; Wallace, K., The role of protein binding of trivalent arsenicals in arsenic carcinogenesis and toxicity. *J. Inorg. Biochem.* **2008,** *102* (3), 532-9; (b) Shen, S.; Li, X.-F.; Cullen, W. R.; Weinfeld, M.; Le, X. C., Arsenic binding to proteins. *Chem. Rev.* **2013**.

6. Flora, S. J., Arsenic-induced oxidative stress and its reversibility. *Free Radic. Biol. Med.* **2011,** *51* (2), 257-81.

7. Marafante, E.; Vahter, M.; Envall, J., The role of the methylation in the detoxication of arsenate in the rabbit. *Chem. Biol. Interact.* **1985,** *56* (2–3), 225-238.

8. Petrick, J. S.; Ayala-Fierro, F.; Cullen, W. R.; Carter, D. E.; Vasken Aposhian, H., Monomethylarsonous acid (MMA(III)) is more toxic than arsenite in Chang human hepatocytes. *Toxicol. Appl. Pharmacol.* **2000,** *163* (2), 203-7.

9. Petrick, J. S.; Jagadish, B.; Mash, E. A.; Aposhian, H. V., Monomethylarsonous acid (MMA(III)) and arsenite: LD(50) in hamsters and in vitro inhibition of pyruvate dehydrogenase. *Chem. Res. Toxicol.* **2001,** *14* (6), 651-6.

10. (a) Le, X. C.; Lu, X.; Li, X.-F., Arsenic speciation. *Anal. Chem.* **2004,** *76* (1), 26 A-33 A; (b) Watanabe, T.; Hirano, S., Metabolism of arsenic and its toxicological relevance. *Arch. Toxicol.* **2013,** *87* (6), 969-79.

11. Medeiros, M.; Zheng, X.; Novak, P.; Wnek, S. M.; Chyan, V.; Escudero-Lourdes, C.; Gandolfi, A. J., Global gene expression changes in human urothelial cells exposed to low-level monomethylarsonous acid. *Toxicol.* **2012,** *291* (1-3), 102-12.

12. Aebersold, R.; Mann, M., Mass spectrometry-based proteomics. *Nature* **2003,** *422* (6928), 198-207.

13. Greenbaum, D.; Colangelo, C.; Williams, K.; Gerstein, M., Comparing protein abundance and mRNA expression levels on a genomic scale. *Genome Biol.* **2003,** *4* (9), 117.

14. Ong, S. E.; Blagoev, B.; Kratchmarova, I.; Kristensen, D. B.; Steen, H.; Pandey, A.; Mann, M., Stable isotope labeling by amino acids in cell culture, SILAC, as a simple and accurate approach to expression proteomics. *Mol. Cell. Proteomics* **2002,** *1* (5), 376-86.

15. Wisniewski, J. R.; Zougman, A.; Nagaraj, N.; Mann, M., Universal sample preparation method for proteome analysis. *Nat. Methods* **2009,** *6* (5), 359-62.

16. Guo, L.; Xiao, Y.; Wang, Y., Hexavalent chromium-induced alteration of proteomic landscape in human skin fibroblast cells. *J. Proteome Res.* **2013,** *12* (7), 3511-3518.

17. Cox, J.; Mann, M., MaxQuant enables high peptide identification rates, individualized p.p.b.-range mass accuracies and proteome-wide protein quantification. *Nat. Biotechnol.* **2008,** *26* (12), 1367-1372.

18. Salomonis, N.; Hanspers, K.; Zambon, A.; Vranizan, K.; Lawlor, S.; Dahlquist, K.; Doniger, S.; Stuart, J.; Conklin, B.; Pico, A., GenMAPP 2: new features and resources for pathway analysis. *BMC Bioinformatics* **2007,** *8* (1), 217.

19. Livak, K. J.; Schmittgen, T. D., Analysis of relative gene expression data using real-time quantitative PCR and the $2^{-\Delta\Delta Ct}$ Method. *Methods* **2001,** *25* (4), 402-8.

20. Martinez, F.; Eschegoyen, S.; Briones, R.; Cuellar, A., Cholesterol increase in mitochondria: a new method of cholesterol incorporation. *J. Lipid Res.* **1988,** *29* (8), 1005-11.

21. Dong, X.; Xiong, L.; Jiang, X.; Wang, Y., Quantitative proteomic analysis reveals the perturbation of multiple cellular pathways in jurkat-T cells induced by doxorubicin. *J. Proteome Res.* **2010,** *9* (11), 5943-51.

22. (a) Charoensuk, V.; Gati, W. P.; Weinfeld, M.; Le, X. C., Differential cytotoxic effects of arsenic compounds in human acute promyelocytic leukemia cells. *Toxicol. Appl. Pharmacol.* **2009,** *239* (1), 64-70; (b) Shen, S.; Lee, J.; Cullen, W. R.; Le, X. C.; Weinfeld, M., Arsenite and its mono- and dimethylated trivalent metabolites enhance the formation of benzo[a]pyrene diol epoxide-DNA adducts in Xeroderma pigmentosum complementation group A cells. *Chem. Res. Toxicol.* **2009,** *22* (2), 382-90.

23. Defesche, J. C., Low-density lipoprotein receptor--its structure, function, and mutations. *Semin. Vasc. Med.* **2004,** *4* (1), 5-11.

24. Espenshade, P. J.; Hughes, A. L., Regulation of sterol synthesis in eukaryotes. *Annu. Rev. Genet.* **2007,** *41*, 401-27.

25. Repa, J. J.; Liang, G.; Ou, J.; Bashmakov, Y.; Lobaccaro, J. M.; Shimomura, I.; Shan, B.; Brown, M. S.; Goldstein, J. L.; Mangelsdorf, D. J., Regulation of mouse sterol regulatory element-binding protein-1c gene (SREBP-1c) by oxysterol receptors, LXRalpha and LXRbeta. *Genes Dev.* **2000,** *14* (22), 2819-30.

26. Mann, K. K.; Padovani, A. M. S.; Guo, Q.; Colosimo, A. L.; Lee, H.-Y.; Kurie, J. M.; Jr, W. H. M., Arsenic trioxide inhibits nuclear receptor function via SEK1/JNK-mediated RXRα phosphorylation. *J. Clin. Invest.* **2005,** *115* (10), 2924-2933.

27. Takemoto, M.; Liao, J. K., Pleiotropic effects of 3-hydroxy-3-methylglutaryl coenzyme a reductase inhibitors. *Arterioscler. Thromb. Vasc. Biol.* **2001,** *21* (11), 1712-9.

28. (a) Dong, X.; Xiao, Y.; Jiang, X.; Wang, Y., Quantitative proteomic analysis revealed lovastatin-induced perturbation of cellular pathways in HL-60 cells. *J. Proteome Res.* **2011,** *10* (12), 5463-71; (b) Zhang, F.; Dai, X.; Wang, Y., 5-Aza-2'-deoxycytidine induced growth inhibition of leukemia cells through modulating endogenous cholesterol biosynthesis. *Mol. Cell. Proteomics* **2012,** *11* (7), M111 016915.

29. Zhu, Y.; Casey, P. J.; Kumar, A. P.; Pervaiz, S., Deciphering the signaling networks underlying simvastatin-induced apoptosis in human cancer cells: evidence for non-canonical activation of RhoA and Rac1 GTPases. *Cell Death Dis.* **2013,** *4*, e568.

30. Ganyc, D.; Talbot, S.; Konate, F.; Jackson, S.; Schanen, B.; Cullen, W.; Self, W. T., Impact of trivalent arsenicals on selenoprotein synthesis. *Environ. Health Perspect.* **2007,** *115* (3), 346-53.

31. (a) Meno, S. R.; Nelson, R.; Hintze, K. J.; Self, W. T., Exposure to monomethylarsonous acid (MMA(III)) leads to altered selenoprotein synthesis in a primary human lung cell model. *Toxicol. Appl. Pharmacol.* **2009,** *239* (2), 130-6; (b) Lin, S.; Cullen, W. R.; Thomas, D. J., Methylarsenicals and arsinothiols are potent inhibitors of mouse liver thioredoxin reductase. *Chem. Res. Toxicol.* **1999,** *12* (10), 924-30.

32. Davis, C. D.; Tsuji, P. A.; Milner, J. A., Selenoproteins and cancer prevention. *Annu. Rev. Nutr.* **2012,** *32*, 73-95.

33. Reeves, M. A.; Bellinger, F. P.; Berry, M. J., The neuroprotective functions of selenoprotein M and its role in cytosolic calcium regulation. *Antioxid. Redox Signal.* **2010,** *12* (7), 809-18.

34. Kensler, T. W.; Wakabayashi, N.; Biswal, S., Cell survival responses to environmental stresses via the Keap1-Nrf2-ARE pathway. *Annu. Rev. Pharmacol. Toxicol.* **2007,** *47*, 89-116.

35. Lau, A.; Whitman, S. A.; Jaramillo, M. C.; Zhang, D. D., Arsenic-mediated activation of the Nrf2-Keap1 antioxidant pathway. *J. Biochem. Mol. Toxicol.* **2013,** *27* (2), 99-105.

36. Wang, X. J.; Sun, Z.; Chen, W.; Eblin, K. E.; Gandolfi, J. A.; Zhang, D. D., Nrf2 protects human bladder urothelial cells from arsenite and monomethylarsonous acid toxicity. *Toxicol. Appl. Pharmacol.* **2007,** *225* (2), 206-13.

37. Lau, A.; Villeneuve, N. F.; Sun, Z.; Wong, P. K.; Zhang, D. D., Dual roles of Nrf2 in cancer. *Pharmacol. Res.* **2008,** *58* (5-6), 262-70.

38. Wang, X. J.; Sun, Z.; Chen, W.; Li, Y.; Villeneuve, N. F.; Zhang, D. D., Activation of Nrf2 by arsenite and monomethylarsonous acid is independent of Keap1-C151: enhanced Keap1-Cul3 interaction. *Toxicol. Appl. Pharmacol.* **2008,** *230* (3), 383-9.

39. Lau, A.; Zheng, Y.; Tao, S.; Wang, H.; Whitman, S. A.; White, E.; Zhang, D. D., Arsenic inhibits autophagic flux, activating the Nrf2-Keap1 pathway in a p62-dependent manner. *Mol. Cell. Biol.* **2013,** *33* (12), 2436-46.

40. Smith, A. H.; Hopenhayn-Rich, C.; Bates, M. N.; Goeden, H. M.; Hertz-Picciotto, I.; Duggan, H. M.; Wood, R.; Kosnett, M. J.; Smith, M. T., Cancer risks from arsenic in drinking water. *Environ. Health Perspect.* **1992,** *97*, 259-67.

**Figure 3.1** Cell viability test with MTT assay of GM00637 cells after 24 h of treatment with 0, 0.25, 0.5, 1, 2, 4, 8 μM monomethylarsonous acid**.**

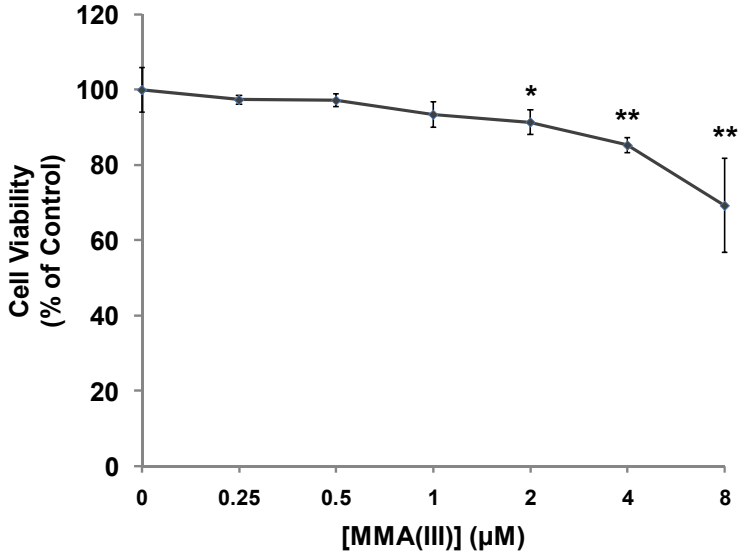

**Figure 3.2** Quantitative analysis of global proteome perturbation induced by monomethylarsonous acid exposure. (A) Flowchart of forward SILAC coupled with LC-MS/MS analysis to reveal the alteration of protein expression in GM00637 cells following monomethylarsonous acid exposure. (B) Venn diagram depicting the number of proteins quantified in two forward and one reverse SILAC experiments. (C) The distribution of expression ratios for the quantified proteins.

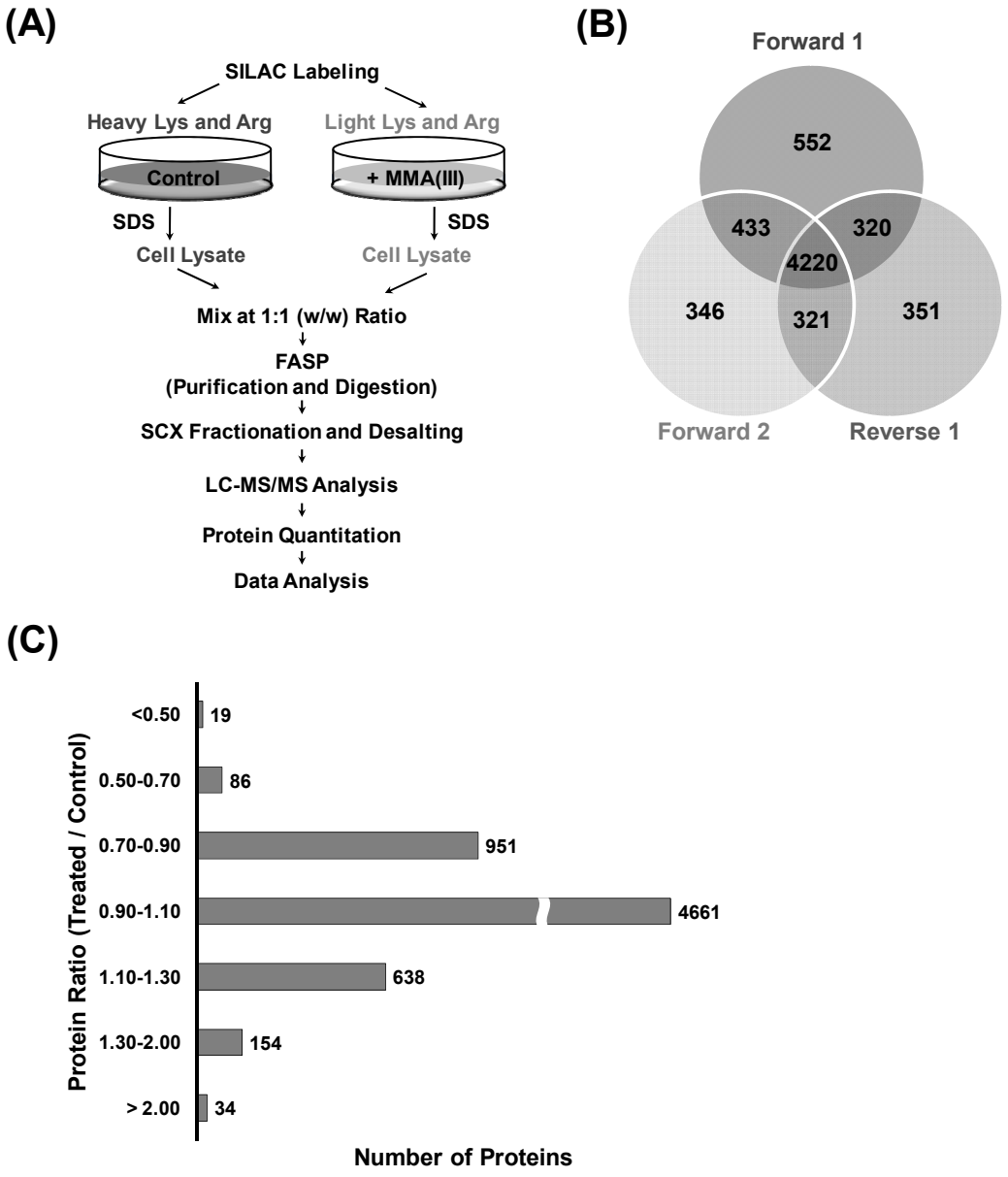
(A)
SILAC Labeling
Heavy Lys and Arg
Light Lys and Arg
Control
+ MMA(III)
SDS
SDS
Cell Lysate
Cell Lysate
Mix at 1:1 (w/w) Ratio
FASP
(Purification and Digestion)
SCX Fractionation and Desalting
LC-MS/MS Analysis
Protein Quantitation
Data Analysis
(B)
Forward 1
552
433
320
4220
346
321
351
Forward 2
Reverse 1
(C)
Protein Ratio (Treated / Control)
<0.50
19
0.50-0.70
86
0.70-0.90
951
0.90-1.10
4661
1.10-1.30
638
1.30-2.00
154
> 2.00
34
Number of Proteins

**Figure 3.3** Western blot for the detection of caspase 3 activity with and without 2 μM monomethylarsonous acid treatment.

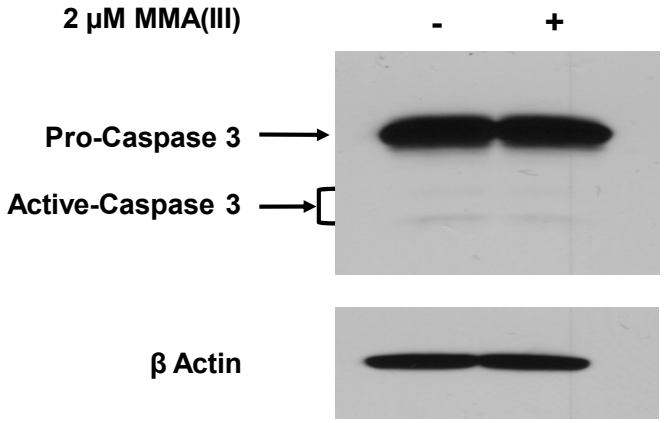

**Figure 3.4** Representative ESI-MS and MS/MS demonstrating the MMA(III)-induced down-regulation of 3-hydroxy-3-methylglutaryl-CoA synthase. Shown are the MS for the $[M+2H]^{2+}$ ions of HMG-CoA synthase peptide MLLNDFLNDQNR and MLLNDFLNDQNR* ("R*" designates the heavy labeled arginine) from one forward (A) and one reverse (B) SILAC experiments. Shown in (C) and (D) are the MS/MS for the $[M+2H]^{2+}$ ions of MLLNDFLNDQNR and MLLNDFLNDQNR*, respectively.

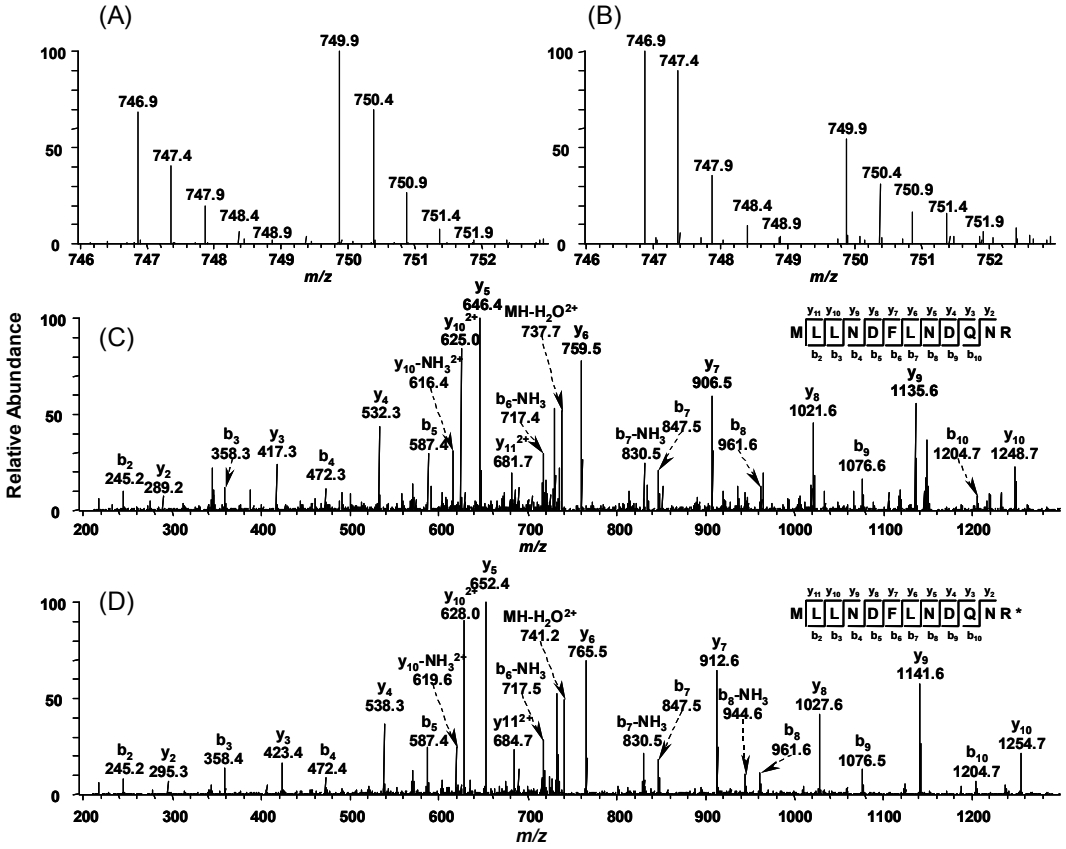

**Figure 3.5** Determination of the threshold value of significantly changed proteins by Perseus.

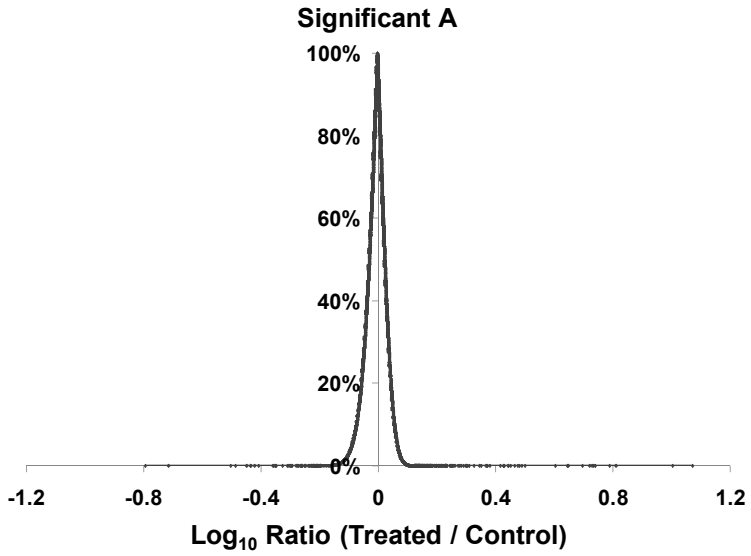

**Figure 3.6** MMA(III) induced down-regulation of enzymes involved in key steps of *de novo* cholesterol biosynthesis. The expression ratios (MMA(III)-treated/control) of quantified enzymes are shown. 'NA', not available; these enzymes were not quantified in any set of the SILAC experiments. The relative mRNA expression levels assessed by real-time PCR are depicted in parenthesis. The values are the mean of results measured from three independent experiments.

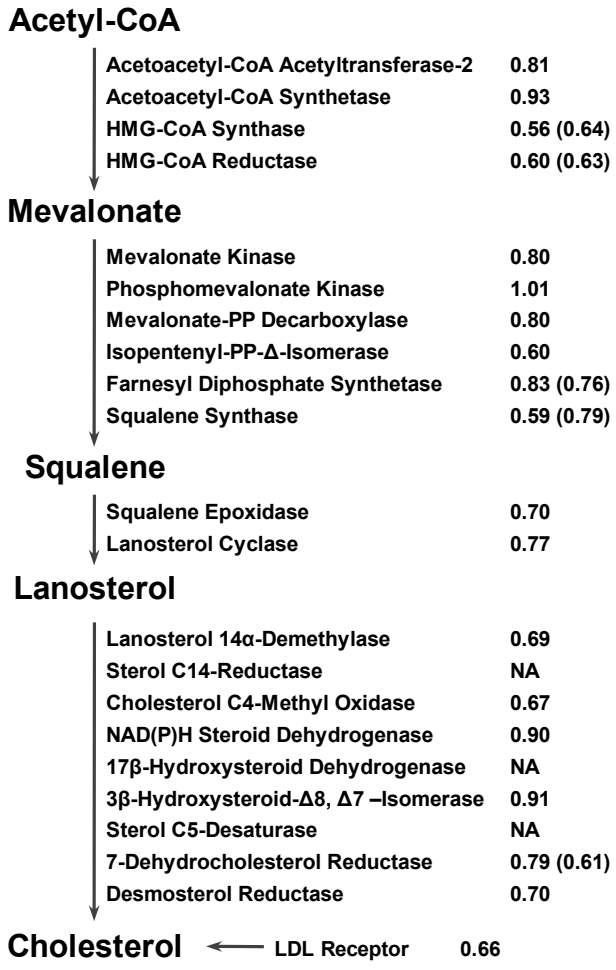

**Figure 3.7** Monomethylarsonous acid perturbed the mRNA expression levels of genes involved *de novo* cholesterol biosynthesis (A) and suppressed cholesterol biosynthesis in cells (B). Depicted in figure (A) are the histograms of relative mRNA expression levels of selected genes in the *de novo* cholesterol biosynthesis pathway in GM00637 cells with or without 2 μM MMA(III) exposure for 24 h. (B) Cholesterol contents of GM00637, WM-266-4 and HEK293T cells that were untreated or treated for 24 h with 2 μM MMA(III), alone or in combination with 60 mg/L cholesterol. Cellular cholesterol amount is normalized to that of the control. The values represent mean ± S.D. of results obtained from three independent experiments. '*', $p < 0.05$; '**', $p < 0.01$. The p values were calculated by using unpaired two-tailed *t*-test.

**(A)**

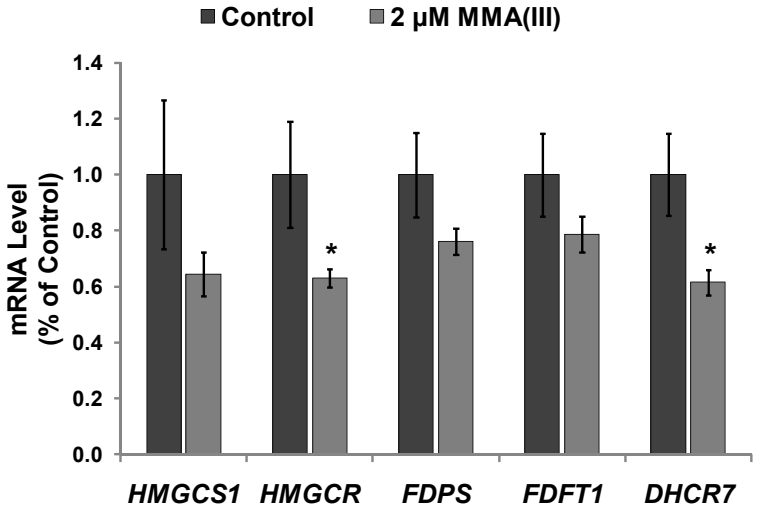
Control
2 μM MMA(III)
mRNA Level (% of Control)
1.4
1.2
1.0
0.8
0.6
0.4
0.2
0.0
*
*
HMGCS1
HMGCR
FDPS
FDFT1
DHCR7

**(B)**

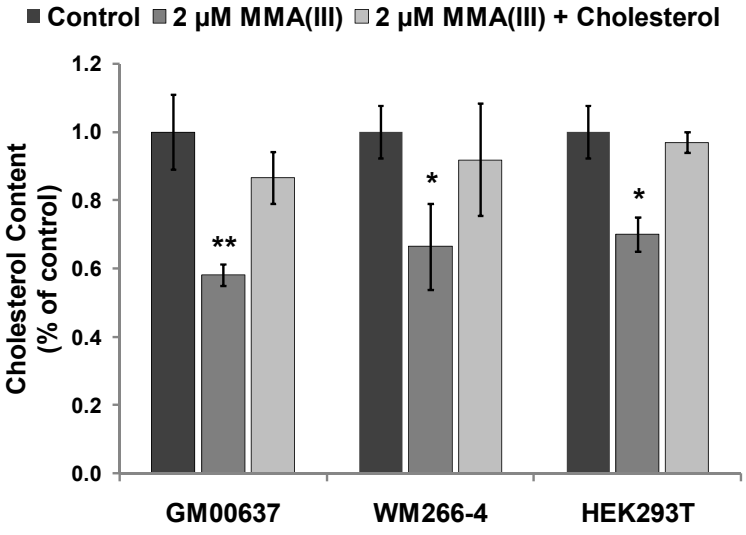
Control
2 μM MMA(III)
2 μM MMA(III) + Cholesterol
Cholesterol Content (% of control)
1.2
1.0
0.8
0.6
0.4
0.2
0.0
**
*
*
GM00637
WM266-4
HEK293T

**Figure 3.8** Monomethylarsonous acid-induced growth inhibition of cells could be abolished by addition of exogenous cholesterol. Number of viable GM00637 (A), WM-266-4 (B) and HEK293T (C) cells measured by trypan blue exclusion assay after 12 or 24 h of treatment with 0 (black dotted line), 30 (dark grey dash line) or 60 mg/L (light grey solid line) cholesterol alone (left), or together with 2 μM MMA(III) (right).

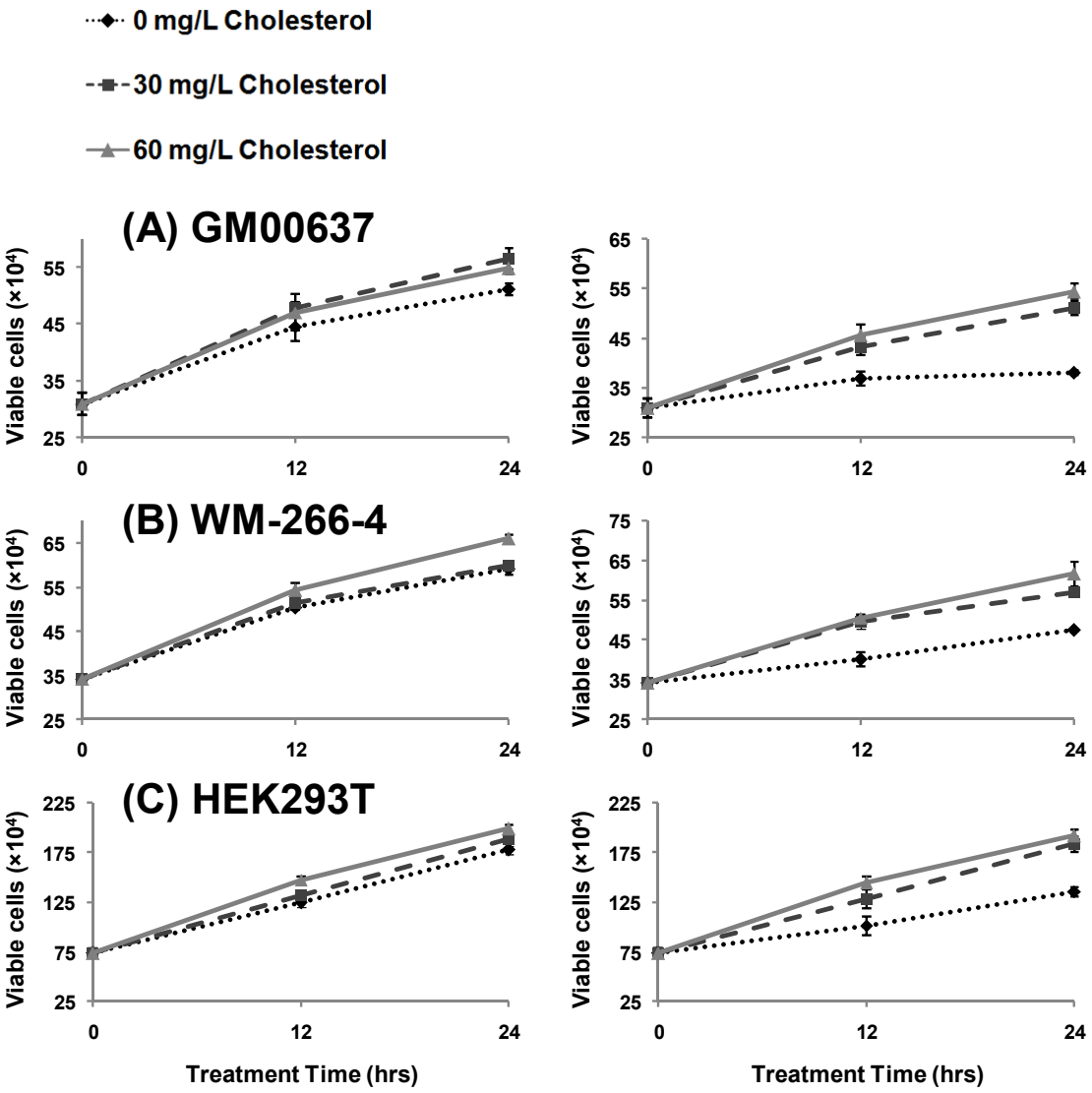

**Figure 3.9** Monomethylarsonous acid-induced decline of cholesterol biosynthesis and growth inhibition of cells cannot be recovered by addition of intermediates of cholesterol biosynthesis pathway. (A) Cholesterol content of GM00637 cell lines that were untreated or treated for 24 h with 2 μM MMA(III), alone or in combination with intermediates [mevalonic acid (MVA), farnesyl pyrophosphate (FPP) and geranylgeranyl pyrophosphate (GGPP)] of cholesterol biosynthesis pathway. Cholesterol content is expressed as fold change of the value from control. The cell viability of GM00637 (B) determined by Trypan Blue assay after 12 and 24 h of treatment intermediates alone (top), or together with 2 μM MMA(III) (bottom).

**(A)**

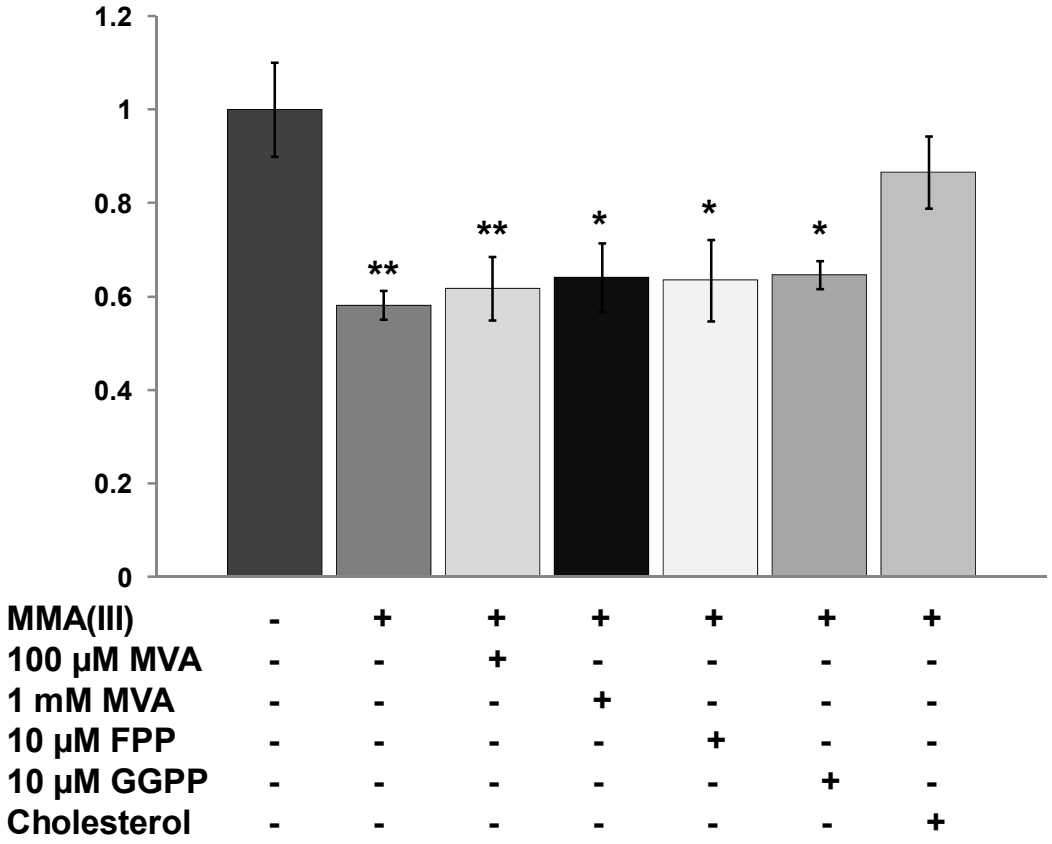
1.2
1
0.8
0.6
0.4
0.2
0
**
**
*
*
*
MMA(III) - + + + + + +
100 µM MVA - - + - - - -
1 mM MVA - - - + - - -
10 µM FPP - - - - + - -
10 µM GGPP - - - - - + -
Cholesterol - - - - - - +

**(B)**

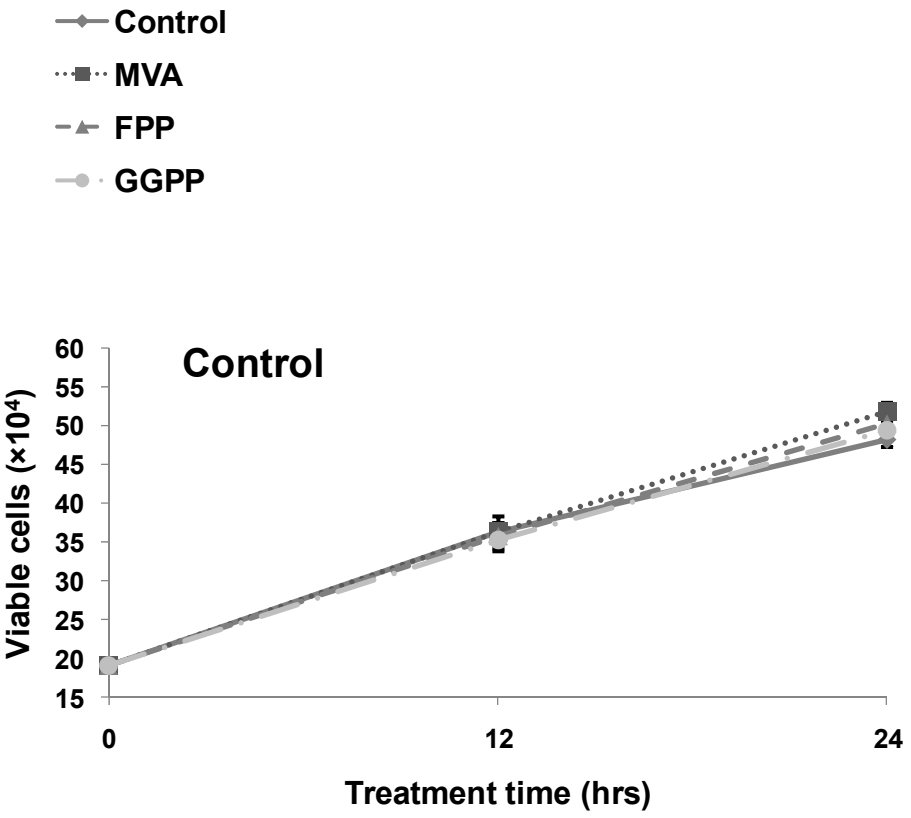
Control
MVA
FPP
GGPP
Control
Viable cells (×10⁴)
60
55
50
45
40
35
30
25
20
15
0
12
24
Treatment time (hrs)

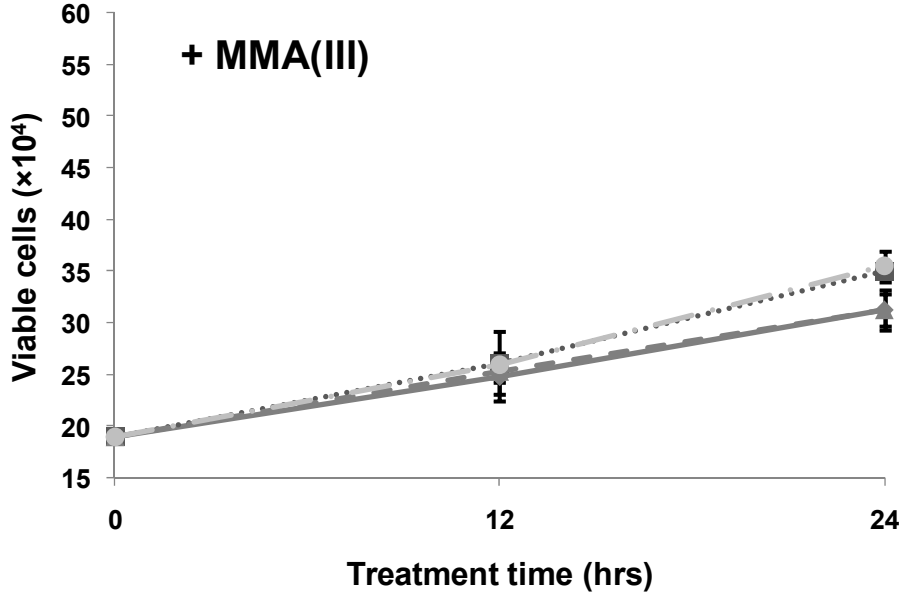
+ MMA(III)
Viable cells (×10⁴)
60
55
50
45
40
35
30
25
20
15
0
12
24
Treatment time (hrs)

**Table 3.1** List of primers for real-time PCR analysis as designed by Primer Premier 5.

| Genes | Forward Primer | Reverse Primer |
|---|---|---|
| *HMGCS1* | 5' - TGA AAA GCA CAG AAG AAC TTA CGC - 3' | 5' - TCT TGG CAG GGC TTG GAA TA - 3' |
| *HMGCR* | 5' - TGG GGA ATT GTC ACT TAT GG - 3' | 5' - GGG CTA TTC AGG CTG TCT TC - 3' |
| *FDPS* | 5' - CAA AAT TGG CAC TGA CAT CC - 3' | 5' - GCC ACT TTC TCA GCC TCC TT - 3' |
| *FDFT1* | 5' - CAA GCA GTG ACC CTG ATG AT - 3' | 5' - CTG AGT CGG GGA TTC TAT GA - 3' |
| *DHCR7* | 5' - TGC CTT ATC TTT ACA CGC TG - 3' | 5' - AAC AGG TCC TTC TGG TGG TT - 3' |

*HMGCS1*, 3-hydroxy-3-methylglutaryl-CoA synthase 1; *HMGCR*, 3-hydroxy-3-methylglutaryl-CoA reductase; *FDPS*, farnesyl diphosphate synthase; *FDFT1*, squalene synthase; *DHCR7*, 7-dehydrocholesterol reductase.

**Table 3.2** List of proteins with significantly changed expression ratio following MMA(III) exposure. The ratio is expressed as the average ratio in MMA(III)-treated cells versus control untreated cells. ('S.D.' designates standard deviation and "Significant A" is a p-value calculated by Perseus as an outlier significance score for logarithmized protein ratios).

| Protein IDs | Protein Names | Ratio | S.D. | Significant A |
|---|---|---|---|---|
| | **Down-regulated** | | | |
| IPI00154588 | signal peptide peptidase-like 2A | 0.16 | | 1.29E-19 |
| IPI00293665 | keratin 6B | 0.19 | | 3.04E-18 |
| IPI00157729 | ubiquitin domain containing 2 | 0.31 | 0.00 | 1.39E-13 |
| IPI00334605 | doublesex and mab-3 related transcription factor 2 | 0.33 | | 3.53E-13 |
| IPI00472416 | HLA class I histocompatibility antigen, B-45 alpha chain | 0.36 | | 4.00E-12 |
| IPI00010808 | interferon gamma receptor 1 | 0.37 | | 8.91E-12 |
| IPI00288988 | isoform 1 of uncharacterized protein KIAA1614 | 0.37 | | 1.00E-11 |
| IPI00783082 | tRNA isopentenyltransferase 1 | 0.38 | | 2.31E-11 |
| IPI00910937 | cDNA FLJ54803, highly similar to cyclin-dependent kinase inhibitor 1A (p21, Cip1) | 0.39 | | 5.32E-11 |
| IPI00063219 | nuclear assembly factor 1 homolog (S. cerevisiae) | 0.44 | | 1.52E-09 |
| IPI00647707 | aarF domain containing kinase 4 | 0.44 | | 1.63E-09 |
| IPI00008601 | glucocorticoid modulatory element binding protein 1 | 0.45 | | 2.50E-09 |
| IPI00884185 | protein-L-isoaspartate (D-aspartate) O-methyltransferase domain containing 2 | 0.45 | | 2.55E-09 |
| IPI00183786 | fatty acid desaturase 2 | 0.45 | 0.08 | 3.03E-09 |
| IPI00784651 | fatty acid desaturase 1 | 0.47 | 0.23 | 1.31E-08 |
| IPI00005502 | atrophin 1 | 0.49 | | 4.18E-08 |
| IPI00216346 | nucleolar protein 3 (apoptosis repressor with CARD domain) | 0.50 | | 6.23E-08 |
| IPI00002251 | pyruvate dehyrogenase phosphatase catalytic subunit 2 | 0.50 | | 8.79E-08 |
| IPI00748877 | centrosomal protein 120kDa | 0.50 | | 9.72E-08 |
| IPI00472138 | HLA class I histocompatibility antigen, B-58 alpha chain | 0.51 | | 1.00E-07 |
| IPI00220113 | isoform 2 of microtubule-associated protein 4 | 0.51 | | 1.25E-07 |
| IPI00000230 | isoform 2 of tropomyosin 1 (alpha) | 0.53 | | 3.46E-07 |
| IPI00419266 | NADH dehydrogenase (ubiquinone) 1 alpha subcomplex, 6, 14kDa | 0.53 | 0.09 | 5.00E-07 |
| IPI00012093 | serine/threonine kinase 25 (STE20 homolog, yeast) | 0.54 | | 5.83E-07 |
| IPI00651738 | acireductone dioxygenase 1 | 0.54 | 0.24 | 7.93E-07 |
| IPI00888042 | zinc finger protein 853 | 0.54 | | 9.51E-07 |
| IPI00103471 | selenoprotein M | 0.55 | | 1.32E-06 |
| IPI00217852 | peptidase M20 domain containing 2 | 0.55 | 0.29 | 1.34E-06 |
| IPI00926423 | cDNA FLJ77768, similar to fatty acid desaturase 1 | 0.55 | | 1.38E-06 |

| Protein IDs | Protein Names | Ratio | S.D. | Significant A |
|---|---|---|---|---|
| IPI00008475 | HMG-CoA synthase | 0.56 | 0.02 | 2.47E-06 |
| IPI00414985 | chromosome 13 open reading frame 27 | 0.56 | | 2.82E-06 |
| IPI00654810 | RANBP2-like and GRIP domain containing 1 | 0.57 | | 2.94E-06 |
| IPI00221233 | B-cell receptor-associated protein 29 | 0.58 | | 5.56E-06 |
| IPI00872352 | HD domain containing 2 | 0.58 | | 7.61E-06 |
| IPI00019590 | plasminogen activator, tissue | 0.58 | 0.03 | 7.77E-06 |
| IPI00470776 | family with sequence similarity 98, member C | 0.59 | | 1.21E-05 |
| IPI00020944 | squalene synthase | 0.59 | 0.09 | 1.23E-05 |
| IPI00554824 | shugoshin-like 1 (S. pombe) | 0.60 | | 1.41E-05 |
| IPI00220014 | isopentenyl-PP-delta-isomerase | 0.60 | 0.08 | 1.66E-05 |
| IPI00827503 | kinesin family member 20B | 0.60 | 0.03 | 2.09E-05 |
| IPI00021770 | HMG-CoA reductase | 0.60 | 0.06 | 2.11E-05 |
| IPI00166767 | F-box and leucine-rich repeat protein 6 | 0.60 | | 2.15E-05 |
| IPI00152815 | collagen and calcium binding EGF domains 1 | 0.61 | | 2.26E-05 |
| IPI00074258 | microtubule associated serine/threonine kinase-like | 0.61 | | 2.28E-05 |
| IPI00782966 | zinc finger protein 106 homolog (mouse) | 0.61 | | 2.78E-05 |
| IPI00397474 | extra spindle pole bodies homolog 1 (S. cerevisiae) | 0.61 | 0.05 | 3.34E-05 |
| IPI00447051 | B-cell CLL/lymphoma 7C | 0.62 | 0.48 | 3.57E-05 |
| IPI00218803 | fibulin 1 | 0.62 | | 3.75E-05 |
| IPI00719446 | chromosome 14 open reading frame 145 | 0.62 | 0.38 | 3.94E-05 |
| IPI00007702 | heat shock 70kDa protein 2 | 0.62 | | 4.12E-05 |
| IPI00151360 | GTP binding protein 2 | 0.62 | 0.47 | 4.65E-05 |
| IPI00304840 | collagen, type VI, alpha 2 | 0.62 | 0.13 | 4.91E-05 |
| IPI00926023 | CTD (carboxy-terminal domain, RNA polymerase II, polypeptide A) small phosphatase 1 | 0.62 | | 5.02E-05 |
| IPI00915334 | ubiquitin protein ligase E3 component n-recognin 3 (putative) | 0.62 | 0.00 | 5.04E-05 |
| IPI00556241 | SECIS binding protein 2 | 0.63 | | 5.99E-05 |
| IPI00018213 | leucine rich repeat containing 8 family, member D | 0.63 | 0.24 | 8.03E-05 |
| IPI00299738 | procollagen C-endopeptidase enhancer | 0.63 | 0.09 | 8.33E-05 |
| IPI00748490 | alanyl-tRNA synthetase domain containing 1 | 0.63 | 0.38 | 8.46E-05 |
| IPI00867551 | isoform 3 of diacylglycerol kinase, zeta 104kDa | 0.63 | | 8.48E-05 |
| IPI00014925 | RecQ protein-like 4 | 0.63 | | 8.62E-05 |
| IPI00177655 | leucine rich repeat containing 42 | 0.63 | | 8.75E-05 |
| IPI00553199 | RAD51 homolog (RecA homolog, E. coli) (S. cerevisiae) | 0.64 | | 1.07E-04 |
| IPI00221172 | ubiquitin protein ligase E3 component n-recognin 7 (putative) | 0.64 | 0.09 | 1.11E-04 |
| IPI00218094 | isoform 3 of protein ALO17 | 0.64 | | 1.18E-04 |
| IPI00018266 | ELK3, ETS-domain protein (SRF accessory protein 2) | 0.64 | | 1.19E-04 |
| IPI00910272 | cDNA FLJ52701, highly similar to calponin 2 | 0.65 | | 1.49E-04 |
| IPI00005573 | 5', 3'-nucleotidase, cytosolic | 0.65 | | 1.70E-04 |
| IPI00018037 | surfeit 2 | 0.65 | 0.16 | 1.76E-04 |
| IPI00101163 | MTERF domain containing 1 | 0.65 | | 1.88E-04 |
| IPI00796914 | aurora kinase B | 0.66 | 0.04 | 2.21E-04 |

| Protein IDs | Protein Names | Ratio | S.D. | Significant A |
|---|---|---|---|---|
| IPI00375915 | minichromosome maintenance complex component 10 | 0.66 | 0.12 | 2.49E-04 |
| IPI00797030 | isoform 1 of non-SMC condensin II complex, subunit G2 | 0.66 | | 2.51E-04 |
| IPI00000070 | low density lipoprotein receptor | 0.66 | 0.19 | 2.91E-04 |
| IPI00794198 | activating transcription factor 7 interacting protein | 0.67 | | 3.70E-04 |
| IPI00433138 | discoidin, CUB and LCCL domain containing 2 | 0.67 | 0.02 | 3.77E-04 |
| IPI00019899 | cholesterol C4-methyl oxidase | 0.67 | 0.13 | 3.94E-04 |
| IPI00023664 | CHK1 checkpoint homolog (S. pombe) | 0.67 | 0.03 | 4.59E-04 |
| IPI00940881 | multiple EGF-like-domains 6 | 0.68 | | 5.57E-04 |
| IPI00412410 | similar to growth arrest-specific 6 | 0.68 | 0.27 | 5.96E-04 |
| IPI00413780 | protein kinase N3 | 0.68 | | 6.19E-04 |
| IPI00010130 | glutamate-ammonia ligase (glutamine synthetase) | 0.68 | 0.34 | 6.38E-04 |
| IPI00292787 | ARP5 actin-related protein 5 homolog (yeast) | 0.68 | | 6.39E-04 |
| IPI00332157 | mitochondrial ribosomal protein L54 | 0.69 | | 7.59E-04 |
| IPI00021431 | nuclear receptor subfamily 2, group F, member 1 | 0.69 | | 7.70E-04 |
| IPI00335589 | RNA methyltransferase like 1 | 0.69 | | 8.46E-04 |
| IPI00294008 | ZW10 interactor | 0.69 | | 8.55E-04 |
| IPI00470629 | chromosome 2 open reading frame 34 | 0.69 | | 9.03E-04 |
| IPI00923477 | transporter 2, ATP-binding cassette, sub-family B (MDR/TAP) | 0.69 | | 9.10E-04 |
| IPI00418221 | mitogen-activated protein kinase kinase kinase 6 | 0.69 | 0.09 | 9.30E-04 |
| IPI00217049 | 2'-5'-oligoadenylate synthetase 2, 69/71kDa | 0.69 | | 9.37E-04 |
| IPI00032292 | TIMP metallopeptidase inhibitor 1 | 0.69 | 0.06 | 9.58E-04 |
| IPI00025418 | collagen, type VII, alpha 1 | 0.69 | 0.11 | 9.66E-04 |
| IPI00792838 | chromosome 19 open reading frame 42 | 0.69 | 0.41 | 9.76E-04 |
| IPI00295772 | lanosterol 14 alpha-demethylase | 0.69 | 0.08 | 1.03E-03 |
| IPI00332567 | isoform 4 of dedicator of cytokinesis 9 | 0.70 | | 1.10E-03 |
| IPI00305992 | RCC1-like G exchanging factor-like | 0.70 | | 1.14E-03 |
| IPI00910712 | cDNA FLJ57036, highly similar to tropomyosin 2 (beta) | 0.70 | | 1.17E-03 |
| IPI00008800 | MYC-associated zinc finger protein (purine-binding transcription factor) | 0.70 | | 1.26E-03 |
| IPI00420070 | ADAM metallopeptidase domain 15 | 0.70 | | 1.30E-03 |
| IPI00399304 | isoform 2 of protein regulator of cytokinesis 1 | 0.70 | | 1.32E-03 |
| IPI00328825 | NEDD4 binding protein 2 | 0.70 | | 1.35E-03 |
| IPI00644322 | PHD finger protein 15 | 0.70 | | 1.35E-03 |
| IPI00759481 | high mobility group AT-hook 2, isoform | 0.70 | | 1.45E-03 |
| IPI00291544 | squalene epoxidase | 0.70 | 0.06 | 1.48E-03 |
| IPI00016703 | desmosterol reductase | 0.70 | 0.09 | 1.57E-03 |
| | **Up-regulated** | | | |
| IPI00384643 | tumor protein p53 inducible protein 3 | 1.30 | 0.45 | 5.17E-04 |
| IPI00059368 | RFT1 homolog (S. cerevisiae) | 1.30 | | 5.04E-04 |
| IPI00021146 | PRP18 pre-mRNA processing factor 18 homolog (S. cerevisiae) | 1.30 | 0.50 | 4.71E-04 |

| Protein IDs | Protein Names | Ratio | S.D. | Significant A |
|---|---|---|---|---|
| IPI00006064 | TBK1 binding protein 1 | 1.30 | | 4.06E-04 |
| IPI00303283 | integrin, beta 3 (platelet glycoprotein IIIa, antigen CD61) | 1.30 | 0.36 | 3.89E-04 |
| IPI00013404 | SMAD family member 4 | 1.30 | | 3.75E-04 |
| IPI00855946 | sorting nexin family member 30 | 1.30 | | 3.72E-04 |
| IPI00003848 | DnaJ (Hsp40) homolog, subfamily B, member 4 | 1.30 | 0.06 | 3.55E-04 |
| IPI00297455 | A kinase (PRKA) anchor protein 8-like | 1.30 | 0.18 | 3.47E-04 |
| IPI00002569 | eukaryotic translation initiation factor 4E binding protein 1 | 1.31 | 0.20 | 3.34E-04 |
| IPI00218054 | chromosome 11 open reading frame 31 | 1.31 | 0.01 | 3.08E-04 |
| IPI00015944 | echinoderm microtubule associated protein like 2 | 1.31 | | 3.04E-04 |
| IPI00166945 | family with sequence similarity 101, member B | 1.31 | 0.04 | 2.64E-04 |
| IPI00184708 | solute carrier family 25, member 29 | 1.31 | 0.32 | 2.61E-04 |
| IPI00166835 | family with sequence similarity 26, member E | 1.31 | 0.03 | 2.51E-04 |
| IPI00022525 | lysophosphatidic acid receptor 1 | 1.31 | | 2.51E-04 |
| IPI00168554 | sulfiredoxin 1 homolog (S. cerevisiae) | 1.31 | | 2.48E-04 |
| IPI00019471 | insulin receptor substrate 1 | 1.31 | 0.23 | 2.41E-04 |
| IPI00334514 | isoform e precursor of sulfatase modifying factor 2 | 1.31 | | 2.23E-04 |
| IPI00418530 | ATP/GTP binding protein 1 | 1.31 | | 2.21E-04 |
| IPI00400838 | N/A | 1.32 | | 2.07E-04 |
| IPI00783902 | HEAT repeat containing 5A | 1.32 | | 1.94E-04 |
| IPI00643781 | PC4 and SFRS1 interacting protein 1 | 1.32 | | 1.87E-04 |
| IPI00793184 | peripherin | 1.32 | | 1.72E-04 |
| IPI00922695 | isoform 3 of GRAM domain containing 3 | 1.32 | | 1.56E-04 |
| IPI00013378 | topoisomerase (DNA) III alpha | 1.32 | | 1.49E-04 |
| IPI00307524 | arsenic (+3 oxidation state) methyltransferase | 1.32 | | 1.44E-04 |
| IPI00332887 | signal-regulatory protein alpha | 1.32 | 0.43 | 1.41E-04 |
| IPI00298199 | RIO kinase 3 (yeast) | 1.32 | | 1.40E-04 |
| IPI00020530 | acyl-CoA thioesterase 13 | 1.32 | 0.70 | 1.40E-04 |
| IPI00856115 | replication initiator 1 | 1.33 | | 1.35E-04 |
| IPI00410034 | solute carrier family 38, member 2 | 1.33 | 0.05 | 1.31E-04 |
| IPI00163565 | actin filament associated protein 1-like 1 | 1.33 | 0.19 | 1.27E-04 |
| IPI00913848 | fermitin family homolog 2 (Drosophila) | 1.33 | 0.53 | 1.26E-04 |
| IPI00954084 | HLA-C MHC class I antigen (fragment) | 1.33 | | 1.24E-04 |
| IPI00015890 | CCR4 carbon catabolite repression 4-like (S. cerevisiae) | 1.33 | | 1.21E-04 |
| IPI00646625 | transporter 1, ATP-binding cassette, sub-family B (MDR/TAP) | 1.33 | 0.63 | 1.20E-04 |
| IPI00219129 | NAD(P)H dehydrogenase, quinone 2 | 1.33 | | 1.05E-04 |
| IPI00030090 | ethanolamine kinase 1 | 1.33 | 0.47 | 9.42E-05 |
| IPI00030578 | vesicle amine transport protein 1 homolog (T. californica)-like | 1.33 | | 9.38E-05 |
| IPI00218539 | collagen, type XI, alpha 1 | 1.34 | 0.93 | 8.11E-05 |
| IPI00307545 | tensin 1 | 1.34 | 0.08 | 7.99E-05 |
| IPI00844046 | gem (nuclear organelle) associated protein 8 | 1.34 | | 7.83E-05 |
| IPI00107698 | fibroblast growth factor receptor substrate 2 | 1.34 | | 7.40E-05 |
| IPI00479793 | methionine sulfoxide reductase B3 | 1.34 | 0.09 | 6.80E-05 |

| Protein IDs | Protein Names | Ratio | S.D. | Significant A |
|---|---|---|---|---|
| IPI00293425 | frataxin | 1.34 | 0.43 | 5.32E-05 |
| IPI00008726 | iron-responsive element binding protein 2 | 1.34 | | 5.30E-05 |
| IPI00302962 | amphiphysin 1 variant CT4 (fragment) | 1.35 | | 5.22E-05 |
| IPI00946154 | fibroblast growth factor 2 (basic) | 1.35 | 0.50 | 4.91E-05 |
| IPI00176532 | junctophilin 2 | 1.35 | 0.12 | 4.00E-05 |
| IPI00166657 | F-box and WD repeat domain containing 8 | 1.35 | | 3.87E-05 |
| IPI00871430 | leupaxin | 1.35 | 1.06 | 3.51E-05 |
| IPI00004573 | polymeric immunoglobulin receptor | 1.36 | | 3.11E-05 |
| IPI00002469 | host cell factor C2 | 1.36 | | 2.84E-05 |
| IPI00761017 | transforming growth factor beta 1 induced transcript 1 | 1.36 | 0.35 | 2.66E-05 |
| IPI00412272 | SH3 domain binding glutamic acid-rich protein like 2 | 1.36 | | 2.28E-05 |
| IPI00027232 | insulin-like growth factor 1 receptor | 1.36 | | 2.17E-05 |
| IPI00856116 | palladin, cytoskeletal associated protein | 1.36 | 0.46 | 1.92E-05 |
| IPI00396967 | four and a half LIM domains 2 | 1.37 | 0.36 | 1.82E-05 |
| IPI00288964 | anoctamin 8 | 1.37 | | 1.51E-05 |
| IPI00553043 | LIM and calponin homology domains 1 | 1.37 | 0.59 | 1.43E-05 |
| IPI00007067 | GLI pathogenesis-related 2 | 1.37 | 0.68 | 1.27E-05 |
| IPI00884896 | thioredoxin reductase 1 | 1.37 | 0.19 | 1.14E-05 |
| IPI00289454 | MUS81 endonuclease homolog (S. cerevisiae) | 1.38 | | 9.86E-06 |
| IPI00179438 | disabled homolog 2, mitogen-responsive phosphoprotein (Drosophila) | 1.38 | 0.57 | 9.74E-06 |
| IPI00384180 | yrdC domain containing (E. coli) | 1.38 | | 9.71E-06 |
| IPI00332828 | carboxylesterase 2 (intestine, liver) | 1.38 | 0.65 | 8.76E-06 |
| IPI00554481 | solute carrier family 3 (activators of dibasic and neutral amino acid transport), member 2 | 1.38 | 0.14 | 8.36E-06 |
| IPI00453458 | nuclear receptor coactivator 7 | 1.38 | 0.10 | 7.53E-06 |
| IPI00470418 | dehydrogenase/reductase (SDR family) member 7 | 1.38 | | 7.08E-06 |
| IPI00306576 | arylsulfatase B | 1.39 | 0.09 | 6.29E-06 |
| IPI00024273 | very low density lipoprotein receptor | 1.39 | 0.82 | 5.80E-06 |
| IPI00001734 | chromosome 8 open reading frame 62 | 1.39 | 0.34 | 4.62E-06 |
| IPI00221375 | neuregulin 1 | 1.39 | | 4.51E-06 |
| IPI00018368 | bicaudal D homolog 1 (Drosophila) | 1.39 | 0.58 | 4.06E-06 |
| IPI00019971 | syntaxin binding protein 2 | 1.40 | | 3.25E-06 |
| IPI00025323 | microtubule-associated protein 9 | 1.40 | | 2.90E-06 |
| IPI00000783 | isoform 1 of proteasome (prosome, macropain) subunit, beta type, 8 | 1.40 | | 2.44E-06 |
| IPI00007694 | protein phosphatase methylesterase 1 | 1.41 | 0.68 | 2.09E-06 |
| IPI00386861 | peroxisomal biogenesis factor 16 | 1.41 | | 1.71E-06 |
| IPI00554777 | asparagine synthetase | 1.41 | 0.30 | 1.57E-06 |
| IPI00909845 | cDNA FLJ56409, highly similar to CHK1 checkpoint homolog (S. pombe) | 1.41 | | 1.39E-06 |
| IPI00018298 | interferon-induced protein with tetratricopeptide repeats 2 | 1.42 | 0.67 | 1.13E-06 |
| IPI00329075 | protein phosphatase 1, regulatory (inhibitor) subunit 12B | 1.42 | | 1.11E-06 |

| Protein IDs | Protein Names | Ratio | S.D. | Significant A |
|---|---|---|---|---|
| IPI00029733 | aldo-keto reductase family 1, member C1 | 1.43 | | 6.48E-07 |
| IPI00012069 | NAD(P)H dehydrogenase, quinone 1 | 1.43 | 0.17 | 4.95E-07 |
| IPI00435947 | WAS/WASL interacting protein family, member 2 | 1.43 | | 4.49E-07 |
| IPI00031821 | integral membrane protein 2B | 1.44 | | 3.40E-07 |
| IPI00455328 | schlafen family member 12-like | 1.44 | | 2.98E-07 |
| IPI00021076 | plakophilin 4 | 1.44 | | 2.78E-07 |
| IPI00015866 | ADP-ribosylation factor-like 2 binding protein | 1.44 | 0.69 | 2.72E-07 |
| IPI00020356 | microtubule-associated protein 1A | 1.44 | 0.85 | 2.21E-07 |
| IPI00027803 | poly (ADP-ribose) polymerase family, member 9 | 1.45 | | 1.92E-07 |
| IPI00398020 | odz, odd Oz/ten-m homolog 3 (Drosophila) | 1.45 | | 1.50E-07 |
| IPI00152875 | zinc finger protein 384 | 1.46 | | 1.03E-07 |
| IPI00021264 | calponin 1, basic, smooth muscle | 1.46 | 0.83 | 9.68E-08 |
| IPI00023529 | cyclin-dependent kinase 6 | 1.46 | 0.14 | 8.67E-08 |
| IPI00016839 | general transcription factor IIH, polypeptide 4, 52kDa | 1.47 | | 4.97E-08 |
| IPI00296360 | doublecortin-like kinase 2 | 1.47 | | 4.69E-08 |
| IPI00871279 | solute carrier family 38, member 1 | 1.47 | | 3.90E-08 |
| IPI00002848 | small nuclear RNA activating complex, polypeptide 1, 43kDa | 1.47 | 0.22 | 3.70E-08 |
| IPI00464978 | insulin receptor substrate 2 | 1.48 | 0.23 | 2.36E-08 |
| IPI00064262 | dachsous 1 (Drosophila) | 1.48 | | 2.18E-08 |
| IPI00645849 | extracellular matrix protein 1 | 1.48 | 1.12 | 2.15E-08 |
| IPI00337574 | ankyrin repeat domain 39 | 1.48 | | 1.53E-08 |
| IPI00783750 | TNFAIP3 interacting protein 1 | 1.49 | | 7.63E-09 |
| IPI00152564 | ring finger protein 141 | 1.50 | | 5.53E-09 |
| IPI00465087 | BRCA1 associated protein-1 | 1.50 | | 5.04E-09 |
| IPI00445977 | lipoma HMGIC fusion partner-like 2 | 1.50 | | 4.49E-09 |
| IPI00922559 | nuclear receptor coactivator 4 | 1.50 | | 3.82E-09 |
| IPI00333063 | transmembrane and coiled-coil domain family 1 | 1.51 | | 3.08E-09 |
| IPI00015476 | solute carrier family 1 (glutamate/neutral amino acid transporter), member 4 | 1.51 | 0.44 | 2.99E-09 |
| IPI00169307 | Rho GTPase activating protein 21 | 1.51 | 0.65 | 1.94E-09 |
| IPI00220272 | triadin | 1.52 | 0.82 | 1.79E-09 |
| IPI00304925 | heat shock 70kDa protein 1A/1B | 1.52 | 0.06 | 1.62E-09 |
| IPI00179473 | sequestosome 1 | 1.52 | 0.27 | 1.27E-09 |
| IPI00410297 | heparanase | 1.52 | | 9.44E-10 |
| IPI00434781 | C75F, uncharacterized protein | 1.53 | 0.06 | 4.37E-10 |
| IPI00444656 | RUN and SH3 domain containing 2 | 1.54 | | 3.54E-10 |
| IPI00307755 | protein kinase, AMP-activated, alpha 2 catalytic subunit | 1.56 | | 9.29E-11 |
| IPI00014399 | four and a half LIM domains 3 | 1.56 | 0.45 | 5.49E-11 |
| IPI00219718 | retinol binding protein 1, cellular | 1.56 | | 4.48E-11 |
| IPI00938337 | hypothetical protein LOC100289775 | 1.57 | | 2.55E-11 |
| IPI00217051 | neuron navigator 3 | 1.58 | 0.14 | 1.22E-11 |
| IPI00014903 | FGFR1 oncogene partner 2 | 1.58 | | 9.80E-12 |

| Protein IDs | Protein Names | Ratio | S.D. | Significant A |
|---|---|---|---|---|
| IPI00061793 | isoform 6 of sorbin and SH3 domain containing 2 | 1.58 | | 8.87E-12 |
| IPI00911039 | cDNA FLJ54408, highly similar to heat shock 70kDa protein 1A | 1.60 | 0.01 | 2.97E-12 |
| IPI00464980 | SIN3 homolog B, transcription regulator (yeast) | 1.61 | 0.74 | 1.47E-12 |
| IPI00006682 | protein phosphatase 1, regulatory (inhibitor) subunit 3D | 1.62 | | 5.82E-13 |
| IPI00376941 | DDHD domain containing 1 | 1.62 | 0.74 | 4.39E-13 |
| IPI00013183 | ubiquitin-like modifier activating enzyme 7 | 1.64 | | 1.00E-13 |
| IPI00152881 | shroom family member 3 | 1.64 | | 5.90E-14 |
| IPI00028564 | guanylate binding protein 1, interferon-inducible, 67kDa | 1.65 | 0.92 | 4.43E-14 |
| IPI00000334 | chromosome 6 open reading frame 35 | 1.65 | | 3.15E-14 |
| IPI00794080 | myosin, heavy chain 3, skeletal muscle, embryonic | 1.66 | | 1.70E-14 |
| IPI00640924 | isoform 1 of neural precursor cell expressed, developmentally down-regulated 4-like | 1.67 | | 3.80E-15 |
| IPI00902997 | cDNA FLJ33692, similar to family with sequence similarity 134, member A | 1.68 | | 1.46E-15 |
| IPI00096899 | chromatin licensing and DNA replication factor 1 | 1.69 | | 8.26E-16 |
| IPI00017504 | chromosome 9 open reading frame 40 | 1.69 | 1.28 | 7.66E-16 |
| IPI00303258 | LIM and cysteine-rich domains 1 | 1.69 | 1.04 | 6.54E-16 |
| IPI00299911 | integrin alpha FG-GAP repeat containing 2 | 1.70 | | 5.05E-16 |
| IPI00296379 | tumor necrosis factor receptor superfamily, member 10b | 1.70 | 0.08 | 4.47E-16 |
| IPI00010090 | glutamate-cysteine ligase, modifier subunit | 1.70 | 0.35 | 3.76E-16 |
| IPI00556381 | CMT1A duplicated region transcript 1 | 1.70 | 0.06 | 3.16E-16 |
| IPI00001640 | N-6 adenine-specific DNA methyltransferase 1 (putative) | 1.70 | | 3.07E-16 |
| IPI00402021 | kelch-like 21 (Drosophila) | 1.70 | | 2.17E-16 |
| IPI00852669 | zinc finger protein 516 | 1.70 | | 2.13E-16 |
| IPI00395572 | mannosyl (alpha-1,6-)-glycoprotein beta-1,6-N-acetyl-glucosaminyltransferase, isozyme B | 1.71 | | 1.00E-16 |
| IPI00100585 | solute carrier family 39 (zinc transporter), member 1 | 1.71 | | 8.11E-17 |
| IPI00218511 | isoform 2 of tuftelin 1 | 1.72 | | 7.26E-17 |
| IPI00025712 | chromosome 21 open reading frame 7 | 1.76 | 1.16 | 1.22E-18 |
| IPI00643763 | PAP associated domain containing 5 | 1.76 | 1.48 | 6.85E-19 |
| IPI00015688 | glypican 1 | 1.78 | | 6.43E-20 |
| IPI00329600 | saccharopine dehydrogenase (putative) | 1.79 | 2.23 | 4.79E-20 |
| IPI00021369 | crystallin, alpha B | 1.79 | | 3.51E-20 |
| IPI00556155 | insulin-like growth factor binding protein 3 | 1.80 | 1.09 | 1.14E-20 |
| IPI00555809 | POTE ankyrin domain family, member F pseudogene | 1.83 | | 3.03E-22 |
| IPI00218486 | slingshot homolog 3 (Drosophila) | 1.87 | | 2.75E-24 |
| IPI00514538 | transmembrane protein 63B | 1.90 | | 1.18E-25 |
| IPI00026602 | major histocompatibility complex, class I, B | 1.92 | 0.00 | 5.21E-27 |
| IPI00940343 | cDNA FLJ16459, moderately similar to tropomyosin 1 (alpha) | 1.96 | | 5.54E-29 |
| IPI00011525 | calsequestrin 1 (fast-twitch, skeletal muscle) | 1.99 | | 1.12E-30 |
| IPI00376221 | erythrocyte membrane protein band 4.1 like 5 | 2.00 | | 2.89E-31 |
| IPI00456628 | RGD motif, leucine rich repeats, tropomodulin domain and proline-rich containing | 2.01 | | 1.23E-31 |

| Protein IDs | Protein Names | Ratio | S.D. | Significant A |
|---|---|---|---|---|
| IPI00011735 | interferon-related developmental regulator 1 | 2.02 | | 2.31E-32 |
| IPI00219563 | phospholipase C, beta 1 (phosphoinositide-specific) | 2.05 | | 4.58E-34 |
| IPI00921911 | cysteine-rich protein 2 | 2.12 | | 7.24E-39 |
| IPI00101524 | SNF8, ESCRT-II complex subunit, homolog (S. cerevisiae) | 2.22 | 1.72 | 5.23E-46 |
| IPI00790757 | DUSP3 23 kDa protien | 2.25 | 1.88 | 7.24E-48 |
| IPI00005668 | aldo-keto reductase family 1, member C2 | 2.34 | | 1.04E-54 |
| IPI00646541 | transmembrane protein 200A | 2.35 | | 1.94E-55 |
| IPI00215979 | 2,3-bisphosphoglycerate mutase | 2.36 | | 2.87E-56 |
| IPI00020977 | connective tissue growth factor | 2.41 | 1.41 | 3.85E-60 |
| IPI00007856 | myosin, heavy chain 2, skeletal muscle, adult | 2.61 | | 4.35E-78 |
| IPI00008780 | stanniocalcin 2 | 2.67 | | 5.34E-84 |
| IPI00001437 | Rho family GTPase 3 | 2.67 | 0.93 | 3.18E-84 |
| IPI00019884 | actinin, alpha 2 | 2.70 | | 1.76E-86 |
| IPI00010539 | sestrin 2 | 2.78 | 0.88 | 7.07E-95 |
| IPI00414008 | leiomodin 1 (smooth muscle) | 2.79 | 0.24 | 6.24E-96 |
| IPI00477812 | tripartite motif-containing 22 | 2.83 | | 1.68E-100 |
| IPI00444820 | cDNA FLJ45145, moderately similar to erythrocyte membrane protein band 4.1-like 2 | 2.92 | | 1.26E-110 |
| IPI00238262 | adhesion molecule with Ig-like domain 2 | 2.99 | | 1.65E-118 |
| IPI00218082 | kin of IRRE like 3 (Drosophila) | 3.03 | | 4.05E-123 |
| IPI00024804 | ATPase, Ca++ transporting, cardiac muscle, fast twitch 1 | 3.09 | | 2.86E-130 |
| IPI00215716 | erythrocyte membrane protein band 4.1-like 3 | 3.17 | 0.46 | 1.33E-139 |
| IPI00183750 | MAM domain containing 2 | 4.02 | | 1.69E-269 |
| IPI00302329 | myosin, heavy chain 8, skeletal muscle, perinatal | 4.42 | | 0.00E+00 |
| IPI00744872 | family with sequence similarity 179, member B | 4.46 | | 0.00E+00 |
| IPI00009384 | cyclin-dependent kinase inhibitor 1A (p21, Cip1) | 4.98 | 0.12 | 0.00E+00 |
| IPI00025685 | RWD domain containing 2B | 5.29 | | 0.00E+00 |
| IPI00002352 | myosin light chain, phosphorylatable, fast skeletal muscle | 5.39 | | 0.00E+00 |
| IPI00945846 | protease, serine, 1 (trypsin 1) | 5.45 | 4.66 | 0.00E+00 |
| IPI00215893 | heme oxygenase (decycling) 1 | 5.49 | 2.40 | 0.00E+00 |
| IPI00064112 | SEC16 homolog B (S. cerevisiae) | 6.15 | | 0.00E+00 |
| IPI00411763 | isoform 3 of kinesin family member 1B | 6.50 | 7.56 | 0.00E+00 |
| IPI00328123 | NLR family, pyrin domain containing 1 | 10.12 | | 0.00E+00 |
| IPI00514201 | myosin, heavy chain 6, cardiac muscle, alpha | 11.80 | | 0.00E+00 |

**Table 3.3** List of pathways altered by monomethylarsonous acid exposure derived by GenMAPP analysis. List of proteins involved in the substantially perturbed pathways.

| Protein IDs | Symbol | Protein Name | Ratio | S.D. | Significant A |
|---|---|---|---|---|---|
| | | **Down-regulated Pathway** | | | |
| | | **Cholesterol Biosynthesis** | | | |
| IPI00008475 | HMGCS1 | HMG-CoA synthase | 0.56 | 0.02 | 2.47E-06 |
| IPI00021770 | HMGCR | HMG-CoA reductase | 0.60 | 0.06 | 2.11E-05 |
| IPI00220014 | IDI1 | isopentenyl-PP-delta-isomerase | 0.60 | 0.08 | 1.66E-05 |
| IPI00020944 | FDFT1 | squalene synthase | 0.59 | 0.09 | 1.23E-05 |
| IPI00295772 | CYP51A1 | lanosterol 14 alpha-demethylase | 0.69 | 0.08 | 1.03E-03 |
| IPI00019899 | SC4MOL | cholesterol C4-methyl oxidase | 0.67 | 0.13 | 3.94E-04 |
| IPI00291544 | SQLE | squalene epoxidase | 0.70 | 0.06 | 1.48E-03 |
| IPI00016703 | DHCR24 | desmosterol reductase | 0.70 | 0.09 | 1.57E-03 |
| | | **Selenium Pathway** | | | |
| IPI00103471 | SELM | selenoprotein M | 0.55 | | 1.32E-06 |
| IPI00000070 | LDLR | low density lipoprotein receptor | 0.66 | 0.19 | 2.91E-04 |
| IPI00019590 | PLAT | plasminogen activator, tissue | 0.58 | 0.03 | 7.77E-06 |
| IPI00884896 | TrxR1 | thioredoxin reductase 1 | 1.37 | 0.19 | 1.14E-05 |
| | | **Up-regulated Pathway** | | | |
| | | **Keap1-Nrf2** | | | |
| IPI00012069 | NQO1 | NAD(P)H dehydrogenase, quinone 1 | 1.43 | 0.17 | 4.95E-07 |
| IPI00010090 | GCLM | glutamate-cysteine ligase, modifier subunit | 1.70 | 0.35 | 3.76E-16 |
| IPI00215893 | HMOX1 | heme oxygenase (decycling) 1 | 5.49 | 2.40 | 0.00E+00 |

# Chapter 4

# The Application of ATP Affinity Probe and Scheduled MRM Analysis for Profiling Global Kinome in Human cells in Response to Arsenite Treatment

## Introduction

As one of the most important family of enzymes, kinases are extensively engaged in numerous cellular pathways, from metabolism to signal transduction.[1] The kinase-mediated phosphorylation of proteins, lipids and carbohydrates controls the activation/deactivation, cellular localization, binding affinity and degradation of the substrate molecules.[2] Thus, regulation of the function and localization of kinases is the foundation to maintain proper cell proliferation, differentiation and apoptosis, while aberrant regulation of kinases may lead to the induction of diseases and development of tumors.[3] Along this line, perturbation of cellular phosphorylation pattern by modulating kinases is one of the primary deleterious effects exerted by environmental toxicants.[4] Thus, a thorough assessment of the alterations of the expression and activity of the entire kinome, which refers to the collection of global kinases, is vital for understanding the

modes of action of various environmental toxicants and for exploiting effective therapeutic interventions against toxicant exposure.

Efforts have been made into exploring effective strategies to interrogate the expression and activities of kinases. Conventional immunoanalysis with kinase/phospho-specific antibodies or peptide chips has provided information on the regulation and enzymatic activities of individual or specific groups of kinases.[5] However, these strategies are restricted by the specificity and availability of kinase antibodies or substrates. Recent advances in MS instrumentation, along with the development of bioinformatic tools, have led to great success in the identification and quantification of global proteome and phosphoproteome[6]. However, since kinases are of relatively low abundance, interference from highly abundant proteins hampers the detection of kinases, rendering the studies of global kinome by MS very challenging. Therefore, it would be highly beneficial to apply efficient kinase enrichment steps prior to MS analysis. To this end, kinase inhibitor-based enrichment method[7] and biotin-conjugated acyl nucleotide probe affinity assay,[8] coupled with LC-MS/MS analysis in the data-dependent acquisition (DDA) mode, have facilitated high-throughput characterizations of the global kinome from whole cell lysates or tissue extracts. However, in the DDA mode, where 10-20 most abundant precursor ions are selected for fragmentation to achieve peptide identification[9], the sensitivity and reproducibility for kinase discovery is limited by the complexity of samples and variations in precursor ion selection. Recently, with application of triple quadrupole mass spectrometer and advances in software development for multiple-reaction monitoring (MRM) analysis,[10] targeted quantification

method has gained advantages over the above-mentioned discovery-based approach in terms of sensitivity, quantification accuracy and reproducibility.[11]

We recently constructed an MRM kinome library consisting of ~ 400 strictly selected peptides representing more than 300 unique kinases based on data acquired in DDA mode on an LTQ Orbitrap Velos mass spectrometer.[10a] With the use of the MRM kinome library, together with the application of desthiobiotin-based isotope-coded ATP-affinity probe (ICAP) for kinase labeling, kinase peptide enrichment and LC-MS/MS analysis on a triple quadrupole mass spectrometer, we were able to reproducibly identify and quantify more than ~ 250 protein and lipid kinases in cancer cells and tissues.[10a] In this highly multiplexed detection, it is essential to perform scheduled MRM analysis where the mass spectrometer is programmed to detect only a limited number of peptides in pre-defined retention time windows. To achieve that, we calculated the "iRT" score for each targeted kinase peptide to accurately predict its retention time in scheduled MRM analysis. In our previous workflow, the global kinome profiling was achieved by monitoring ~ 2000 transitions in 4 LC-MRM runs with the duration of retention time window being set at 10 min. We used relatively wide retention time window in our previous study mainly due to the observed retention time shift between sequential LC-MS/MS runs; although the elution order of peptides follows strictly the iRT scales, systematic retention time shift of peptides was observed possibly due to sample loading. To correct for retention time shift, here we adopted "on-the-fly" recalibration[12] of retention time shift with spiked-in reference peptides in the targeted kinome analysis. With the increased accuracy in retention time prediction, we were able to shorten the

retention time window of our scheduled MRM analysis to 6 min, thereby enabling the monitoring of the same number of transitions within two LC-MS/MS runs without compromising the overall analytical performance.

By coupling SILAC labeling[13] with the ATP-affinity probe in the targeted quantitative kinome analysis for the first time, we achieved an in-depth analysis of inorganic As(III)-induced global kinome perturbation in GM00637 human skin fibroblasts. We were able to quantify 234 kinases from one forward and two reverse SILAC labeling experiments. Among them, 8 and 9 kinases were found to be significantly decreased and increased, respectively, in protein expression level and ATP binding activity. To our best knowledge, this is the first report about the investigation of global human kinome response under exposure to an environmental toxicant. Moreover, we demonstrated that the targeted MRM-based kinome analysis is amenable to both chemical and metabolic labeling, and is a powerful tool in the exploration of the disturbance in cellular signaling network after external stimuli.

## Materials and methods

### Cell culture

All reagents unless otherwise stated were purchased from Sigma-Aldrich (St. Louis, MO). GM00637 human skin fibroblasts were kindly provided by Prof. Gerd P. Pfeifer (the City of Hope) and cultured at 37°C in an atmosphere containing 5% $CO_2$ in Dulbecco's Modified Eagle's Media (DMEM, ATCC, Manassas, VA), supplemented with 10% fetal bovine serum (FBS, Life Technologies, Grand Island, NY) and 1% antibiotic-antimycotic solution (Life Technologies).

MTT assay was performed using Cell Proliferation Kit 1 (Roche, Basel, Switzerland) as previously described.[14] For metabolic labeling using SILAC, GM00637 cells were cultured in DMEM media for SILAC (DMEM media minus L-lysine and L-arginine, Thermo Scientific, Rockford, IL) supplemented with light lysine and arginine, or heavy stable isotope-labeled [$^{13}C_6$,$^{15}N_2$]-L-lysine and [$^{13}C_6$]-L-arginine (Sigma-Aldrich), following previously published procedures.[15] SILAC GM00637 cells were maintained under the same conditions as noted above, except that dialyzed FBS (Life Technologies) was used. The cells were cultured in the heavy or light medium for at least five passages prior to arsenite exposure to ensure nearly complete incorporation of the stable isotope-labeled amino acids.

**Sodium arsenite treatment and cell lysis**

After SILAC labeling, light and heavy-labeled GM00637 cells at a density of ~ $5\times10^5$ cells/mL were treated with 5 μM sodium arsenite [iAs(III)] for 24 h without dialyzed FBS in forward and reverse SILAC labeling experiments, respectively. Cells were then harvested with trypsin-EDTA solution (ATCC) and washed with ice-cold phosphate-buffered saline (PBS) for three times. The pelleted cells were lysed with 0.7% CHAPS in a solution containing 50 mM HEPES (pH 7.4), 0.5 mM EDTA, 100 mM NaCl and a protease inhibitor cocktail (100:1, Sigma-Aldrich). Supernatant was then collected after centrifugation at 16000× *g* for 30 min, and the total protein concentration determined by Bicinchoninic Acid Kit for Protein Determination (Sigma-Aldrich). The light-labeled, iAs(III)-treated cell lysate was mixed with the heavy-labeled, control cell lysate at 1:1 ratio (w/w) in the forward SILAC experiment. In the reverse SILAC experiment, both the labeling and iAs(III) treatment were reversed. The cell lysate mixture was further purified through Illustra NAP-25 Columns (GM Healthcare Bio-Sciences, Pittsburgh, PA) to remove endogenous nucleotides.

**ATP affinity probe labeling and sample preparation**

The detailed procedures for ATP affinity probe labeling, tryptic digestion, affinity purification of desthiobiotin-labeled peptides were reported previously.[10a] Briefly, after incubation with the ATP affinity probe for 2.5 h,[8b, 16] the labeled cell lysate mixture was reduced with dithiothreitol, alkylated with iodoacetamide, and digested with sequencing grade trypsin (Roche Applied Science, Indianapolis, IN). The resultant desthiobiotin-labeled peptides were enriched by using avidin-agarose resin and eluted with a buffer

containing 1% TFA in $CH_3CN$:$H_2O$ (7:3, v/v). The resulting enriched peptide samples were desalted by employing OMIX $C_{18}$ pipette tips (Agilent, Santa Clara, CA).

**Scheduled LC-MRM analysis and on-the-fly correction of retention time shift**

A TSQ Vantage triple-quadrupole mass spectrometer (Thermo Fisher, San Jose, CA) was utilized for the scheduled LC-MRM analysis with on-the-fly correction for retention time (RT) shift. The mass spectrometer was coupled to an EASY n-LCII HPLC system with a nanoelectrospray ionization source (Thermo Fisher). The experimental conditions for the scheduled LC-MRM analysis were described elsewhere.[10a] To achieve on-the-fly recalibration of retention time shift, standard reference peptides (Pierce Peptide Retention Time Calibration Mixture) with pre-generated iRT values (Table 4.1) were spiked into samples. In the process of an LC-MRM run, RT shift was evaluated based on the RTs of the reference peptides. The RT window of the subsequent peptides was then adjusted in real time according to the linearregression of the two preceding reference peptides. Thus, the improved accuracy in RT prediction increased overall analytical robustness and allowed for the use of shortened RT window in scheduled MRM analysis. The retention time windows for the reference peptides (IGDYAGIK and TASEFDSAIAQDK) and the remaining peptides were set up as 16 min and 6 min, respectively. Therefore, the ~ 2000 transitions corresponding to ~ 400 peptides from ~ 300 kinases could be monitored in two LC-MRM runs. Data were processed against the MRM-based kinome library[10a] adapted for SILAC labeling on Skyline, version 1.4.0.4421.[10b]

## Results and discussion

### 1. Quantitative analysis of global kinome by ATP affinity probe with SILAC labeling

Recently we constructed a human MRM kinome library on the basis of large-scale shotgun proteomic analysis of kinases enriched by desthiobiotin-based isotope-coded ATP affinity probes from the whole cell lysates of six different cell lines (K562, IMR-90, HeLa-S3, Jurkat-T, WM-115 and WM-266-4).[10a] The acquired tandem mass spectra and retention time information of kinase-derived peptides with desthiobiotin labeling were then processed using Skyline for the MRM library construction. However, the use of isotope-coded ATP affinity probes in the previous study required customized synthesis, which may limit its general application in analytical laboratories. To accommodate for more widely used quantitative approach using SILAC, we re-constructed the human MRM kinome library by setting up variable modifications with mass shifts introduced by heavy isotope labeling with lysine (+8 Da) and arginine (+6 Da). Current SILAC-compatible MRM kinome library consists of 395 peptides, corresponding to 285 kinases, which allows for in-depth kinome profiling that covers all the seven major human kinase families (Figure 4.1A).

To achieve quantitative analysis of the global kinome, we employed metabolic labeling with SILAC (Figure 4.1B). After complete incorporation of the light- and heavy-labeled amino acids, the cells were exposed to sodium arsenite and subsequently lysed. The light and heavy cell lysates were then incubated with ATP affinity probe, mixed at 1:1 ratio (w/w), and digested with trypsin. After avidin agarose enrichment, the

desthiobiotin-conjugated peptides were eluted and subjected to scheduled LC-MRM analysis.

Our results revealed that accurate MRM identification and quantification of SILAC-labeled human kinome can be achieved by referring to the spectra of targeted peptides in our SILAC-compatible MRM kinome library. LC-MRM results of a representative peptide DIK*PQNLLLDPDTAVLK (K* is desthiobiotin-labeled lysine) from glycogen synthase kinase-3 beta are depicted in Figure 4.2. Based on the MS/MS in the kinome library obtained from data-dependent analysis, transitions of three abundant y ions ($y_7$, $y_8$ and $y_9$) were selected for MRM monitoring of light- and heavy-labeled kinase peptides (Figure 4.2A). Subsequent MRM analysis results revealed reliable monitoring of the corresponding light and heavy forms of these three ions (Figure 4.2B and C). The relative abundances of the three y ions from both light- and heavy-SILAC labeled kinase peptides were consistent with those in the original spectrum in the library, confirming the unbiased identification and quantification of this peptide. Therefore, our MRM-based targeted kinome analysis is fully compatible with SILAC labeling, thereby further broadening the application of this method for global kinome profiling.

**2. Scheduled MRM analysis with on-the-fly correction of retention time shift**

To achieve large-scale global kinome analysis for more than 300 kinases, it is essential to perform scheduled MRM analysis, which necessitates accurate prediction of retention time. In our previous workflow, we predicted the retention time for individual peptides based on their empirically determined iRT scores.[10a] However, a wide variety of factors can give rise to retention time variations. For example, sample loading, difference

in column packing, instabilities of LC systems and mobile phase flow rate can all lead to unexpected shift in retention time, which decreases the reproducibility and accuracy for quantification by scheduled MRM analysis. In our previous experiment, although the targeted kinase peptides follow strictly the elution order according to their iRT scores, we also observed a 2-3 min delay in retention time after multiple sample injections, which may result in the failure in detecting some kinase peptides if a narrow detection window is imposed in scheduled MRM analysis.

To correct for systematic retention time shift during scheduled LC-MRM analysis, we incorporated on-the-fly correction[12] in our MRM detection workflow, during which the instrument automatically detects the shift in retention time for pre-defined reference peptides and adjust, in real-time, the retention time window for subsequently eluted targeted peptides. Since this recalibration of retention time occurred in real-time, it could greatly reduce the chance of peak loss arising from retention time shift during scheduled MRM analysis. In our test experiment for monitoring the tryptic digestion mixture of BSA, we found that peptides with large retention time shift can still be successfully captured with the on-the-fly technique. For instance, Figure 4.3A shows the chromatograms for two peptides (AEFVEVTK and LGEYGFQNALIVR) from tryptic digestion mixture of BSA. With an intentionally delayed gradient, the actual retention times of these two peptides were postponed by 9 and 8 min, respectively, from previous LC-MRM runs. Thus, without on-the-fly correction of retention time shift, transitions of these two peptides would not be captured in the predicted retention time window. However, using the same detection windows, these two BSA peptides with very large

retention time shifts can still be successfully detected with the real-time adjustment of detection window. Therefore, on-the-fly technique is expected to easily correct for retention time shift observed in our kinome MRM analysis, which generally lies within 2-3 min range.

To achieve on-the-fly recalibration of retention time shift for our MRM-based kinome analysis, we spiked a set of commercially available standard peptides into the sample.[12b] The iRT values of these reference peptides were also recalculated by co-injection with tryptic peptides of BSA, whose iRT scores are well-defined in the kinome library (Table 4.1). In our experience, we found that employing two reference peptides as retention time markers is sufficient for systematic correction of retention time, whereas too many reference peptides may adversely affect the real-time detection window adjustment by the interference from complex sample matrices. In addition, the early-eluted standard peptides, which generally have large retention time variations, were not employed as the reference peptides. Therefore, we chose the third and fourth eluted standard peptides IGDYAGIK and TASEFDSAIAQDK as the reference peptides for on-the-fly corrections and the detection time window was set at 16 min so that no reference could be missed even with large retention time shift. As a result, the detection window for subsequently eluted target peptides will be adjusted according to a linear fit through the predicted and actual RTs of reference peptides IGDYAGIK and TASEFDSAIAQDK. Owing to this on-the-fly adjustment and the resultant increased accuracy in retention time prediction, the duration of retention time window could be shortened from 10 min, as used in our previous study,[10a] to 6 min. As depicted in Figure 4.3B, for monitoring a total

of more than 2000 transitions with a 10-min scheduled retention time window, four LC-MRM analytical runs are required since the maximum capacity for LC-MRM analysis is around 170 transitions per cycle. With a 6-min retention time window, the MS was capable of monitoring the same number of transitions in 2 scheduled LC-MRM runs. Thus, this method improved the analytical throughput, reduced the amount of analyte required, and increased the analytical robustness and accuracy.

**3. Sodium arsenite-induced perturbation of the entire kinome**

Previously we utilized the isotope-coded ATP affinity probes in conjunction with scheduled MRM analysis to achieve a comparative analysis of the global kinome of a pair of melanoma cell lines derived from the primary (WM-115) and metastatic (WM-266-4) tumor sites of the same individual.[10a] However, this targeted MRM analysis was not applied to study the global kinome response upon external chemical stimulus, which has broad applications in research in cell signaling and environmental toxicology. Therefore, in the current study, we further expanded the application of this technique to elucidate, with the use of an SILAC-based approach, the perturbation of the entire kinome induced by an environmental toxicant, sodium arsenite. In this vein, exposure to arsenic species in drinking water is a widespread public health concern worldwide. Researchers from disparate fields have explored the mechanisms of action of arsenic species from different perspectives, ranging from speciation to metabolism.[17] Owing to the importance of kinases in cell signaling, we decided to employ the MRM-based method to conduct an in-depth profiling of the alteration of global kinome in human cells in response to sodium arsenite exposure.

GM00637 human skin fibroblast cells were treated with 5 μM sodium arsenite [iAs(III)] for 24 h. The subsequent ATP affinity probe labeling and sample preparation were as described in Figure 4.1B. The resulting enriched kinase peptides were analyzed by two scheduled MRM runs with a 6-min retention time window and on-the-fly retention time correction strategy. In total, we quantified 234 kinases from one forward and two reverse SILAC experiments. In addition, the excellent correlation between the measured retention time with iRT demonstrated the effectiveness of this strategy (Figure 4.3C). Depicted in Figure 4.4 is the histogram of kinome quantification results, which revealed that kinases from all kinase groups except the PKL group were quantified. Although the expression levels and ATP binding affinities of the majority of the kinases in the kinome remained unchanged towards iAs(III) treatment, 8 and 9 kinases were significantly down- and up-regulated, respectively (Figures 4.4, 4.5 and 4.6, and Table 4.2).

It is worth discussing the analytical performances of the MRM-based kinome profiling method. First, we found that the method provided an excellent dynamic range for kinome quantification; signal intensities, as reflected by peak areas found in the selected-ion chromatograms for MRM transitions, vary from $10^3$ to $10^6$ (Figure 4.7). Thus, kinases with expression levels differing by 2 to 3 orders of magnitude can be simultaneously monitored and quantified. Second, to achieve high specificity in the MRM-based kinome analysis, we chose only those kinase peptides that are directly associated with ATP binding or possess known ATP-binding motifs (HRDxKxxN, VAxK or GxxxxGK) for the construction of the kinome MRM library.[10a] As a result,

quantifications of the majority of kinases were based on single unique peptides. Nevertheless, 66 out of the 234 kinases were quantified based on multiple peptides. Quantitative variations among the multiple unique peptides for any of the 66 kinases are relatively small, as manifested by an average relative standard deviation (RSD) of 12.6%.

**4. Sodium arsenite exposure induced hyperactivation of CDK1 and other cell cycle-related protein kinases**

Different mechanisms were proposed about how arsenic species exert their cytotoxic effects, which include induction of oxidative stress and dysfunction of proteins through binding to vicinal thiol groups.[18] Especially, cell cycle arrest induced by inorganic arsenic exposure has been observed by multiple research groups.[19]

In the current study, we observed the over-expression of multiple protein kinases associated with cell cycle progression. For instance, we observed an elevated level of cyclin-dependent kinase 1 (CDK1) in both forward and reverse SILAC experiments (ratio of 2.07, Figures 4.8A and 4.6). Along this line, our Western blot analysis independently confirmed the increased expression of CDK1, as illustrated in Figure 4.8B. In agreement with our observation, cDNA microarray analysis also revealed the augmented expression of CDK1 in sodium arsenite-treated HFW human fibroblast cells.[20]

CDK1 plays pivotal roles in regulating mammalian cell cycle progression, which is an evolutionarily conserved and highly regulated process. Sustained activation of CDK1 was found to arrest cells in the metaphase and cause mitotic failure which eventually induces cell death.[21] In this vein, hyperactivation of CDK1 was observed to induce mitotic arrest in A375 leukemia cells after arsenite exposure.[22] Thus, aberrant

hyperactivation of CDK1 may account, in part, for the cytotoxicity of sodium arsenite, and inhibition of CDK1 may result in a decreased sensitivity towards sodium arsenite exposure. To test this hypothesis, we co-treated GM00637 cells with sodium arsenite and an effective CDK inhibitor, flavopiridol,[23] and monitored the proliferation of the cells using the MTT assay. Our results showed that treatment with flavopiridol rescued in part the arsenite-induced growth inhibition (Figure 4.8C). Therefore, inhibition of CDK1 hyperactivities could reduce the cytotoxicity of sodium arsenite in human skin fibroblasts.

Apart from CDK1, we found that arsenite exposure also led to the up-regulation of several other kinases involved in cell cycle progression. In this vein, we observed elevated levels of all three members of Aurora kinases (AurA, AurB and AurC) by 1.85-, 1.37- and 1.68-fold, respectively, following arsenite treatment. Aurora kinases play vital roles in regulating cell cycle progression. Different members of Aurora kinases possess distinct functions and subcellular localizations; however, there is partial overlap and coordination of their functions.[24] AurA is implicated in centrosome segregation, spindle assembly and it controls the transition between different phases of the cell cycle, whereas AurB is involved in chromatin modification, spindle checkpoint signaling and cytokinesis.[25] The function of AurC is ambiguous owing to the paucity of studies; however, it may serve as a potential chromosomal passenger protein as AurB and regulate spindle checkpoint.[26] Overexpression of Aurora kinases has been linked to centrosome amplification, multi-nuclei formation and aneuploidy.[27] The activation of individual Aurora kinases upon arsenite treatment was observed previously. For

example, AurA was found to be elevated in immortalized keratinocytes upon treatment with a low dose (<1 μM) of arsenite.[28] Likewise, AurB was found to be increased in Hela-S3 cells upon exposure with arsenic trioxide.[29] Here, facilitated by this global kinome analysis technique, we demonstrated unambiguously the global elevated expression/activation for all three Aurora kinases upon arsenite treatment, which may induce cell cycle dysregulation. Thus, the aberrant expression and activation of cell cycle-related kinases and the ensuing perturbation in mitotic progression may account, in part, for the cytotoxic and carcinogenic effects of arsenite.

**Conclusions**

Maturation of targeted proteomic approach provides a solid foundation for global kinome profiling. By interrogating this important family of enzymes, more information can be garnered on the details of critical cellular processes, such as cell signaling and cell proliferation. In the present study, a reactive ATP affinity probe, coupled with SILAC labeling and scheduled MRM analysis, was harnessed for global kinome profiling. By adopting "on-the-fly" recalibration of retention time shift with "spiked-in" reference peptides to the targeted kinome analysis, we were able to shorten the duration of retention time window from 10 to 6 min. In doing so, ~2000 transitions of ~ 400 kinase peptides can be monitored in two LC-MRM runs without compromising the overall analytical performance. By taking advantage of the above-described method, we achieved, for the first time, an in-depth analysis of arsenic-induced global kinome perturbation in GM00637 human skin fibroblasts. This further demonstrated that the ATP affinity labeling method is amendable to both chemical and metabolic labeling, and the method is also powerful for exploring the disturbance in cell signaling network in response to environmental toxicant exposure.

A total of 245 unique peptides, representing 234 unique kinases, were quantified from three independent SILAC experiments. Several kinases involved in cell cycle progression were found to be hyperactivated. Among them, the expression level of CDK1 was increased by ~ 2 fold, which was further confirmed by Western analysis. Additionally, treatment with a CDK1 inhibitor, flavopiridol, could partly rescue the cells from arsenite-induced growth inhibition. Thus, we reason that sodium arsenite may exert

its cytotoxic effect, in part, through aberrant activation of CDK1 and the resultant disturbance of cell cycle progression. In addition, other kinases involved in the mitotic progression, including Aurora kinases, were found to be activated, which may give rise to mitotic instability and, eventually, cell death. Together, the above findings strongly support that MRM- and ATP affinity probe-based kinome profiling constitutes a powerful tool for the discovery of molecular mechanisms of action of environmental toxicants.

**References**


1. Cheng, H. C.; Qi, R. Z.; Paudel, H.; Zhu, H. J., Regulation and function of protein kinases and phosphatases. *Enzyme Res.* **2011,** *2011*, 794089.

2. Johnson, L. N., The regulation of protein phosphorylation. *Biochem. Soc. Trans.* **2009,** *37* (Pt 4), 627-41.

3. Lahiry, P.; Torkamani, A.; Schork, N. J.; Hegele, R. A., Kinase mutations in human disease: interpreting genotype-phenotype relationships. *Nat. Rev. Genet.* **2010,** *11* (1), 60-74.

4. Carpenter, R. L.; Jiang, B. H., Roles of EGFR, PI3K, AKT, and mTOR in heavy metal-induced cancer. *Curr. Cancer Drug Targets* **2013,** *13* (3), 252-66.

5. (a) Stains, Cliff I.; Tedford, Nathan C.; Walkup, Traci C.; Luković, E.; Goguen, Brenda N.; Griffith, Linda G.; Lauffenburger, Douglas A.; Imperiali, B., Interrogating signaling nodes involved in cellular transformations using kinase activity probes. *Chem. Biol.* **2012,** *19* (2), 210-217; (b) Houseman, B. T.; Huh, J. H.; Kron, S. J.; Mrksich, M., Peptide chips for the quantitative evaluation of protein kinase activity. *Nat. Biotechnol.* **2002,** *20* (3), 270-274.

6. (a) Mann, M., Functional and quantitative proteomics using SILAC. *Nat. Rev. Mol. Cell Biol.* **2006,** *7* (12), 952-8; (b) Tao, W. A.; Wollscheid, B.; O'Brien, R.; Eng, J. K.; Li, X. J.; Bodenmiller, B.; Watts, J. D.; Hood, L.; Aebersold, R., Quantitative phosphoproteome analysis using a dendrimer conjugation chemistry and tandem mass spectrometry. *Nat. Methods* **2005,** *2* (8), 591-8.

7. Daub, H.; Olsen, J. V.; Bairlein, M.; Gnad, F.; Oppermann, F. S.; Körner, R.; Greff, Z.; Kéri, G.; Stemmann, O.; Mann, M., Kinase-selective enrichment enables quantitative phosphoproteomics of the kinome across the cell cycle. *Mol. Cell* **2008,** *31* (3), 438-448.

8. (a) Patricelli, M. P.; Szardenings, A. K.; Liyanage, M.; Nomanbhoy, T. K.; Wu, M.; Weissig, H.; Aban, A.; Chun, D.; Tanner, S.; Kozarich, J. W., Functional interrogation of the kinome using nucleotide acyl phosphates. *Biochemistry* **2007,** *46* (2), 350-8; (b) Xiao, Y.; Guo, L.; Jiang, X.; Wang, Y., Proteome-wide discovery and characterizations of nucleotide-binding proteins with affinity-labeled chemical probes. *Anal. Chem.* **2013,** *85* (6), 3198-206.

9. Olsen, J. V.; Schwartz, J. C.; Griep-Raming, J.; Nielsen, M. L.; Damoc, E.; Denisov, E.; Lange, O.; Remes, P.; Taylor, D.; Splendore, M.; Wouters, E. R.; Senko, M.; Makarov, A.; Mann, M.; Horning, S., A dual pressure linear ion trap Orbitrap instrument with very high sequencing speed. *Mol. Cell. Proteomics* **2009,** *8* (12), 2759-69.

10. (a) Xiao, Y.; Guo, L.; Wang, Y., A targeted quantitative proteomics strategy for global kinome profiling of cancer cells and tissues. *Mol. Cell. Proteomics* **2014,** *13* (4), 1065-75; (b) MacLean, B.; Tomazela, D. M.; Shulman, N.; Chambers, M.; Finney, G. L.; Frewen, B.; Kern, R.; Tabb, D. L.; Liebler, D. C.; MacCoss, M. J., Skyline: an open source document editor for creating and analyzing targeted proteomics experiments. *Bioinformatics (Oxford, England)* **2010,** *26* (7), 966-8.

11. Picotti, P.; Aebersold, R., Selected reaction monitoring-based proteomics: workflows, potential, pitfalls and future directions. *Nat. Methods* **2012,** *9* (6), 555-66.

12. (a) Escher, C.; Reiter, L.; MacLean, B.; Ossola, R.; Herzog, F.; Chilton, J.; MacCoss, M. J.; Rinner, O., Using iRT, a normalized retention time for more targeted measurement of peptides. *Proteomics* **2012,** *12* (8), 1111-21; (b) Kiyonami, R.; Schoen, A.; Zabrouskov, V., On-the-fly retention time shift correction for multiple targeted peptide quantification by LC-MS/MS. *Thermo Fisher Scientific, Application Note 503* **2010**.

13. (a) Chen, X.; Smith, L. M.; Bradbury, E. M., Site-specific mass tagging with stable isotopes in proteins for accurate and efficient protein identification. *Analytical chemistry* **2000,** *72* (6), 1134-43; (b) Zhu, H.; Pan, S.; Gu, S.; Bradbury, E. M.; Chen, X., Amino acid residue specific stable isotope labeling for quantitative proteomics. *Rapid Commun. Mass Spectrom.* **2002,** *16* (22), 2115-23; (c) Ong, S. E.; Blagoev, B.; Kratchmarova, I.; Kristensen, D. B.; Steen, H.; Pandey, A.; Mann, M., Stable isotope labeling by amino acids in cell culture, SILAC, as a simple and accurate approach to expression proteomics. *Molecular & cellular proteomics : MCP* **2002,** *1* (5), 376-86.

14. Guo, L.; Xiao, Y.; Wang, Y., Monomethylarsonous acid inhibited endogenous cholesterol biosynthesis in human skin fibroblasts. *Toxicology and applied pharmacology* **2014,** *277* (1), 21-9.

15. Guo, L.; Xiao, Y.; Wang, Y., Hexavalent chromium-induced alteration of proteomic landscape in human skin fibroblast cells. *Journal of proteome research* **2013,** *12* (7), 3511-8.

16. Xiao, Y.; Guo, L.; Wang, Y., Isotope-coded ATP probe for quantitative affinity profiling of ATP-binding proteins. *Analytical chemistry* **2013,** *85* (15), 7478-86.

17. (a) Watanabe, T.; Hirano, S., Metabolism of arsenic and its toxicological relevance. *Arch. Toxicol.* **2013,** *87* (6), 969-79; (b) Planer-Friedrich, B.; Suess, E.; Scheinost, A. C.; Wallschlager, D., Arsenic speciation in sulfidic waters: reconciling contradictory spectroscopic and chromatographic evidence. *Analytical chemistry* **2010,** *82* (24), 10228-35.

18. Shen, S.; Li, X. F.; Cullen, W. R.; Weinfeld, M.; Le, X. C., Arsenic binding to proteins. *Chem. Rev.* **2013,** *113* (10), 7769-92.

19. McCollum, G.; Keng, P. C.; States, J. C.; McCabe, M. J., Jr., Arsenite delays progression through each cell cycle phase and induces apoptosis following G2/M arrest in U937 myeloid leukemia cells. *The Journal of pharmacology and experimental therapeutics* **2005,** *313* (2), 877-87.

20. Yih, L. H.; Peck, K.; Lee, T. C., Changes in gene expression profiles of human fibroblasts in response to sodium arsenite treatment. *Carcinogenesis* **2002,** *23* (5), 867-76.

21. Castedo, M.; Perfettini, J.-L.; Roumier, T.; Andreau, K.; Medema, R.; Kroemer, G., Cell death by mitotic catastrophe: a molecular definition. *Oncogene* **2004,** *23* (16), 2825-2837.

22. McNeely, S. C.; Taylor, B. F.; States, J. C., Mitotic arrest-associated apoptosis induced by sodium arsenite in A375 melanoma cells is BUBR1-dependent. *Toxicology and applied pharmacology* **2008,** *231* (1), 61-7.

23. Shapiro, G. I., Preclinical and clinical development of the cyclin-dependent kinase inhibitor flavopiridol. *Clinical cancer research : an official journal of the American Association for Cancer Research* **2004,** *10* (12 Pt 2), 4270s-4275s.

24. Hochegger, H.; Hégarat, N.; Pereira-Leal, J. B., Aurora at the pole and equator: overlapping functions of Aurora kinases in the mitotic spindle. *Open Biol.* **2013,** *3* (3), 120185.

25. (a) Santaguida, S.; Vernieri, C.; Villa, F.; Ciliberto, A.; Musacchio, A., Evidence that Aurora B is implicated in spindle checkpoint signalling independently of error correction. *The EMBO journal* **2011,** *30* (8), 1508-19; (b) Nikonova, A. S.; Astsaturov, I.; Serebriiskii, I. G.; Dunbrack, R. L., Jr.; Golemis, E. A., Aurora A kinase (AURKA) in normal and pathological cell division. *Cellular and molecular life sciences : CMLS* **2013,** *70* (4), 661-87.

26. Sasai, K.; Katayama, H.; Stenoien, D. L.; Fujii, S.; Honda, R.; Kimura, M.; Okano, Y.; Tatsuka, M.; Suzuki, F.; Nigg, E. A.; Earnshaw, W. C.; Brinkley, W. R.; Sen, S., Aurora C kinase is a novel chromosomal passenger protein that can complement Aurora-B kinase function in mitotic cells. *Cell motility and the cytoskeleton* **2004,** *59* (4), 249-63.

27. Fu, J.; Bian, M.; Jiang, Q.; Zhang, C., Roles of Aurora kinases in mitosis and tumorigenesis. *Molecular cancer research : MCR* **2007,** *5* (1), 1-10.

28. Wu, C. H.; Tseng, Y. S.; Kao, Y. T.; Sheu, H. M.; Liu, H. S., Low concentration of arsenic-induced aberrant mitosis in keratinocytes through E2F1 transcriptionally regulated Aurora-A. *Toxicological sciences : an official journal of the Society of Toxicology* **2013,** *132* (1), 43-52.

29. Yih, L. H.; Hsu, N. C.; Wu, Y. C.; Yen, W. Y.; Kuo, H. H., Inhibition of AKT enhances mitotic cell apoptosis induced by arsenic trioxide. *Toxicology and applied pharmacology* **2013,** *267* (3), 228-37.

**Figure 4.1** Targeted human kinases mapped in the dendrogram of SILAC-compatible kinome library (A) and a general workflow of SILAC-based multiple reaction monitoring (MRM) analysis for global kinome profiling using ATP affinity probe (B).

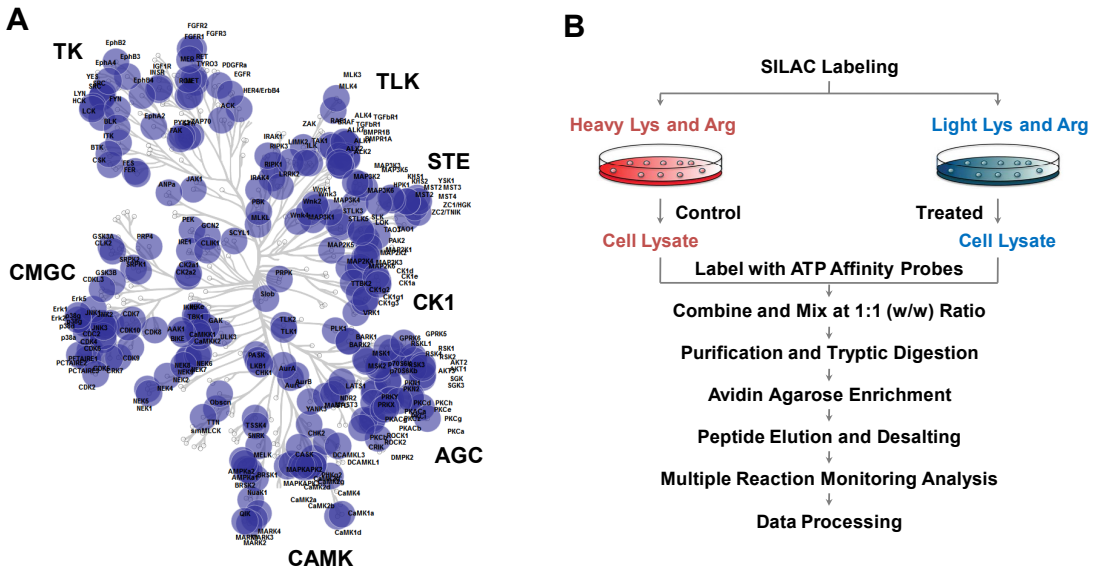

**Figure 4.2** Representative MS/MS data revealed the reliable identification of glycogen synthase kinase-3 beta. (A) The MS/MS of glycogen synthase kinase-3 beta peptide DIK*PQNLLLDPDTAVLK ("K*" designates the desthiobiotin-labeled lysine) in the kinome library based on data-dependent analysis. (B-C) MS/MS for the same peptide from targeted analysis with light- and heavy-labeled lysine, respectively.

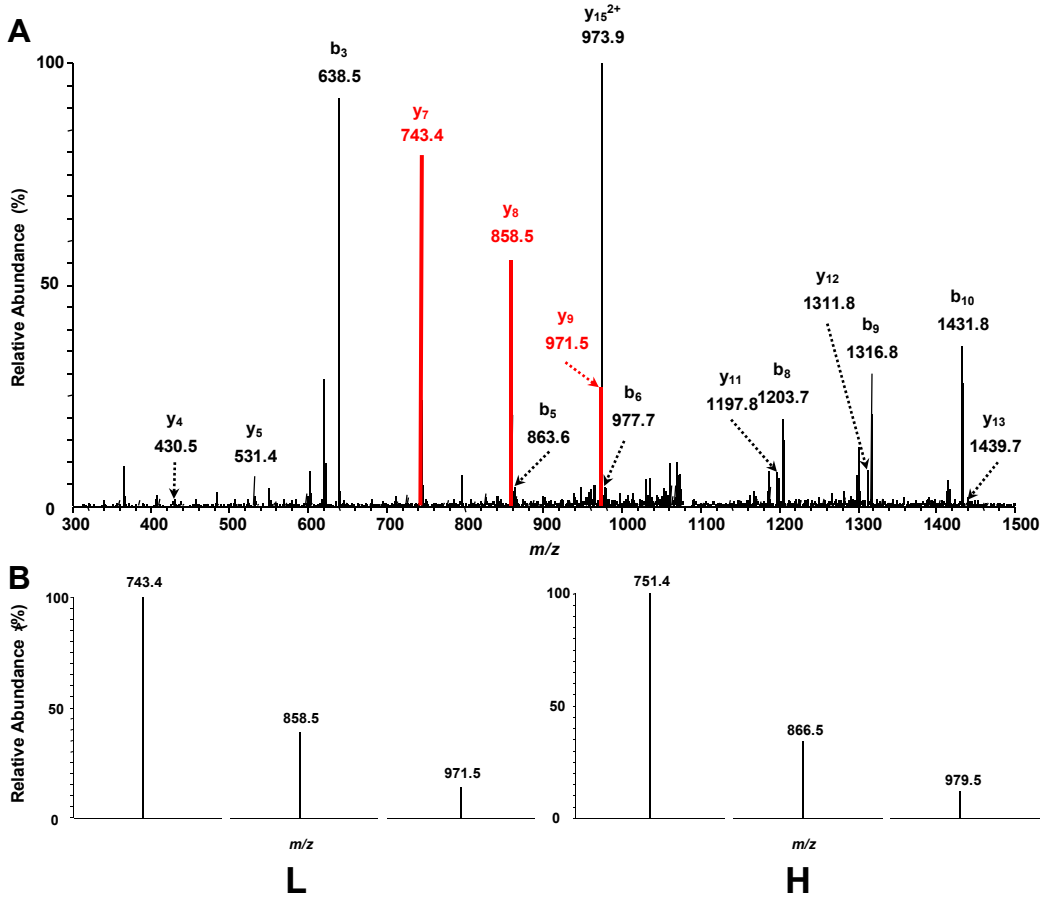

**Figure 4.3** Proof of concept for on-the-fly retention time calibration using tryptic peptides of BSA (A-B) and linearity of calculated iRT versus measured retention time based on LC-MS/MS analysis on a TSQ Vantage mass spectrometer (C). (A) Extracted-ion chromatograms for two representative BSA peptides AEFVEVTK and LGEYGFQNALIVR from two LC-MRM analyses with different gradients. The traces acquired in the initial and intentionally delayed gradients are shown in green and red, respectively. The blue line depicts the predicted retention time window. (B) Number of transitions scheduled in each cycle with a 6 and 10 min retention time window, respectively. (C) iRT-based retention time prediction achieved a good correlation with a $R^2$ value of 0.999 on the measurement of 245 peptides with a 130-min linear gradient.

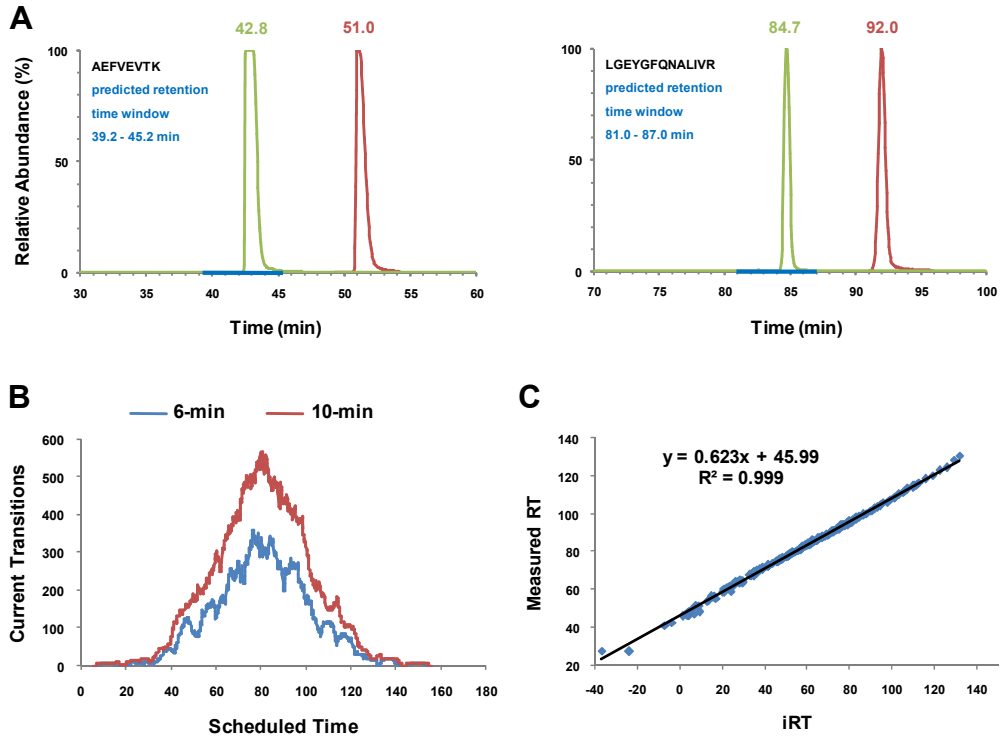

**Figure 4.4** Global kinome profiling for GM00637 human skin fibroblasts after treatment with 5 μM sodium arsenite for 24 h. Blue and red bars denote kinases that are down- and up-regulated after sodium arsenite exposure, respectively.

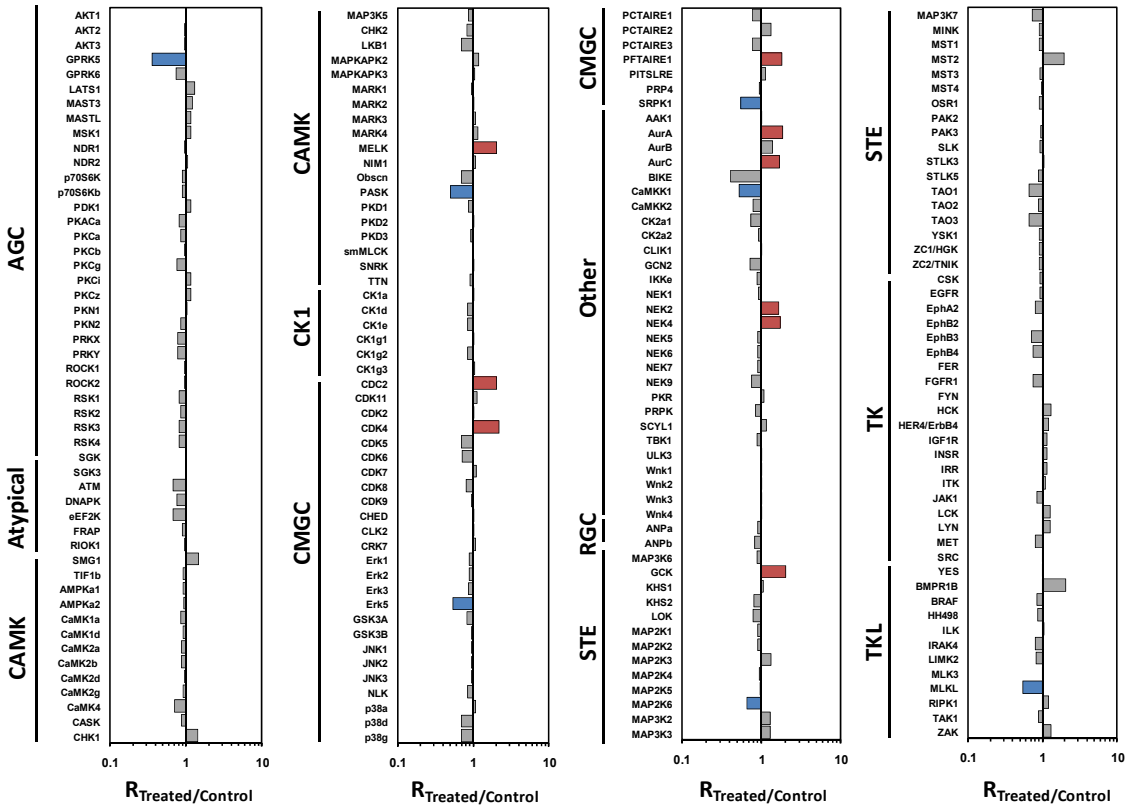

**Figure 4.5** MS/MS obtained from MRM analysis of GK*FGNVYLAR (K* is desthiobiotin-labeled lysine) from Aurora kinase A based on forward (top panels) and reverse (bottom panels) SILAC labeling experiments. The signal intensities for the corresponding light (left panels) and heavy (middle panels) labeled peptides revealed the arsenite-induced overexpression and/or activation of this kinase. The extracted-ion chromatograms for three transitions monitored for the peptide with light (red) and heavy (blue) labels in corresponding SILAC experiments.

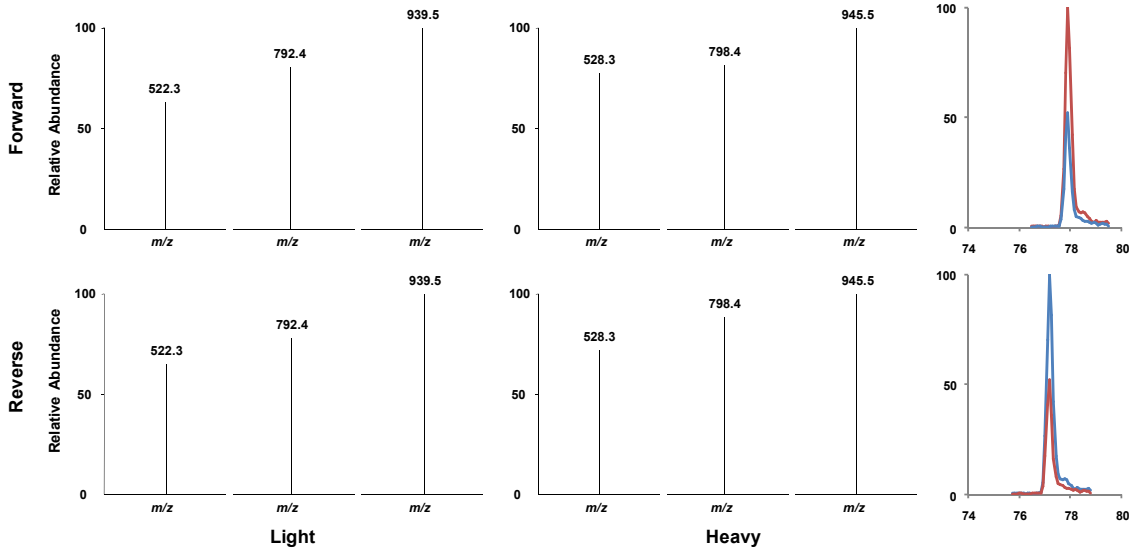

**Figure 4.6** MS/MS obtained from MRM analysis of K*VLALQAR (K* is desthiobiotin-labeled lysine) from SRSF protein kinase 1 based on forward (top panels) and reverse (bottom panels) SILAC labeling experiments. The signal intensities for the corresponding light (left panels) and heavy (middle panels) labeled peptides revealed the arsenite-induced down-regulation and/or deactivation of this kinase. The extracted-ion chromatograms for three transitions monitored for the peptide with light (red) and heavy (blue) labels in corresponding SILAC experiments.

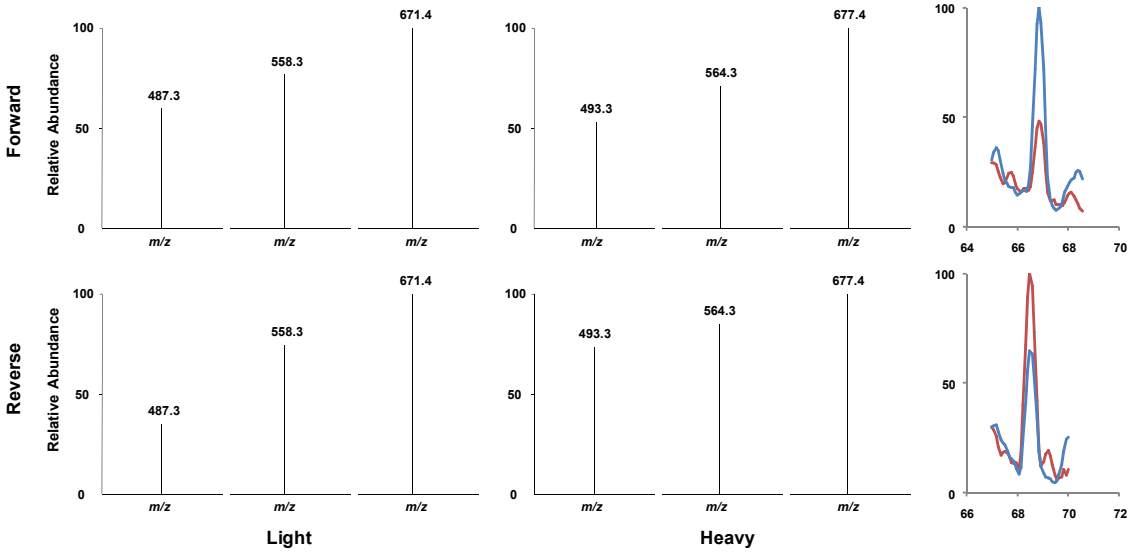

**Figure 4.7** Quantification results for ETGALAAAK*VIETK (K* is desthiobiotin-labeled lysine) from serine/threonine-protein kinase 10 (A) and DLK*PSNLLINTTCDLK from mitogen-activated protein kinase 3 (B). The results showed that a dynamic range of 2-3 orders of magnitude can be achieved with the use of the MRM-based kinome method.

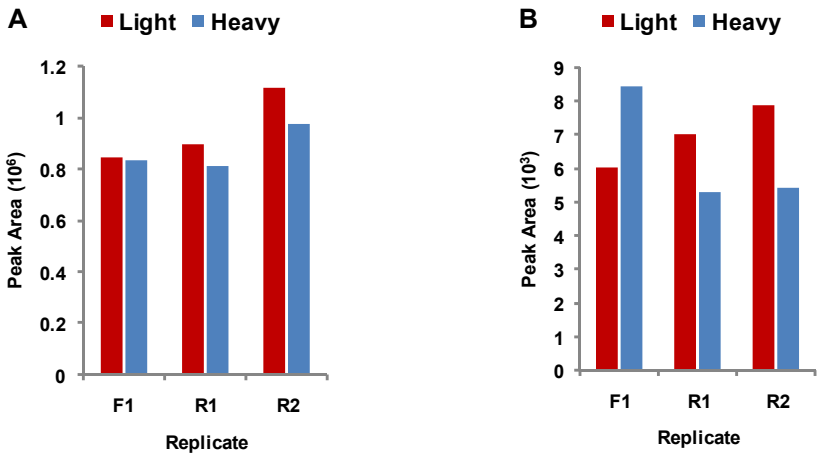

**Figure 4.8** Sodium arsenite induced elevated expression of cyclin-dependent kinase 1 (CDK1) (A-B), and arsenite-induced growth inhibition of cells can be rescued by a CDK inhibitor, flavopiridol (C). (A) Quantitative results by LC-MRM analysis for peptide DLK*PQNLLIDDK ("K*" designates the desthiobiotin-labeled lysine) from CDK1. Shown are the extracted-ion chromatograms for three transitions monitored for the peptide with light (Red) and heavy (Blue) labels in forward (Left) and reverse (Right) SILAC experiments. (B) Western blot analysis revealed the elevated expression of CDK1 upon arsenite treatment. (C) MTT assay showed that flavopiridol could significantly restore the cell proliferation rate after sodium arsenite treatment. '*', $p < 0.05$; '**', $p < 0.01$; '***', $p < 0.001$. The p values were calculated by using unpaired two-tailed t-test. The values represent mean of results obtained from three independent experiments.

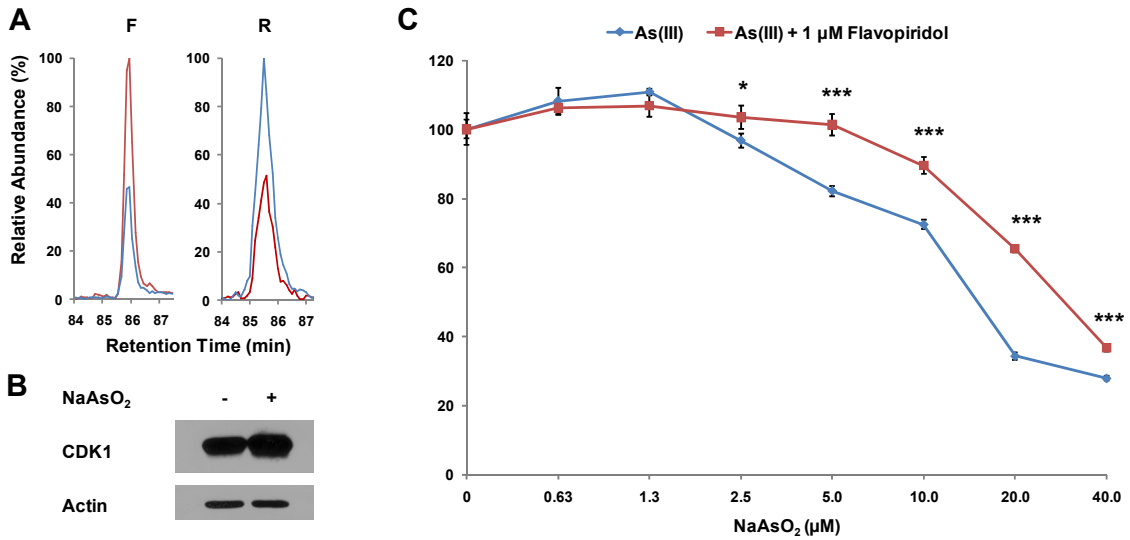

**Table 4.1** List of iRTs for reference peptides used in on-the-fly retention time calibration (A) and peptide from the tryptic digestion of BSA (B).

(A)

| Sequence | iRT |
|---|---|
| **GISNEGQNASIK** | -23.6 |
| **HVLTSIGEK** | -17.11 |
| **IGDYAGIK** | -3.57 |
| **TASEFDSAIAQDK** | 7.76 |
| **SAAGAFGPELSR** | 14 |
| **ELGQSGVDTYLQTK** | 22.55 |
| **GILFVGSGVSGGEEGAR** | 41.42 |
| **LTILEELR** | 58.5 |
| **ELASGLSFPVGFK** | 69.13 |
| **LSSEAPALFQFDLK** | 80.16 |

(B)

| Sequence | iRT |
|---|---|
| **AEFVEVTK** | 0 |
| **DAFLGSFLYEYSR** | 100 |
| **DLGEEHFK** | -11.06 |
| **HLVDEPQNLIK** | 13.76 |
| **LGEYGFQNALIVR** | 58.51 |
| **LVTDLTK** | -4.9 |
| **QTALVELLK** | 50.95 |
| **LVNELTEFAK** | 38.44 |
| **YLYEIAR** | 16.96 |
| **DDSPDLPK** | -13.05 |

**Table 4.2** List of kinases quantified as significantly changed after $NaAsO_2$ exposure. Listed are the expression ratios of GM00637 cells with $NaAsO_2$ treatment versus untreated control cells.

| IPI No. | Kinase Name | Description | Ratio |
|---|---|---|---|
| **IPI00414058** | GPRK5 | G protein-coupled receptor kinase 5 | 0.36 ± 0.18 |
| **IPI00513919** | PAN3 | Isoform 1 of PAB-dependent poly(A)-specific ribonuclease subunit 3 | 0.49 ± 0.12 |
| **IPI00398824** | PASK | Isoform 1 of PAS domain-containing serine/threonine-protein kinase | 0.51 ± 0.09 |
| **IPI00017083** | CaMKK1 | Isoform 1 of Calcium/calmodulin-dependent protein kinase kinase 1 | 0.53 ± 0.10 |
| **IPI00149048** | Erk5 | Isoform 2 of Mitogen-activated protein kinase 7 | 0.54 ± 0.13 |
| **IPI00180781** | MLKL | Isoform 1 of Mixed lineage kinase domain-like protein | 0.54 ± 0.05 |
| **IPI00290439** | SRPK1 | 74 kDa protein | 0.56 ± 0.09 |
| **IPI00003814** | MAP2K6 | Isoform 1 of Dual specificity mitogen-activated protein kinase kinase 6 | 0.66 ± 0.04 |
| **IPI00021331** | NEK2 | Isoform 1 of Serine/threonine-protein kinase Nek2 | 1.67 ± 0.10 |
| **IPI00099756** | AurC | Isoform 1 of Serine/threonine-protein kinase 13 | 1.68 ± 0.27 |
| **IPI00021333** | NEK4 | Isoform 1 of Serine/threonine-protein kinase Nek4 | 1.75 ± 0.18 |
| **IPI00165249** | PFTAIRE1 | Isoform 1 of Cell division protein kinase 14 | 1.80 ± 0.24 |
| **IPI00298940** | AurA | Serine/threonine-protein kinase 6 | 1.85 ± 0.39 |
| **IPI00149094** | GCK | Mitogen-activated protein kinase kinase kinase kinase 2 | 2.01 ± 1.01 |
| **IPI00006471** | MELK | Maternal embryonic leucine zipper kinase | 2.07 ± 0.31 |
| **IPI00007811** | CDK4 | Cell division protein kinase 4 | 2.18 ± 0.97 |
| **IPI00026689** | CDC2 | Cyclin-dependent kinase 1 | 2.07 ± 0.15 |

# Chapter 5

# Profiling Global Kinome Signatures of the Radioresistant MCF-7/C6 Breast Cancer Cells Using MRM-based Targeted Proteomics

## Introduction

There are increasing public concerns about the safety of environmental ionizing radiation as well as industrial and medical applications of ionizing radiation. Ionizing radiation, arising from both natural and anthropogenic sources, may cause damage to exposed individuals depending on radiation dose and duration.[1] In this vein, ionizing radiation may emanate from secondary particles from cosmic rays or decay of naturally occurring radioisotopes, and arise from nuclear reactors or during high-energy physics experiments.[2] Inadvertent exposure to ionizing radiation may result in DNA damage, cell death, and ultimately leading to human diseases including cancer.[2a] On the other hand, the ionizing radiation's capability in damaging DNA also forms the basis for cancer radiotherapy.[3] However, cellular response toward ionizing radiation varies among different cell types; the toxic effects on normal cells and tissues may elicit adverse human health consequences, whereas resistance of tumor cells toward ionizing radiation may render cancer radiation therapy less effective.[4] Accumulating evidence suggests that mammalian cells including many types of tumor cells are able to develop adaptive

radioresistance against ionizing radiation by activating a prosurvival signaling network.[5] The so-called tumor adaptive radioresistance creates a barrier for further improving cancer patient survival by ionizing radiation-based anti-cancer modalities.[5b]

Tumor aggressiveness in metastatic lesions is the lethal cause of cancer patients and is associated with the tumor-initiating cells, a.k.a. cancer stem cells, which display enhanced self-renewal, elevated DNA repair capacity and radioresistance.[4, 6] Radioresistant cells are capable of surviving under many genotoxic stress conditions including the therapeutic ionizing radiation, and this defective response in radiation therapy may be innate or acquired.[7] Along this line, radioresistance may arise from self-repair mechanisms in cells, mainly DNA damage repair,[8] and/or repopulation of radioresistant cancer stem cells.[5b, 9] Tumor heterogeneity was linked with different levels of radioresistance and a group of clones isolated from the MCF-7 breast cancer cells after long-term fractionated radiation were found to be more resistant to radiation than the parental MCF-7 tumor cells,[10] supporting the concept of the presence of cancer stem cells.[8, 11] One of the radioresistant clones, i.e. MCF-7/C6 [12], was found to be enriched in breast cancer stem cells (BCSCs; $ALDH^{+}/CD44^{+}/CD24^{-/low}$) and exhibit an enhanced prosurvival network of NF-κB and HER-2 expression,[5b, 13] suggesting that the radioresistant MCF-7/C6 cells are present as the most aggressive breast cancer cells. However, the precise mechanisms underlying this radioresistant phenotype remain elusive.

Kinases are an important superfamily of enzymes catalyzing the phosphorylation of small intracellular molecules and proteins that are critical in the maintenance of a

homeostatic cellular environment.[14] Aberrant regulation of kinases affects a myriad of cellular processes including cell signaling, proliferation and apoptosis. As mentioned above, HER-2 is implicated in the development of radioresistance.[5b, 13] In addition, several other kinase-mediated cell signaling pathways were found to play an important role in cancer radioresistance.[15] Thus, a thorough interrogation of the kinome reprogramming in cells with tumor radioresistance will not only provide practical perspectives about increasing the efficacy of cancer radiotherapy, but also afford important knowledge for developing potential effective molecules that can significantly prevent or treat tumors that are resistant to cancer radiation therapy.

With the advances in mass spectrometry instrumentation and the availability of bioinformatic tools, studies of global proteome and kinome become feasible.[16] Recently, we developed a multiple-reaction monitoring (MRM)-based approach, together with the use of isotope-coded ATP-affinity probes, for global kinome profiling, which enabled the simultaneous assessment of the expression/activity of more than 300 kinases in human cells and tissues.[17] In this approach, the binding moiety of the ATP affinity probe interacts specifically with ATP-binding proteins, including kinases, and subsequently forms covalent bond with lysine near the ATP binding sites, which enables efficient labeling, enrichment and identification of ATP-binding proteins from complex protein mixtures.[18] The stable isotope-coded linker of the ATP affinity probe further facilitates quantitative comparison of kinase expression/activity between different samples.[16b] Moreover, with a pre-constructed MRM kinome library, scheduled MRM analysis can be achieved with precisely predicted retention time window, rendering high-throughput and

simultaneous quantification of protein kinases feasible.[17] This MRM-based targeted proteomic analysis exhibited better sensitivity, accuracy and reproducibility than discovery-based shotgun proteomic method.[17] In the current study, we employed the same approach and conducted differential kinome analysis of MCF-7/WT human breast-cancer cells and the corresponding radioresistant MCF-7/C6 cells.

## Materials and methods

### Cell culture

All reagents unless otherwise stated were obtained from Sigma-Aldrich (St. Louis, MO). MCF-7/WT human breast cancer cells were purchased from ATCC (Manassas, VA). MCF-7+FIR30 (MCF-7/C6) radioresistant clone is a single clone (#6) surviving from 15 fractionated ionizing radiations at 2 Gy each [10, 12a]. MCF-7/WT and MCF-7/C6 cells were cultured in Eagle's Minimum Essential Medium (EMEM, ATCC) supplemented with 10% fetal bovine serum (FBS, Life Technologies, Grand Island, NY) and 1% antibiotic-antimycotic solution (Life Technologies). Cells were maintained in a humidified atmosphere with 5% $CO_2$ at 37°C, with media renewal in every 2-3 days.

### Sample preparation and isotope-coded ATP affinity probe labeling

MCF-7/WT and MCF-7/C6 cells were harvested at 80% confluency, at a density of ~ $5\times10^5$ cells/mL. Cells were collected and lysed as previously described.[17] Briefly, after washing with ice-cold phosphate-buffered saline (PBS) for three times, the cells were lysed with 0.7% CHAPS lysis buffer and further homogenized with a cell homogenizer. The cell lysates were passed through Illustra NAP-25 columns (GM Healthcare Bio-Sciences, Pittsburgh, PA) for the removal of endogenous nucleotides, and protein concentrations in the resultant lysates were subsequently determined by Bicinchoninic Acid Kit for Protein Determination.

The isotope-coded ATP affinity probes were synthesized previously.[16b, 19] Cell lysates (1.5 mg) from MCF-7/WT and MCF-7/C6 cells were incubated with heavy or light isotope-coded ATP affinity probe until its final concentration reached 100 μM. As

described elsewhere,[17] after incubation at room temperature for 2.5 h, heavy and light ATP probe-labeled cell lysates were mixed at 1:1 ratio (w/w). Subsequently, 10 kDa Amicon Ultra-15 centrifugal filter units (EMD Millipore, Billerica, MA) and sequencing-grade trypsin (Roche Applied Science, Indianapolis, IN) were employed for sample purification and tryptic digestion with the use of the filter-aided sample preparation method.[20] After enrichment using avidin-agarose resin, the eluted peptides were desalted by using OMIX $C_{18}$ pipette tips (Agilent, Santa Clara, CA).

**Scheduled LC-MRM analysis and data processing**

Scheduled LC-MRM analyses were performed on a TSQ Vantage triple-quadrupole mass spectrometer (Thermo Fisher, San Jose, CA) coupled with a nanoelectrospray ionization source and an EASY n-LCII HPLC system (Thermo Fisher). Detailed experimental conditions were described previously.[17] Briefly, the HPLC separation was conducted automatically with a 40-mm trapping column (150 μm i.d.) and a 200-mm analytical column (75 μm i.d., PicoTip Emitter, New Objective), packed with 5 and 3 μm reversed-phase ReproSil-Pur C18 material (120 Å in pore size, Dr. Maisch, Germany), respectively. The peptides were separated using a 130-min linear gradient of 2-35% acetonitrile in 0.1% formic acid at a flow rate of 230 nL/min. The spray voltage was 1.9 kV, and Q1 and Q3 resolutions were 0.7 Da. According to the maximum number of transitions per cycle, the cycle time was set at 4-5 s. Data were then processed against the MRM-based kinome library[17] on Skyline, version 1.4.0.4421.[21] Subsequent KEGG pathway and GO analysis was conducted using DAVID Bioinformatics Resources, version 6.7.[22]

**Western blot**

Western blot was performed as described elsewhere.[17] Briefly, equal amounts of lysates from MCF-7/WT and MCF-7/C6 cells were electrophoresed on a 12% SDS-PAGE gel with a 4% stacking gel. After protein transfer, the nitrocellulose membrane was blocked and incubated with the corresponding primary and then secondary antibodies. CHK1 (2G1D5) mouse mAb (Cell Signaling, Beverly, MA), CDK1 (E161) rabbit mAb (Abcam, Cambridge, MA) and CDK2 (78B2) rabbit mAb (Cell Signaling) were employed as the primary antibodies, and actin was used as the loading control.

## Results and discussions

### 1. Strategy for global kinome profiling

Despite being extensively studied, the exact mechanisms underlying tumor adaptive radioresistance to therapeutic ionizing radiation remain unresolved.[5b,23] We found that tumor heterogeneity plays a key role in cell repopulation in breast cancer cells and the radioresistant clones.[10] The radioresistant clones including MCF-7/C6[12] were found to be enriched with breast cancer stem cells (BCSCs; $ALDH^+/CD44^+/CD24^{-/low}$),[5b, 13] suggesting that the radioresistant MCF-7/C6 cells represent the most aggressive breast cancer cells.[24] Therefore, revealing active factors signaling the radioresistant phenotype of MCF-7/C6 cells may allow for the discovery of specific targets or development of small-molecule inhibitors for the prevention and treatment of radioresistant cancer. To exploit the kinome reprogramming accompanied with the development of radioresistance, we conducted an in-depth comparative analysis of the global kinome of MCF-7/WT and MCF-7/C6 human breast cancer cells. To this end, we adopted a previously established global kinome profiling method relying on LC-MRM and isotope-coded ATP affinity probes.[16b, 17] The probe consists of a binding moiety of ATP, an enrichment moiety of desthiobiotin, and an isotope-coded linker with six hydrogens or deuterons for light or heavy isotope labeling.

Figure 5.1 depicted the general workflow for the scheduled LC-MRM analysis. After reaching 80% confluency, MCF-7/WT and the corresponding γ-radiation-selected radioresistant MCF-7/C6 cells were harvested and lysed separately. In the forward labeling experiment, lysates of MCF-7/WT and MCF-7/C6 cells were incubated with the

heavy and light isotope-coded ATP affinity probes, respectively. The labeling was reversed in the reverse labeling experiment. To achieve reliable differential analysis of the global kinome of these two lines of cells, we conducted one forward and two reverse labeling experiments. As noted previously,[19] the ATP component of the affinity probe binds to the ATP-binding pocket of kinases during incubation. Upon binding, the acyl phosphate group in the probe reacts with the side chain amino group of the nearby conserved lysine residue, which gives rise to the labeling of kinases. After the incubation, the heavy and light ATP probe-labeled cell lysates were mixed together in equal mass. Subsequently, the filter-aided sample preparation method was utilized for protein purification and tryptic digestion. The resulting peptides were subsequently enriched using avidin-agarose. After peptide elution and desalting, the samples were subjected to scheduled LC-MRM analysis (Figure 5.1). For kinase quantification, integration of peak areas for the monitored transitions of kinase peptides was processed using Skyline.[21]

To achieve global kinome quantification in high throughput, we utilized our previously constructed kinome library for scheduled MRM analysis.[17] For the kinome library construction, large-scale data-dependent analyses of isotope-coded desthiobiotinylated kinome were performed, from which the tandem mass spectra and retention times for kinase peptides were extracted for scheduled MRM analysis using Skyline. With this method, we were able to monitor a total of ~ 2000 transitions, corresponding to approximately 400 peptides derived from more than 300 kinases, in two LC-MRM analyses. As illustrated on Figure 5.2A, the tandem mass spectrum (MS/MS)

of GK*FGNVYLAR (K* designates isotope-labeled desthiobiotin-conjugated lysine residue) derived from Aurora kinase A was acquired from previous data-dependent analysis for the kinome library construction. Based on the MS/MS, transitions for the formation of the three most abundant y ions ($y_4$, $y_7$, and $y_8$) were chosen for the scheduled MRM analysis of this kinase peptide. Transitions monitored in the current LC-MRM analysis for the corresponding light- and heavy-labeled peptides are shown in Figure 5.2B and C, respectively. The distribution patterns of the three y ions derived from the light- and heavy-labeled peptides were very similar to that in the MS/MS acquired from previous data-dependant analysis, which supports the reliable identification and quantification of the corresponding peptides.

**2. Global kinome of radioresistant MCF-7/C6 breast cancer cells versus parental MCF-7 cells**

In the current study, we were able to identify 195 kinases, among which 120 were quantified, from one forward and two reverse labeling experiments. The average relative standard deviation for all the quantified kinases is 14%. Thus, we employed cutoff ratios of > 1.5 and < 0.67 to define the significantly up- and down-regulated kinases, respectively. With the use of this criterion, 24 and 13 of the quantified kinases were significantly up- and down-regulated in MCF-7/C6 relative to MCF-7/WT cells, respectively (Table 5.1 and Figure 5.3). To the best of our knowledge, this represents the first in-depth analysis of the alteration of the entire kinome after breast cancer cells develop radioresistance. Kinases from all kinase families except the RGC and PKL family were successfully detected. These kinases cover a major part of cellular

components and are involved in a large collection of cellular pathway, as revealed by GO and KEGG pathway analysis (Figure 5.4). Figure 5.4A-B lists the GO cellular components and KEGG pathways as well as the number of kinases in each component or pathway with a p-value < 0.05. For example, 25, 10 and 8 key kinase modulators involved in MAPK, Toll-like receptor (TLR) and ErbB signaling pathways were successfully quantified with our method. Among them, TLR signaling pathway is well-known for its critical role in innate immune response.[25] Some members of TLRs such as TLR5 and TLR9 were found to trigger cancer recurrence after radiotherapy.[26]

It is worth noting that in the current labeling strategy, the ATP-affinity probe forms a covalent amide bond with the side chain of lysine residue at the ATP-binding site and may share conserved sequence.[16b, 27] To increase the specificity and reliability of this approach, we excluded those labelings emanating from non-specific interactions. In this vein, only peptides containing the pre-determined ATP-binding motifs (HRDxKxxN, VAxK or GxxxxGK) or those without a binding motif but were frequently identified in previous shotgun proteomic studies were chosen for the scheduled MRM monitoring.[17] Thus, some targeted peptides may be attributed to multiple protein kinases and quantification was only based on unique peptides when they are available. In the current study, among the 195 kinases identified, 120 (62%) were quantified with at least one unique peptides to unambiguously identify the targeted kinase isoform, whereas the rest 75 (38%) were identified based on peptides that may originate from multiple kinases. The quantification results of the entire kinome are depicted in the histogram in Figure 5.3. As mentioned above, 69% of quantified kinases exhibited very similar levels of

expression/activation in the MCF-7/WT and MCF-7/C6 cells. The remaining 20% and 11% kinases were significantly increased and decreased, respectively. Among the different kinase families, the cell kinase 1 family displayed the most distinct alterations in expression level/activity, with all the kinases quantified in this family being elevated in the radioresistant cells. Similarly, for tyrosine kinase-like and atypical families of kinases, all significantly altered kinases were up-regulated in MCF-7/C6 cells. On the other hand, considerably more kinases in the protein kinase A/G/C family were significantly decreased in MCF-7/C6 cells than those that were increased. From KEGG pathway analysis of these kinases, we discovered that a variety of pathways were altered in the radioresistant cells compared to the parental MCF-7 cells. As depicted in Figure 5.4C-D, most pathways are unambiguously activated or inhibited in the radioresistant MCF-7/C6 cells. However, for certain pathways, such as MAPK signaling pathway, the regulation of kinase expression/activity displayed opposite trend, which may suggest the roles of some of these kinases in other cellular pathways or the aberrant regulation of some kinases in this pathway is compensated by others in the same pathway.

**3. Ionizing radiation perturbed the expression/activity of kinases in cell cycle progression as well as DNA damage response and repair**

Four kinases involved in cell cycle regulation and DNA damage response/repair were found to be overexpressed/activated in the radioresistant MCF-7/C6 relative to MCF-7/WT cells, which include CHK1, cyclin-dependent kinases 1 and 2 (CDK1 and CDK2) and the catalytic subunit of DNA-dependent protein kinase (DNA-PKcs). Figure 5.5A-C shows the extracted ion-chromatograms of DIK*PENLLLDER from CHK1 (ratio

of 5.46), DLK*PQNLLIDDK from CDK1 (ratio of 2.76) and DLK*PQNLLINTEGAIK from CDK2 (ratio of 1.82), where K* denotes isotope-labeled desthiobiotin-conjugated lysine residue. To further confirm these quantification results, we monitored the expression levels of CHK1, CDK1 and CDK2 in these two lines of cells by Western blot analysis. Our results showed that all three kinases displayed elevated expression in MCF-7/C6 relative to MCF-7/WT cells, which is in agreement with our MRM quantification results (Figure 5.5D). Therefore, enabled by this global kinome analysis, we demonstrated unambiguously the elevated expression/activation of kinases involved in cell cycle regulation in the radioresistant cells, which may better facilitate cell cycle progression in the presence of genotoxic stress introduced by ionizing radiation.

Cancer radiation therapy relies primarily on the radiation-induced DNA lesions, particularly DNA strand breaks.[3, 28] Differences in DNA repair capacities may contribute directly to variations in the efficacies of cancer radiation therapy.[29] In this regard, radioresistant cancer may possess a more robust DNA damage repair machinery through inherited or acquired mechanisms.[4] Most DNA repair events require the initiation of cell cycle arrest, which provides time for genome repair before continuing cell cycle progression.[30] Along this line, CHK1 is activated in response to DNA damage, which facilitates transduction of checkpoint signal for the induction of cell cycle arrest.[31] Thus, activation of CHK1 could be a critical contributor to cancer radioresistance. In this vein, the connection between CHK1 activation and induction of radioresistance was reported previously.[32] CHK1's role in radioresistance may stem from the zinc-finger E-box binding homeobox 1-enhanced ubiquitin-specific-processing protease 7 activity, which

controls the activation and deubiquitination of CHK1 via an ATM-dependent mechanism.[33] To overcome the CHK1-induced radioresistance, inhibitors have been utilized for the improvement of radiotherapy.[34] Likewise, as a cell cycle regulator, CDK1 was found to be up-regulated in radioresistant cells in our study, which was believed to contribute to radioresistance through phosphorylation of checkpoint proteins and modulators of DNA repair.[30] In this context, it was found recently that CDK1 can relocate to mitochondria, which leads to the phosphorylation of a cluster of mitochondrial targets including complex I and enhances mitochondrial ATP generation at G2/M transition in fast-growing cells.[35] The results from the present study further support the notion that CDK1 may exert two layers of function in enhancing cell survival, i.e., by increasing the DNA repair capacity and by augmenting cellular energy supply through modulation of mitochondrial metabolism. Nevertheless, the interplay of these two functions of cell survival, especially in tumor adaptive radioresistance, awaits further investigation.

Non-homologous end-joining constitutes the major mechanism for repairing ionizing radiation-induced DNA double strand breaks.[36] We found that DNA-PKcs, a key component of this repair pathway, was overexpressed/activated in the present study, which is consistent with its documented role in cancer radioresistance.[37] It was reported that DNA-PKcs participates in acquired radioresistance through the activation of protein kinase B and inactivation of glycogen synthase kinase-3β in a positive feedback loop, thereby leading to cyclin D1 overproduction and triggering the DNA damage response pathway in cancer cells upon exposure to ionizing radiation.[38] In keeping with this

notion, inhibition of DNA-PKcs was shown to sensitize MCF-7, MDA-MB-231 and T47D human breast cancer cells toward ionizing radiation.[39] Aside from the aforementioned kinases whose overexpression is known to be important in radioresistance, we also observed the overexpression/activation of a number of other kinases, including MLKL, EphB4, etc. These kinases may constitute novel targets for ameliorating radioresistance in cancer therapy, and further studies are needed to determine whether this is the case.

**Conclusions**

Although extensively studied, the mechanisms underlying tumor adaptive radioresistance remain unclear. The innate or acquired radioresistance compromises the effectiveness of radiation therapy for cancer patients, an urgent clinical issue that needs to be addressed. To unveil the molecular mechanisms of radioresistance, we performed quantitative comparison of the global kinome of MCF-7 human breast cancer cells and the corresponding ionizing radiation-selected radioresistant clone, i.e. MCF-7/C6 cells. In this vein, we employed scheduled LC-MRM coupled with isotope-coded desthiobiotin-conjugated ATP affinity probes for the quantification of the entire kinome of these two cell lines. We were able to quantify a total of 120 kinases, which covered around 25% of the entire human kinome. Approximately one third of these quantified kinases displayed significant alterations in expression and/or activity, which consists of a majority of cellular components and regulates multiple cellular processes.

Notably, several key regulators of cell cycle progression and maintenance of genomic stability were found to be overexpressed/hyperactivated in the radioresistant MCF-7/C6 cells, including CHK1, CDK1, CDK2 and DNA-PKcs. The elevated expression of CHK1, CDK1 and CDK2 was further confirmed by Western blot analysis. Given that DNA lesion induction is one of the major deleterious effects elicited by ionizing radiation,[3] efficiency in DNA repair is a deciding factor for the cellular sensitivity toward ionizing radiation. Cell cycle arrest is indispensable for providing cells enough time to complete DNA repair.[40] The above-mentioned kinases play pivotal roles in triggering cell cycle checkpoint and regulating cell cycle progression. In addition,

some of these kinases are also actively engaged in the phosphorylation of mediators in DNA repair pathways. Thus, the above findings of global kinome alterations associated with radioresistance provide new knowledge for understanding tumor adaptive radioresistance and offer potential targets for sensitizing cancer cells toward radiation therapy, so as to achieve better remission of cancer.

**References**


1. Little, M., Risks associated with ionizing radiation: environmental pollution and health. *Br. Med. Bull.* **2003,** *68* (1), 259-275.

2. (a) Doll, R., Hazards of ionising radiation: 100 years of observations on man. *Br. J. Cancer* **1995,** *72* (6), 1339-49; (b) Melott, A. L.; Thomas, B. C., Astrophysical ionizing radiation and Earth: a brief review and census of intermittent intense sources. *Astrobiology* **2011,** *11* (4), 343-61.

3. Prise, K. M.; Schettino, G.; Folkard, M.; Held, K. D., New insights on cell death from radiation exposure. *Lancet Oncol.* **2005,** *6* (7), 520-8.

4. Baumann, M.; Krause, M.; Hill, R., Exploring the role of cancer stem cells in radioresistance. *Nat. Rev. Cancer* **2008,** *8* (7), 545-554.

5. (a) Ahmed, K. M.; Li, J. J., NF-kappa B-mediated adaptive resistance to ionizing radiation. *Free Radic. Biol. Med.* **2008,** *44* (1), 1-13; (b) Duru, N.; Candas, D.; Jiang, G.; Li, J. J., Breast cancer adaptive resistance: HER2 and cancer stem cell repopulation in a heterogeneous tumor society. *J. Cancer Res. Clin. Oncol.* **2014,** *140* (1), 1-14.

6. (a) Bao, S.; Wu, Q.; McLendon, R. E.; Hao, Y.; Shi, Q.; Hjelmeland, A. B.; Dewhirst, M. W.; Bigner, D. D.; Rich, J. N., Glioma stem cells promote radioresistance by preferential activation of the DNA damage response. *Nature* **2006,** *444* (7120), 756-760; (b) Rich, J. N., Cancer stem cells in radiation resistance. *Cancer Res.* **2007,** *67* (19), 8980-4.

7. (a) Conger, A. D.; Luippold, H. J., Studies on the mechanism of acquired radioresistance in cancer. *Cancer Res.* **1957,** *17* (9), 897-903; (b) Liu, C.; Zhang, C.; Mitchel, R. E.; Cui, J.; Lin, J.; Yang, Y.; Liu, X.; Cai, J., A critical role of toll-like receptor 4 (TLR4) and its' in vivo ligands in basal radio-resistance. *Cell Death Dis.* **2013,** *4*, e649.

8. Bao, S.; Wu, Q.; McLendon, R. E.; Hao, Y.; Shi, Q.; Hjelmeland, A. B.; Dewhirst, M. W.; Bigner, D. D.; Rich, J. N., Glioma stem cells promote radioresistance by preferential activation of the DNA damage response. *Nature* **2006,** *444*, 756-60.

9. Reya, T.; Morrison, S. J.; Clarke, M. F.; Weissman, I. L., Stem cells, cancer, and cancer stem cells. *Nature* **2001,** *414* (6859), 105-11.

10. Li, Z.; Xia, L.; Lee, M. L.; Khaletskiy, A.; Wang, J.; Wong, J. Y. C.; Li, J. J., Effector genes altered in MCF-7 human breast cancer cells after exposure to fractionated ionizing radiation. *Radiat. Res.* **2001,** *155* (4), 543-553.

11. Pajonk, F.; Vlashi, E.; McBride, W. H., Radiation resistance of cancer stem cells: the 4 R's of radiobiology revisited. *Stem Cells* **2010,** *28* (4), 639-48.

12. (a) Ahmed, K. M.; Dong, S.; Fan, M.; Li, J. J., Nuclear factor-kappaB p65 inhibits mitogen-activated protein kinase signaling pathway in radioresistant breast cancer cells. *Mol. Cancer Res.* **2006,** *4* (12), 945-55; (b) Guo, G.; Wang, T.; Gao, Q.; Tamae, D.; Wong, P.; Chen, T.; Chen, W. C.; Shively, J. E.; Wong, J. Y.; Li, J. J., Expression of ErbB2 enhances radiation-induced NF-kappaB activation. *Oncogene* **2004,** *23* (2), 535-45; (c) Cao, N.; Li, S.; Wang, Z.; Ahmed, K. M.; Degnan, M. E.; Fan, M.; Dynlacht, J. R.; Li, J. J., NF-kappaB-mediated HER2 overexpression in radiation-adaptive resistance. *Radiat. Res.* **2009,** *171* (1), 9-21.

13. Duru, N.; Fan, M.; Candas, D.; Menaa, C.; Liu, H. C.; Nantajit, D.; Wen, Y.; Xiao, K.; Eldridge, A.; Chromy, B. A.; Li, S.; Spitz, D. R.; Lam, K. S.; Wicha, M. S.; Li, J. J., HER2-associated radioresistance of breast cancer stem cells isolated from HER2-negative breast cancer cells. *Clin. Cancer Res.* **2012,** *18* (24), 6634-47.

14. Cheng, H. C.; Qi, R. Z.; Paudel, H.; Zhu, H. J., Regulation and function of protein kinases and phosphatases. *Enzyme Res.* **2011,** *2011*, 794089.

15. Skvortsova, I.; Skvortsov, S.; Stasyk, T.; Raju, U.; Popper, B. A.; Schiestl, B.; von Guggenberg, E.; Neher, A.; Bonn, G. K.; Huber, L. A.; Lukas, P., Intracellular signaling pathways regulating radioresistance of human prostate carcinoma cells. *Proteomics* **2008,** *8* (21), 4521-33.

16. (a) Mann, M., Functional and quantitative proteomics using SILAC. *Nat. Rev. Mol. Cell Biol.* **2006,** *7* (12), 952-958; (b) Xiao, Y.; Guo, L.; Wang, Y., Isotope-coded ATP probe for quantitative affinity profiling of ATP-binding proteins. *Anal. Chem.* **2013,** *85* (15), 7478-86.

17. Xiao, Y.; Guo, L.; Wang, Y., A targeted quantitative proteomics strategy for global kinome profiling of cancer cells and tissues. *Mol. Cell. Proteomics* **2014,** *13* (4), 1065-75.

18. (a) Patricelli, M. P.; Szardenings, A. K.; Liyanage, M.; Nomanbhoy, T. K.; Wu, M.; Weissig, H.; Aban, A.; Chun, D.; Tanner, S.; Kozarich, J. W., Functional interrogation of the kinome using nucleotide acyl phosphates. *Biochemistry* **2007,** *46* (2), 350-8; (b) Qiu, H.; Wang, Y., Probing adenosine nucleotide-binding proteins with an affinity-labeled nucleotide probe and mass spectrometry. *Anal. Chem.* **2007,** *79* (15), 5547-56.

19. Xiao, Y.; Guo, L.; Jiang, X.; Wang, Y., Proteome-wide discovery and characterizations of nucleotide-binding proteins with affinity-labeled chemical probes. *Anal. Chem.* **2013,** *85* (6), 3198-206.

20. Wisniewski, J. R.; Zougman, A.; Nagaraj, N.; Mann, M., Universal sample preparation method for proteome analysis. *Nat. Methods* **2009,** *6* (5), 359-62.

21. MacLean, B.; Tomazela, D. M.; Shulman, N.; Chambers, M.; Finney, G. L.; Frewen, B.; Kern, R.; Tabb, D. L.; Liebler, D. C.; MacCoss, M. J., Skyline: an open source document editor for creating and analyzing targeted proteomics experiments. *Bioinformatics (Oxford, England)* **2010,** *26* (7), 966-8.

22. Huang da, W.; Sherman, B. T.; Lempicki, R. A., Bioinformatics enrichment tools: paths toward the comprehensive functional analysis of large gene lists. *Nucleic. Acids Res.* **2009,** *37* (1), 1-13.

23. Bourguignon, L. Y.; Shiina, M.; Li, J. J., Hyaluronan-CD44 Interaction Promotes Oncogenic Signaling, microRNA Functions, Chemoresistance, and Radiation Resistance in Cancer Stem Cells Leading to Tumor Progression. *Adv. Cancer Res.* **2014,** *123*, 255-75.

24. Phillips, T. M.; McBride, W. H.; Pajonk, F., The response of CD24(-/low)/CD44+ breast cancer-initiating cells to radiation. *J. Natl. Cancer Inst.* **2006,** *98* (24), 1777-85.

25. Akira, S.; Takeda, K., Toll-like receptor signalling. *Nat. Rev. Immunol.* **2004,** *4* (7), 499-511.

26. (a) Kauppila, J. H.; Mattila, A. E.; Karttunen, T. J.; Salo, T., Toll-like receptor 5 (TLR5) expression is a novel predictive marker for recurrence and survival in squamous cell carcinoma of the tongue. *Br. J. Cancer* **2013,** *108* (3), 638-643; (b) Gao, C.; Kozlowska, A.; Nechaev, S.; Li, H.; Zhang, Q.; Hossain, D. M.; Kowolik, C. M.; Chu, P.; Swiderski, P.; Diamond, D. J.; Pal, S. K.; Raubitschek, A.; Kortylewski, M., TLR9 signaling in the tumor microenvironment initiates cancer recurrence after radiotherapy. *Cancer Res.* **2013,** *73* (24), 7211-21.

27. Manning, G.; Whyte, D. B.; Martinez, R.; Hunter, T.; Sudarsanam, S., The protein kinase complement of the human genome. *Science* **2002,** *298* (5600), 1912-34.

28. Jackson, S. P., Sensing and repairing DNA double-strand breaks. *Carcinogenesis* **2002,** *23* (5), 687-96.

29. Buchholz, T. A., Radiation therapy for early-stage breast cancer after breast-conserving surgery. *N. Engl. J. Med.* **2009,** *360* (1), 63-70.

30. Branzei, D.; Foiani, M., Regulation of DNA repair throughout the cell cycle. *Nat. Rev. Mol. Cell Biol.* **2008,** *9* (4), 297-308.

31. Zhang, Y.; Hunter, T., Roles of Chk1 in cell biology and cancer therapy. *Int. J. Cancer* **2014,** *134* (5), 1013-23.

32. Wang, W. J.; Wu, S. P.; Liu, J. B.; Shi, Y. S.; Huang, X.; Zhang, Q. B.; Yao, K. T., MYC regulation of CHK1 and CHK2 promotes radioresistance in a stem cell-like population of nasopharyngeal carcinoma cells. *Cancer Res.* **2013,** *73* (3), 1219-31.

33. Zhang, P.; Wei, Y.; Wang, L.; Debeb, B. G.; Yuan, Y.; Zhang, J.; Yuan, J.; Wang, M.; Chen, D.; Sun, Y.; Woodward, W. A.; Liu, Y.; Dean, D. C.; Liang, H.; Hu, Y.; Ang, K. K.; Hung, M. C.; Chen, J.; Ma, L., ATM-mediated stabilization of ZEB1 promotes DNA damage response and radioresistance through CHK1. *Nat. Cell Biol.* **2014**.

34. Bolderson, E.; Richard, D. J.; Zhou, B. B.; Khanna, K. K., Recent advances in cancer therapy targeting proteins involved in DNA double-strand break repair. *Clin. Cancer Res.* **2009,** *15* (20), 6314-20.

35. Wang, Z.; Fan, M.; Candas, D.; Zhang, T. Q.; Qin, L.; Eldridge, A.; Wachsmann-Hogiu, S.; Ahmed, K. M.; Chromy, B. A.; Nantajit, D.; Duru, N.; He, F.; Chen, M.; Finkel, T.; Weinstein, L. S.; Li, J. J., Cyclin B1/Cdk1 coordinates mitochondrial respiration for cell-cycle G2/M progression. *Dev. Cell* **2014,** *29* (2), 217-32.

36. Lieber, M. R.; Ma, Y.; Pannicke, U.; Schwarz, K., Mechanism and regulation of human non-homologous DNA end-joining. *Nat. Rev. Mol. Cell. Biol.* **2003,** *4* (9), 712-20.

37. Kienker, L. J.; Shin, E. K.; Meek, K., Both V(D)J recombination and radioresistance require DNA-PK kinase activity, though minimal levels suffice for V(D)J recombination. *Nucleic. Acids Res.* **2000,** *28* (14), 2752-61.

38. Shimura, T.; Kakuda, S.; Ochiai, Y.; Nakagawa, H.; Kuwahara, Y.; Takai, Y.; Kobayashi, J.; Komatsu, K.; Fukumoto, M., Acquired radioresistance of human tumor cells by DNA-PK/AKT/GSK3beta-mediated cyclin D1 overexpression. *Oncogene* **2010,** *29* (34), 4826-37.

39. Ciszewski, W. M.; Tavecchio, M.; Dastych, J.; Curtin, N. J., DNA-PK inhibition by NU7441 sensitizes breast cancer cells to ionizing radiation and doxorubicin. *Breast Cancer Res. Treat.* **2014,** *143* (1), 47-55.

40. Zhou, B. B.; Elledge, S. J., The DNA damage response: putting checkpoints in perspective. *Nature* **2000,** *408* (6811), 433-9.

**Figure 5.1** General workflow for the quantitative scheduled multiple-reaction monitoring (MRM) analysis of the entire kinome using isotope-coded ATP affinity probes. Flowcharts of the forward labeling and LC-MRM experiment.

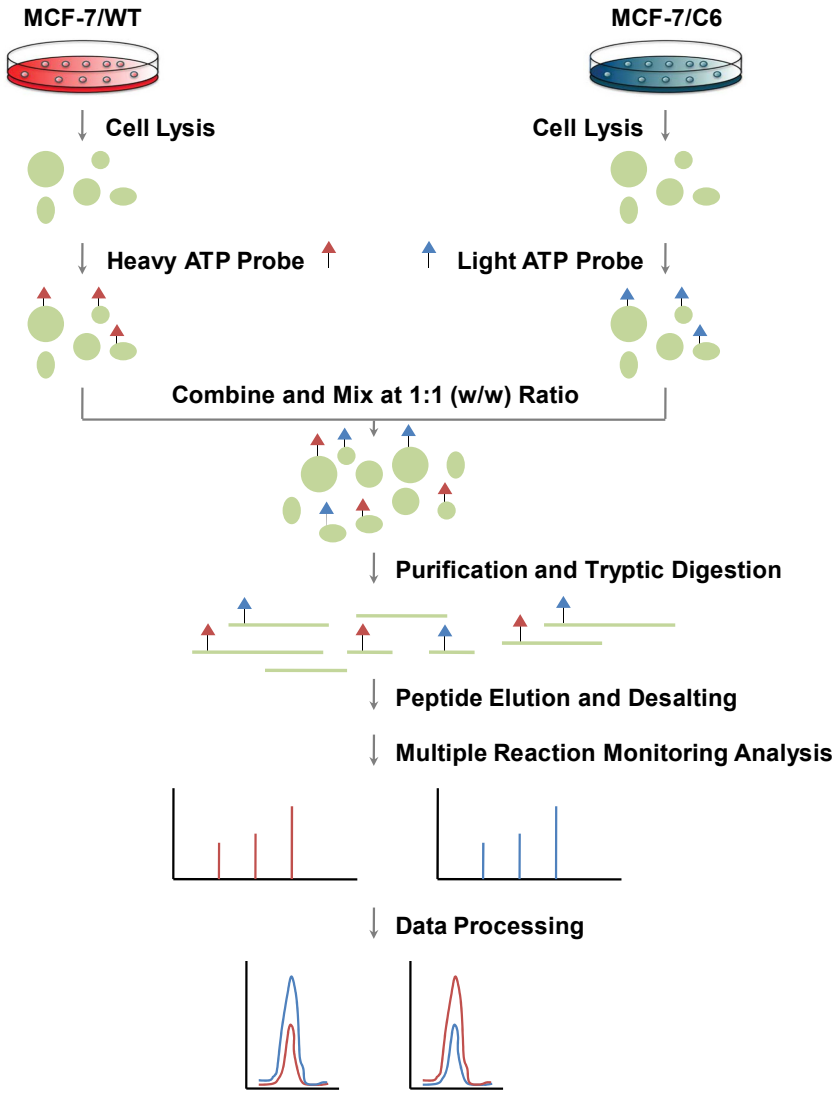

**Figure 5.2** Representative MS/MS depicted the reliable quantification of Aurora kinase A. (A) The MS/MS of Aurora kinase A peptide GK*FGNVYLAR (K* designates isotope-labeled desthiobiotin-conjugated lysine) in the kinome library from previous data-dependent analysis. (B-C) The monitored transitions from the current LC-MRM analysis for the same light and heavy-labeled desthiobiotinylated peptides, respectively.

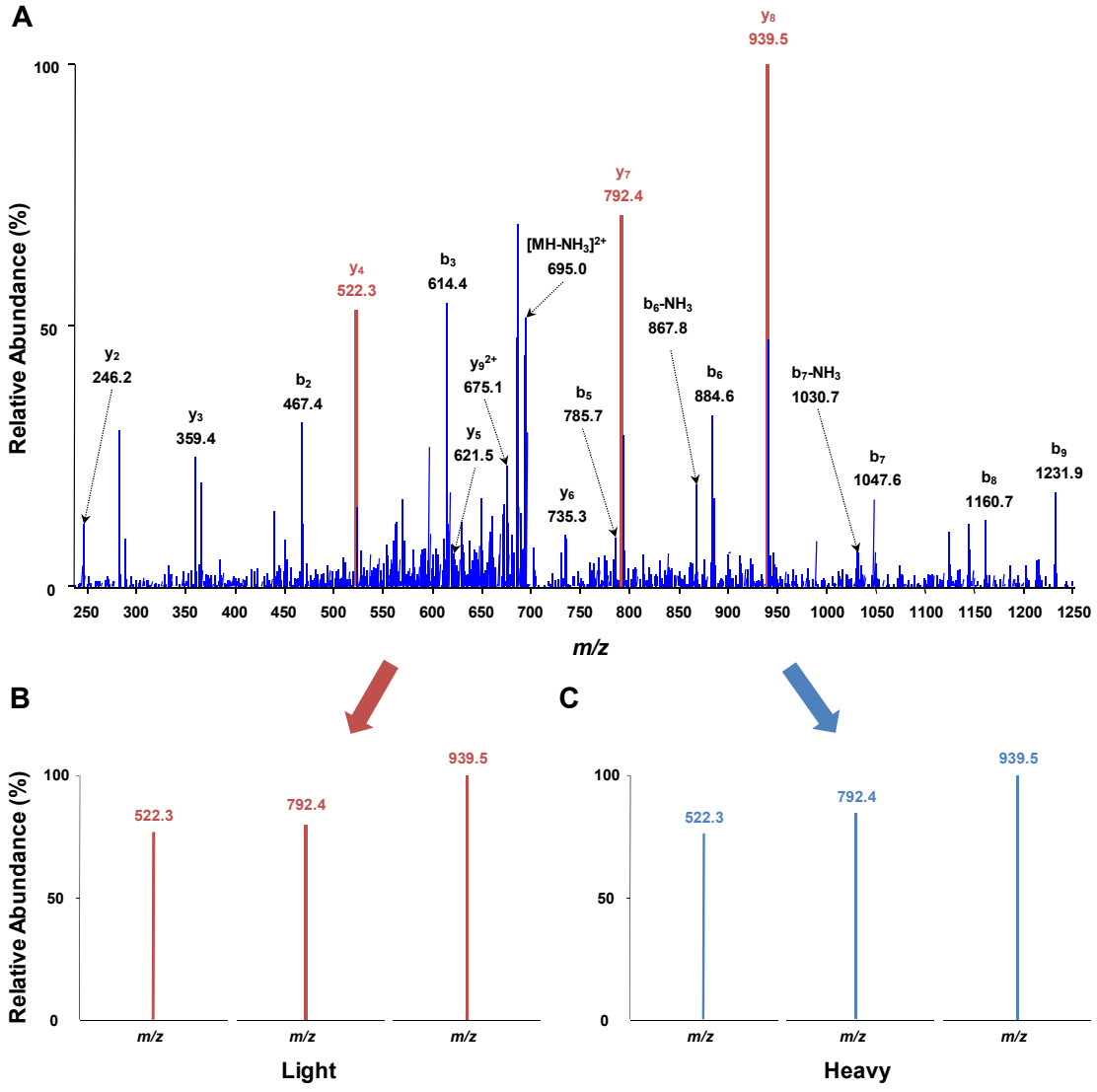

**Figure 5.3** Global kinome comparison of MCF-7/WT and radioresistant MCF-7/C6 human breast cancer cells. Shown in the histogram are the quantification results of the entire kinome in the two cell lines. Blue and red bars represent those kinases that are significantly down- and up-regulated in MCF-7/C6 relative to MCF-7/WT cells, respectively.

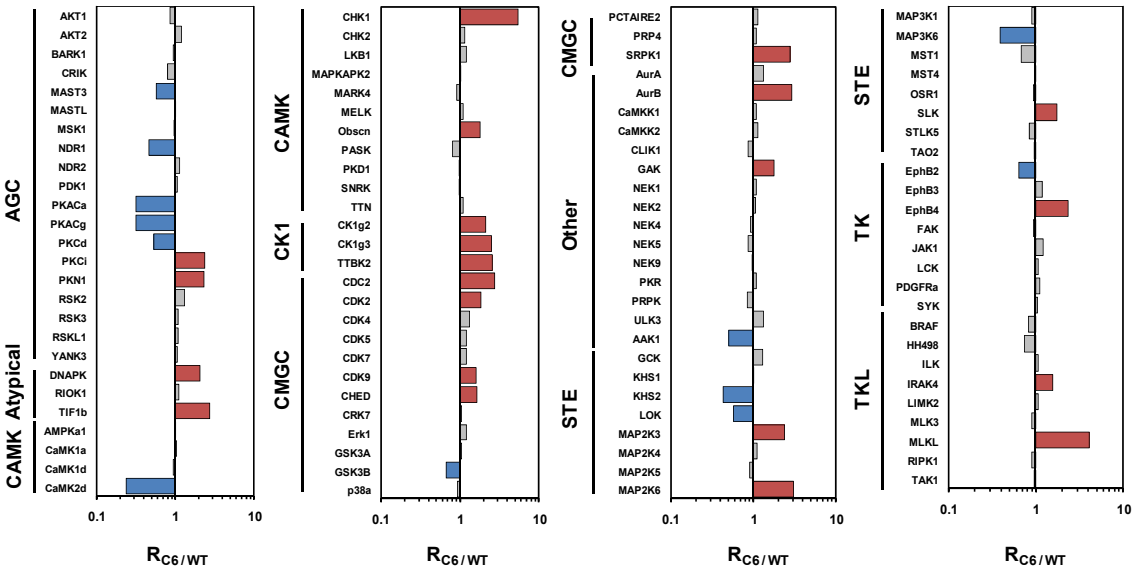

**Figure 5.4** GO and KEGG pathway analysis of kinases detected in the LC-MRM analysis. The number of kinases in the GO cellular components (A) and KEGG pathways (B) with a p-value < 0.05 are listed. Displayed are also the significantly down- (C) and up- (D) regulated kinases involved KEGG pathways in MCF-7/C6 relative to MCF-7/WT cells.

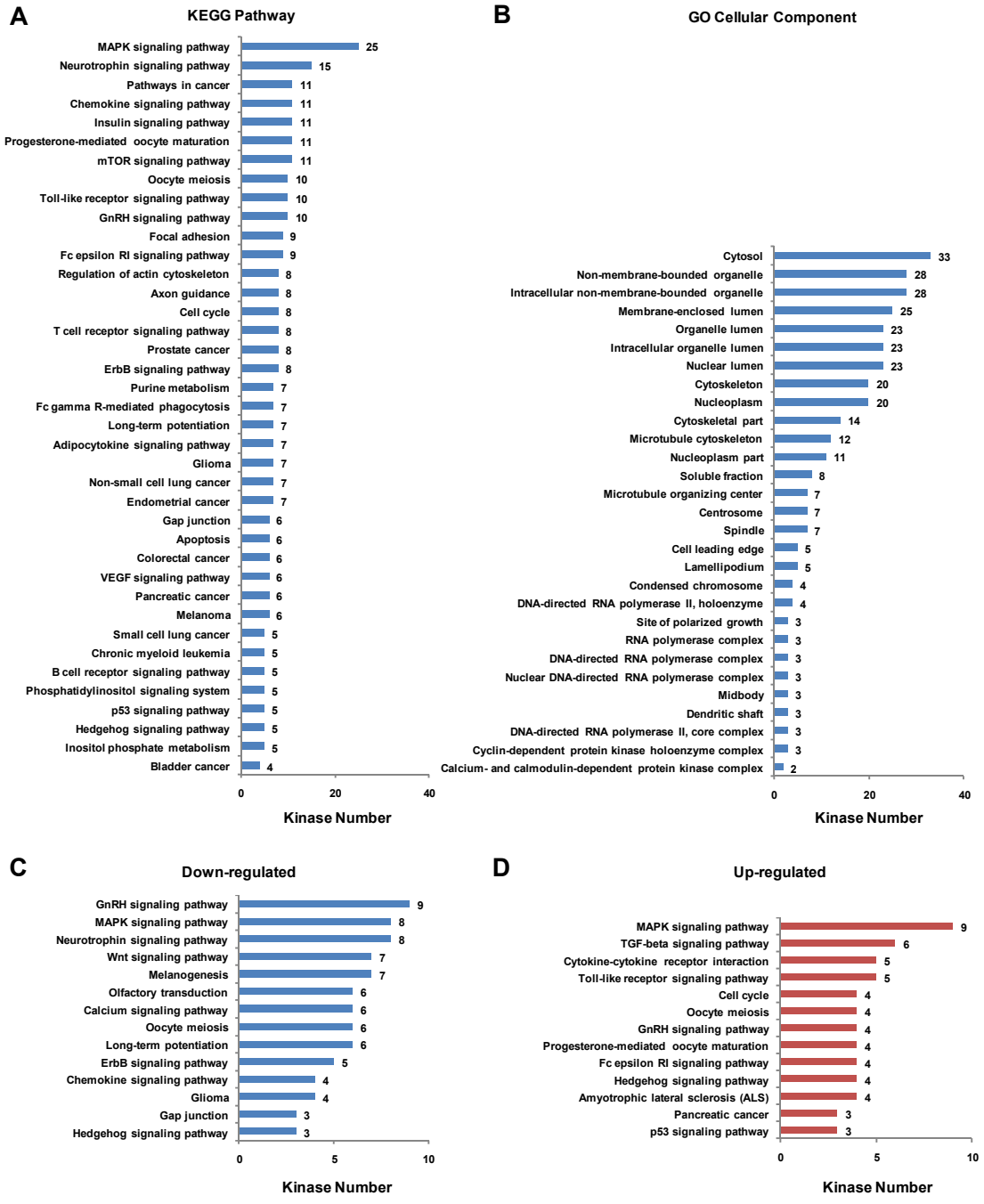
A
KEGG Pathway
MAPK signaling pathway 25
Neurotrophin signaling pathway 15
Pathways in cancer 11
Chemokine signaling pathway 11
Insulin signaling pathway 11
Progesterone-mediated oocyte maturation 11
mTOR signaling pathway 11
Oocyte meiosis 10
Toll-like receptor signaling pathway 10
GnRH signaling pathway 10
Focal adhesion 9
Fc epsilon RI signaling pathway 9
Regulation of actin cytoskeleton 8
Axon guidance 8
Cell cycle 8
T cell receptor signaling pathway 8
Prostate cancer 8
ErbB signaling pathway 8
Purine metabolism 7
Fc gamma R-mediated phagocytosis 7
Long-term potentiation 7
Adipocytokine signaling pathway 7
Glioma 7
Non-small cell lung cancer 7
Endometrial cancer 7
Gap junction 6
Apoptosis 6
Colorectal cancer 6
VEGF signaling pathway 6
Pancreatic cancer 6
Melanoma 6
Small cell lung cancer 5
Chronic myeloid leukemia 5
B cell receptor signaling pathway 5
Phosphatidylinositol signaling system 5
p53 signaling pathway 5
Hedgehog signaling pathway 5
Inositol phosphate metabolism 5
Bladder cancer 4
0 20 40
Kinase Number
B
GO Cellular Component
Cytosol 33
Non-membrane-bounded organelle 28
Intracellular non-membrane-bounded organelle 28
Membrane-enclosed lumen 25
Organelle lumen 23
Intracellular organelle lumen 23
Nuclear lumen 23
Cytoskeleton 20
Nucleoplasm 20
Cytoskeletal part 14
Microtubule cytoskeleton 12
Nucleoplasm part 11
Soluble fraction 8
Microtubule organizing center 7
Centrosome 7
Spindle 7
Cell leading edge 5
Lamellipodium 5
Condensed chromosome 4
DNA-directed RNA polymerase II, holoenzyme 4
Site of polarized growth 3
RNA polymerase complex 3
DNA-directed RNA polymerase complex 3
Nuclear DNA-directed RNA polymerase complex 3
Midbody 3
Dendritic shaft 3
DNA-directed RNA polymerase II, core complex 3
Cyclin-dependent protein kinase holoenzyme complex 3
Calcium- and calmodulin-dependent protein kinase complex 2
0 20 40
Kinase Number
C
Down-regulated
GnRH signaling pathway 9
MAPK signaling pathway 8
Neurotrophin signaling pathway 8
Wnt signaling pathway 7
Melanogenesis 7
Olfactory transduction 6
Calcium signaling pathway 6
Oocyte meiosis 6
Long-term potentiation 6
ErbB signaling pathway 5
Chemokine signaling pathway 4
Glioma 4
Gap junction 3
Hedgehog signaling pathway 3
0 5 10
Kinase Number
D
Up-regulated
MAPK signaling pathway 9
TGF-beta signaling pathway 6
Cytokine-cytokine receptor interaction 5
Toll-like receptor signaling pathway 5
Cell cycle 4
Oocyte meiosis 4
GnRH signaling pathway 4
Progesterone-mediated oocyte maturation 4
Fc epsilon RI signaling pathway 4
Hedgehog signaling pathway 4
Amyotrophic lateral sclerosis (ALS) 4
Pancreatic cancer 3
p53 signaling pathway 3
0 5 10
Kinase Number

**Figure 5.5** Development of radioresistance is correlated with elevation of kinases involved in cell cycle progression and checkpoint control. Shown are the extracted-ion chromatograms for transitions monitored for the following peptides: (A) DIK*PENLLLDER (K* designates isotope-labeled desthiobiotin-conjugated lysine residue) from CHK1; (B) DLK*PQNLLIDDK from CDK1; (C) DLK*PQNLLINTEGAIK from CDK2 in the LC-MRM experiments. Light- (Red) and heavy- (Blue) labeled peptides in forward (Left) and reverse (Right) labeling experiments. (D) Western blot analysis reveals the increased expression of CHK1, CDK1 and CDK2 in MCF-7/C6 relative to MCF-7/WT cells.

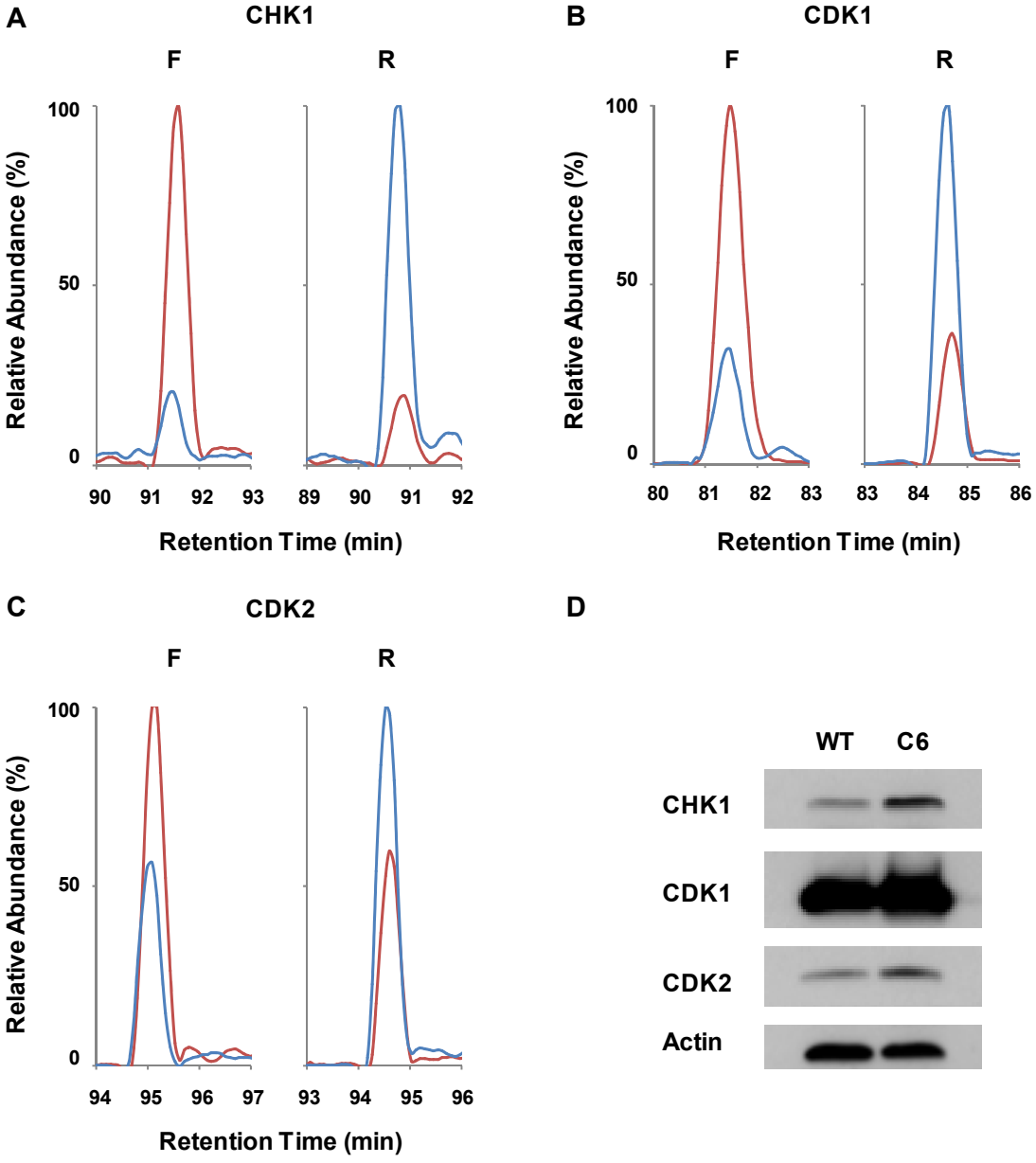
A
CHK1
F
R
100
50
0
Relative Abundance (%)
90 91 92 93 89 90 91 92
Retention Time (min)
B
CDK1
F
R
100
50
0
Relative Abundance (%)
80 81 82 83 83 84 85 86
Retention Time (min)
C
CDK2
F
R
100
50
0
Relative Abundance (%)
94 95 96 97 93 94 95 96
Retention Time (min)
D
WT
C6
CHK1
CDK1
CDK2
Actin

**Table 5.1** List of kinases quantified as significantly changed in radioresistant MCF-7/C6 compared to MCF-7/WT human breast cancer cells. Listed are the expression ratios of kinases in MCF-7/C6 versus MCF-7/WT.

| IPI No. | Kinase Name | Description | Ratio |
|---|---|---|---|
| | | **Up-regulated** | |
| **IPI00007641** | IRAK4 | IRAK4 Interleukin-1 receptor-associated kinase 4 | 1.57 ± 0.11 |
| **IPI00301923** | CDK9 | CDK9 Isoform 1 of Cell division protein kinase 9 | 1.59 ± 0.15 |
| **IPI00029162** | CHED | CDK13 Isoform 2 of Cell division protein kinase 13 | 1.64 ± 0.11 |
| **IPI00022827** | SLK | SLK Isoform 1 of STE20-like serine/threonine-protein kinase | 1.73 ± 0.22 |
| **IPI00298949** | GAK | GAK Cyclin-G-associated kinase | 1.78 ± 0.04 |
| **IPI00288940** | Obscn | OBSCN Isoform 1 of Obscurin | 1.82 ± 0.50 |
| **IPI00031681** | CDK2 | CDK2 Cell division protein kinase 2 | 1.82 ± 0.13 |
| **IPI00296337** | DNAPK | PRKDC Isoform 1 of DNA-dependent protein kinase catalytic subunit | 2.06 ± 0.63 |
| **IPI00031627** | POLR2A | POLR2A DNA-directed RNA polymerase II subunit RPB1 | 2.06 ± 0.71 |
| **IPI00100329** | ITPK1 | ITPK1 Isoform 1 of Inositol-tetrakisphosphate 1-kinase | 2.09 ± 0.79 |
| **IPI00297767** | CK1g2 | CSNK1G2 Casein kinase I isoform gamma-2 | 2.13 ± 0.38 |
| **IPI00002803** | PKN1 | PKN1 Isoform 1 of Serine/threonine-protein kinase N1 | 2.33 ± 0.52 |
| **IPI00186826** | EphB4 | EPHB4 Ephrin receptor | 2.37 ± 0.36 |
| **IPI00016639** | PKCi | PRKCI Protein kinase C iota type | 2.39 ± 0.73 |
| **IPI00218857** | MAP2K3 | MAP2K3 Isoform 1 of Dual specificity mitogen-activated protein kinase kinase 3 | 2.40 ± 0.45 |
| **IPI00181294** | CK1g3 | CSNK1G3 Isoform 1 of Casein kinase I isoform gamma-3 | 2.51 ± 0.55 |
| **IPI00217437** | TTBK2 | TTBK2 Tau-tubulin kinase | 2.55 ± 0.70 |
| **IPI00438229** | TIF1b | TRIM28 Isoform 1 of Transcription intermediary factor 1-beta | 2.73 ± 0.33 |
| **IPI00026689** | CDC2 | CDK1 Putative uncharacterized protein DKFZp686L20222 | 2.76 ± 0.48 |
| **IPI00290439** | SRPK1 | SRPK1 74 kDa protein | 2.78 ± 0.26 |
| **IPI00176642** | AurB | AURKB Serine/threonine-protein kinase 12 | 2.94 ± 0.44 |
| **IPI00003814** | MAP2K6 | MAP2K6 Isoform 1 of Dual specificity mitogen-activated protein kinase kinase 6 | 3.07 ± 0.36 |
| **IPI00180781** | MLKL | MLKL Isoform 1 of Mixed lineage kinase domain-like protein | 4.14 ± 0.25 |
| **IPI00023664** | CHK1 | CHEK1 Serine/threonine-protein kinase Chk1 | 5.46 ± 1.33 |

| IPI No. | Kinase Name | Description | Ratio |
|---|---|---|---|
| | | **Down-regulated** | |
| **IPI00172636** | CaMK2d | CAMK2D Isoform Delta 6 of Calcium/calmodulin-dependent protein kinase type II subunit delta | 0.24 ± 0.01 |
| **IPI00009688** | PIP4K2A | PIP4K2A Phosphatidylinositol-5-phosphate 4-kinase type-2 alpha | 0.29 ± 0.06 |
| **IPI00217960** | PKACa | PRKACA Isoform 2 of cAMP-dependent protein kinase catalytic subunit alpha | 0.32 ± 0.05 |
| **IPI00219592** | PKACg | PRKACG CAMP-dependent protein kinase CatalytiC subunit gamma | 0.32 ± 0.05 |
| **IPI00418221** | MAP3K6 | MAP3K6 Isoform 1 of Mitogen-activated protein kinase kinase kinase 6 | 0.39 ± 0.20 |
| **IPI00217024** | KHS2 | MAP4K3 Isoform 1 of Mitogen-activated protein kinase kinase kinase kinase 3 | 0.43 ± 0.05 |
| **IPI00027251** | NDR1 | STK38 Serine/threonine-protein kinase 38 | 0.46 ± 0.02 |
| **IPI00479760** | AAK1 | AAK1 Isoform 2 of AP2-associated protein kinase 1 | 0.50 ± 0.21 |
| **IPI00329236** | PKCd | PRKCD Protein kinase C delta type | 0.54 ± 0.30 |
| **IPI00028932** | MAST3 | MAST3 Microtubule-associated serine/threonine-protein kinase 3 | 0.58 ± 0.07 |
| **IPI00304742** | LOK | STK10 Serine/threonine-protein kinase 10 | 0.58 ± 0.06 |
| **IPI00021275** | EphB2 | EPHB2 Isoform 1 of Ephrin type-B receptor 2 | 0.64 ± 0.09 |
| **IPI00028570** | GSK3B | GSK3B Isoform 1 of Glycogen synthase kinase-3 beta | 0.66 ± 0.06 |

# Chapter 6

## Conclusions and Perspectives

In this dissertation, we utilized mass spectrometry-based approaches for quantitative proteomic analysis. By applying discovery-based and targeted proteomic analysis, we have successfully achieved global proteome and kinome profiling to reveal environmental toxicant exposure- and disease-related alterations in global protein expression level and kinase expression/activity.

In Chapters 2 and 3, we adopted discovery-based quantitative proteomic strategy with SILAC and LC-MS/MS analysis to achieve a large-scale quantification of the alterations of the whole proteome of GM00637 human skin fibroblast cells in response to treatment with potassium dichromate [Cr(VI)] and monomethylarsonous acid [MMA(III)]. These two compounds are common pollutants in the environment that can induce the development of cancer and other diseases among the exposed population. This analysis provided us with unbiased information of changes in protein expression for elucidating the mechanisms through which Cr(VI) and MMA(III) exert their deleterious effects. Initially, with in-gel digestion, we were able to quantify 4608 proteins from three sets of SILAC experiments. Later, with improved sample preparation method using filter-aided sample preparation coupled with SCX fractionation, we increased the number

of quantified proteins to ~6500. From downstream pathway analysis, we found the cholesterol biosynthesis pathway was significantly perturbed upon the toxicant treatments. It worth noting that, Cr(VI) and MMA(III) exerted distinct effects on cellular cholesterol production. While Cr(VI) exposure significantly activated the process, MMA(III) treatment greatly inhibited that. One possible explanation may be that the maintenance of steady cholesterol production is very critical to cellular function and interference with the process may cause deleterious effect to cell proliferation. Taken together, the novel insights into the mechanisms of cytoxicity of Cr(VI) and MMA(III) could provide us with new opportunity for the development of effective approaches for the therapeutic intervention following the exposure to Cr(VI) and MMA(III). In addition, the abundance of cellular cholesterol may serve as a new biomarker for Cr(VI) and MMA(III) exposure.

In Chapters 4 and 5, we utilized targeted proteomic approach to profile the global kinome. By interrogating this important family of enzymes, more information can be garnered on the details of critical cellular processes, such as cell signaling and cell proliferation. For quantitative analysis, we combined the use of an isotope-coded reactive ATP affinity probe with scheduled MRM analysis. The application of this probe is further expanded to accommodate the SILAC-based metabolic labeling. By adopting "on-the-fly" recalibration of retention time shift with "spiked-in" reference peptides to the targeted kinome analysis, we were able to shorten the duration of retention time window from 10 to 6 min. In doing so, ~2000 transitions of ~ 400 kinase peptides can be monitored in two LC-MRM runs without compromising the overall analytical

performance. By taking advantage of the above-described methods, we achieved, for the first time, an in-depth analysis of arsenic-induced global kinome perturbation in GM00637 human skin fibroblasts as well as kinome profiling of MCF-7 human breast cancer cells and the corresponding ionizing radiation-selected radioresistant clone, i.e. MCF-7/C6 cells. This demonstrated that the ATP affinity labeling method is amendable to both chemical and metabolic labeling, and the method is also powerful for exploring the disturbance in cell signaling network in response to environmental toxicant or disease-related changes.

Recently, to increase the proteome coverage, especially for the detection of proteins with low abundance, data-independent (DIA) approach has been utilized.[1] Unlike the traditional data-dependant acquisition method, whose detection relies on the signal intensity of the precursor ions in the full scan, the DIA approach allows systematic fragmentation of all peptides. To be specific, the DIA method involved cyclic recording of successive survey scans and fragment ion spectra of all precursors in each predetermined isolation window sequentially.[1-2] This prevents bias towards detection of proteins with high abundance and enables a more complete coverage of the proteome as well as increases reproducibility of the analysis.[3]

The DIA-based technique can also be applied to perform targeted analysis such as sequential windowed acquisition of all theoretical fragment ion mass spectra (SWATH).[2] Instead of targeted MS acquisition, the SWATH method is based on targeted data extraction.[2, 4] Specifically, the SWATH approach extracts mass spectra of targeted

peptides from SWATH MS analysis in the guidance of pre-constructed spectral libraries for the systematic identification and quantification of these peptides. The SWATH approach greatly increases the throughput and quantitative accuracy for the measurement of complex samples.[2] With the development of bioinformatic tools, the DIA acquisition approach may further expand the depth and breadth of MS-based proteomics.[5]

## References


1. Law, K. P.; Lim, Y. P., Recent advances in mass spectrometry: data independent analysis and hyper reaction monitoring. *Expert Rev. Proteomics* **2013,** *10* (6), 551-66.

2. Gillet, L. C.; Navarro, P.; Tate, S.; Rost, H.; Selevsek, N.; Reiter, L.; Bonner, R.; Aebersold, R., Targeted data extraction of the MS/MS spectra generated by data-independent acquisition: a new concept for consistent and accurate proteome analysis. *Mol. Cell. Proteomics* **2012,** *11* (6), O111 016717.

3. Tabb, D. L.; Vega-Montoto, L.; Rudnick, P. A.; Variyath, A. M.; Ham, A. J.; Bunk, D. M.; Kilpatrick, L. E.; Billheimer, D. D.; Blackman, R. K.; Cardasis, H. L.; Carr, S. A.; Clauser, K. R.; Jaffe, J. D.; Kowalski, K. A.; Neubert, T. A.; Regnier, F. E.; Schilling, B.; Tegeler, T. J.; Wang, M.; Wang, P.; Whiteaker, J. R.; Zimmerman, L. J.; Fisher, S. J.; Gibson, B. W.; Kinsinger, C. R.; Mesri, M.; Rodriguez, H.; Stein, S. E.; Tempst, P.; Paulovich, A. G.; Liebler, D. C.; Spiegelman, C., Repeatability and reproducibility in proteomic identifications by liquid chromatography-tandem mass spectrometry. *J. Proteome Res.* **2010,** *9* (2), 761-76.

4. Liu, Y.; Hüttenhain, R.; Collins, B.; Aebersold, R., Mass spectrometric protein maps for biomarker discovery and clinical research. *Expert Rev. Mol. Diagn.* **2013,** *13* (8), 811-825.

5. (a) Tsou, C. C.; Avtonomov, D.; Larsen, B.; Tucholska, M.; Choi, H.; Gingras, A. C.; Nesvizhskii, A. I., DIA-Umpire: comprehensive computational framework for data-independent acquisition proteomics. *Nature methods* **2015**; (b) MacLean, B.; Tomazela, D. M.; Shulman, N.; Chambers, M.; Finney, G. L.; Frewen, B.; Kern, R.; Tabb, D. L.; Liebler, D. C.; MacCoss, M. J., Skyline: an open source document editor for creating and analyzing targeted proteomics experiments. *Bioinformatics (Oxford, England)* **2010,** *26* (7), 966-8.